



The
University
Of
Sheffield.

The role of Transmembrane Protein 33 and calcium signalling during angiogenesis

By:

Aaron Michael Savage

A thesis submitted in partial fulfilment of the requirements for the degree of
Doctor of Philosophy

The University of Sheffield
Faculty of Medicine, Dentistry & Health
Department of Infection, Immunity & Cardiovascular Disease

March 2018

Table of Contents

List of Tables	9
List of abbreviations.....	10
Acknowledgements.....	12
1 Introduction	14
1.1 The endothelial cell and the clinical importance of angiogenesis.....	14
1.2 Transmembrane Protein 33 (<i>tmem33</i>)	16
1.3 Previous work relating to the project.	18
1.4 Endothelial cell origins and vasculogenesis.	25
1.5 Angiogenesis.	28
1.5.1 Signalling pathways regulating angiogenesis.....	31
1.5.2 Lymphangiogenesis.....	36
1.5.3 Regulation of the actin cytoskeleton and calcium signalling during angiogenesis. 37	
1.6 Kidney development in zebrafish.....	40
1.7 The Regulation of intracellular Calcium levels and Calcium Signalling.....	42
1.8 TRP channels	47
1.9 Developments in genome editing.....	49
1.9.1 Forward genetics and mutagenesis screens.	49
1.9.2 Reverse genetic approaches – morpholino knockdown.....	51
1.9.3 Reverse genetic approaches – targeted mutagenesis via Zinc Finger nucleases and TALENs.	52
1.9.4 Reverse genetic approaches – the CRISPR/Cas9 endonuclease system and recent adaptations.	53
1.10 The phenomenon of genetic compensation.....	56
1.11 Thesis Aims and hypotheses	57
2 Materials and Methods.....	60
2.1 Materials.	60
2.1.1 Zebrafish maintenance and husbandry.	60
Table 2.1 Transgenic lines characterised in this study.....	61
2.1.2 Morpholinos.....	69
Table 2.2 Morpholinos used in study.....	70
2.1.3 CRISPR/CRISPRi.	70
Table 2.3 List of gRNAs.....	70
2.1.4 Primers and probes used in study.....	71
Table 2.4 List of genotyping primers.....	71
Table 2.5 List of primers used to generate <i>in situ</i> hybridisation probes.	72
Table 2.6 List of primers used during cloning.	75

Table 2.7 List of Taqman probes.....	76
2.1.5 Generation of <i>tmem33</i> full length mRNA and <i>tmem33-gfp</i> fused mRNA	77
2.1.6 List of chemical inhibitors.....	79
Table 2.8 List of chemical inhibitors.....	79
2.1.7 Buffers and solutions.	79
Table 2.9 List of Buffers/Solutions	79
2.2 Methodology.....	81
2.2.1 Molecular biology.	81
2.2.4 Hybridisation and Immunohistochemistry.	89
2.2.5 Microscopy.....	92
2.2.6 Quantification and statistical analysis.	94
3 <i>Tmem33</i> is a novel regulator of endothelial and kidney calcium signalling during angiogenesis and kidney development.....	97
3.1 Introduction	97
3.2 <i>TMEM33</i> displays amino acid conservation from teleost fish to mammals.....	98
3.3 <i>tmem33-eGFP</i> mRNA localises to the endoplasmic reticulum and nuclear pore within zebrafish endothelial cells.	100
3.4 <i>Tg(fli1a:gff)ubs3;Tg(uas-GCaMP7a)sh392</i> is a genetically encoded calcium indicator (GECI), allowing visualisation of calcium signalling in endothelial cells in real-time and modulation of calcium signalling induces changes in <i>Tg(fli1a:gff)ubs3;Tg(uas:GCaMP7a)sh392</i> fluorescence levels.	102
3.5 VEGF signalling is required for endothelial calcium oscillations.....	105
3.6 <i>tmem33</i> morphants display impaired angiogenesis and reduced endothelial calcium oscillations.	108
3.6.1 Thapsigargin-mediated elevations in cytosolic Ca ²⁺ are reduced in <i>tmem33</i> morphants.....	111
3.7 <i>tmem33</i> morphants display reduced pronephric calcium signalling.....	112
3.8 Development of an endothelial F-actin reporter line to quantify filopodia dynamics during angiogenesis.	115
3.9 Latrunculin B inhibits formation of endothelial filopodia but does not alter endothelial calcium oscillation frequency.	118
3.10 <i>tmem33</i> knockdown inhibits endothelial filopodia formation.....	119
3.11 <i>tmem33</i> ^{sh443} mutants exhibit nonsense mediated decay but normal angiogenesis.....	122
3.12 <i>tmem33</i> ^{sh448} mutants are protected from the effects of <i>tmem33</i> morpholinos.....	124
3.13 Discussion.....	127
3.13.1 Overview	127
3.13.2 <i>tmem33</i> is expressed ubiquitously early in development, and is expressed in both pronephros and endothelial cells later in development, probably localising to the ER	128
3.13.3 <i>tmem33</i> knockdown impairs angiogenesis.....	129

3.13.4	The role of calcium signalling in angiogenesis and angiogenic signalling pathways	130
3.13.5	<i>tmem33</i> knockdown impairs calcium signalling and actin cytoskeleton regulation	131
3.13.6	<i>tmem33</i> is required for normal calcium signalling in both developing endothelial and kidney cells, suggesting a wider function than just during VEGF-mediated calcium signalling	133
3.13.7	<i>tmem33</i> mutants appear to display genetic compensation	134
4	Development of a strategy for conditional knockdown of genes via CRISPR interference to validate and extend functional analysis of <i>tmem33</i>	137
4.1	Introduction	137
4.1.1	VHL and Hypoxia-induced angiogenesis	137
4.2	Development of <i>vhl-phd3</i> pathway as a novel test-bed for CRISPRi	139
4.3	Knockdown of <i>vhl</i> induces angiogenic branching defects and kidney filtration defects	146
4.4	Development of tissue-specific CRISPRi as a tool to conditionally modulate gene expression	149
4.4.1	Developing kidney specific gene knockdown by CRISPRi: <i>vhl</i> is required in a tissue specific manner for normal kidney function	150
4.5	Knockdown of <i>tmem33</i> using CRISPR interference reduces <i>tmem33</i> mRNA expression and induces vascular and kidney defects	152
4.6	<i>tmem33</i> overexpression rescues <i>tmem33</i> crispant phenotype	156
4.7	<i>tmem33</i> knockdown by CRISPRi attenuates endothelial calcium oscillations	158
4.8	<i>tmem33</i> knockdown by CRISPRi reduces endothelial filopodia dynamics and number	160
4.9	Transient knockdown of <i>tmem33</i> by tissue-specific CRISPRi can uncouple kidney and vascular defects	162
4.10	Transient knockdown of <i>tmem33</i> using tissue specific CRISPRi is comparable to global <i>tmem33</i> knockdown by morpholinos or global CRISPRi	163
4.11	Generation of a stable <i>Tg(fli1a:dcas9,cryaa:CFP)sh512</i> transgenic zebrafish line	165
4.12	Endothelial specific <i>dll4</i> knockdown by CRISPRi in stable <i>Tg(fli1a:dcas9;craa:CFP)^{sh512}</i> transgenics induces aberrant DLAV patterning	167
4.13	Endothelial specific knockdown of <i>tmem33</i> by CRISPRi in stable <i>Tg(fli1a:dcas9;craa:CFP)^{sh512}</i> transgenics induces vascular branching defects but not glomerular expansion	168
4.14	<i>tmem33</i> functions downstream of VEGF signalling during angiogenesis	171
4.15	<i>tmem33</i> promotes Notch signalling during angiogenesis	176
4.16	<i>tmem33</i> promotes endothelial MAPK/ERK signalling during angiogenesis	179
4.17	Both <i>flt4</i> and <i>dll4</i> function downstream of calcium signalling	180
4.18	Inhibition of Store Operated Calcium Entry (SOCE) delays angiogenesis	182
4.19	Inhibition of SOCE via SKF96365 reduces frequency of endothelial calcium oscillations	183
4.20	Inhibition of SOCE reduces endothelial Notch signalling and filopodia dynamics	184

Table 4.1 A summary and comparison of phenotypes observed following <i>tmem33</i> knockdown and SKF96365 treatment.....	187
4.21 Discussion.....	188
4.21.1 General discussion: development of tissue-specific CRISPRi as a strategy to conditionally modulate gene expression.	188
4.21.2 EC-specific knockdown of <i>tmem33</i> using CRISPRi reveals <i>tmem33</i> is required in ECs for normal angiogenesis.	191
4.21.3 TMEM33 maintains normal migrational endothelial cell biology via regulation of calcium signalling, integrating VEGF, ERK and Notch signalling pathways.....	193
4.21.4 Calcium signalling is required for normal endothelial cell behaviour.	195
4.21.5 Much still remains unknown regarding TMEM33 function <i>in vivo</i>	198
5 Investigation of putative genetic interactions of <i>tmem33</i> with TRP channels.....	203
5.1 Introduction	203
5.2 Knockdown of <i>tmem33</i> in <i>pkd2</i> mutants does not increase glomerular area.	204
5.3 Abnormal glomerular development induced by <i>tmem33</i> knockdown is not enhanced by knockdown of <i>pkd2</i>	206
5.4 <i>tmem33</i> ^{-/-} ; <i>pkd2</i> ^{-/-} double mutants do not display an increase in glomerular area.....	207
5.4 Axial curvature is not affected in <i>tmem33</i> ^{-/-} ; <i>pkd2</i> ^{-/-} double mutants.....	209
5.4.1 <i>tmem33</i> knockdown in <i>elipsa</i> mutants does not increase glomerular area.....	210
5.5 Expression analysis of transient receptor potential (TRP) channels during zebrafish embryogenesis.....	212
5.6 TRPV4 is required for calcium signalling during flow-independent angiogenesis.....	220
5.6.1 <i>trpv4</i> antagonist treatment delays angiogenic sprouting in zebrafish embryos. 220	
5.6.2 <i>trpv4</i> antagonist reduces endothelial calcium oscillations in <i>Tg(fi1a:gff)ubs3;Tg(uas:GCaMP7a)sh392</i> embryos.....	222
5.6.3 <i>trpv4</i> CRISPRi reduces frequency of calcium oscillations in <i>Tg(fi1a:gff)ubs3;Tg(uas:GCaMP7a)sh392</i> embryos.....	223
5.6.4 <i>trpv4</i> CRISPRi reduces TRPV4 gene expression.....	225
5.6.5 Endothelial-specific knockdown of <i>trpv4</i> by CRISPRi reduces calcium oscillation frequency in ECs in <i>Tg(fi1a:gff)ubs3;Tg(uas:GCaMP7a)sh392</i> embryos.	226
5.7 Discussion.....	228
5.7.1 My data provides no evidence for genetic compensation between <i>tmem33</i> and <i>pkd2</i> but does not discount possible interaction during zebrafish development.	228
5.7.2 TRPV4 contributes to endothelial calcium oscillations during sprouting angiogenesis.....	230
5.7.3 Limitations and future work.....	232
6 Overall Discussion: A more general role for <i>tmem33</i> in calcium signalling?	234
7 Bibliography	243

List of Figures

Figure 1.1 – TMEM33 protein structure.	17
Figure 1.2 <i>tmem33</i> displays enrichment of expression in the developing kidney and endothelium during zebrafish embryogenesis.	20
Figure 1.3 A 28 hpf zebrafish embryo to illustrate imaging parameters.	21
Figure 1.4 <i>tmem33</i> morpholino knockdown impairs angiogenesis and lymphatic development.	23
Figure 1.5 <i>tmem33</i> morpholino knockdown induces glomerular expansion in zebrafish embryos.	24
Figure 1.6 – Midline migration and vasculogenesis in zebrafish embryos.	27
Figure 1.7 – Zebrafish trunk angiogenesis.	30
Figure 1.8 – Key signalling regulating angiogenesis.	31
Figure 1.9 – Intracellular signalling during angiogenesis.	34
Figure 1.10 An overview of calcium signalling mechanisms.	44
Figure 1.11 – Store operated calcium entry via STIM and ORAI proteins.	47
Figure 1.12 – Genetic manipulation by CRISPR-mediated knockout and CRISPR interference.	56
Figure 1.13 A summary of proposed <i>tmem33</i> interactions and integration within the endothelial signalling pathway hierarchy.	59
Figure 2.1 <i>Tg(fli1a:LifeACT-mClover)sh467</i> labels probable F-Actin structures within endothelial cells.	63
Figure 2.2 <i>Tg(fli1a:AC-TagRFP)sh511</i> labels F-Actin-like structures in endothelial cells.	66
Figure 2.3 <i>Tg(fli1a:DsRedEx2)sh495</i> embryos display endothelial DsRed protein and apparent nuclear exclusion.	68
Figure 3.1 Protein alignment of TMEM33 across species shows conservation of transmembrane domains.	99
Figure 3.2 <i>tmem33</i> is expressed in the endothelium during zebrafish embryonic development.	100
Figure 3.3 <i>tmem33-eGFP</i> appears to be expressed in the ER and nuclear envelope.	101
Figure 3.4 <i>Tg(fli1a:gff)ubs3;Tg(uas:GCaMP7a)sh392</i> fluorescence can be modulated by modulating calcium signalling.	104
Figure 3.5. Modulation of VEGF and Notch signalling modify frequency of endothelial Ca^{2+} oscillations.	107
Figure 3.6. <i>tmem33</i> knockdown impairs EC migration.	109
Figure 3.7. <i>tmem33</i> knockdown reduces Ca^{2+} oscillations in endothelial tip cells.	110
Figure 3.8 <i>tmem33</i> morphants do not display Thapsigargin-mediated increases in cytosolic Ca^{2+}	112
Figure 3.9 <i>tmem33</i> knockdown by morpholino reduces calcium signalling within the developing kidney.	114
Figure 3.10 <i>Tg(fli1a:LifeACT-mClover)sh467;Tg(fli1a:DsRedEx2)sh511</i> embryos display spatially distinct fluorophores and <i>Tg(fli1a:LifeACT-mClover)sh467</i> highlights endothelial filopodia. ...	117

Figure 3.11 Endothelial Ca ²⁺ oscillations within tip cells are not disrupted following loss of filopodia..	119
Figure 3.12 <i>tmem33</i> knockdown by morpholino reduces endothelial filopodia activity..	121
Figure 3.13 <i>tmem33</i> ^{sh443} mutants are predicted loss of function and display nonsense-mediated decay but normal angiogenesis.	124
Figure 3.14 <i>tmem33</i> ^{sh443} mutants are partially protected from morpholino-induced angiogenic and glomerular defects.	126
Figure 3.15 <i>tmem33</i> functions to regulate calcium efflux from the ER, which is important for normal F-actin mobilisation, including filopodia formation.....	127
Figure 4.1. Schematic representation of <i>vhl</i> gRNA superimposed on <i>vhl</i> genomic sequence .	141
Figure 4.2 Embryonic survival is reduced at by injection of high concentrations of dCas9 or gRNA.....	142
Figure 4.3 <i>vhl</i> -gRNA-1 induces double strand breaks when co-injected with active Cas9, but not with dCas9.....	143
Figure 4.4 <i>vhl</i> CRISPRi knockdown transiently activates <i>phd3:eGFP</i> expression.....	145
Figure 4.5 <i>vhl</i> CRISPRi knockdown induces mild ectopic angiogenesis at 120 hpf.	147
Figure 4.6 <i>vhl</i> CRISPRi knockdown induces kidney filtration defects comparable with <i>vhl</i> mutants.....	148
Figure 4.7 Schematic representation of tissue-specific CRISPRi constructs.	150
Figure 4.8 Tissue-specific knockdown of <i>vhl</i> by CRISPRi increases GFP in the kidney of <i>Tg(phd3:GFP)</i> embryos.	151
Figure 4.9 Kidney-specific knockdown of <i>vhl</i> by CRISPRi is sufficient to induce kidney filtration defects observed following global knockdown of <i>vhl</i> by CRISPRi.....	152
Figure 4.10 Guide RNA design for <i>tmem33</i>	153
Figure 4.11 <i>tmem33</i> CRISPRi recapitulates <i>tmem33</i> morpholino phenotypes	155
Figure 4.12 <i>tmem33</i> CRISPRi-induced defects can be rescued by overexpression of full-length <i>tmem33</i> mRNA.....	157
Figure 4.13 <i>tmem33</i> CRISPRi reduces endothelial calcium signalling frequency.	159
Figure 4.14 <i>tmem33</i> CRISPRi reduces endothelial filopodia numbers during sprouting angiogenesis.....	161
Figure 4.15 Transient tissue-specific <i>tmem33</i> CRISPRi induces defects during angiogenesis and kidney development independently at 55 hpf	163
Figure 4.16 Transient tissue-specific <i>tmem33</i> CRISPRi induces both vascular and kidney developmental defects comparable to global knockdown.....	165
Figure 4.17 <i>Tg(fli1a:dCas9,cryaa:CFP)sh512</i> embryos express <i>dCas9</i> in endothelial cells.	167
Figure 4.18 Tissue-specific <i>dll4</i> CRISPRi increases DLAV vascularisation.....	168
Figure 4.19 Tissue-specific <i>tmem33</i> CRISPRi induces vascular developmental defects but not glomerular expansion..	170
Figure 4.20 <i>tmem33</i> functions downstream of VEGF during endothelial proliferation and the regulation of calcium signalling.	173
Figure 4.21 <i>tmem33</i> CRISPRi reduces expression of <i>flt4</i> , but not other VEGF receptors.....	175

Figure 4.22 <i>tmem33</i> knockdown reduces Notch signalling in the endothelium.	179
Figure 4.23 <i>tmem33</i> CRISPRi reduces endothelial ERK phosphorylation.	180
Figure 4.24 <i>flt4</i> knockdown does not significantly affect calcium oscillation frequency..	181
Figure 4.25 SKF96365 treatment induces angiogenic delays.	183
Figure 4.26 Inhibition of SOCE reduces frequency of endothelial calcium oscillations.....	184
Figure 4.27 Endothelial Notch signalling and filopodia dynamics are reduced by SKF96365 treatment.....	186
Figure 4.28 A proposed role for <i>tmem33</i> within the angiogenic hierarchy.....	202
Figure 5.1 Glomerulus area is not affected by <i>tmem33</i> knockdown in <i>pkd2</i> ^{hu2173} mutants....	205
Figure 5.2 Abnormal glomerular development induced by <i>tmem33</i> knockdown is not enhanced by knockdown of <i>pkd2</i>	207
Figure 5.3 No significant change in glomerular area is observed in <i>tmem33</i> ^{sh443} ; <i>pkd2</i> ^{hu2173} double mutants.....	208
Figure 5.4 <i>tmem33</i> ^{sh443} ; <i>pkd2</i> ^{hu2173} mutants display no significant difference in axial curvature.	210
Figure 5.5 <i>tmem33</i> knockdown does not increase glomerular expansion in <i>elipsa</i> mutants. .	212
Figure 5.6 No canonical TRP channel displays enrichment in endothelial cells at 24 hpf.	214
Figure 5.7 No canonical TRP channel displays enrichment in endothelial cells at 24 hpf.	215
Figure 5.8 No Ankyrin or melanostatin TRP channel displays enrichment in endothelial cells at 24 hpf.	216
Figure 5.9 No melanostatin TRP channel displays enrichment in endothelial cells at 24 hpf. .	217
Figure 5.10 No mucolipin or polycystin TRP channel displays enrichment in endothelial cells.	218
Figure 5.11 No vanilloid TRP channel displays enrichment in endothelial cells.....	219
Figure 5.12 TRPV4 Antagonist III treatment causes angiogenesis delays in <i>Tg(fli1a:EGFP)y1</i> embryos.	222
Figure 5.13 TRPV4 Antagonist III treatment reduces calcium oscillation frequency during angiogenesis.....	223
Figure 5.14 TRPV4 CRISPRi reduces endothelial calcium oscillation frequency in migrating SeAs	224
Figure 5.15 TRPV4 CRISPRi reduces TRPV4 expression.....	225
Figure 5.16 Endothelial-specific TRPV4 CRISPRi reduces endothelial calcium oscillation frequency..	227
Figure 6.1 <i>TMEM33</i> is required for VEGFA-mediated angiogenesis in Human Umbilical Vein Endothelial Cells (HUVECs).	236
Figure 6.2 <i>tmem33</i> -mediated Ca ²⁺ signalling functions downstream of VEGF signalling to regulate downstream signalling.....	240

List of Tables

Table 2.1 Transgenic lines characterised in this study.....	61
Table 2.2 Morpholinos used in study.....	70
Table 2.3 List of gRNAs.....	70
Table 2.4 List of genotyping primers.....	71
Table 2.5 List of primers used to generate <i>in situ</i> hybridisation probes.	72
Table 2.6 List of primers used during cloning.	75
Table 2.7 List of Taqman probes.	76
Table 2.8 List of chemical inhibitors	79
Table 2.9 List of Buffers/Solutions	79
Table 4.1 A summary and comparison of phenotypes observed following <i>tmem33</i> knockdown and SKF96365 treatment.	187

List of abbreviations

+/+	Wild type
+/-	Heterozygote
-/-	Homozygote
AV951	Tivozanib (AVEO pharmaceuticals)
Ca ²⁺	Calcium ion
Cas9	CRISPR-associated protein 9
COMO	Control morpholino
CRAC	Calcium release-activated calcium channel
CRACM1	Calcium release-activated calcium membrane protein 1 (now <i>orai1</i>)
CRISPR	Clustered regularly interspaced short palindromic repeats
CRISPRa	CRISPR activation
CRISPRi	CRISPR interference
CVP	Caudal vein plexus
DA	Dorsal aorta
DAPT	N-[N-(3,5-Difluorophenoacetyl-L-alanyl)]-S-phenylglycine t-Butyl Ester
dCas9	Deactivated Cas9
DLAV	Dorsal longitudinal anastomotic vessel
DLP	Dorso-lateral plate mesoderm
<i>dll4</i>	Delta-like ligand 4
Dpf	Days post fertilisation
EC	Endothelial cell
EGF	Epidermal growth factor-like domain
EGFP	Enhanced green fluorescent protein
<i>Enpep</i>	Glutamyl aminopeptidase
ERK	Extracellular signal regulated kinase kinase
<i>fli1</i>	Friend leukaemia integration 1 transcription factor
<i>flk1</i>	Foetal liver kinase (now <i>kdrl</i> in zebrafish)
<i>flt1</i>	Fms-related tyrosine kinase 1
<i>flt4</i>	Fms-related tyrosine kinase 4
GFP	Green fluorescent protein
gRNA	Guide RNA
Hh	Hedgehog (signalling)
HIF	Hypoxia-inducible factor
Hpf	Hours post fertilisation
HSC	Haematopoietic stem cell
ISV	Intersegmental vessel
aISV	Arterial intersegmental vessel
vISV	Venous intersegmental vessel
KD	Knockdown
<i>Kdr</i>	Kinase insert domain receptor
<i>Kdrl</i>	Kinase insert domain receptor-like
KO	Knockout
KRAB	Krüppel-associated box
LEC	Lymphatic endothelial cell
LPM	Lateral plate mesoderm
MAB	Maleic acid buffer
MAPK	Mitogen-activated protein kinase
<i>Mib</i>	<i>mind bomb</i>

MO	Morpholino
NICD	Notch intracellular domain
NS	Not significant
ORAI	Calcium release-activated calcium channel protein 1 (In Greek mythology, the <i>Orai</i> are the keepers of the gates of heaven)
PBS	Phosphate buffered saline
PCV	Posterior cardinal vein
PHD	Prolyl hydroxylase
PI3K	Phosphatidylinositol 3-kinase
PKD	Polycystic kidney disease
PLC- γ	Phospholipase C-gamma
<i>prox1</i>	Prospero homeobox 1
SC	Stalk cell
SeA	Segmental artery
Shh	Sonic hedgehog
SIV	Sub-intestinal vein
SOCE	Store-operated calcium entry
STIM	Stromal interaction molecule
TD	Thoracic duct
TRP	Transient receptor potential (channel)
TRPA	Ankyrin transient receptor potential subfamily
TRPC	Canonical transient receptor potential subfamily
TRPM	Melanostatin transient receptor potential subfamily
TRPML	Mucolipin transient receptor potential subfamily
TRPP	Polycystin transient receptor potential subfamily
TRPV	Vanilloid transient receptor potential subfamily
VEGF	Vascular endothelial growth factor
VEGFR	Vascular endothelial growth factor receptor
<i>vhl</i>	von Hippel-Lindau
VOC	Voltage-operated calcium channel
WT	Wild type
<i>wt1b</i>	Wilm's tumour 1b

Acknowledgements

I would like to take this opportunity to thank those who have contributed both to this thesis and to my development technically. Firstly, I would like to acknowledge the experimental contributions to this thesis provided by both Dr Rob Wilkinson and Dr Freek van Eeden in section 1.2. All other experiments were performed and analysed by myself.

I would also like to thank my supervisors Tim and Rob, for scientific and technical guidance over the three years, and to Freek during the first year of my PhD. I would like to thank Karen, Rich, Aylin and Jane for teaching me new techniques and giving me tips (both in advice and pipette form).

Abstract

In this thesis I present the first functional analysis of *tmem33* in multicellular organisms. I have determined the function of *tmem33* and endothelial calcium oscillations during angiogenesis utilising developing zebrafish embryos. I show that *tmem33* is required downstream of VEGF signalling during VEGF-mediated angiogenesis and functions to promote calcium oscillations within endothelial cells. Furthermore, *tmem33* knockdown attenuates downstream signalling pathways including Dll4/Notch and ERK, indicating a requirement for calcium signalling in integrating VEGF signalling with Notch and MAP kinase signalling.

Interestingly, *tmem33* mutants are morphologically normal and homozygous viable, yet these displayed significantly reduced *tmem33* mRNA expression, indicating induction of nonsense mediated decay. *tmem33* mutants displayed protection from morpholino-induced angiogenesis and kidney defects, suggesting *tmem33* mutants display compensation via transcriptional adaptation. To overcome this, I have developed a novel approach to achieve tissue specific loss-of-function, using CRISPR interference to specifically abrogate *tmem33* function in endothelial cells and the developing kidney. Using this approach, I find *tmem33* is required in endothelial cells for both normal angiogenesis and is required within the developing kidney for normal calcium oscillations and glomerular development. *tmem33* is also required for endothelial migration during primary angiogenesis and formation of filopodia. Importantly, through analysis of *tmem33* function I identify novel functions for endothelial calcium oscillations in promoting formation of filopodia during endothelial migration, promoting VEGF-mediated endothelial proliferation and to link VEGF signalling with downstream Dll4/Notch and ERK signalling.

1 Introduction

1.1 The endothelial cell and the clinical importance of angiogenesis.

Developing and adult vertebrate organisms require a vascular system to supply nutrients and oxygen and remove waste products. The endothelial cell is a specialised epithelial cell which lines the inner lumens of vessels and is exposed to circulating haematopoietic cells and plasma (Eelen et al., 2018). During development, endothelial cells can migrate to form new vessels via a process known as angiogenesis, before becoming quiescent as vessels become patent. Endothelial cells lining the vessel lumen comprise a system known as the endothelium. This functions not only as a barrier between blood and respiring tissues, but is able to regulate oxygen transfer, as well as functions such as angiocrine factor secretion (Eelen et al., 2018; Rajendran et al., 2013).

Endothelial dysfunction underlies many diseases, including atherosclerosis, diabetes and cancer. During atherosclerosis, fatty plaques build up underneath the endothelium (Tabas et al., 2015), and during cancer progression, tumours require a vascular network to grow and later metastasise (Yadav et al., 2015). Therefore, understanding how endothelial function is regulated may allow us to develop therapies to treat diseases where pathology either results from or causes aberrant endothelial function (Eelen et al., 2018; Rajendran et al., 2013).

Understanding the pathways that regulate angiogenesis has implications for disease therapy. For example, anti-angiogenic therapies to treat cancer have targeted VEGF signalling, the master regulator of angiogenesis, to prevent tumour vascularisation (Yadav et al., 2015). However, most anti-angiogenic

treatments have been unsuccessful (Meadows and Hurwitz, 2012), suggesting a greater understanding of downstream intracellular signalling mechanisms regulating angiogenesis is required. Similarly, pro-angiogenic treatment to stimulate vascularisation in regions surrounding vascular occlusion may benefit patients suffering from arterial or microvascular disease.

One such component of downstream signalling implicated in angiogenesis is calcium signalling. While it is established that calcium signalling is induced downstream of VEGF signalling (Fearnley et al., 2015; Oike et al., 1994; Vaca and Kunze, 1994; Zadeh et al., 2009), a greater understanding of the role of calcium signalling during angiogenesis is required. One class of highly characterised calcium channel is the transient receptor potential (TRP) channel family, suggesting they may be suitable candidates for manipulating endothelial calcium signalling *in vivo* and therapeutically. However, such a large number of TRP channels exist (18 in humans, 34 in zebrafish) that a degree of redundancy is likely to exist. Therefore, identifying other components of calcium signalling may be important to understand how calcium signalling regulates endothelial development and homeostasis.

Previous work by Dr. Eric Honore in collaboration with Dr. Robert Wilkinson and Dr. Freek van Eeden identified several proteins, via pull-down assays, which interact with members of the TRP family of non-selective ion channels. The calcium channels PKD1 and PKD2 were used in this study. TMEM33 was one such protein. Therefore, I aim to use the zebrafish to characterise *tmem33* function and understand how calcium signalling regulates angiogenesis *in vivo*.

In this chapter I will discuss what is currently known about the gene *tmem33*, vascular and kidney development, calcium signalling and genome editing, as these areas pertain to the data I will present.

1.2 Transmembrane Protein 33 (*tmem33*)

Transmembrane protein 33 (*tmem33*), originally cloned as DB83 in rat liver samples (Nakadai et al., 1998), is a 3-pass transmembrane domain protein (Figure 1.1) localised to the ER membrane (Sakabe et al., 2015). Little is known about *tmem33* function *in vivo*, and *tmem33* function has not been examined in multicellular organisms.

Much of the analysis of *tmem33* has examined the orthologues in budding yeast, *Saccharomyces cerevisiae* and fission yeast, *Saccharomyces pombe*, Pom33/Per33 and Tts1, respectively (Floch et al., 2015; Zhang and Oliferenko, 2014), or more recently cell culture (Chapman et al., 2015; Huang et al., 2016; Sakabe et al., 2015; Urade et al., 2014). While the majority of data suggests a function for *tmem33* in the endoplasmic reticulum, it has been implicated in a variety of roles. In both yeast species, *tmem33* is suggested to regulate the nuclear envelope and nuclear pore. *tmem33* binds to nuclear pore complex proteins such as the nuclear import factor, Kap123 (Floch et al., 2015), and is implicated in the insertion of spindle bodies during mitosis in fission yeast (Zhang and Oliferenko, 2014).

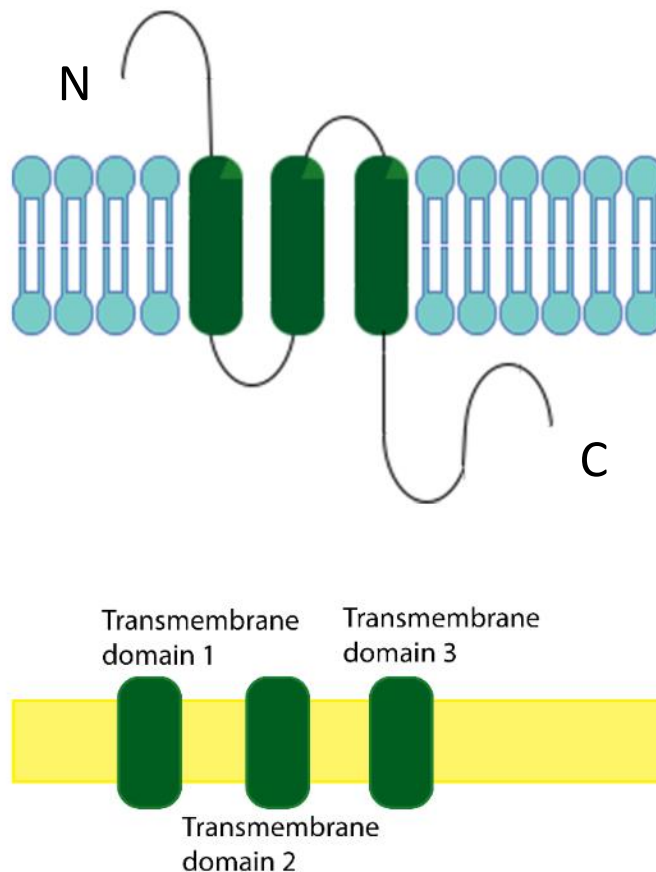


Figure 1.1 – TMEM33 protein structure. *Tmem33* displays a three-transmembrane structure, with an extra-ER N-terminal tail, intra-ER C-terminal tail and two alternating intra- and extra-ER loops.

In cell culture, *tmem33* has been shown to be upregulated during ER stress, leading to induction of the unfolded protein response (UPR) (Sakabe et al., 2015). Furthermore, *tmem33* has been linked to the ER-associated degradation (ERAD) pathway, in which it participates with the Cyclophilin C-mediated degradation of major histocompatibility complex class I (MHC I) molecules (Chapman et al., 2015). *tmem33* has also been implicated in cancer cell adhesion and invasion (Huang et al., 2016), and in regulation of ER tubule formation (Urade et al., 2014). *tmem33* is differentially expressed in the melanocytes of east Asian populations,

compared to African populations, suggesting it may play a role in pigmentation changes in this population (Hider et al., 2013).

Furthermore, *tmem33* has been suggested to interact with reticulon binding proteins, suggesting *tmem33* functions in regulating ER shape (Urade et al., 2014). Interestingly, *tmem33* has also been shown to interact with the ER stress-sensor, PERK (Sakabe et al., 2015). PERK has recently been implicated in the resolution of store-operated calcium signalling (SOCE), via regulation of ER shape (van Vliet et al., 2017). These findings suggest that *tmem33* may function during calcium signalling, via regulation of ER shape.

No study, thus far, has implicated *tmem33* in developmental processes in multicellular organisms. In this thesis, I determine the function of *tmem33* in migrating endothelial cells during angiogenesis and establish the relationships between *tmem33* and pathways controlling angiogenesis, including VEGF and Notch.

1.3 Previous work relating to the project.

Data from collaborators identified TMEM33 in interaction with PKD1/2 and further implicated interaction between TMEM33 and PKD2 via a series of experiments, including lipid bilayer reconstitution, in which the calcium channel activity of PKD2 was enhanced by the presence of TMEM33, suggesting TMEM33 may function during the regulation of calcium signalling.

Preliminary work undertaken by Dr. Robert Wilkinson prior to my arrival in the laboratory analysed *tmem33* expression by *in situ* hybridisation. Ubiquitous *tmem33* expression was observed during early zebrafish development, increasing between the 17 and 19 somite stages (Figure 1.2 A, B). By 25 hpf, *tmem33* was more expressed within the developing kidney (Figure 1.2 C, white arrowhead) and somite boundaries at 25 hpf (black arrowhead). Sections of 25 hpf embryos confirmed *tmem33* expression within pronephric tubules (Figure 1.2 D, black arrows) and the posterior cardinal vein (Figure 1.2 D, green arrowhead). By 30 hpf reduction in *tmem33* expression was observed, although its expression was maintained within the pronephric duct (Figure 1.2 E, white arrowhead). By 50 hpf, *tmem33* expression was reduced within the pronephric duct and endothelium (Figure 1.2 F).

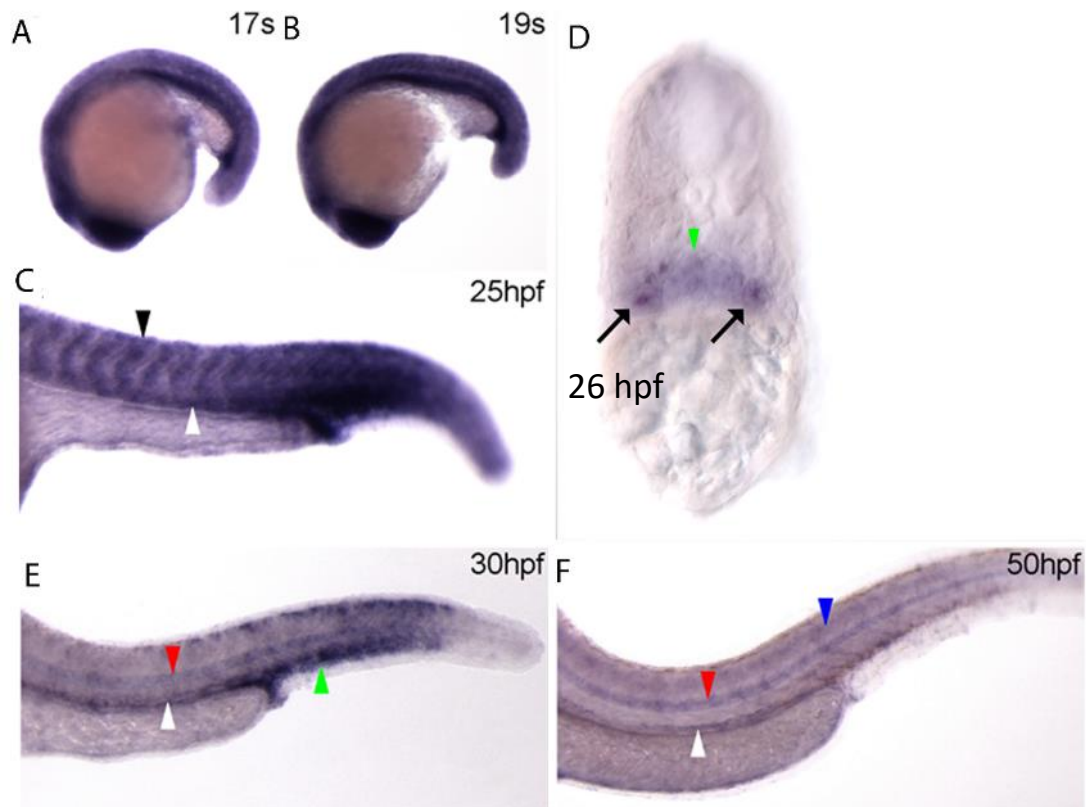


Figure 1.2 *tmem33* displays enrichment of expression in the developing kidney and endothelium during zebrafish embryogenesis. (A-B) *tmem33* displays ubiquitous expression at 17 and 19 somite stages. (C) *tmem33* displays largely ubiquitous expression, with enrichment in the kidney (white arrowhead) and somite boundaries (black arrowhead) at 25 hpf. (D). Enriched *tmem33* expression is seen in the pronephric tubules (black arrows) and in the PCV (green arrowhead) in a 25 hpf section (E) By 30 hpf, *tmem33* expression diminishes , with some enrichment in the pronephric tubules (white arrowhead), floor plate (red arrowhead) and CVP (green arrowhead). (F) By 50 hpf, no restricted expression is observed.

Data courtesy of Dr. Robert Wilkinson.

Next, splice blocking morpholinos were designed to induce mis-splicing of *tmem33* pre-mRNA in transgenic zebrafish lines labelling endothelial cells to visualise the developing vasculature. Morpholino knockdown of *tmem33* in endothelial transgenic reporter embryos was performed by Dr Robert Wilkinson prior to my arrival in the laboratory. For reference, all images of the vasculature

taken throughout this thesis are of the region dorsal to the yolk cell extension, beginning anterior to the cloaca; highlighted in the example below (Figure 1.3).

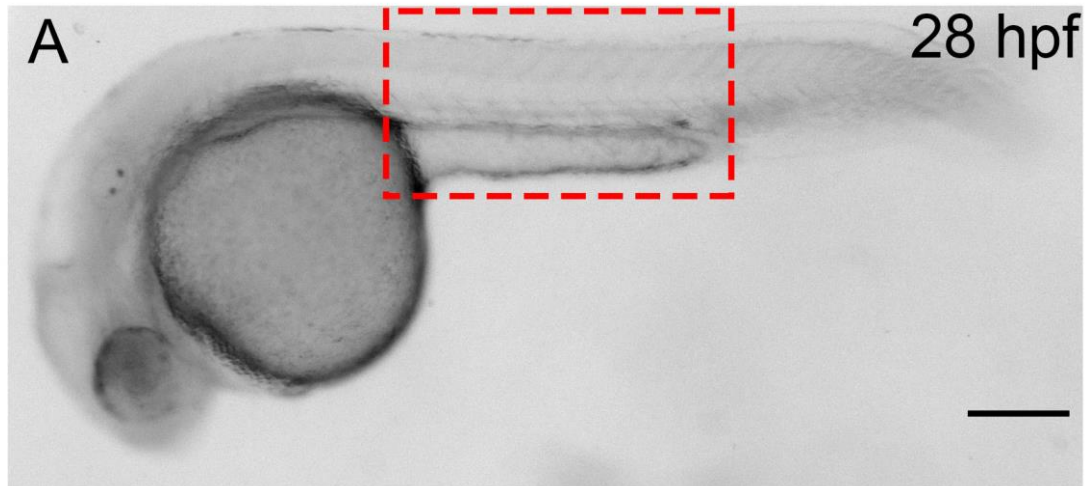


Figure 1.3 A 28 hpf zebrafish embryo to illustrate imaging parameters. The red box indicates the location at which all images of vascular development throughout this thesis were captured. The box contains 15 somites located dorsal to the yolk cell extension. At the caudal end of the yolk cell extension lies the cloaca. Between the somites develop 14 pairs of intersegmental vessels, a selection of which were imaged during this study in each experiment.

Following *tmem33* morpholino knockdown, delayed SeA sprouting was observed in *Tg(fli1a:eGFP)y1* transgenic embryos at 30 hpf (Figure 1.4 B, B'). Migrating SeAs stalled around the level of the horizontal myoseptum in morphants (Figure 1.4 E), whereas control embryos displayed complete dorsal migration after which SeAs began to anastomose and form the dorsal longitudinal anastomotic vessel (DLAV) (Figure 1.4 A, A'). Stalled SeAs are consistent with phenotypes observed following reduced VEGF signalling (Covassin et al., 2006). This suggests *tmem33* knockdown may impair SeAs response to migratory VEGF signals or

that *tmem33* may be responsible for modulation of cell biology in response to VEGF signals.

By 53 hpf, *tmem33* morphant SeAs displayed complete dorsal migration, However, *tmem33* SeAs did not display normal, chevron-shaped development, as in controls (Figure 1.4 C, C', yellow arrowheads), instead branching aberrantly and resulting in discontinuous DLAV formation (Figure 1.4 D, D', yellow arrowheads). Furthermore, aberrantly migrating SeAs were frequently observed in *tmem33* morphants (Figure 1.4 D, white arrowhead) and *tmem33* morphants displayed an increase in abnormal DLAV formation (Figure 1.4 D, D').

In addition, *tmem33* morphants lacked lymphatic vasculature (Figure 1.4 D, D', red arrowheads; H, white asterisks). Lymphangiogenesis is dependent on *vegfc* signalling via *flt4* (VEGF receptor 3), which enables lymphangioblasts to migrate from the posterior cardinal vein (PCV) to form parachordal lymphangioblasts, which align along the horizontal myoseptum (refer to figure). While control morphants developed a parachordal lymphangioblasts (Figure 1.4 C, C', red arrowheads), *tmem33* morphants did not (Figure 1.4 B, B', red arrowheads). At later stages, *tmem33* morphants failed to develop a thoracic duct (TD) (Figure 1.4 E, F, white asterisks). The TD is formed from lymphangioblasts which migrate ventrally from the parachordal lymphangioblasts (Figure 1.4 E, white arrowheads). Since, *tmem33* morphants did not develop parachordal lymphangioblasts, TD formation was restricted (Figure 1.4 F, white asterisks).

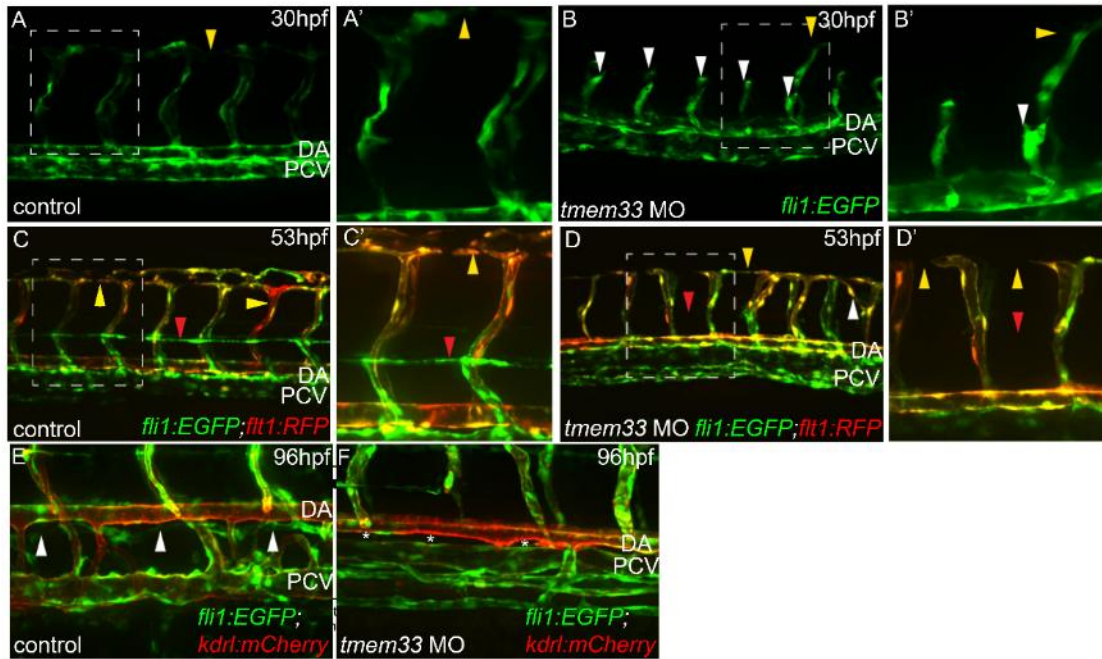


Figure 1.4 *tmem33* morpholino knockdown impairs angiogenesis and lymphatic development. (A-B') *tmem33* morphants display delayed migration of *Tg(fli1a:eGFP)y1* positive SeAs, which stall at the horizontal myoseptum (B, B', white arrowheads), compared to control *Tg(fli1a:eGFP)y1* embryos (A, A'), which begin to anastomose by 30 hpf (yellow arrowheads). (C-D') By 53 hpf, *Tg(fli1a:eGFP)y1;Tg(-0.8flt1:enhRFP)hu5333* *tmem33* morphant SeAs complete dorsal migration, but display incomplete DLA formation (D, D', yellow arrowheads), misdirected migration (white arrowheads) and lack lymphatic vasculature (red arrowheads). At 53 hpf *Tg(fli1a:eGFP)y1;Tg(-0.8flt1:enhRFP)hu5333* control embryos display secondary angiogenesis (C, C', yellow arrowheads) and parachordal lymphangioblasts (red arrowhead). (E-F) Thoracic duct formation is impaired in *tmem33* morphants (white asterisks), compared to control embryos (white arrowheads).

Data courtesy of Dr Robert Wilkinson

tmem33 is expressed in the developing kidney (Figure 1.2). To determine whether *tmem33* functions during kidney development, *tmem33* was knocked down in *Tg(-26wt1b:eGFP)li1* embryos using morpholinos by Dr Freek van Eeden (Figure 1.5 A, B). *tmem33* morphants displayed expanded glomeruli from 52 hpf onwards (Figure 1.5 C), similar to *pkd2* morphants (Sun, 2004), suggesting

tmem33 may function during kidney development in addition to vascular development. Furthermore, data from my collaborator suggests TMEM33 interacts with PKD family members (Eric Honore, data not shown), it is possible that TMEM33 and PKD may interact during kidney development. This will be addressed in Chapter 5.

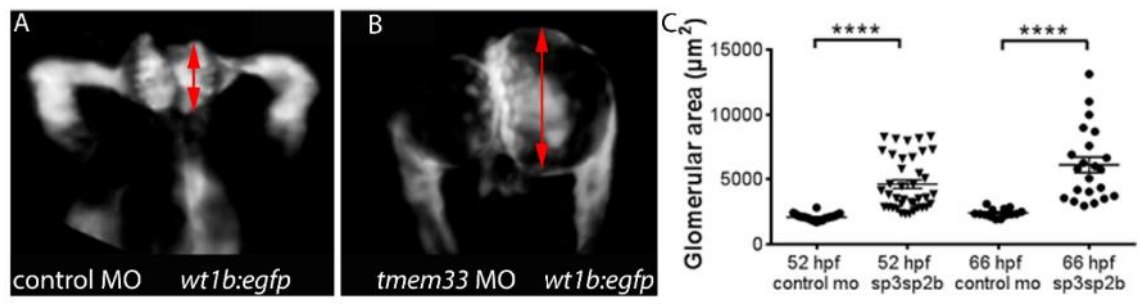


Figure 1.5 *tmem33* morpholino knockdown induces glomerular expansion in zebrafish embryos. (A-B) *tmem33* morphants display increased glomerular area (indicated by red arrow), when compared to control morphants (red arrow). (C) Glomerular area is significantly increased at both 52 hpf and 66 hpf in *tmem33* morphants (One-way ANOVA **** $p < 0.0001$).

Data courtesy of Dr Freek van Eeden.

The work undertaken before I joined the lab suggested that *tmem33* functions during vascular and kidney development, and is expressed within kidney cells. However it was not clear whether *tmem33* is expressed in endothelial cells. Furthermore the precise mode of *tmem33* function is not known from this analysis. Therefore more detailed analysis of the effect of loss-of *tmem33* function on endothelial cell biology is required. Previous work in other labs has suggested *tmem33* functions during ER homeostasis (Chadrin et al., 2010; Floch et al., 2015; Sakabe et al., 2015; Urade et al., 2014). Since the ER functions as the primary calcium store, and *tmem33* has been shown to interact with *pkd1* and

pkd2 in vitro, Dr. Wilkinson generated zebrafish endothelial GCaMP (Nakai et al., 2001) transgenic lines to quantify Ca²⁺ oscillations during angiogenesis in the presence and absence of *tmem33* function. No current study has implicated *tmem33* function in calcium signalling directly and no current study has analysed *tmem33* function in multicellular organisms.

1.4 Endothelial cell origins and vasculogenesis.

Both blood and endothelium are derived from the mesoderm and it has been shown that fibroblast growth factor 2 (FGF2) and bone morphogenic protein 4 (BMP4) are required for, initially, the specification of mesoderm, but later for differentiation to blood and endothelium (Nostro et al., 2008; Schier and Shen, 2000). Furthermore, mutant embryos in which downstream BMP effector signalling is impaired display reduced vascular formation, such as Endoglin and Smad4/5 mutant mice (Mao et al., 2012; McAllister et al., 1994; Yang et al., 1999).

During embryogenesis, the axial vessels form via *vasculogenesis*, in which free endothelial precursors (angioblasts) migrate to the midline and coalesce in the aorta-gonad-mesonephros (AGM) region (Brown et al., 2000). Prior to migration, both endothelial and haematopoietic cells arise in close proximity within the ventral mesoderm, along with pronephric (kidney) precursors (Gering, 2003; Perens et al., 2016). Furthermore, It has been suggested that both endothelial and haematopoietic cell types arise from a common precursor; the haemangioblast (Murray, 1932). Mouse embryonic stem cells cultured with VEGF induce two populations of cells expressing haematopoietic or endothelial markers (Choi et al., 1998). During early gastrulation, a subset of the posterior lateral

mesoderm (PLM) become haemangioblasts (Vogeli et al., 2006), with *cloche* being identified as the master regulator of this process (Liao et al., 1997; Stainier et al., 1995). *cloche* was later identified as *npas4l* (Reischauer et al., 2016) and regulates both haematopoietic and angiogenic lineages and is expressed earlier than endothelial and haematopoietic markers such as *etsrp/etv2* or *scl/Tal1*, respectively (Reischauer et al., 2016; Stainier et al., 1995). Interestingly, *etsrp2* has been shown to regulate angioblast migration to the midline (Sumanas and Lin, 2006).

Initially, in both zebrafish and *Xenopus* embryos, haemangioblasts in the dorsal lateral plate mesoderm (DLP) express both endothelial and haematopoietic markers before beginning migration to the embryonic midline (Bussmann et al., 2007; Ciau-Uitz et al., 2010, 2013; Gering, 2003). However, a subset of specified angioblasts, expressing both *scl*, and *fli1* (Gering et al., 1998; Thompson et al., 1998), can be observed in the PLM of zebrafish at 12 hpf. By 10 somites (~14hpf), the primitive blood and endothelial lineages have completely diverged (Gering and Patient, 2005). Their migration requires *sonic hedgehog (shh)* (Gering & Patient, 2005). In zebrafish, angioblasts expressing endothelial genes such as *fli1a*, *kdr* and *etsrp*, migrate from the lateral mesoderm to the midline, ventral to the notochord, where they coalesce and form the dorsal aorta (Figure 1.6) (Brown et al., 2000; Jin et al., 2005; Sumanas and Lin, 2006). Interestingly, angioblast migration is not ablated following *vegfa* or *plcg1* knockdown, but reduced numbers of migratory angioblasts are observed. This suggests VEGF signalling may be dispensable for angioblast migration in zebrafish (Brown et al., 2000; Jin et al., 2005; Lawson and Weinstein, 2002; Lawson et al., 2002; Sumanas and Lin, 2006). Conversely, in *Xenopus* embryos, VEGF does influence angioblast

migration (Cleaver and Krieg, 1998). Despite being dispensable for zebrafish angioblast migration, VEGF upstream Hedgehog (Hh) signalling are required for arterial fate specification.

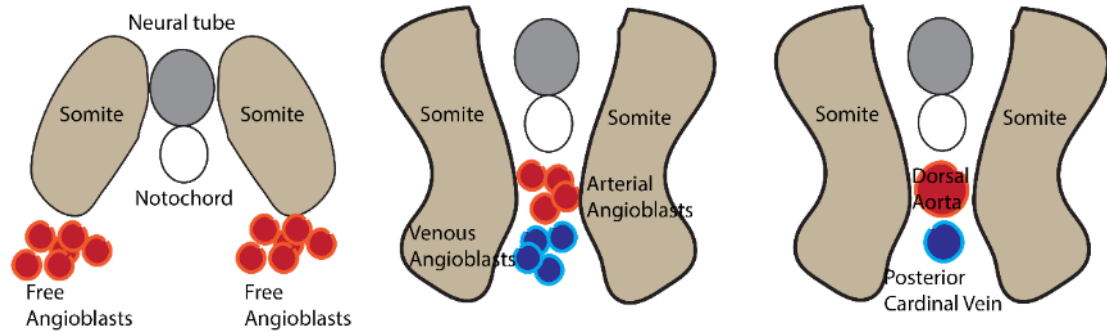


Figure 1.6 – Midline migration and vasculogenesis in zebrafish embryos. During vasculogenesis, angioblasts migrate medially from the lateral mesoderm to form two clusters of cells, which coalesce and form the dorsal aorta (red) and posterior cardinal vein (blue). This figure shows a cross-sectional view of the developing trunk of a zebrafish embryo.

Once migration to the midline is complete, in zebrafish, the free angioblasts coalesce and lumenise to form the DA and PCV (Figure 1.6) (Jin et al., 2005). The mechanism by which angioblasts adopt an arterial or venous fate has been contested. It has been suggested that location within the PLM may play a role, with more medial progenitors giving rise to the DA, which forms first, and more lateral progenitors giving rise to the PCV shortly afterwards (Kohli et al., 2013). Interestingly, it has recently been shown that Notch signalling is activated in the PLM, and that cells in which Notch signalling is active give rise to the DA (Quillien et al., 2014). However, other research has also suggested a third mechanism in which ventral sprouting from the DA between 21-24 hpf gives rise to at least some cells of the PCV (Herbert et al., 2009).

Distinct differences in how Shh and VEGF signalling interact and regulate vasculogenesis exist between mouse and zebrafish models. In mice, Shh signalling induces vasculogenesis in a VEGF-dependent and -independent manner and does not regulate VEGF expression. Instead, Shh signalling directly induces Notch signalling via regulation of Dll4 expression (Coultas et al., 2010). Conversely, in zebrafish, Shh signalling is required for induction of VEGF signalling in somites. Loss of Shh signalling abrogates arterial differentiation, which can be rescued by addition of VEGF. Furthermore, VEGF is required downstream for arterial-venous differentiation, via Notch signalling induction (Lawson et al., 2002). Interestingly, however, *shh* signalling can bypass VEGF-mediated arterial differentiation in zebrafish via calcitonin receptor-like A (*clra*). This indicates a complex relationship between VEGF and Shh signalling during DA formation (Wilkinson et al., 2012).

Completion of DA and PCV formation concludes vasculogenesis, and subsequent blood vessels develop via *angiogenesis*.

1.5 Angiogenesis.

Angiogenesis is the process by which new vessels form from pre-existing vasculature, giving rise to the entire, essential vascular network. In zebrafish, angiogenesis begins around 22 hpf (Figure 1.7), with parallel pairs of segmental arteries (SeAs) sprouting from the dorsal aorta between somite boundaries (Isogai et al., 2001). Sprouting occurs asynchronously, with pairs of SeAs sprouting anterior to posterior. However, a degree of stochasticity is observed and occasionally posterior SeAs migrate prior to a more anterior pair (Isogai et

al., 2001). Once SeAs complete dorsal migration, endothelial cells migrate along the anterior-posterior axis of the zebrafish, and fuse to form two parallel dorsal longitudinal anastomotic vessels (DLAVs) (Isogai et al., 2001) (Figure 1.7).

Following primary sprouting, secondary sprouting begins from 32 hpf. During secondary angiogenic sprouting, venous endothelial cells migrate from the posterior cardinal vein (PCV) and from venous intersegmental vessels (vISVs) via fusion with existing SeAs, which are now termed arterial intersegmental vessels (aISVs). While in many cases, aISVs and vISVs alternate along the body of the zebrafish, this is not always the case (Bussmann et al., 2010). Although the majority of secondary sprouting occurs dorsally, utilising VEGF signalling, the caudal vein plexus, located at the posterior of the zebrafish, migrates ventrally, via alternative signalling. Ventral migration of venous angioblasts is instead regulated by BMP signalling, working against the VEGF gradient driving dorsal migration (Wiley et al., 2011).

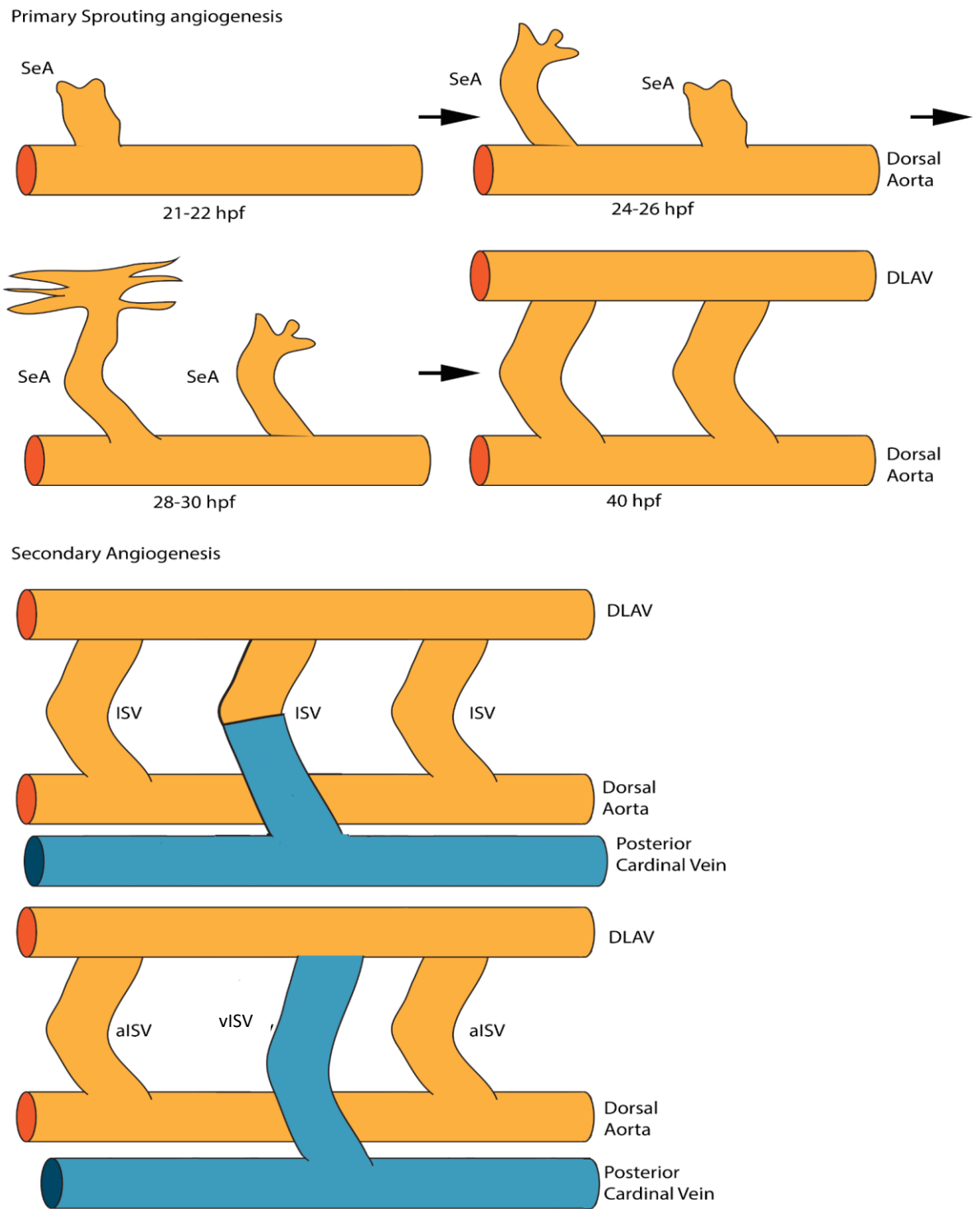


Figure 1.7 – Zebrafish trunk angiogenesis. During primary sprouting angiogenesis, endothelial cells migrate dorsally beginning with rostral tip cells, before migrating along the anteroposterior axis and fusing during anastomosis. During secondary sprouting, endothelial cells migrate from the posterior cardinal vein to fuse with arterial ISVs (aISVs) to form venous ISVs (vISVs).

1.5.1 Signalling pathways regulating angiogenesis.

Primary sprouting angiogenesis is regulated by two main signalling pathways; VEGF and Notch (Figure 1.8). However, complex signalling regulating how the endothelial tip cells respond to VEGF signalling are also activated downstream of VEGF signalling, adding to the complexity of endothelial cell biology. Current understanding of these processes will be presented in this section.

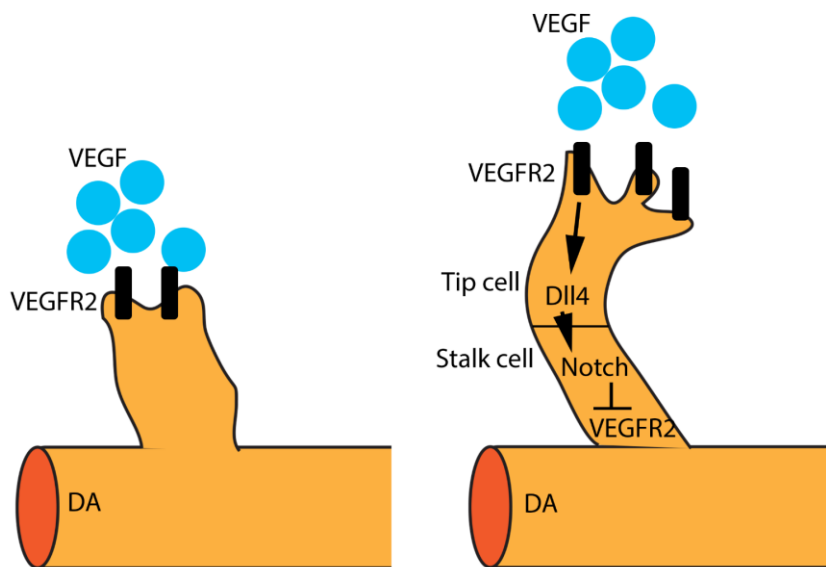


Figure 1.8 – Key signalling regulating angiogenesis. During angiogenesis, VEGF signalling via VEGF receptors induces a downstream signalling cascade culminating in the expression of *dll4* in tip cells, which induces Notch signalling in neighbouring cells. Notch signalling functions to inhibit the response to VEGF in stalk cells via transcriptional repression of VEGFR2.

Primary sprouting angiogenesis is initiated in response to VEGF signalling, which is induced by Sonic Hedgehog (Shh) signalling (Lawson et al., 2002). VEGFA is the primary driver of arterial angiogenesis and two paralogues exist in zebrafish, *vegfaa* and *vegfab* (Bahary et al., 2007; Covassin et al., 2009; Lawson et al., 2002; Nasevicius et al., 2000). *vegfab* is expressed at lower levels within

developing somatic tissues than *vegfaa* during zebrafish development and knockdown induces a milder phenotype compared to *vegfaa* knockdown (Bahary et al., 2007; Nasevicius et al., 2000). VEGFA bind to VEGF receptors on endothelial cells to induce sprouting and migration. Signalling of VEGFA via the receptor KDR induces primary angiogenic sprouting in most species (Terman et al., 1992; Zeng et al., 2001). However, in zebrafish, two KDR paralogues exist, *kdr* and *kdr1* (Bahary et al., 2007). *kdr1* is the dominant signalling receptor and is functionally conserved with *KDR*, but *kdr* and *kdr1* co-operate during primary angiogenesis (Bahary et al., 2007; Covassin et al., 2006). Since VEGF receptors function as dimers, different combinations of homo- and heterodimers exist which respond differently to each VEGF ligand, creating a degree of redundancy between VEGF receptors (Koch and Claesson-Welsh, 2011; Nilsson et al., 2010). This is evident in zebrafish due to the fact that VEGFC influences both primary angiogenesis and lymphangiogenesis (Covassin et al., 2006; Le Guen et al., 2014) and angiogenesis can occur in the absence of KDR via FLT4 in conditional mouse knockout models (Benedito et al., 2012). However, VEGFC/FLT4 signalling may be suppressed by DLL4 signalling in aISVs (Hogan et al., 2009a). Therefore, context- and timing-dependent mechanisms exist by which migratory angiogenesis is co-ordinated.

Phospholipase C gamma 1 (*plcy1*) signalling is induced downstream of VEGF receptor signalling and zebrafish *plcy1* mutants display a loss of arterial sprouting, akin to pan-VEGF receptor inhibition (Covassin et al., 2006; Fong et al., 1999; Lawson et al., 2003). Indeed phosphorylation of *plcy1* is induced by KDR and phosphorylated PLCG1 is important for downstream signalling, including MAP kinase signalling in cell culture (Takahashi and Shibuya, 1997;

Takahashi et al., 2001). Many studies demonstrate a requirement for both the Ras/Raf/MEK/ERK and PI3K/AKT signalling pathways in endothelial cells (Gerber et al., 1998; Graupera et al., 2008; Meadows et al., 2001; Serban et al., 2008). Zebrafish studies show that ERK signalling downstream of VEGF signalling is required for vascular development (Shin et al., 2016), while loss of ERK1 and 2 impairs normal vascular development in mice (Selcher, 2001; Srinivasan et al., 2009). Further evidence exists for a role for MAP kinase signalling in endothelial cells, with increased ERK activity associated with vascularisation in mice (Deng et al., 2013a). Interestingly, reduced MEK signalling impairs angiogenesis in tumours (Mavria et al., 2006) and reduces mouse placental angiogenesis, leading to embryonic death (Giroux et al., 1999). Tight control of the Ras/Raf/MEK/ERK pathway is required with context-specific regulation of Akt/PI3K signalling regulating this pathway (Hellesoy and Lorens, 2015). Furthermore, negative feedback of Ras/Raf/MEK/ERK via Angiopoietin-like 4 has been implicated (Yang et al., 2008). Taken together, these findings suggest a complex interaction between signalling pathways downstream of VEGF signalling (Figure 1.9).

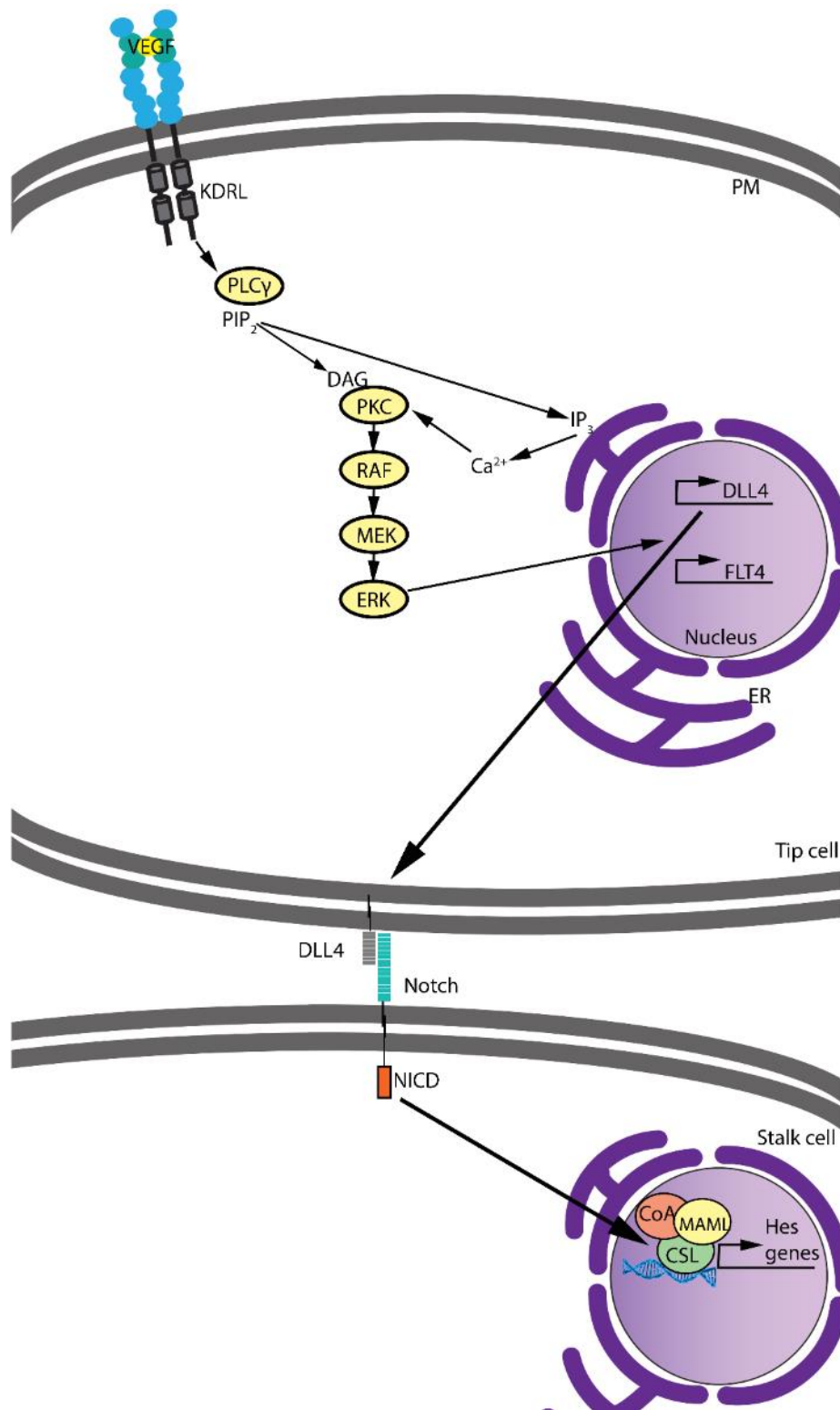


Figure 1.9 – Intracellular signalling during angiogenesis. Downstream of VEGF signalling, a signalling cascade including PLCG1, calcium signalling and ERK signalling induces the expression of *dll4* in tip cells. DLL4 expression on tip cells induces Notch signalling in stalk cells, leading to the upregulation of Notch-responsive genes.

Transduction of VEGF signalling culminates in downstream Notch signalling, via upregulation of *dll4* expression (Hellström et al., 2007) (Figure 1.9). Endothelial cells in which *dll4* is upregulated begin to migrate to form a new vessel; these are termed the “tip cell” of the angiogenic sprout. Neighbouring cells, which express *notch* more highly than *dll4* have traditionally been thought to follow the tip cell and form the remainder of the angiogenic sprout (termed “stalk” or “phalanx” cells) (Herbert and Stainier, 2011). However, recent data suggests tip and stalk cell fate may not be fixed and that relative distribution of VEGF receptors is important to establish tip-and stalk cell fate following asymmetric cell division of tip cells (Costa et al., 2016). Furthermore, while mouse studies have shown tip cells do not proliferate during angiogenesis (Gerhardt et al., 2003), this is not true in zebrafish, in which tip cells proliferate more frequently than stalk cells (Costa et al., 2016). Conditional mouse Raf1 mutants, in which ERK1 signalling is activated, display increased expression of Notch signalling components, including Dll4 (Deng et al., 2013b, 2013a). This suggests that Notch signalling via induction of *dll4* expression occurs downstream of ERK signalling, implying a direct pathway from VEGF signalling to Notch signalling via PLCG1 signalling and the Ras/Raf/MEK/ERK pathway. DLL4 haploinsufficiency impairs vascular development in mouse embryos (Duarte et al., 2004), with increased vascular branching (Suchting et al., 2007). Following upregulation of *dll4* signalling, Notch signalling is induced in neighbouring endothelial cells via lateral inhibition. Neighbouring Notch-expressing cells join the sprout as stalk cells (Siekman and Lawson, 2007). Notch signalling limits the response to VEGF by upregulation of the decoy VEGF receptor, *flt1* (VEGFR1) (Krueger et al., 2011), and suppression of Notch signalling results in increased angiogenic sprouting, *in vitro* (Sainson et al., 2005) and *in vivo* (Hellström et al., 2007; Leslie et al., 2007; Siekman and

Lawson, 2007; Suchting et al., 2007; [CSL STYLE ERROR: reference with no printed form.]). At later stages, blood flow inhibits endothelial Notch signalling by downregulation of *dll4* (Watson et al., 2013). Furthermore, maintenance of stalk cell fate is regulated independently of VEGF and Notch signalling, via H2.0 homeobox-like 1, suggesting an additional level of control may exist to regulate cell fate during angiogenesis (Herbert et al., 2012).

1.5.2 Lymphangiogenesis.

Lymphatic angiogenesis begins from 2 dpf in zebrafish. Sprouting ECs destined to become lymphatic vasculature are termed lymphatic endothelial cells (LECs). LECs migrate simultaneously with secondary angiogenic sprouts which become vISVs (Bussmann et al., 2010; Hogan et al., 2009b; Isogai et al., 2001). LECs migrate to the horizontal myoseptum, before migrating laterally forming the parachordal chain. After this, they migrate ventrally and seed the lymphatic vasculature, including the thoracic duct. Embryos deficient in VEGFC/FLT4 signalling display impaired lymphatic development in zebrafish (Hogan et al., 2009b; Villefranc et al., 2013; Yaniv et al., 2006).

It is likely that conserved signals regulate venous endothelial cell and LEC migration from venous progenitors. That lymphatic endothelial cells are derived from a subpopulation of Prox1+ venous cells was first proposed in mice (Sathish Srinivasan and Oliver, 2011). Indeed, *prox1* is expressed in LECs in zebrafish, both in the parachordal lymphangioblasts and the PCV before dorsal migration (Koltowska et al., 2015; Shin et al., 2017). In zebrafish, two paralogues of *prox1* exist, *prox1a* and *prox1b*. While *prox1a* labels LECs in zebrafish (Dunworth et al.,

2014), *prox1b* does not (Tao et al., 2011). However, mutations in neither *prox1a* nor *prox1b* impair vascular development, while double mutants display only minor defects (van Impel et al., 2014; Tao et al., 2011). This suggests a divergent role for Prox1 in zebrafish compared to mice, in which Prox1 is essential for lymphatic formation (Yang et al., 2012).

Little is currently known about signalling pathways involved in lymphangiogenesis downstream of VEGFC/FLT4. In common with aISVs, ERK signalling is essential for lymphatic formation in zebrafish (Shin et al., 2016, 2017). Furthermore, ERK signalling has been implicated in lymphatic fate specification *in vitro* (Deng et al., 2013b), suggesting signalling downstream of FLT4 may share commonalities between angiogenesis and lymphangiogenesis.

1.5.3 Regulation of the actin cytoskeleton and calcium signalling during angiogenesis.

Angiogenesis requires endothelial cells to undergo rapid and transient changes in cell biology and morphology during migration without losing structural integrity (Kapustina et al., 2013). The actin cytoskeleton maintains cellular structure while sensing the environment into which cells migrate (Pollard and Cooper, 2009). Rearrangement of the actin cytoskeleton into cellular projections such as filopodia and lamellipodia enables the cell to change morphology, migrate mechanically and sense the environment (Chhabra and Higgs, 2007). Furthermore, the actin cytoskeleton maintains focal adhesions and adherens junctions for cell-cell contact during migration (Bayless and Johnson, 2011).

Filopodia are present on many migrating tissue types, during development, including the well-characterised *Drosophila* tracheal tubes (Myat et al., 2005; Ribeiro et al., 2002). The importance of filopodia during retinal angiogenesis in mice has been demonstrated (Gerhardt et al., 2003; Sawamiphak et al., 2010). Visualisation of F-actin *in vivo* is possible due to the LifeACT motif, which binds F-actin (Riedl et al., 2008). LifeACT-fluorophore fusions have been used in mouse and zebrafish to observe filopodial behaviour during development and angiogenesis (Fraccaroli et al., 2012; Phng et al., 2013; Riedl et al., 2010). While evidence exists to suggest VEGF signalling stimulates production of filopodia during angiogenesis in mouse (Gerhardt et al., 2003) and cell culture (Morales-ruiiz et al., 2014), zebrafish studies suggest filopodia are dispensable during primary angiogenesis (Phng et al., 2013). Interestingly, inhibition of filopodia formation via Latrunculin B treatment did not ablate angiogenesis but caused angiogenic delays, suggesting filopodial loss reduces the rate of angiogenic migration. However, chemical inhibition may not entirely ablate F-actin structures required for migration (Phng et al., 2013). Furthermore, loss of *cdh5* in zebrafish resulted in impaired cytoskeleton formation during angiogenesis, suggesting *cdh5* may function as an anchor point for the cytoskeleton of migrating stalk cells (Sauteur et al., 2014).

It has long been established that a calcium-dependent element of actin cytoskeletal organisation exists, via calcium-dependent regulation of actin modifying proteins (Ikebuchi and Waismanj, 1990; Sakurai et al., 1991; Young et al., 1994). In cell culture, calcium influx regulates organisation of the actin cytoskeleton of immune cells via store-operated calcium entry (SOCE) (Hartzell et al., 2016), and calcium efflux from the ER regulates actin cytoskeleton-

mediated ER translocation during calcium signalling (van Vliet et al., 2017). Furthermore, calcium signalling is essential during actin cytoskeletal rearrangements in neural cell migration (Martini and Valdeolmillos, 2010). In cancer cells, the calcium channel TRPM2 regulates the actin cytoskeleton in response to H₂O₂ by increasing intracellular Ca²⁺ and Mg²⁺ (Li et al., 2016). Furthermore, a “calcium-mediated actin reset” has been suggested, wherein a burst of intracellular calcium is induced immediately prior to cytoskeletal rearrangement (Wales et al., 2016), while “calcium flickers” have been observed at the leading edge of migrating fibroblasts (Wei et al., 2009).

Endothelial cells are generally thought to be non-excitabile and as such utilise store-operated calcium entry (SOCE) as their primary means to maintain Ca²⁺ levels in the ER after influx (Oike et al., 1994; Vaca and Kunze, 1994). Calcium signalling is VEGF-dependent in cultured ECs (Fearnley et al., 2015; Hamdollah Zadeh, 2008) and induction of Ca²⁺ oscillations downstream of VEGF *in vivo* has been demonstrated during flow-independent angiogenesis in zebrafish during the timeframe of this thesis (Yokota et al., 2015). Endothelial cells replenish ER calcium stores after signalling primarily via the calcium release-activated calcium (CRAC) channel, comprised of STIM1 (Jones et al., 2005; Roos et al., 2005) and ORAI1 (Cheng et al., 2011; Feske et al., 2006; Vig, 2006). SOCE relies on modulation of the actin cytoskeleton, which requires calcium-dependent proteins for motility (van Vliet et al., 2017). Furthermore, protein kinase signalling is calcium-dependent, and functions upstream of the MEK-ERK signalling pathway in ECs (Hollenbach et al., 2013; Wong and Jin, 2005). Calcium signalling will be discussed in greater detail in section 1.7.

1.6 Kidney development in zebrafish

The kidney is the site at which the vascular system comes into contact with the urinary tract. In the kidney, blood is filtered, resulting in the removal of waste products and maintenance of essential ions (Drummond and Davidson, 2016). The kidney provides a second function in zebrafish as the site of adult haematopoiesis, analogous to bone marrow in mammals (Drummond and Davidson, 2016).

In the zebrafish, the kidney develops from cells within the ventrolateral mesoderm, overlapping with regions giving rise to blood and endothelial cells (Kimmel et al., 1990). BMP signalling is important for the determination of the kidney- and blood-forming ventrolateral mesoderm. Embryos lacking *swirl* (BMP2) display a loss of ventral tissues including blood and pronephros (Kishimoto et al., 1997). During embryogenesis, the ventrolateral mesoderm gives rise to the intermediate mesoderm (IM) and lateral mesoderm (LM). The nephrogenic component of this region is determined by expression of factors such as *hnf1ba*, *pax2a*, *pax8*, and *lhx1a* (Bedell et al., 2012a; Naylor et al., 2013; Pfeffer et al., 1998; Swanhart et al., 2010) and is found adjacent to the blood-forming region (Kimmel et al., 1990). Furthermore, loss of *wnt8a* reduces the pool of renal progenitors during zebrafish kidney development (Naylor et al., 2017).

Kidney progenitor cells form within the IM, as a pair of lateral stripes of cells from around the 2-somite stage. The IM is flanked by the lateral mesoderm, which gives rise to blood and endothelial cells (Perens et al., 2016). Interestingly, *hand2* has been shown to promote both kidney and endothelial progenitor development

in zebrafish (Perens et al., 2016). However, other evidence exists of antagonistic genetic interaction between the IM and LM. For example, Odd skipped related 1 (*Osr1*) is widely expressed in the developing mesoderm before becoming restricted to renal progenitors in mice (Mugford et al., 2008) while zebrafish *osr1* morphants display reduced pronephric but expanded vascular marker expression and increased venous development (Mudumana et al., 2008). Furthermore, *scf* and *lmo2* overexpression reduces *pax2* but promotes blood and endothelial marker expression in zebrafish (Gering, 2003; Gering et al., 1998). Such findings indicate an antagonistic interaction between these two developing domains. The IM gives rise to the pronephric tubules, which form bilaterally, while blood and endothelial precursors migrate medially to form the vascular system (Brown et al., 2000; Jin, 2005; Sumanas and Lin, 2006). Collective cell migration drives the development of different domains within the developing kidney, including glomeruli (Naylor et al., 2016; Vasilyev et al., 2009).

From 40-48 hpf, endothelial cells begin to invade the glomerulus (Drummond and Davidson, 2016). During this time, podocytes within the glomerulus express VEGFA to promote angiogenesis (Eremina et al., 2003; Veron et al., 2010a, 2010b). Loss of function of several genes known to function during kidney development induces an expanded glomerulus, including *pkd1a*, *pkd1b*, *pkd2* and *wt1b*, while *wt1a* knockdown causes a failure to form glomeruli (Mangos et al., 2010; Perner et al., 2007; Sun, 2004). Such expanded glomerular phenotypes usually develop after 40 hpf and loss of both *pkd1a* and *pkd2* has been associated with vascular developmental defects (Coxam et al., 2014; Heckel et al., 2015). Interestingly, an interaction between *pkd2* and *trpv4* has been suggested both in epithelial cells of the renal collecting duct and in endocardial

cells, suggesting conserved functions for calcium channels in both renal and endothelial/endocardial cells may exist (Heckel et al., 2015; Zhang et al., 2013).

1.7 The Regulation of intracellular Calcium levels and Calcium Signalling

The calcium ion (Ca^{2+}) is a second messenger in many evolutionarily conserved signalling pathways. Calcium levels are tightly regulated and maintained within the cell, where it is largely stored in the endoplasmic reticulum (ER) at concentrations of around 100 μM (Putney, 2010). Ca^{2+} perpetually cycles out of the ER into the cytoplasm, where concentrations rarely exceed 10 nM under normal conditions and back into the ER again, through a series of channels and pumps on the membrane of the ER. Ca^{2+} is also stored in mitochondria, and Ca^{2+} release from the ER results in mitochondrial Ca^{2+} entry (Giacomello et al., 2010). Resting mitochondrial Ca^{2+} concentration is 100 nM but may reach 100 μM during calcium signalling (Pozzan et al., 2000).

Small changes in intracellular Ca^{2+} concentration can trigger downstream signalling events. To initiate calcium signalling, extracellular signalling molecules bind targets on the plasma membrane, such as receptor tyrosine kinases (Katz et al., 2012) and G-coupled protein receptors (GPCRs) (Lopez-illasaca, 1998), which then activate phospholipase C proteins (PLCs) (Ji et al., 1997; Katz et al., 2012; Lopez-illasaca, 1998) (Figure 1.10). PLCs catalyse formation of inositol 1, 4, 5- triphosphate (IP_3) from phosphatidylinositol 4,5-bisphosphate (PIP_2) (Noh et al., 1995). During calcium signalling, IP_3 binds to IP_3 receptors (IP_3Rs) located on the ER membrane to induce calcium release from the ER (Bootman, 2012) (Figure 1.10). Furthermore, IP_3 receptor activity can be modulated by

phosphorylation via non-receptor tyrosine kinases (Jayaraman et al., 1996). Another ER membrane calcium receptor is the ryanodine receptor (RyR), commonly found in excitable cell types such as skeletal muscle, which functions in voltage-gated calcium entry via coupling with the Caveolin-3 (Cav-3) voltage gated calcium channel (Whiteley et al., 2012).

As Ca^{2+} is exported from the ER during calcium signalling, calcium stores in the ER must be replenished. ATPase pumps, along with sarco-endoplasmic reticular Ca^{2+} ATPases (SERCAs) (MacLennan et al., 1985) actively transport calcium ions back into the ER. ATPases on the plasma membrane are known as plasma membrane Ca^{2+} pumps (PMCAs). PMCAs actively pump excess Ca^{2+} out of the cell into the extracellular matrix (Verma et al., 1988).

It is becoming increasingly clear that mitochondria play an important role during calcium signalling (Pozzan et al., 2000). It has long been known that mitochondria interact with the ER and take up Ca^{2+} ions through “ Ca^{2+} hot spots” (Giacomello et al., 2010; Rizzuto et al., 1998), while more recent studies implicate mitochondria in regulation of SOCE (Glitsch et al., 2002; Naghdi et al., 2010). Recently, the mitochondrial calcium uniporter (MCU) has been studied, with mutant zebrafish displaying impaired cell migration during early gastrulation (Prudent et al., 2013). Furthermore, MCU knockdown in cell culture reduces intracellular $[\text{Ca}^{2+}]$, cell polarity, and cell migration, while impairing focal adhesions and F-actin, producing more cortical F-actin with increase focal adhesion number (Prudent et al., 2016).

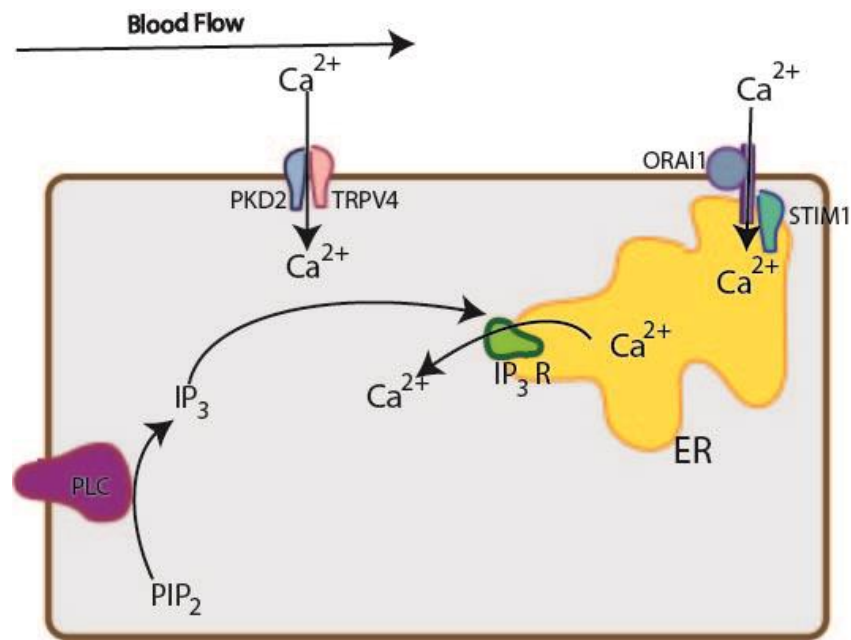


Figure 1.10 An overview of calcium signalling mechanisms. Ca²⁺ ions are stored in the endoplasmic reticulum (ER) from which they are released into the cytosol via the IP₃ receptor. To replenish cellular calcium in non-excitable cells, flow responsive calcium channel complexes (eg TRP channels) and the calcium release-activated calcium (CRAC) channel comprised of ORAI and STIM proteins are utilised.

Ca²⁺ trafficking between ER storage, mitochondrial storage and the cytosol induces intracellular calcium oscillations (Pozzan et al., 2000). It has been hypothesised that intracellular calcium oscillations are induced by intracellular Ca²⁺ load or concentration (Sneyd et al., 2004). Testing of this hypothesis showed that inhibition of calcium influx into cells after, but not prior to, the onset of calcium signalling halted Ca²⁺ oscillations (Sneyd et al., 2004). These were rescued by induction of ER calcium efflux, suggesting the interplay between calcium load and ER membrane flux dictates whether calcium oscillations occur (Sneyd et al., 2004). Furthermore, IP₃ recognition by IP₃R may induce calcium influx from external sources as well as regulating ER calcium efflux (van Rossum et al., 2004).

The process of calcium signalling differs considerably between cell types. Excitable cells, such as neural and muscle tissue, respond to and generate electrical signals. When excitable cells undergo calcium signalling, a change in membrane potential occurs, initiating activation of a signalling cascade, often through voltage-operated calcium channels (VOCs) (Turner et al., 2011).

The ER membrane contains proteins that sense changes in ER Ca^{2+} concentration. One such is stromal interaction molecule 1 (STIM1), an ER membrane-spanning protein, which has a sensory C-terminal tail embedded in the ER lumen (Figure 1.11) (Jones et al., 2005). While ER calcium levels are normal, the C-terminal tail interacts with calcium ions. Upon calcium release from the ER, Ca^{2+} concentration decreases, freeing the luminal N-terminal tail of STIM1 (Jones et al., 2005). STIM1 then undergoes a conformational change (Ma et al., 2015). STIM1 forms pairs of homodimers that interact with ORAI1 in the plasma membrane (Feske et al., 2006; Vig, 2006). The complex formed by ORAI1 and STIM1 is known as the calcium release-activated calcium (CRAC) channel (Figure 1.11), which is a calcium-selective ion channel (Jones et al., 2005; Li et al., 2011; Liou et al., 2007; Roos et al., 2005). The CRAC channel links the ER to the cell surface membrane to facilitate Ca^{2+} influx (Soboloff et al., 2012). Interaction between ORAI1 and STIM1 has been confirmed, with the cytoplasmic c-terminal tails of both ORAI1 and STIM1 essential for this interaction (Li et al., 2007; Zhou et al., 2010).

For calcium influx to occur via the CRAC channel, the ER must translocate to the PM, utilising both intracellular free Ca^{2+} ions and regulation of the actin cytoskeleton (van Vliet et al., 2017), resulting in formation of an ER-PM microdomain (Cao et al., 2015). Ca^{2+} ions travel through the CRAC channel from the extracellular space into the ER, restoring the ER Ca^{2+} concentration. Calcium-dependent negative feedback regulation of the CRAC channel complex has been suggested, both via a rise in intracellular Ca^{2+} concentration and a calmodulin-dependent mechanism (Li et al., 2017; Zweifach and Lewis, 1995), suggesting normalisation of Ca^{2+} levels is required for resolution of SOCE via the CRAC channel.

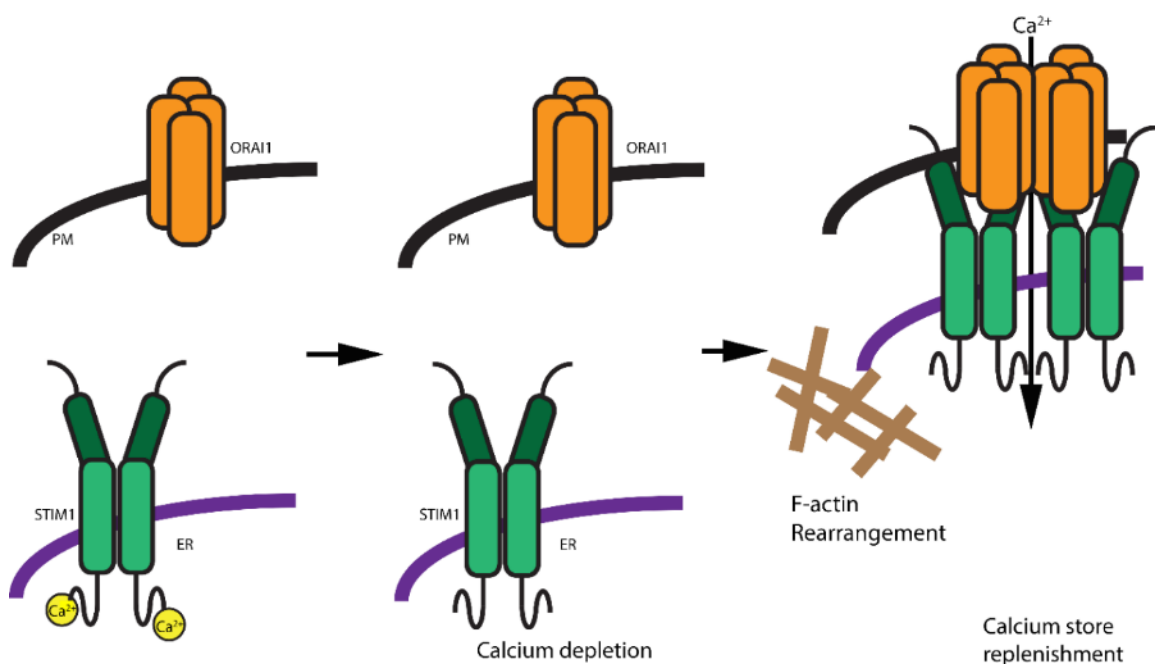


Figure 1.11 – Store operated calcium entry via STIM and ORAI proteins. STIM proteins in the ER membrane sense when calcium stores become depleted during calcium signalling, dimerise and form a complex with ORAI proteins on the cell membrane to form the calcium release-activated calcium (CRAC) channel.

1.8 TRP channels

Calcium signalling occurs via selective channels found both on the ER and cell membrane. One family of channels is the transient receptor potential (TRP) channels. The first TRP channel was identified in *Drosophila*, termed *trp*. *trp* mutant *Drosophila* showed only a transient reaction to light, behaving as if blind (Cosens and Manning, 1969). *trp* was later characterised as a membrane protein (Montell and Rubin, 1989). *Trp* mutant *Drosophila* also showed a defect in calcium influx. The TRP superfamily consists of seven subfamilies. TRP channels are expressed widely, but some are enriched in specific tissues (Graham et al., 2013; Von Niederh??usern et al., 2013; Zhang et al., 2013).

The protein structures of the *trp* superfamily show topology which resembles voltage-gated ion channels, such as those involved with K⁺, Na⁺ and Ca²⁺ influx and efflux. Such channels are porous, with several membrane-spanning domains coalescing to form the pore (Moiseenkova-Bell and Wensel, 2011)(Moiseenkova-Bell and Wensel, 2011)(Moiseenkova-Bell and Wensel, 2011) *trp* channels consist of around six membrane spanning domains, although this varies depending on subfamily. The membrane spanning domains form a pore (Moiseenkova-Bell and Wensel, 2009). TRP proteins form homotetramers, with each monomer contributing two membrane-spanning domains to the channel pore. Recent findings, however, suggest TRP channels can function as pairs of

homodimers (Köttgen et al., 2008; Zhang et al., 2013) or even with three different TRPs contributing to a single channel. Indeed *trpc1*, *trpv4* and *trpp2* can form a heteromeric channel, however the combination in which they act remains unclear (Du et al., 2014).

In vivo function of TRP channels remains largely unclear, with most studies taking place in cell culture. TRPs play a role in endothelial permeability, whereby VEGF signalling increases vascular permeability through activation of *trpc1*-dependent plasmalemmal Ca^{2+} entry, which is inhibited by the action of *angiopoietin-1* (*ang-1*) (Jho et al., 2005). TRP channels are also implicated in flow sensing through formation of heterotetrameric channels (Du et al., 2014). The role of *trpc* channels in angiogenesis have been well-documented, with roles in VEGF-mediated vascular permeability described, in particular for TRPC6 (Ge et al., 2009; Pocock et al., 2004). *Trpc6* has been implicated as a regulator of VEGF-mediated calcium signalling in endothelial cell lines (Brock et al., 1991; Zadeh et al., 2009), while it has been suggested that *trpc1* is essential for angiogenesis in zebrafish (Yu et al., 2010).

Many studies have analysed the functions of the *trp* channels TRPP2/PKD2, TRPV4 and TRPV1 and have attempted to understand how these channels interact (Graham et al., 2013; Köttgen et al., 2008; Ma et al., 2013; Zhang et al., 2013). Several roles for both *trpv1* and *trpv4* have been suggested. Roles for *trpv1* have been suggested in motility, utilising its calcium channel function in actin cytoskeletal projections in both keratinocytes (Graham et al., 2013) and in heat-induced locomotion (Gau et al., 2013). *Trpv4* has been implicated in a

sensory role, sensing flow and osmolarity (Wu et al., 2007). *trpp2*, also known as *pkd2*, is one of the two genes mutated in autosomal dominant polycystic kidney disease; the other being *pkd1*. *trpp2* has also been proposed to act as a heteromeric flow- and pressure-sensing channel with other *trp* proteins (Du et al., 2014; Sharif-Naeini et al., 2009; Zhang et al., 2013).

1.9 Developments in genome editing.

The ability to manipulate a gene's expression or function is essential in understanding its function. New advances in loss-of-function techniques and genome editing have contributed to my ability to perform genetic functional analysis. Since my work applies a number of these approaches, I will here summarise the different methods available.

1.9.1 Forward genetics and mutagenesis screens.

Forward genetic approaches rely on blind induction of phenotypes, without prior knowledge of which gene is mutated. Classically, this is applied in human inherited diseases, in which a family is identified with a particular phenotype but the causative mutation is not known. To understand developmental pathways, mutagenesis screens were first performed in invertebrates such as *C. elegans* and *D. melanogaster* (Brenner, 1974; Nusslein-Volhard and Wieschaus, 1980). Later, this approach was applied to vertebrates, initially the zebrafish and more recently mouse (Driever et al., 1996; Horner and Caspary, 2011). The zebrafish has inherent advantages over mammalian models, including the large numbers of progeny, and external fertilisation and development, making it highly suitable for forward genetics screens (Chakrabarti et al., 1983; Grunwald et al., 1988;

Streisinger et al., 1986). Forward genetic screens using zebrafish were conducted at the Max Planck Institute, Tübingen, and Harvard Medical School, Boston (MA), in the 1990s (Driever et al., 1996; Haffter et al., 1996; Mullins et al., 1994). Mutants generated by these screens have been used to study development of a range of tissues, including the brain and cardiovascular systems (DY et al., 1996; J et al., 1997; Neuhauss et al., 1996; Schier et al., 1996; Solnica-Krezel et al., 1996; Whitfield et al., 1995).

When a forward genetics approach produces a phenotype, the mutated gene is not known. Typically, positional cloning is utilised to identify the genetic locus. To position the mutation, maps of microsatellite markers, or simple sequence length polymorphisms (SSLPs), were developed, and later a radiation map of SSLPs was developed, leading to accurate identification of SSLP markers, mapped to the zebrafish genome (Geisler et al., 1999; Knapik et al., 1996, 1998; Shimoda et al., 1999). By PCR amplification and sequence comparison, the precise locations of mutations could then be determined. However, the limitations of positional cloning meant that the master regulator of haematopoiesis and angiogenesis, *cloche*, remained unidentified for over 20 years (Reischauer et al., 2016; Stainier et al., 1995). Despite this limitation, forward genetics screens represent an unbiased method to analyse gene function, which have led to better understanding of genes required for a number of biological processes. However, with the advent of comprehensive genome sequencing (Sanger and Coulson, 1975) it is now more common to first identify a gene and then attempt to target it specifically, via reverse genetic strategies.

1.9.2 Reverse genetic approaches – morpholino knockdown.

Contrary to forward genetics, reverse genetics aims to discern gene function through a targeted inactivation of a known gene. Armed with the sequence of the target gene, reagents are designed to reduce or abolish gene function. Reverse genetic approaches include gene knockdown, for example by morpholino or RNAi, and targeted mutagenesis via zinc finger or TALE nucleases or, more recently, the CRISPR/Cas9 endonuclease system.

The zebrafish has been widely used for reverse genetics studies, in particular, transient knockdown via antisense morpholino oligonucleotides. Morpholinos (MOs) target mRNA and induce improper translation via blocking translation initiation or pre-mRNA splicing (Bill et al., 2009). Morpholinos were first tested *in vivo* in *Xenopus*, before the first study in zebrafish, in which ubiquitous EGFP was knocked down, along with reproduction of known mutant phenotypes, including *no tail* and *one-eyed pinhead* (Heasman et al., 2000; Nasevicius and Ekker, 2000).

Recently, however, morpholinos have come under scrutiny, due to concerns regarding off-target effects (Schulte-Merker and Stainier, 2014), and difficulty in interpreting results (Stainier et al., 2017). Many morphant phenotypes require co-injection with *p53* morpholinos to offset non-specific induction of this pathway (Robu et al., 2007) and many morphant phenotypes cannot be recapitulated in

loss-of-function mutants (Kok et al 2015). Subsequently, however, a recent study has shown mutants without such phenotypes can be protected from morpholino-induced phenotypes, suggesting compensatory pathways induced by the mutation, that are not activated in morphants (Rossi et al 2015). However, the mechanism by which this occurs is poorly understood (El-Brolosy and Stainier, 2017) and will be further discussed in section 1.8.

1.9.3 Reverse genetic approaches – targeted mutagenesis via Zinc Finger nucleases and TALENs.

It is now possible to induce stable mutations in target genes via site-directed mutagenesis. Two commonly utilised methods are zinc finger nucleases (ZFNs) (Kim et al., 1996) and transcription activator-like effector nucleases (TALENs) (Cermak et al., 2011a). ZFNs utilise sequential arrays of zinc finger DNA binding domains specific to a particular nucleotide triplet, to which a *FokI* restriction enzyme is bound. ZFNs function in pairs, flanking a *FokI* restriction site, with one of each pair binding opposing strands of DNA to induce a double strand break (reviewed in Urnov et al., 2010). Likewise, TALENs function in a pair, designed to target specific nucleotide sequences. TALENs were derived from naturally occurring TALE repeats encoded by *Xanthomonas* bacteria species, which function to regulate transcription in plant cells by binding specific nucleotides. TALENs are comprised of a series of TALE repeats, which recognise different nucleotides fused to a *FokI* restriction enzyme to induce double strand DNA breaks (reviewed in Joung and Sander, 2013).

Zebrafish mutant lines have been generated successfully using both approaches. For example, *kdr*, *brachyury* and *golden* (Nacre) mutations were generated using ZFNs (Doyon et al., 2008; Meng et al., 2008) while the *cdh5* mutant line was generated via TALEN-mediated mutagenesis (Bedell et al., 2012b).

1.9.4 Reverse genetic approaches – the CRISPR/Cas9 endonuclease system and recent adaptations.

More recently, the CRISPR/Cas9 (clustered regularly interspaced short palindromic repeats/CRISPR-associated protein) system has become the technique of choice owing to its simplicity, rapidity and efficacy (Chira et al., 2017). CRISPR/Cas9 utilises guide RNAs (gRNAs), which target specific regions of the genome, in combination with the Cas9 endonuclease. The gRNA-Cas9 complex functions to induce a double strand break at the specified locus, leading to DNA repair by error-prone non-homologous end joining (NHEJ) (Chira et al., 2017; Kim et al., 2017).

CRISPR/Cas9 was first identified as an adaptive immune mechanism in archaea and bacteria, as a protection against pathogenic genetic material (Kim et al., 2017), which is cleaved by Cas proteins, most commonly Cas9, a type-II CRISPR-associated protein from *Streptococcus pyogenes* (Mali et al., 2013). Endogenous Cas9 utilises a duplex of two RNAs: crRNAs and tracrRNAs. tracrRNAs bind to both the sequence-specific crRNA and the Cas protein to form a functional complex, which cleaves genetic material in a sequence-specific manner (Wang et al., 2016).

In order to adapt this system for laboratory use, the Cas9 enzyme was isolated and the binding sequence for the crRNAs and tracrRNAs were identified. Later, strategies simplified the system by fusing the crRNA and tracrRNA into a single guide RNA (sgRNA), making in-house transcription of sgRNAs possible for large-scale screens (Clontech, 2016; Gilbert et al., 2014). For simplicity, all variants of guide RNAs (crRNAs, tracrRNAs and sgRNAs) will be hereafter referred to as “gRNAs”, unless direct comparisons are being made between the function of the variants.

To induce double strand breaks, gRNA-Cas9 complexes must bind to both the target DNA and gRNAs which guide it to a specific target region. gRNAs contain two key regions: the specific DNA binding region, and the Cas9 binding region (Josephs et al., 2015; Shibata et al., 2017). The Cas9 binding region is comprised of stem-loops which anchor the gRNA into the Cas9 protein. Cas9 is predicted to have a bilobed structure, with a nuclease lobe and a recognition lobe. The lobes contain nuclease and gRNA target recognition domains (Josephs et al., 2015; Shibata et al., 2017). The Cas9 protein recognises and envelops the DNA-gRNA complex, before cleaving the DNA, resulting in double-stranded breaks (Ran et al., 2013).

Recent modifications to Cas9 endonuclease have extended its utility, including development of the dCas9 (deactivated Cas9) protein (Gilbert et al., 2013; Larson et al., 2014; Qi et al., 2013). Although dCas9 retains its ability to recognise gRNA-DNA complexes, mutations in the endonuclease domain prevent dCas9 from

cleaving DNA. Therefore, dCas9 blocks transcription through steric hindrance, termed CRISPR interference (CRISPRi) (Qi et al., 2013) (Figure 1.12).

Other modifications to the dCas9 protein aim to increase the level of transcriptional control available. To increase transcriptional repression dCas9-KRAB (Krüppel-associated box) fusions have been developed (Gilbert et al., 2013, 2014; Qi et al., 2013). Furthermore, a recent publication has similarly utilised a dCas9-eng (engrailed) fusion during zebrafish development to disrupt BMP function (Mouillesseaux et al., 2016). dCas9 fusion enzymes can effectively repress enhancers, suggesting tissue-specific control of gene expression may be possible (Kearns et al., 2015). Conversely, activation of transcription via activating modifications to dCas9 have been explored, termed CRISPRa, initially with modest transcriptional upregulation (Gilbert et al., 2013). CRISPRa utilises dCas9 fused to transcriptional activation domains such as VP64 or P65 (Gilbert et al., 2013). However, recent studies have sought to increase the effectiveness of CRISPRa by producing new dCas9 fusions which incorporate elements of various transcriptional activation domains (Gilbert et al., 2014; Horlbeck et al., 2016; Lin et al., 2015). Furthermore, a modified version of the Cas9 enzyme has been utilised to induce targeted mutagenesis of single DNA base pairs (Gaudelli et al., 2017; Zhang et al., 2017), so called base-editing, allowing determination of precise functions of amino acids and reproduction of disease-causing mutations.

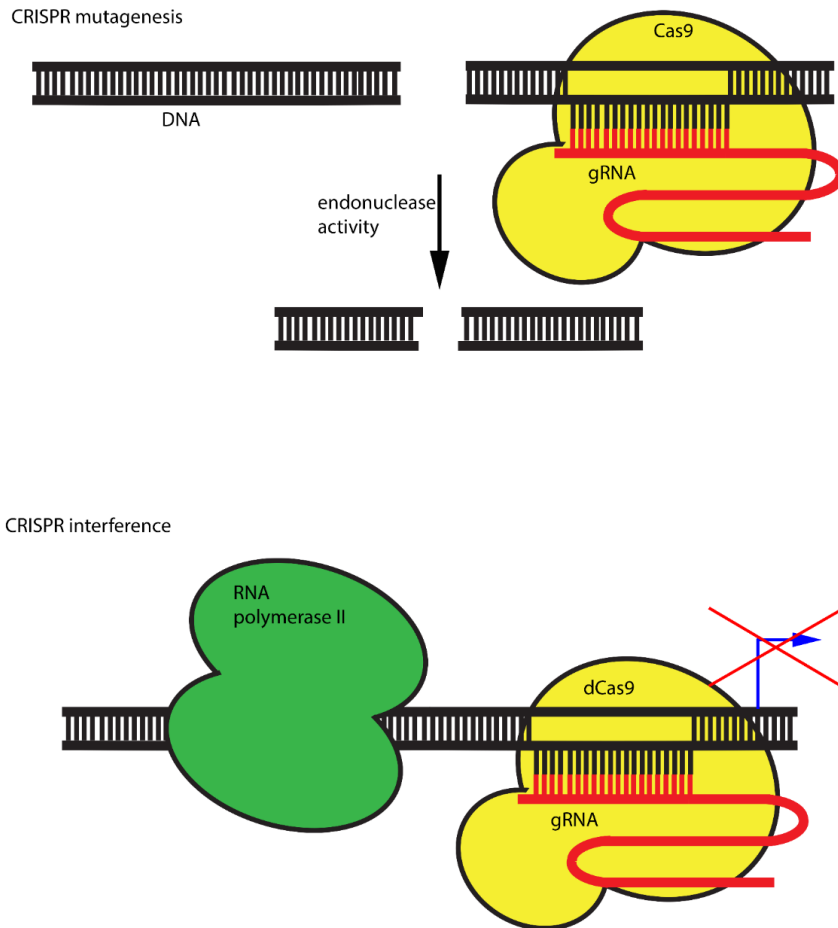


Figure 1.12 – Genetic manipulation by CRISPR-mediated knockout and CRISPR interference. Active Cas9 enzyme is directed to a specific genomic site by a gRNA, which it cleaves via endonuclease function. dCas9 lacks endonuclease function but binds DNA. dCas9 therefore functions to inhibit transcription sterically.

1.10 The phenomenon of genetic compensation.

TALEN and CRISPR mutagenesis has greatly facilitated production of zebrafish mutant lines. Consistently, however, many such mutants do not display phenotypes previously observed using genetic knockdown. Recent studies have suggested stable zebrafish mutants may undergo genetic compensation via transcriptional adaptation, wherein the effects of a deleterious mutation can be bypassed by transcriptional upregulation of an independent gene that functions

in place of the mutated gene (Rossi et al., 2015). This phenomenon is not limited to zebrafish, however, with reports of aphenotypic mutants in both mouse and Arabidopsis (Bouché and Bouchez, 2001; White et al., 2013). Recent studies suggest that nonsense-mediated decay (NMD) of incomplete mRNA transcripts can induce compensatory machinery and that knockdown of NMD components can increase phenotypic severity (Schuermann et al., 2015). Furthermore, upstream open reading frames, mRNA surveillance pathways and RNA binding proteins, among others, are potential mechanisms by which compensatory machinery may act to rescue the effects of a mutation (El-Brolosy and Stainier, 2017).

1.11 Thesis Aims and hypotheses

In this introduction, I have highlighted key elements of the current literature relating to this thesis, ranging from angiogenesis to current genetic tools used in manipulation of gene expression, in addition to current knowledge regarding *tmem33* and the work undertaken previously to analyse *tmem33* function in zebrafish by Dr Robert Wilkinson and Dr Freek van Eeden.

In this thesis, I aim to expand upon the preliminary work undertaken and determine the role of endothelial calcium signalling during angiogenesis *in vivo* and to identify epistasis between known regulators of endothelial cell biology and calcium signalling, such as VEGF and Notch signalling. Furthermore, I aim to understand the function of *tmem33* during vascular development (see Figure 1.13 for a visual hypothesis).

I therefore hypothesise that:

1. *tmem33* is expressed specifically within endothelial and kidney cells during development.
2. *tmem33* is required for normal endothelial and kidney development.
3. *tmem33* regulates endothelial cell biology, including calcium signalling and actin cytoskeleton dynamics.
4. *tmem33* functions to regulate endothelial cell biology downstream of VEGF during VEGF-mediated angiogenesis, by modulating downstream signalling pathways including Notch signalling.
5. *tmem33* interacts with *pkd2* during renal development.

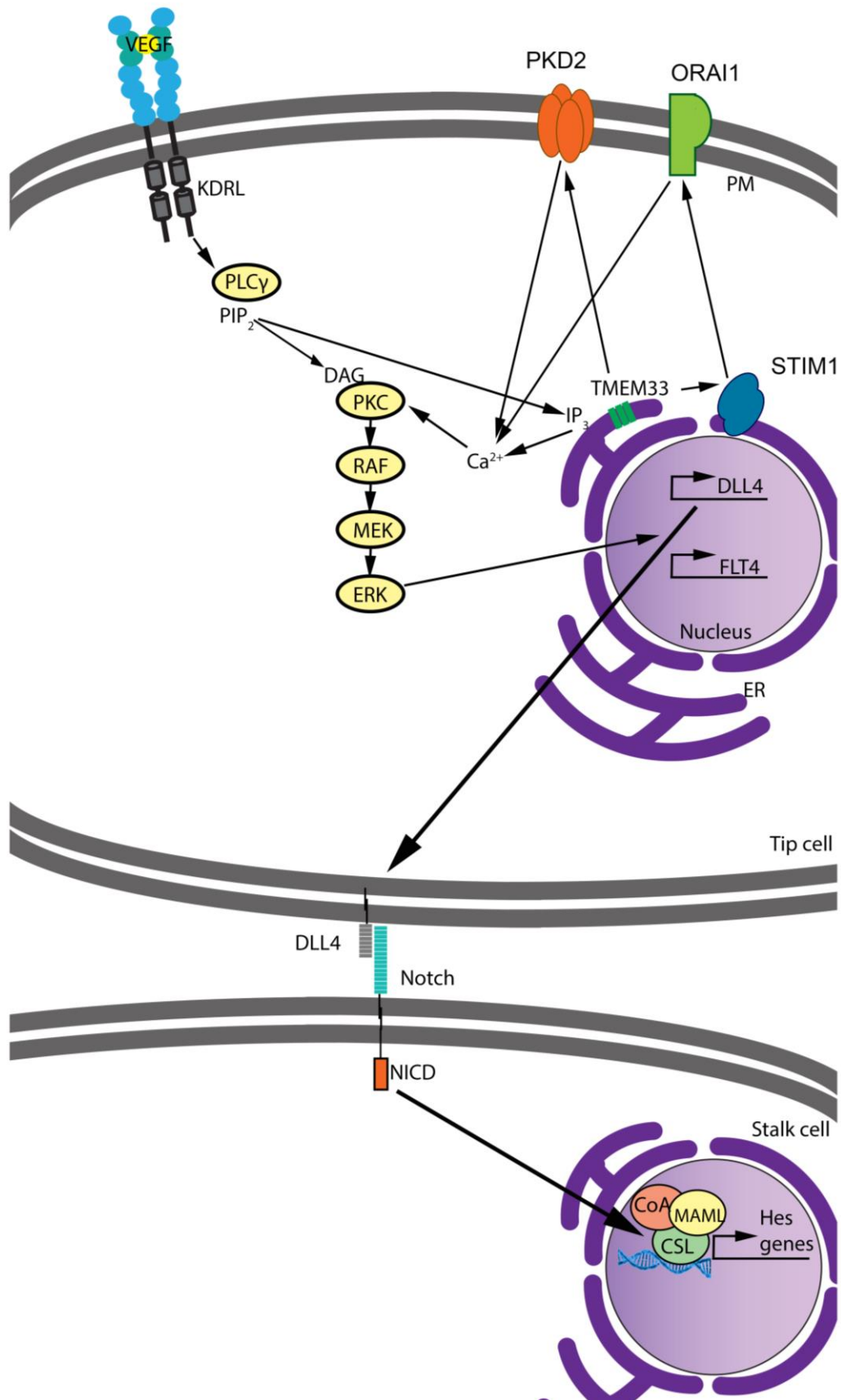


Figure 1.13 A summary of proposed tmem33 interactions and integration within the endothelial signalling pathway hierarchy.

2 Materials and Methods

2.1 Materials.

In this section, I list the materials used throughout the study. In section 2.2, I provide detailed protocols describing the techniques used.

2.1.1 Zebrafish maintenance and husbandry.

All experiments were conducted on Home Office Project Licence 70/8588 held by Professor Tim Chico. Adult zebrafish were maintained at $28.0\pm 1.0^{\circ}\text{C}$ and pH 7.5 ± 0.5 ; and subjected to a light/dark cycle of 14 hours of light and 10 hours of darkness. Adult zebrafish were fed a diet of artemia and food pellets.

When mating zebrafish, a marble box was placed in tanks to harvest progeny, or individual pairs were mated, separated by a divider, to ensure accurate timing of fertilisation and intercrossing of specific lines of zebrafish, such as two different transgenic lines. The wild type lines used in this study were as follows: AB, London Wild Type (LWT), *Tupfel long fin* (TL) and Nacre.

2.1.1.1. Transgenic zebrafish lines.

The following transgenic lines were obtained from other groups: *Tg(fli1a:EGFP)y1* (Bussmann et al., 2010), *Tg(-0.8flt1:enhRFP)hu5333* (Lawson et al., 2002), *Tg(-26wt1b:EGFP)li1* (Bollig et al., 2009), *Tg(flk1:EGFP-NLS)zf109* (Blum et al., 2008), *Tg(kdrl:HRAS-mCherry-CAAX)s916* (Chi et al., 2008) and *Tg(CSLBS:Venus)qmc61* (Gray et al., 2013).

Other transgenic lines were generated during or prior to this study within the University of Sheffield. These include: *Tg(fli1a:gff)ubs3;Tg(uas:GCaMP7a)sh392*, *Tg(fli1a:gff)ubs3;Tg(uas:GCaMP7a)sh393*, *Tg(fli1a:LifeACT-mClover)sh467*, *Tg(fli1a:AC-TagRFP)sh511*, *Tg(PHD3:eGFP)i144*, *Tg(fli1a:DsRedEx2)sh495*, *Tg(fli1a:dCas9,cryaa:CFP)sh512* and *Tg(enpep:gff)ubs3;Tg(uas:GCaMP7a)*. The transgenics I generated are described in more detail below.

Table 2.1 Transgenic lines characterised in this study

Transgenic line	Expression pattern/function
<i>Tg(fli1a:gff)ubs3;Tg(uas:GCaMP7a)sh392</i> , <i>Tg(fli1a:gff)ubs3;Tg(uas:GCaMP7a)sh393</i>	Endothelial GCaMP expression enabling real-time visualisation of calcium signalling dynamics during angiogenesis.
<i>Tg(fli1a:LifeACT-mClover)sh467</i>	Endothelially-expressed green fluorophore which localises to filamentous actin, to visualise actin cytoskeleton dynamics
<i>Tg(fli1a:AC-TagRFP)sh511</i>	Endothelially-expressed red fluorophore which localises to filamentous actin, to visualise actin cytoskeletal/filopodia dynamics
<i>Tg(fli1a:DsRedEx2)sh495</i>	Cytoplasmic red fluorophore expressed in endothelial cells
<i>Tg(enpep:gff)ubs3;Tg(uas:GCaMP7a)</i>	GCaMP expressed in developing pronephric tubules, enabling real-time visualisation of calcium signalling dynamics during kidney development.
<i>Tg(fli1a:dCas9,cryaa:CFP)sh512</i>	Endothelially-restricted dCas9 to enable endothelial-specific knockdown.

2.1.1.2. Generation of the endothelial F-actin reporter line *Tg(fli1a:LifeACT-mClover)sh467*.

LifeACT is a 17 amino acid peptide which can be inserted upstream of a fluorophore sequence to induce the fluorophore to bind to F-actin (Riedl et al.,

2008). The *fli1a:lifeACT-mClover* transgene was generated by PCR amplification of the mClover transgene utilising primers which introduced appropriate restriction enzyme sites and the LifeACT sequence. This was cloned into a middle entry vector and Gateway® cloning performed in combination with a 5' entry vector containing the *fli1a* promoter and a 3' entry vector containing a polyA sequence (Kwan et al., 2007; Villefranc et al., 2007). The *Tg(fli1a:LifeACT-mClover)sh467* transgenic line was generated by injection of the *fli1a:LifeACT-mClover* transgene into wild type embryos. Embryos were screened for endothelial mClover expression and raised until adulthood as potential transgenic line founders. Potential founders were outcrossed and progeny were screened for expression of the *fli1a:LifeACT-mClover* transgene. Once a founder had been identified, a tank of outcrossed embryos was raised to form the *Tg(fli1a:LifeACT-mClover)sh467* transgenic line.

To characterise reporter expression in the *Tg(fli1a:LifeACT-mClover)sh467* line, time-lapse microscopy using light-sheet microscopy was performed. *Tg(fli1a:LifeACT-mClover)sh467* embryos were imaged at 30 hpf and 120 hpf (Figure 2.1 A, B) and endothelial expression of the transgene was confirmed. To determine how effectively embryos labelled endothelial F-actin dynamics and filopodial extensions, embryos were imaged during angiogenesis from 22-30hpf. Clear cellular extensions were observed (Figure 2.1 C, white arrowheads), confirming that the reporter allows visualisation of filopodia.

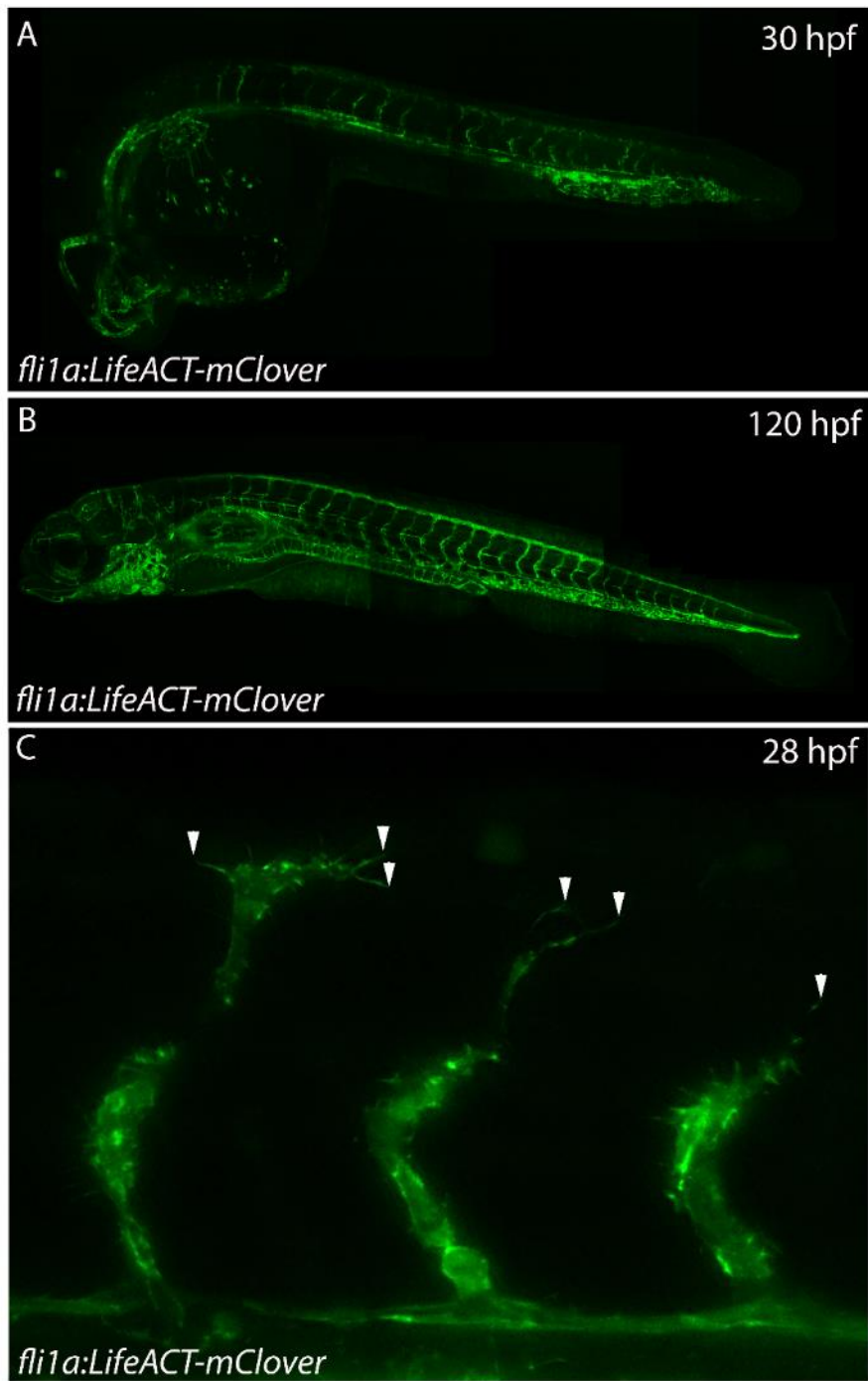


Figure 2.1 *Tg(fli1a:LifeACT-mClover)sh467* labels probable F-Actin structures within endothelial cells. *Tg(fli1a:LifeACT-mClover)sh467* embryo displaying endothelial mClover fluorescence at 30hpf (A) 120 hpf (B) and 28hpf (C). White arrowheads indicate filopodia in C.

2.1.1.3. Generation of the endothelial F-actin reporter line *Tg(fli1a:AC-TagRFP)sh511*.

The calcium reporter transgenic lines *Tg(fli1a:gff)ubs3;Tg(uas:GCaMP7a)sh392* and *Tg(fli1a:gff)ubs3;Tg(uas:GCaMP7a)sh393* express GCaMP7a, which fluoresces following stimulation with 488nm wavelength. Since my actin reporter *Tg(fli1a:LifeACT-mClover)sh467* fluoresces similarly it was not possible to image actin dynamics and calcium signalling simultaneously. Therefore, I deemed it necessary to generate an F-actin reporter line which utilised a fluorophore which fluoresced at a different wavelength, in order to distinguish structures. Recent studies have engineered antibodies from the Camelidae family, which contain a short monomeric heavy-chain fragment, termed nanobodies (Dmitriev et al., 2016; Panza et al., 2015). As with conventional antibodies, nanobodies bind to specific antigens. It is possible to fuse a fluorophore to nanobodies, termed chromobodies. Since chromobodies are turned over rapidly, they may act as real-time markers of intracellular dynamics. Therefore, I generated a novel transgenic line, that labeled F-actin utilising the TagRFP chromobody.

Tg(fli1a:AC-TagRFP)sh511 transgenic fish were generated by co-injection of the *fli1a:AC-TagRFP* transgene with Tol2 mRNA into 1-cell stage embryos. Embryos were raised and a transgenic line was established as described in section 2.1.2.2. At 30 hpf, *Tg(fli1a:AC-TagRFP)sh511* transgenic embryos display TagRFP fluorescence throughout the endothelium (Figure 2.2 A), which is maintained until 120 hpf (Figure 2.2 B). Higher magnification images of the line during angiogenesis show increased TagRFP fluorescence in cell membranes, at probably at apical cell boundaries between two cells, making this a useful marker for determining cell-cell boundaries (Figure 2.2 C, arrowheads). However, it is

difficult to observe filopodial extensions using this line (Figure 2.2 C). It was therefore necessary to study actin and calcium dynamics independently.

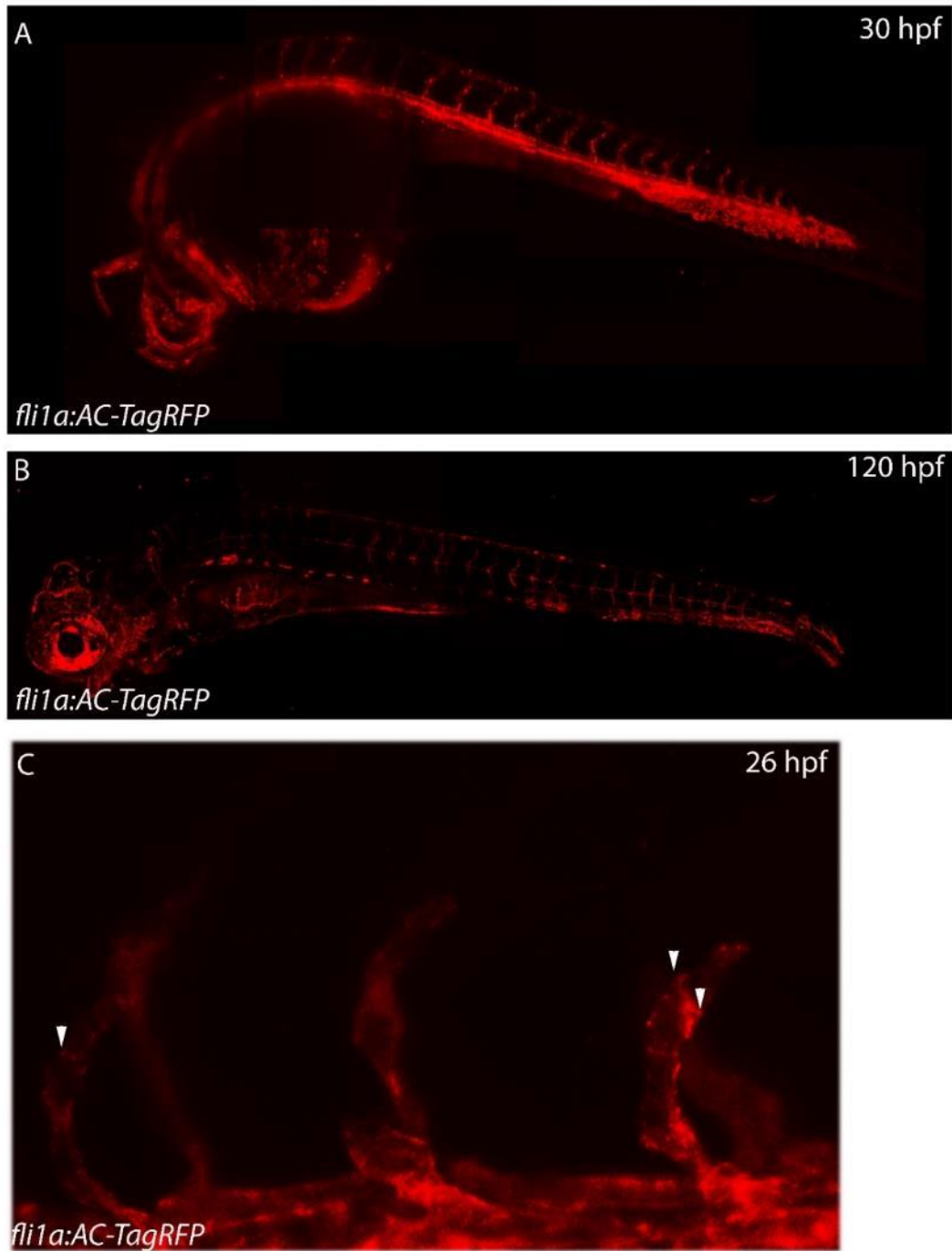


Figure 2.2 *Tg(fli1a:AC-TagRFP)sh511* labels F-Actin-like structures in endothelial cells. (A) 30 hpf *Tg(fli1a:AC-TagRFP)sh511* embryo displaying endothelial Chromobody-TagRFP fluorescence. (B) 120 hpf *Tg(fli1a:AC-TagRFP)sh511* embryo displaying endothelial Chromobody-TagRFP fluorescence. (C) 26 hpf *Tg(fli1a:AC-TagRFP)sh511* embryo displaying endothelial Chromobody-TagRFP fluorescence in migrating segmental arteries. White arrowheads indicate regions of high actin density, in regions likely to be cell boundaries.

2.1.1.4. Generation of the endothelial endoplasmic reticulum reporter line *Tg(fli1a:DsRedEx2)sh495*.

Tmem33 is predicted to localise to the ER membrane (Sakabe et al., 2015). To confirm this, full length *tmem33* mRNA fused to GFP was generated. To show ER localisation in ECs, the *Tg(fli1a:DsRedEx2)sh495* transgenic line was generated. KDEL motifs cause proteins to be shuttled into the ER (Munro and Pelham, 1987), conferring enriched fluorophore expression within the ER to cells expressing the transgene. *Tg(fli1a:DsRedEx2)sh495* embryos display clear endothelial fluorescence at day 1 through until day 5, but no obvious ER enrichment of expression in images taken at 20x magnification (Figure 2.3 A, C, D). When observing the retina at 32x magnification and imaging the retina, nuclear exclusion (Figure 2.3 B, white arrowhead) could be observed. However, no clear ER localisation was observed, suggesting this line does not sufficiently label the ER in endothelial cells. Therefore, this line will be renamed *Tg(fli1a:DsRedEx2)sh495*.

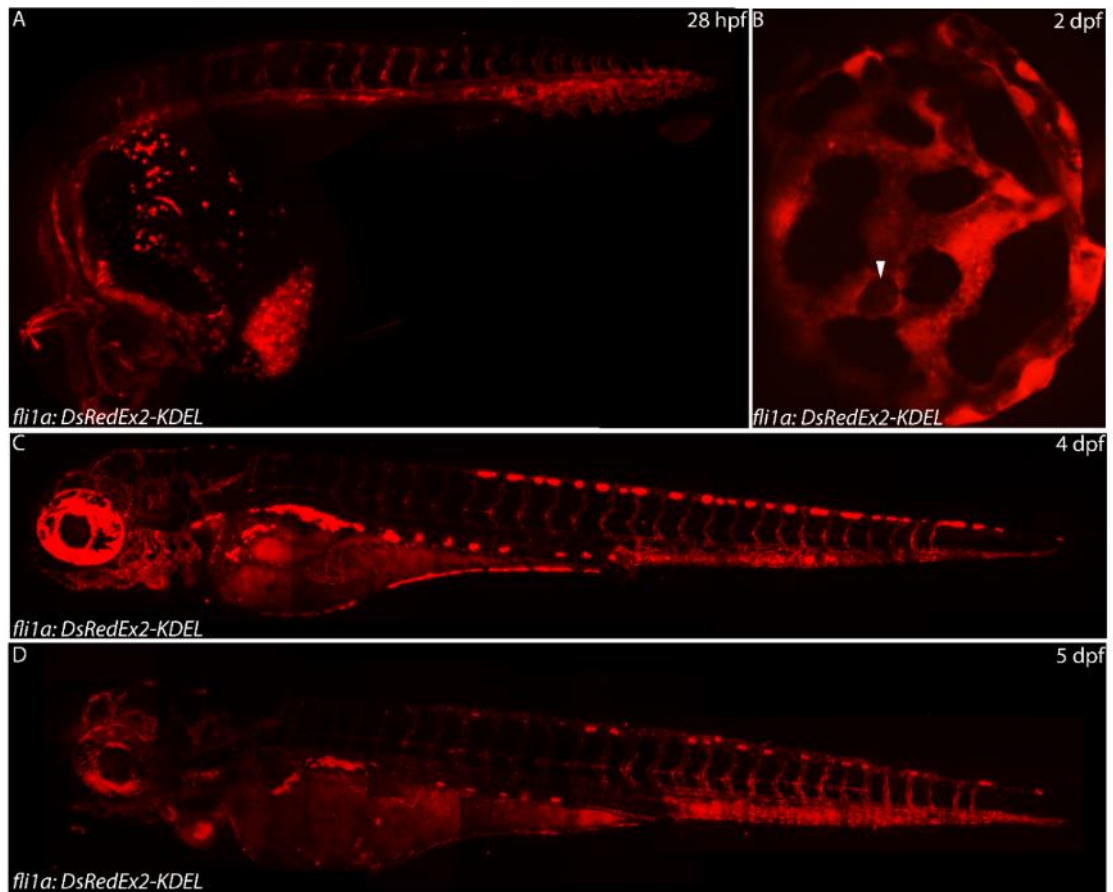


Figure 2.3 *Tg(fli1a:DsRedEx2)sh495* embryos display endothelial DsRed protein and apparent nuclear exclusion. (A-D) *Tg(fli1a:DsRedEx2)sh495* embryos display endothelial fluorescence. Expression is observed in developing blood vessels from the first embryonic day (A), through to the fourth and fifth embryonic days (C, D). At higher magnifications, nuclear exclusion of DsRed protein can be observed. This example uses the retinal vasculature at 2 dpf (B, white arrowhead).

2.1.1.5. Mutant zebrafish lines.

During this study, I used two mutant zebrafish lines: *tmem33^{sh443}* and *vh^{hu2117}*. This *tmem33^{sh443}* zebrafish line consists of a 2bp deletion within the coding sequence of exon 3, causing a frameshift and leading to a premature truncation in exon 4 (Figure 3.13). This is predicted to be a loss of function as it is located

within the conserved transmembrane domains. The *vh^{hu2117}* mutation has been described previously (Rooijen et al., 2009).

2.1.1.6. E3 medium.

Zebrafish larvae were maintained until day 5.2 in E3 medium. E3 medium is composed of 5 mM NaCl, 0.17 mM KCl, 0.33 mM MgSO₄ and 0.33 mM CaCl₂. Methylene blue is added as an anti-fungal agent.

2.1.1.7. Calcium-free Ringer's Solution.

For calcium chelation experiments, zebrafish larvae were treated in Ca²⁺-free Ringer's solution so that Ca²⁺ chelation did not occur within the medium before chelating agents could diffuse into the embryo. Ca²⁺-free Ringer's solution is composed of 100 mM NaCl, 2mM KCl, 1mM EGTA, 1mM MgCl₂, 5M HEPES.

2.1.2 Morpholinos.

In this study, three morpholinos were used; two targeting *tmem33* and one targeting *pkd2*. The *tmem33* morpholinos were designed to bind downstream of exon 3 and upstream of exon 4 to induce improper splicing and retention of exon 3-4. The *pkd2* morpholino targets the ATG sequence to inhibit translation.

Table 2.2 Morpholinos used in study.

<i>tmem33-sp2b</i>	AATTGCTAACACAGACATGACAA
<i>tmem33-sp3</i>	TTATAGGAGAACATGACTCACCCAA
<i>pkd2</i>	AGGACGAACGCGACTGGAGCTCATC

2.1.3 CRISPR/CRISPRi.

During this study, CRISPR interference was used for genetic knockdown. Guide RNAs (gRNAs) were first tested using active Cas9 protein for ability to drive Cas9 endonuclease function.

2.1.3.1. Cas9 endonuclease variants.

All gRNAs were tested using the commercially available active Cas9 protein (Sigma-Aldrich). Functional gRNAs were then tested using dCas9. The dCas9 plasmid is zebrafish codon-optimised and was a kind gift from the Stainier lab (Rossi et al., 2015).

2.1.3.2. Guide RNAs used for CRISPR experiments.

The following gRNAs were employed during this study:

Table 2.3 List of gRNAs

<i>tmem33 5'UTR</i>	AAAGCACCGACTCGGTGCCACTTTTTCAAGTTGATAAC GGACTAGCCTTATTTTAACTTGCTATTTCTAGCTCTAAA ACGAGGTCGGCTGGCTCAGCTGACCCTATAGTGAGTC GTATTACGC
---------------------	---

<i>tmem33 ex1</i>	AAAGCACCGACTCGGTGCCACTTTTTCAAGTTGATAAC GGACTAGCCTTATTTTAACTTGCTATTTCTAGCTCTAAA ACTCCTCCTCCTCCTCAGGCTGGGGCTATAGTGAGTCG TATTACGC
<i>tmem33 5'UTR ctrl</i>	AAAGCACCGACTCGGTGCCACTGAGGTTCGGCTGGCTC AGCTGACCCTATAGTGAGTCGTATTACGC
<i>tmem33 ex1 ctrl</i>	AAAGCACCGACTCGGTGCCACTCCTCCTCCTCCTCAG GCTGGGGCTATAGTGAGTCGTATTACGC
<i>vhl-gRNA-1</i>	AAAGCACCGACTCGGTGCCACTTTTTCAAGTTGATAAC GGACTAGCCTTATTTTAACTTGCTATTTCTAGCTCTAAA ACGTATCCGGCTGATCAGAGACCTATAGTGAGTCGTAT TACGC
<i>vhl-gRNA-1 ctrl</i>	AAAGCACCGACTCGGTGCCACAAACGTATCCGGCTGA TCAGAGACCTATAGTGAGTCGTATTACGC
<i>trpv4 5'UTR 1</i>	AAAGCACCGACTCGGTGCCACTTTTTCAAGTTGATAAC GGACTAGCCTTATTTTAACTTGCTATTTCTAGCTCTAAA ACAAATGTAAAACCCGAGCTCAACCCTATAGTGAGTCG TATTACGC
<i>trpv4 5'UTR 2</i>	AAAGCACCGACTCGGTGCCACTTTTTCAAGTTGATAAC GGACTAGCCTTATTTTAACTTGCTATTTCTAGCTCTAAA ACAGTTAAAGCAATGACTGACCAACCCTATAGTGAGTC GTATTACGC
<i>trpv4 ex1</i>	AAAGCACCGACTCGGTGCCACTTTTTCAAGTTGATAAC GGACTAGCCTTATTTTAACTTGCTATTTCTAGCTCTAAA ACCGACCAGAAGCAGAACATGCACCCTATAGTGAGTC GTATTACGC
<i>trpv4 6TM 5'</i>	AAAGCACCGACTCGGTGCCACTTTTTCAAGTTGATAAC GGACTAGCCTTATTTTAACTTGCTATTTCTAGCTCTAAA ACGAGGCCTTAACTCACTGGAACCCTATAGTGAGTCG TATTACGC
<i>trpv4 6TM 3'</i>	AAAGCACCGACTCGGTGCCACTTTTTCAAGTTGATAAC GGACTAGCCTTATTTTAACTTGCTATTTCTAGCTCTAAA ACGACCATCTGCCCTGATAAGGACCCTATAGTGAGTCG TATTACGC

2.1.4 Primers and probes used in study.

Genotyping primers were used to select for mutants and to determine whether gRNAs coupled with Cas9 were sufficient to cause DNA double strand breaks.

The following primers were used:

Table 2.4 List of genotyping primers.

<i>tmem33 ex3F</i>	GCCTCAAGCTGCTGCTAACTT
--------------------	-----------------------

<i>tmem33 ex3R</i>	AACTCCTACCCCATCACAA
<i>tmem33 ex8F</i>	CACATCATCTGGCGGTTTCC
<i>tmem33 ex8R</i>	TCACAGAGCTGCGCATCTTA
<i>tmem33 gRNA F</i>	TTTGTGCAATCCAGAGGTCTG
<i>tmem33 gRNA R</i>	TGCGCATAATAACATAGTCAAA
<i>vhl F</i>	TAAGGGCTTAGCGCATGTTC
<i>vhl R</i>	CTATCTACGCGTTTAACTCG
<i>trpv4 5'UTR 1 F</i>	AATAGCAAGTCAGACGGGG
<i>trpv4 5'UTR 1 R</i>	AGAGCGTGTGAACAGACAGA
<i>trpv4 5'UTR 2 F</i>	CTCTTGCAGACCCTCAGACA
<i>trpv4 5'UTR 2 R</i>	GGTGGTGAGGAGACAGACAA
<i>trpv4 ex1 F</i>	AGAGGCAGCAGATGGAGATC
<i>trpv4 ex1 R</i>	GGAACCTAATCCGCATGTTCT
<i>trpv4 6TM 5' F</i>	TACTCTGTGTTGGTGCTGGT
<i>trpv4 6TM 5' R</i>	TGGATCATGATGCTGTAAGT
<i>trpv4 6TM 3' F</i>	CATTAGTGTCGCTGTTGA
<i>trpv4 6TM 3' R</i>	TGTAGGTGACCAGCAGAATG

The following primers were used to generate probes for *in situ* hybridisation:

Table 2.5 List of primers used to generate *in situ* hybridisation probes.

<i>dCas9 ISH F</i>	AATTAACCCTCACTAAAGGCCCTAAGAAGTATGGAGGCT
<i>dCas9 ISH R</i>	TAATACGACTCACTATAGGGGCTGAGACAGGTCAATCCTT
<i>trpa1a ISH F</i>	AATTAACCCTCACTAAAGGTGCAAAGGCCATTCTCCACT
<i>trpa1a ISH R</i>	TAATACGACTCACTATAGGGGTTGGTGACCTCCCTCCTTG

<i>trpa1b ISH F</i>	AATTAACCCTCACTAAAGGCCAGTCTGCTGCACTATGCT
<i>trpa1b ISH R</i>	TAATACGACTCACTATAGGGCAAACAGCGTGGCTCTATGC
<i>trpm1a ISH F</i>	AATTAACCCTCACTAAAGGGGAGGTCATATCAACAAGGCC
<i>trpm1a ISH R</i>	TAATACGACTCACTATAGGGGGAGGTCATATCAACAAGGCC
<i>trpm1b ISH F</i>	AATTAACCCTCACTAAAGGTGGTGAAGGAATGGCAGCTA
<i>trpm1b ISH R</i>	TAATACGACTCACTATAGGG TGGTGAAGGAATGGCAGCTA
<i>trpm2 ISH F</i>	AATTAACCCTCACTAAAGGACCAGAACCAAGACACAGGAC
<i>trpm2 ISH R</i>	TAATACGACTCACTATAGGG ACCAGAACCAAGACACAGGAC
<i>trpm3 ISH F</i>	AATTAACCCTCACTAAAGGGCTGCTCATCTCTGTTACAG
<i>trpm3 ISH R</i>	TAATACGACTCACTATAGGGGCTGCTCATCTCTGTTACAG
<i>trpm4a ISH F</i>	AATTAACCCTCACTAAAGGTCTGGGGAAGTGGAAGCATT
<i>trpm4a ISH R</i>	TAATACGACTCACTATAGGG TCTGGGGAAGTGGAAGCATT
<i>trpm4b ISH F</i>	AATTAACCCTCACTAAAGGCACAAAGAGCTGGGTCCCAA
<i>trpm4b ISH R</i>	TAATACGACTCACTATAGGGCACAAAGAGCTGGGTCCCAA
<i>trpm4c ISH F</i>	AATTAACCCTCACTAAAGGCAAACCTGGAAGCAACGACCA
<i>trpm4c ISH R</i>	TAATACGACTCACTATAGGGCAAACCTGGAAGCAACGACCA
<i>trpm5 ISH F</i>	AATTAACCCTCACTAAAGGGTGGTGGGATTGTCATGCAG
<i>trpm5 ISH R</i>	TAATACGACTCACTATAGGGGTGGTGGGATTGTCATGCAG
<i>trpm6 ISH F</i>	AATTAACCCTCACTAAAGGTGCGTCTTTCCTGTGACTCT
<i>trpm6 ISH R</i>	TAATACGACTCACTATAGGG TCGTCTTTCCTGTGACTCT
<i>trpm7 ISH F</i>	AATTAACCCTCACTAAAGGGCACAACCAGATCACACGTG
<i>trpm7 ISH R</i>	TAATACGACTCACTATAGGGGCACAACCAGATCACACGTG
<i>trpm11a ISH F</i>	AATTAACCCTCACTAAAGGTAAATCGCTGACATGGCCG
<i>trpm11a ISH R</i>	TAATACGACTCACTATAGGGTTCCTGACTCGGGTCTC
<i>trpm11b ISH F</i>	AATTAACCCTCACTAAAGGTTCACAGACCCTCAGCTCAG

<i>trpml1b</i> ISH R	TAATACGACTCACTATAGGGCCAGACACATTGGGGTCTCT
<i>trpml2</i> ISH F	AATTAACCCTCACTAAAGGAGTACAGAACCCGACGACAG
<i>trpml2</i> ISH R	TAATACGACTCACTATAGGGAGCTGGAGAATCGCTGAAGT
<i>trpp1a</i> ISH F	AATTAACCCTCACTAAAGGGCGTCCATGGAGTTTCGTAC
<i>trpp1a</i> ISH R	TAATACGACTCACTATAGGGCACTGGCGATGTGGAAGATG
<i>trpp1b</i> ISH F	AATTAACCCTCACTAAAGGAAGATGGTGGGAATCCTGCA
<i>trpp1b</i> ISH R	TAATACGACTCACTATAGGGCTTCCTCCATCCAGTGCAGA
<i>trpp2</i> ISH F	AATTAACCCTCACTAAAGGGCGTATCCCAACTTTGAGCCG
<i>trpp2</i> ISH R	TAATACGACTCACTATAGGGGACGATGCTGCCAATTGAGT
<i>trpv1</i> ISH F	AATTAACCCTCACTAAAGGAAGAGGAGAGGACAAAGGCC
<i>trpv1</i> ISH R	TAATACGACTCACTATAGGGGATGTCTGCAGCCCATAAGC
<i>trpv4</i> ISH F	AATTAACCCTCACTAAAGGGCACTTCTCAACCTGCACAA
<i>trpv4</i> ISH R	TAATACGACTCACTATAGGGGCCAACATCTCATGCCGATT
<i>trpv6</i> ISH F	AATTAACCCTCACTAAAGGCTCCAGGGTCGATGAACACT
<i>trpv6</i> ISH R	TAATACGACTCACTATAGGGAGAGCTCGTCACGTTCTTGA

All forward primers contain T3 promoter sequences and all reverse primers contain T7 promoter sequences. Plasmids containing *in situ* hybridisation probes for *trpc1*, *trpc2a*, *trpc2b*, *trpc3*, *trpc4a*, *trpc4b*, *trpc5a*, *trpc5b*, *trpc6a*, *trpc6b*, *trpc7a* and *trpc7b* were kindly donated by the Neuhauss lab (Von Niederh??usern et al., 2013). Probes for *vegfaa*, *kdr*, *flt1*, *kdrl*, *flt4* and *cdh5* were already available in the lab.

The following primers were used during cloning to generate novel transgenic lines:

Table 2.6 List of primers used during cloning.

LifeAct-CloverF (EcoRI)	<u>GAATTC</u> ATGGGCGTGGCCGACTTGATCAAGAAGTTCGAGT CCATCTCCAAGGAGGAGGGGGATCCACCGGTCGCCACCA TGGTGAGCAAGGGCGAG
Clover R (XhoI)	<u>CTCGAGT</u> TACTTGTACAGCTCGTCC
LACloverattB1F	GGGACAAGTTTGTACAAAAAAGCAGGCTTCATGGGCGTG GCCGACTTG
LACloverattB2R	GGGACCACTTTGTACAAGAAAGCTGGTCTTACTTGTACAG CTCGTCC
Actinvhh-attb1R	GGGACAAGTTTGTACAAAAAAGCAGGCTTCATGGCTCAG GTGCAGCTGG
Tagrfp-attb2R	GGGACCACTTTGTACAAGAAAGCTGGGTCTCAATTAAGTT TGTGCCC
Full-length tmem33F (BamHI)	<u>GGATCC</u> ATGGCAGACACCGAGCAAAG
Full-length tmem33 R (XhoI)	<u>CTCGAGT</u> TAGACGCCGTTGGAGCGA

Restriction enzyme sites within primers are underlined in sequence.

The following Taqman probes were used in the study:

Table 2.7 List of Taqman probes.

Probe name	Probe number	Custom probe target sequence/exons targeted
<i>ef1a</i>	Dr03432748_m1	Exons 1-2
<i>flt1</i>	Dr03109249_m1	Exons 12-13
<i>Kdr</i>	Dr03116242_m1	Exons 15-16
<i>flt4</i>	Dr03138049_m1	Exons 6-7
<i>Kdrl</i>	Dr03432904_m1	Exons 9-10
<i>tmem33</i>	Dr03140164_m1	Exons 3-4
<i>p53</i>	Dr03112089_m1	Exons 9-10
<i>notch1a</i>	Dr03112160_m1	Location 2620
<i>notch1b</i>	Dr03086775_m1	Exons 32-33
<i>notch3</i>	Dr03432941_g1	Exons 11-12
<i>Nrarp</i>	Dr03125445_s1	Exon 1
<i>dll4</i>	Dr03428646_m1	Exons 8-9
<i>jag1a</i>	Dr03093489_m1	Exons 25-26
<i>jag1b</i>	Dr03080071_m1	Exons 24-25
<i>her6</i>	Dr03176397_s1	Exon 1
<i>her9</i>	Dr03112436_g1	Exons 3-4
<i>her12</i>	Dr03133031_m1	Exons 1-2
<i>hey1</i>	Dr03438956_g1	Exons 4-5

<i>hey2</i>		GGAATGAAGTTTGAGACCTCCATTTCGACGGCTCGGGGCG TGTTTTCTATTTTTTTTTTACGGTGGGTGTTCCCGAAGCAG GACGTGGGCGTGAATGTGAGACTGAGGCTCCAGCGGTT CGTGGGAAAGGCGCTCAGAGAGTTTTTGGTGTCTGTACC TGCGCGCACTGCATCATGAAGCGGCCCTGTGAGGACAG CACGTCCGACAGCGACATGGATGAAACCATTGATGTGGG CAGCGAGAATAACTACTCTGGCCAAAGCAATGGTTCATT ATAAGATGTGGCTCACCTACAACGACATCCCAAGTCATG GCCAGAAAGAAGCGGAGAGG
-------------	--	---

2.1.5 Generation of *tmem33* full length mRNA and *tmem33-gfp* fused mRNA

To determine the subcellular localisation of *tmem33* in zebrafish, the full length cDNA sequence of *tmem33* was cloned. Primers were designed to incorporate the entire *tmem33* processed mRNA transcript (See supplementary primer table 2.5) and RT-PCR was performed on extracted RNA from 24 hpf zebrafish embryos.

Once sequenced, the amplified *tmem33* cDNA sequence was found to contain a single base pair change from the reference sequence. The sequence was amplified twice more, using RNA obtained from different wild type strains each time. Each amplification contained the same base pair change, suggesting this is likely to be a sequence variant in the zebrafish stocks at the University of Sheffield.

The base pair change was identified as a C->T change (Not shown), which altered the amino acid sequence from a phenylalanine codon to a serine codon (Figure 2.4 A). The sequence change occurs in the less conserved looped regions between transmembrane domains and was predicted to have a neutral effect on protein structure (Figure 2.4 B). The full length *tmem33* was cloned into the pGEM-T easy vector, for rescue assays and then recombined into pCs2-mtGFP, using the Gateway® system, which fuses GFP to the transcript, for subcellular localisation assays. Given that provean analysis suggested a no change to function, I decided against site-directed mutagenesis.

A

```

MADTEQRSPPPPPPPPQAGAAQFLLSNKLETAMWLSRLFTVYCSIMFILPLLGPQAAANFY
QRALLANALTSALRLHQRLPHFQLSRAFLAQALQEDSCHYLLYSLILVNSYPITMSIFPV
FLFSL LHATTYTKKVLDTMGPNSLMFVRN FLNKLT SNQQN ILKFIACNEIFLMPATVFML
FSGQGSLLQPFIIYYRFLTRYSSRRNPYCRTLFTELRLLEHFVMKPCPVFFRRMCLNS
IAFVSR LAPTGV

MADTEQRSPPPPPPPPQAGAAQFLLSNKLETAMWLSRLFTVYCSIMFILPLLGPQAAANFY
QRALLANALTSALRLHQRLPHFQLSRAFLAQALQEDSCHYLLYSLILVNSYPITMSIFPV
FLFSL LHATTYTKKVLDTMGPNSLMFVRN SLNKLT SNQQN ILKFIACNEIFLMPATVFML
FSGQGSLLQPFIIYYRFLTRYSSRRNPYCRTLFTELRLLEHFVMKPCPVFFRRMCLNS
IAFVSR LAPTGV

```

B

PROVEAN Prediction - Job ID: 171555045072466

- Query sequence (fasta)
- Supporting sequence set used for prediction
Number of sequences: 110 (fasta, E-values)
Number of clusters: 30
- Score thresholds for prediction
(1) Default threshold is -2.5, that is:
-Variants with a score equal to or below -2.5 are considered "deleterious,"
-Variants with a score above -2.5 are considered "neutral."
(2) How to use a more stringent threshold.

Variant	PROVEAN score	Prediction (cutoff= -2.5)
F150S	-1.095	Neutral

Figure 2.4 Generation of full-length *tmem33* mRNA. (A) A nucleotide sequence change of C->T resulted in an amino acid alteration from phenylalanine to serine. Amino acid change is highlighted in red. **(B)** Provean protein structure analysis predicts that the change is neutral with regard to protein function.

2.1.6 List of chemical inhibitors.

Table 2.8 List of chemical inhibitors

Chemical	Supplier	Function
Thapsigargin	AbCam (ab120286)	SERCa-ATPase inhibitor – induces calcium release from ER
2-APB	Tocris (1224)	IP3 receptor inhibitor – impairs calcium release from ER
DAPT	Sigma-Aldrich (D4952)	Gamma secretase inhibitor- impairs Notch signalling
AV951	Selleckchem (S1207)	VEGF receptor inhibitor
Latrunculin B	Sigma-Aldrich (L5288-1MG)	Actin depolymerising agent – prevents formation of F-actin
SKF96365	Tocris (1147)	Store-operated calcium entry inhibitor
TRPV4 Antagonist III	Glaxo Smith-Kline (GSK205)	Blocks TRPV4 function.

2.1.7 Buffers and solutions.

Standard buffers and solutions were used throughout the study, the compositions of which are listed here:

Table 2.9 List of Buffers/Solutions

Buffer/Solution	Composition
0.03% PTU	0.03g of 1-phenyl 2-thiourea per 100ml of dH ₂ O
10x BSA	0.1g Bovine Serum Albumin per 10ml of dH ₂ O
20x SSC	3M NaCl; 0.3M Sodium Citrate
4% PFA	2g paraformaldehyde per 50ml 1xPBS
50x TAE	2M Tris-acetate; 50mM EDTA

BCL III	0.1mM Tris-HCL (pH9.5); 0.1mM NaCl; 50mM MgCl ₂ ; 0.1% Tween20
Hybe +/-	50% Formamide; 5xSSC; 9.2mM Citric acid; 0.1% Tween20; 0.5mg/ml tRNA; 50mg/ml Heparin
Hybe -/-	50% Formamide; 5xSSC; 9.2mM Citric acid; 0.1% Tween20
Maleic Acid Buffer (MAB)	pH7.5 0.1M Maleic acid; 0.15M NaCl (pH adjusted with NaOH)
Maleic Acid Buffer Block	2% Roche Blocking Reagent in Maleic Acid Buffer
Phosphate Buffered Saline (PBS)	150mM Phosphate buffer; 0.85% NaCl RT
PBS Tween (PBSTw)	1xPBS; 0.1% Tween20 RT
Proteinase K	10mg/ml of proteinase K in glycerol
PSI broth	4mM MgSO ₄ ; 10mM KCl; LB medium up to 250ml
TBF1 buffer (pH 5.8)	100mM RbCl; 50mM MnCl ₂ ; 30mM potassium acetate; 20mM CaCl ₂ ; 15% Glycerol
TBF2 buffer (pH 8.0)	10mM MOPS; 10mM RbCl; 75mM CaCl ₂ ; 15% Glycerol
Tricaine (MS222)	pH7-7.5 4g Tricaine methanesulfonate in 1L dH ₂ O (pH adjusted with NaOH)
Tris Buffered Saline (TBS)	Tris/HCL ph 7.5
TBS-Block	TBS; 10% goat serum; 1% BSA
TBS-Triton X-100	TBS; 0.025% Triton X-100 RT

2.2 Methodology.

In this section, I describe the methodology of the techniques used in detail. For details on reagents used, please see section 2.1.

2.2.1 Molecular biology.

2.2.1.1. PCR.

PCR was utilised during this study to amplify gene products during cloning, genotyping, *in situ* hybridisation probe synthesis and gRNA synthesis. PCRs were performed to manufacturer's specifications using 2x ReddyMix (Thermo Scientific) or Phusion High-Fidelity DNA Polymerase (New England BioLabs). See primer tables above for lists of primers in PCR (Table 2.4; Table 2.5; Table 2.6).

2.2.1.2. RT-PCR.

RT-PCR was performed during the amplification of *in situ* hybridisation probes and generation of full length mRNAs. RT-PCR was performed using the SuperScript® III One-Step RT-PCR System with Platinum® *Taq* DNA Polymerase (Thermo Fisher), according to manufacturer's guidelines. A list of primers used in RT-PCR is included in this section (Table 2.7).

2.2.1.3. Gel electrophoresis.

1 or 3% agarose gels were made by adding the specified amount of agarose powder to 1% TAE buffer. 05.mg/ml ethidium bromide was added for visualisation

of gel bands. Samples were loaded in 1x loading buffer alongside suitable DNA markers (100bp/1kb DNA ladders, NEB). Gel electrophoresis was performed at 120V, until gels were resolved.

2.2.1.4. Gel extraction and PCR purification.

Gel extraction was performed on selected bands on resolved gels. Selected bands were excised using a clean scalpel and transferred to a 2ml tube. A QIAquick® Gel Extraction Kit (QIAGEN) was used to extract samples in agarose gels and when no gel was necessary, a PCR QIAquick® Purification Kit (QIAGEN) was used to purify PCR samples. Both protocols were performed as per manufacturer guidelines.

2.2.1.5. Restriction enzyme DNA digestion.

All restriction enzymes used were obtained from New England Biolabs (NEB). For each 1mg of DNA digested, 10 units of enzyme were used alongside a 1x dilution of the specified buffer, using dH₂O, up to a total volume of 20-100 µl as appropriate.

2.2.1.6. DNA ligation.

DNA ligations were set up in a 1:3 (vector:insert) ratio in a 10 µl total reaction volume, using 3 units of T4 DNA ligase (NEB) and a 1x dilution of T4 ligase buffer. Ligations were performed at 4°C overnight.

2.2.1.7. Generation of competent *E. coli* cells.

100 ml of LB medium was inoculated with *E. coli* and incubated, shaking, at 37°C until OD_{578nm} reaches a value of 0.5. Inoculated LB was then centrifuged at 4500 rpm and 4°C for 10 minutes. Pellets were resuspended in 30 ml TBF1 buffer and incubated on ice for 90 minutes. Cells were centrifuged for 10 minutes at 4500 rpm and 4°C and resuspended in 3ml TBF2 buffer. 125 µl aliquots were made and snap frozen using liquid nitrogen. Frozen aliquots were stored at -80°C.

2.2.1.8. Transformation.

Competent *E. coli* cells were thawed on ice for 10 minutes before addition of 2-5 µl of ligation mix. The reaction mix was incubated on ice for 30 minutes followed by a 30 second heat shock at 42 °C. The reaction mix was again incubated on ice for 5 minutes, at which point 950 µl of LB broth was added and the mix was incubated at 37 °C for 1 hour, shaking. The culture was plated out onto LB plates containing the appropriate antibiotic and incubated at 37 °C overnight. Single colonies were then picked and grown in LB broth containing the appropriate antibiotic. For minipreps, a volume of 6 ml was used per colony and midipreps were grown in 100 ml LB broth.

Plasmid DNA was isolated from cultures using a QIAprep Spin Mini Kit (QIAGEN) for minipreps, or using a NucleoBond® Xtra Midi Kit (Machery-Nagel) for midipreps, as per manufacturer guidelines.

2.2.1.9. Gateway® Cloning.

Gateway® cloning reactions were set up using three entry vectors (5' entry, middle entry and 3' entry vectors), and a destination vector. All entry clones were diluted to 10 fmoles and destination vectors were diluted to 20 fmoles, prior to addition to a reaction mix. Reaction mixes were set up to contain 1 µl of each of the three entry vectors and destination vector. LR Clonase™ was then removed from storage at -20°C and thawed on ice for 2 minutes, then vortexed twice for 2 seconds. 2 µl was added to the reaction mix and the total volume was made up to 10 µl by addition of dH₂O. The reaction was incubated at 25°C for 16 hours before 1 µl of proteinase K was added and incubated at 37°C to stop reaction.

2.2.1.10. gDNA extraction from whole embryos.

To obtain genomic DNA (gDNA) from whole embryos, anaesthetised embryos were individually selected and placed in 0.2 ml microcentrifuge tubes containing 20 µl 50mM NaOH, which was then heated to 95°C for 10 minutes and cooled to 12°C. The reaction was stopped by addition of 0.5 µl Tris-HCl pH9.5.

2.2.1.11. gDNA extraction from fin biopsy.

To obtain gDNA from fin biopsies, adult zebrafish were anaesthetised in 100 ml aquarium water containing 4.2 ml tricaine. A small section of the caudal fin (less than one third) was removed using clean scissors and placed in a 0.2 ml microcentrifuge tube containing 50 µl 50mM NaOH. Once fin clips had been taken from the required number of fish, the samples were then heated to 95°C for 10

minutes and cooled to 12°C. The reaction was stopped by addition of 0.5 µl Tris-HCl pH9.5.

2.2.1.12. Whole embryo RNA extraction.

Embryos were selected and anaesthetised. 100 embryos were used for making RNA stocks for developmental time points and 20 embryos were used for qRT-PCR analysis. Embryos were homogenised embryos in 1 ml Trizol® solution and 0.2 ml chloroform was added before mixing for 15 seconds. Samples were incubated at room temperature for 5 minutes and centrifuged for 10 minutes at 12,000xg and 4°C. The upper aqueous phase was removed and 0.5 ml isopropanol was added and mixed. Samples were incubated for 10 minutes at room temperature and centrifuged again for 10 minutes at 12,000xg and 4°C. Samples were washed with 0.5 ml 75% ethanol and centrifuged for 5 minutes at 7,500xg and 4°C. Pellets were then resuspended in 100 µl for RNA stocks and 20 µl for qRT-PCR.

2.2.1.13. cDNA preparation from whole embryo RNA.

Concentrations of RNA samples were established using a NanoDrop™ 1000 spectrophotometer (Thermo Scientific™). To obtain cDNA, VERSO™ kits were used, in which 4 µl 5X buffer, 2 µl RNA primer, 1 µl RT enhancer, 1 µl enzyme mix and 3 µl dH₂O were added to 2.5 µl of RNA diluted to 500ng/reaction. Samples were then incubated at 42°C for 30 minutes followed by 95°C for 15 minutes. 40 µl water was then added to each reaction to make 5 ng/µl.

2.2.1.14. qRT-PCR.

qRT-PCR was set up using cDNA obtained from whole embryo RNA for required experimental conditions. A 384 well plate was set up, with 1 μ l cDNA, 10 μ l TaqMan PCR Master Mix, 8 μ l dH₂O and 1 μ l primer per well. Samples were run using an Applied Biosystems 7900 Real-Time PCR machine and analysed using Applied Biosystems SDS 2.4 and SDS RQ Manager software. Expression data was exported to Excel and analysed in GraphPad Prism

2.2.2. Small molecule inhibition.

Small molecules were used to inhibit gene function or pathways. All small molecule inhibition occurred via immersion of zebrafish embryos in E3 medium (unless otherwise stated) containing the molecule in solution. The following concentrations and incubation times were used.

Thapsigargin	5 μ M	30 minutes
2-APB	100 μ M	2 hours
BAPTA-AM	500 μ M	3-6 hours
DAPT	100 μ M	12 hours
AV951	0.5 μ M	1 hour
Latrunculin B	397 μ M	1 hour
SKF96365	50 μ M	3 hours
TRPV4 Antagonist III	100 μ M	3-5 hours

2.2.3. Genetic Manipulation.

2.2.3.1. Morpholino knockdown.

Morpholino knockdown was performed by microinjection into 1-cell stage zebrafish embryos. All morpholinos were injected at 2ng/embryo. Morpholinos used are listed in Table 2.3. This study utilises novel *tmem33* morpholinos and a previously published *pkd2* morpholino (Sun, 2004). All morpholinos were synthesised by Gene Tools LLC.

2.2.3.2. TALEN generation of *tmem33^{sh443}*.

The mutant zebrafish line, *tmem33^{sh443}*, was generated prior to my joining the lab by Dr. Robert Wilkinson. TALENs were designed against to target an EcoNI site at the following sequence 5'- cttcctggcccaggctt-3'. TALENs were assembled using the Golden Gate TALEN and TAL Effector Kit (Addgene, MA, USA) (Cermak et al., Voytas, Nuc. Acids Res 2011) to generate the pTmem33Tal1L&R plasmids, which were transcribed and injected into zebrafish embryos. To genotype, gDNA was extracted from individual embryos which was analysed by PCR amplification of the TALEN target region, subject to EcoNI digestion. Adult founders were identified by fin clip in the same way.

2.2.3.3. CRISPR mutagenesis and screening of gRNAs.

To perform CRISPR mutagenesis, gRNAs were first designed to the coding sequence of genes, targeting a restriction enzyme to enable identification of mutant embryos via PCR (see 2.1.1.1) and restriction digest of extracted DNA (see 2.2.1.5). gRNAs were generated by *in vitro* transcription using a T7

MEGashortscript™ Kit. Cas9 protein was obtained from Sigma-Aldrich and an injection mix of gRNA and Cas9 protein was prepared, using 1 ng of gRNA and 200pg of Cas9 protein per nl. 1 nl was injected into single-cell stage embryos, which were raised until 1dpf. DNA was extracted from potential mutants (see 2.2.1.10) and PCR using specific primers was performed. Following this, PCR products were digested with specific restriction endonucleases to determine whether a mutation had been produced.

2.2.3.4. CRISPR interference.

CRISPR interference gRNAs and dCas9 were generated by *in vitro* transcription using a T7 MEGashortscript™ Kit and a T3 mMACHINE™ Kit (Invitrogen), respectively, following the manufacturer's guidelines. CRISPR interference was performed by microinjection of gRNAs and dCas9 into 1-cell stage zebrafish embryos. dCas9 was injected at 250-500 pg/embryo and gRNAs were injected at 500-1000 pg/embryo. For gRNA sequences, see Table 2.3.

2.2.3.5. Transient tissue-specific CRISPR interference.

Transient tissue-specific CRISPR interference utilised gRNAs synthesised as in CRISPR interference (described above). gRNAs were injected into 1-cell stage zebrafish embryos at 500-1000 pg/embryo alongside Tol2 mRNA at 50-100 pg/embryo and plasmid DNA at 25-50 pg/embryo. The plasmids used were either *fli1a:dCas9;cryaa:CFP* or *enpep:dCas9;cryaa:CFP*.

2.2.3.6. Stable tissue-specific CRISPR interference.

For CRISPR interference in stable dCas9-expressing embryos, gRNAs were microinjected into 1-cell stage zebrafish embryos at 500-1000 pg/embryo, when using gRNAs transcribed in the lab (see CRISPR interference) or at 50 pg/embryo when using commercial tracrRNA and crRNAs (Sigma-Aldrich).

2.2.4 Hybridisation and Immunohistochemistry.

2.2.4.1. *In situ* hybridisation probe synthesis.

RNA probes for *in situ* hybridisation were generated by *in vitro* transcription. Probes were transcribed from either linearised plasmids or directly from amplified PCR products. 1 µg of linearised plasmid or PCR product was used along with 2 µl DIG-UTP labelling mix, 4 µl 5x transcription buffer, 0.5 µl RNase inhibitor and 1 µl of appropriate polymerase. The reaction was made up to 20 µl with dH₂O.

This reaction was incubated at 37°C for two hours before addition of 1 µl of DNase I, incubated at 37°C for 15 minutes, which is stopped by the addition of 1 µl of EDTA. 80 µl of deionised water was added to the reaction and vortexed, which was precipitated by addition of 33 µl of 10M NH₄Ac and 350 µl of ice cold ethanol and incubating at least 2 hours at -20°C. Following this, the reaction was centrifuged for 30 minutes at 4°C before removal of supernatant which was washed with 70% ethanol, centrifuged for 15 minutes at 4°C. The pellet was resuspended in 20 µl deionised water and stored at -20°C.

2.2.4.2. Chromometric in situ hybridisation.

Prior to *in situ* hybridisation, embryos were selected at different time points and under different conditions (mutants, morphants, etc.) and fixed in 4% PFA in PBS at 4°C overnight. Fixed embryos were then dehydrated sequentially into methanol.

To begin the *in situ* hybridisation, embryos stored in methanol were rehydrated sequentially into PBS Tween, followed by 4 x 5 minute washes in PBS Tween is required. Following this, embryos were washed in 50% PBS Tween: 50% Hybe+/+ solution for 5 minutes and pre-hybridised in Hybe +/+ solution for 1 hour at 65°C. Hybe+/+ was replaced with Hybe+/+ solution containing 1:200 dilution of the required probe and left overnight at 65°C.

The next day, the probe was removed and replaced in storage at -20°C. Embryos were sequentially washed from 100% Hybe-/- to 0.2X SSC at 65°C, using 10-15 minute wash steps. Embryos were then sequentially washed from 0.2XSSC into 100% MAB at room temperature in 5 minute washes. Embryos were washed into blocking reagent in MAB for one hour at room temperature, rocking, before being replaced by blocking solution (Roche 11096176001) in MAB containing 2% anti-DIG antibody overnight at 4°C.

Embryos were removed from 4°C incubation and incubated at room temperature for one hour, rocking. They were then washed in MAB Tween for 8 x 15 minutes; equilibrated with developing buffer, BCLIII, for 3 x 5 minutes at room temperature.

To stain, this was replaced with 50% BCLIII: 50% BM Purple for as long as required. To stop reaction, embryos were refixed in PFA for 20 minutes at room temperature, washed 3 x 5 minutes in PBS tween and transferred into 80% glycerol for storage.

2.2.4.3. Fluorescent *in situ* hybridisation with antibody co-stain.

Fluorescent *in situ* hybridisation to detect gene expression alongside co-staining for fluorescent proteins was performed to determine co-expression of genes. The *in situ* was performed as in colorimetric *in situ* until addition of antibodies in MAB blocking solution, at which point anti-DIG POD (Roche 1 207 733) at 1:500 dilution and the primary antibody (anti-GFP (Torrey Pines Biolabs), 1:1000 dilution) were added and rocked overnight at 4°C.

The next day embryos were washed for 7 x 15 minutes in MAB Tween and once in PBS Tween in the dark. 100 l of Fluorescein tyramide (Cy3) were added and incubated for 30 minutes. Embryos were briefly washed into PBS Tween and then washed in PBS Tween for 4 x 30 minutes. Embryos were washed into TNT solution and stained for 3 hours in the dark, before being washed into Slowfade® Antifade solution (Thermo Fisher S2828) for long term storage.

2.2.4.4. Immunohistochemistry.

Before beginning immunohistochemistry, embryos were fixed and dehydrated sequentially into methanol, then quenched using 3% H₂O₂ and stored in methanol. To begin staining, embryos were rehydrated into PBS Tween and

permeabilised by incubating in dH₂O on ice for 45 minutes and then TBSTw/1% TritonX100 on ice for 30minutes. Embryos were washed in Citrate buffer and heated to 98°C for 20 minutes and then cooled. Embryos were then washed into PBS Tween five times before washing into blocking solution (PBSTw/0.5%TritonX100/10%DMSO/1%goat serum/5%BSA). Finally, embryos were washed in blocking solution containing primary rabbit antibody against phospho-protein and 1/500 mouse anti-GFP antibody (Santa Cruz, sc-9996) and left overnight.

Samples were washed in PBS Tween five times and then washed in blocking solution containing 1/1000 anti-rabbit IgG-HRP and 1/500 anti-mouse IgG-Alexa488 at 4°C for O/N.

Samples were washed in PBS Tween five times and then washed in PBS once. Samples were then washed into 1/50 Tyramide-Cy3 in 1x amplification diluent for three hours in the dark. Samples were finally washed in TBSTw/0.1%TritonX100 overnight to wash out background staining and stored in 4% PFA in PBS prior to imaging.

2.2.5 Microscopy.

2.2.5.1. Light microscopy.

Standard light microscopy was used when analysing *in situ* hybridisation samples. Embryos were imaged using a Leica M165 FC microscope and analysed using LASv4.3 software.

2.2.5.2. Fluorescent microscopy.

For image acquisition, embryos were first anaesthetised in E3 medium containing tricaine. Imaging and analysis of samples using fluorescence was performed using two microscopes during this study, a Leica M165 FC microscope, on which samples were analysed using LASv4.3 software and a Zeiss AXIO Zoom V16, on which samples were analysed using Zen Blue software.

2.2.5.3. Confocal Microscopy.

For confocal microscopy, embryos were anaesthetised using tricaine and mounted in 1% agarose, over which E3 medium containing tricaine was placed, to ensure samples remained anaesthetised. Still images were taken using an Ultraview VOX confocal spinning disc system (Perkin Elmer) and Zeiss LSM880 with Airyscan. Images were analysed using Volocity®V5.3.2 or ZEN software (Zeiss).

2.2.5.4. Light sheet microscopy.

For light sheet microscopy, anaesthetised embryos were immobilised using 1 % agarose. Embryos were mounted in a glass capillary and held in place by agarose. Embryos were suspended in the imaging chamber by protrusion of the agarose cylinder from the capillary. The chamber contained a mixture of E3 and tricaine, to ensure embryos remained anaesthetised throughout the imaging process. A Z.1 Light Sheet (Zeiss) was used for image acquisition and images were processed using ZEN Black software (Zeiss).

2.2.6 Quantification and statistical analysis.

2.2.6.1. Quantification of aberrant vascular development.

Aberrant vascular development was quantified at two stages during development; at 30 hpf and 53 hpf. At 30 hpf, aberrant vascular development was defined as intersegmental vessels which displayed migrational delay compared to others within the same embryo. At 53 hpf, aberrant vascular development was defined as either delayed/stalled intersegmental vessels, gaps/maldeveloped sections in dorsal longitudinal anastomotic vessel development or formation of collateral vessels. In both cases, the number of abnormalities was quantified and number per embryo was determined.

2.2.6.2. Quantification of calcium oscillations.

In order to determine the frequency of endothelial calcium oscillations, 5-10 minute time-lapse movies of endothelial cells in both *Tg(fi1a:gff)ubs3; Tg(uas:GCaMP7a)sh392* and *Tg(fi1a:gff)ubs3;Tg(uas:GCaMP7a)sh393* embryos were acquired, using light sheet microscopy. The number of calcium peaks in endothelial tip cells was counted and divided by the length of the time-lapse and again by the number of tip cells present in the time-lapse. A ratio of calcium oscillations per minute, per tip cell was obtained.

To obtain the frequency of pronephric calcium signalling oscillations, the entire pronephric tubule was imaged over the course of 8 hours. Regions of recurrently oscillating cells were observed and counted and the absolute number of

oscillations observed during the timecourse was quantified. A ratio was obtained as in endothelial calcium signalling measurement.

2.2.6.3. Quantification of filopodia.

Images of endothelial filopodia were obtained using light-sheet microscopy, taking high-resolution images of *Tg(fli1a:LifeACT-mClover)sh467* embryos. Endothelial filopodia numbers and lengths were quantified using Fiji (ImageJ). The number of cellular extensions was determined and the length in μm was measured.

2.2.6.4. Quantification of glomerular area.

Images of glomeruli in *Tg(-26wt1b:EGFP)li1* were obtained using standard fluorescent microscopy. Embryos were anaesthetised in E3 medium containing tricaine and mounted in methylcellulose so that they could be imaged dorsally. Images captured were then used to quantify glomerular area on Fiji (ImageJ) by measuring around the glomerulus and comparing morphants to controls.

2.2.6.5. Statistical analysis.

All statistical analysis employed two-tailed tests and are described in figure legends. All data were subjected to D'Agustino's normality test before performing statistical analysis. Parametric tests, such as independent t-tests, were performed on data found to be parametric and non-parametric equivalents (Mann-Whitney U-tests) were performed on non-parametric data. All error bars display the mean and standard deviation except for qPCR error bars, which display the mean and standard error of the mean. Each experiment was repeated at least three times,

though not all data is necessarily shown. P values, unless exact value is listed, are as follows: *= <0.05 , **= <0.01 , ***= <0.001 , ****= <0.0001 . F-values, t-values and degrees of freedom are listed in individual figure legends. Statistical analysis was performed using GraphPad Prism.

Power calculations were performed *a priori* using a β -value of 0.8 to determine necessary group sizes.

2.2.6.6. Scale Bars.

Scale bars have been included in figures, where appropriate. The following scales have been used: 100 μm , where four or more segmental arteries or intersegmental vessels have been shown; 5 μm , where either one or two segmental arteries are shown; 1 μm , where subcellular localisation is shown; 200 μm where kidney glomeruli are measured; 50 μm , where pronephric tubules are shown.

3 Tmem33 is a novel regulator of endothelial and kidney calcium signalling during angiogenesis and kidney development

3.1 Introduction

Data from my collaborator Eric Honoré indicated TMEM33 interacts with PKD1 in mice and can increase the likelihood that PKD2 functions as a calcium channel in a lipid bilayer reconstitution assay. This suggests *tmem33* may regulate calcium signalling. The role of TMEM33 during blood vessel formation or indeed during embryonic development generally remains unknown.

Currently very little is understood regarding *tmem33* function. Previous studies have taken place using yeast cells or human cell culture and have implicated *tmem33* function in a variety of processes linked to endoplasmic reticulum homeostasis, including interaction with the unfolded protein response, regulation of endoplasmic reticulum morphology and regulation of the actin cytoskeleton and nuclear pore during cell division (Floch et al., 2015; Sakabe et al., 2015; Urade et al., 2014; Zhang and Oliferenko, 2014; Zhang et al., 2010). Here I present the first characterisation of *tmem33* function during angiogenesis and the first characterisation of *tmem33* function in a multicellular organism. I utilise morpholino knockdown to show that *tmem33* is required for endothelial calcium signalling and the regulation of endothelial F-actin, which supports previous data from the lab indicating that *tmem33* knockdown impairs angiogenic migration. Together, these data show that *tmem33* does indeed regulate angiogenesis in zebrafish.

3.2 TMEM33 displays amino acid conservation from teleost fish to mammals.

Human studies predict that TMEM33 protein has a 3-transmembrane structure and resides in the ER membrane (Sakabe et al., 2015) (Figure 3.1 A). I performed protein sequence analysis to determine similarities in TMEM33 sequence throughout evolution. Regions of conserved sequence may suggest regions of functional importance. I observed conservation at the amino acid level, from teleost fish through to amphibians, birds and mammals (Figure 3.1B). The three predicted transmembrane domains within TMEM33 comprise 21 amino acids each (Sakabe et al., 2015) (Figure 3.1 B, blue boxes). Stretches of approximately 20 hydrophobic amino acids anchor the transmembrane domains in the ER membrane by forming alpha helices (reviewed in De Marothy and Elofsson, 2015). In each of the three predicted transmembrane domains of TMEM33, 17 of the 21 (81%) amino acids are hydrophobic, suggesting these regions are likely to form transmembrane domains (Figure 3.1 B).

The conserved predicted transmembrane domains display the greatest amino acid homology, particularly the third transmembrane domain, wherein the mammalian and teleost sequences are identical (Figure 3.1 B). The first and second transmembrane domains differ by six and two amino acids, respectively. The high degree of conservation between predicted transmembrane domains suggests they are important for Tmem33 function.

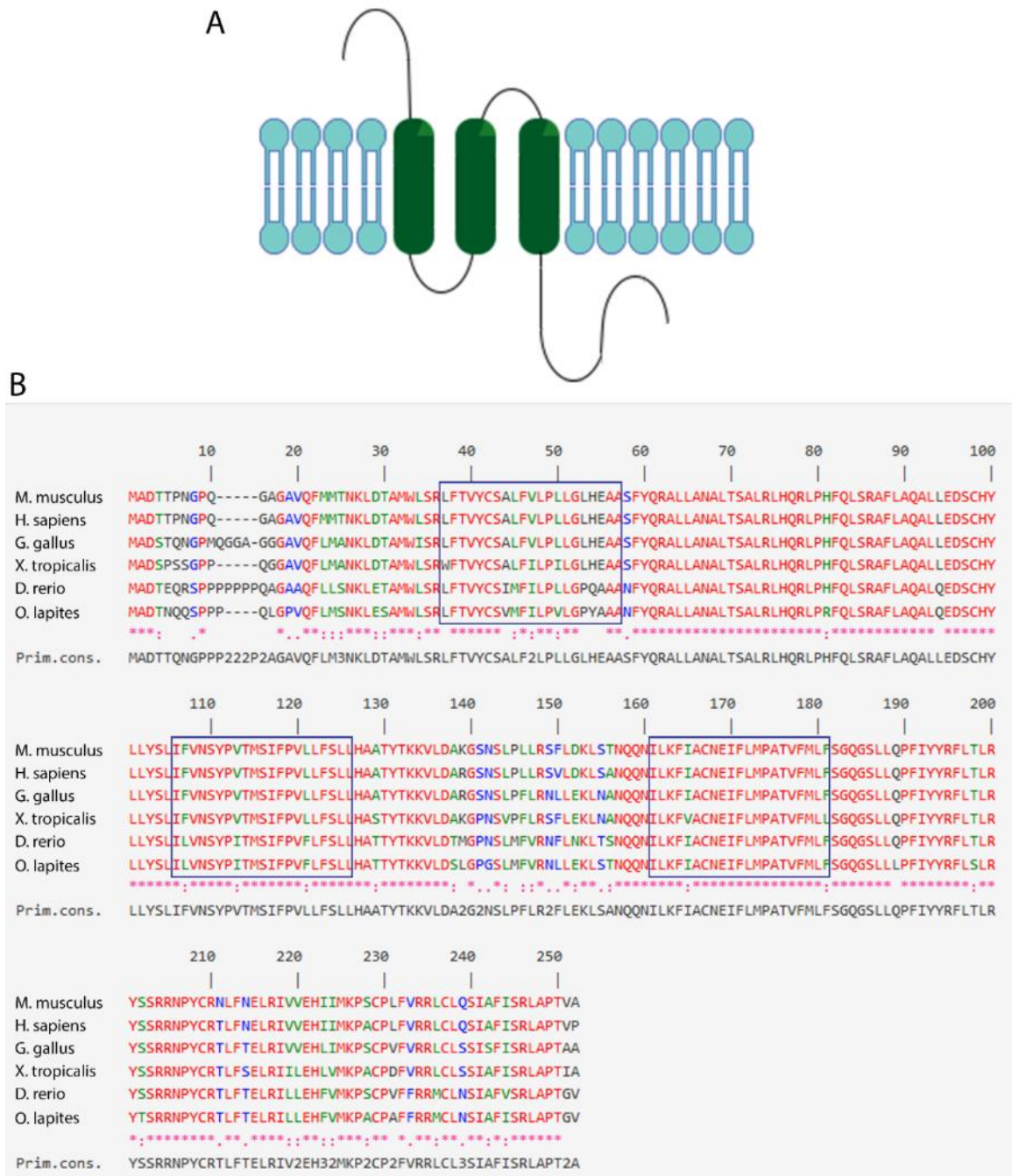


Figure 3.1 Protein alignment of TMEM33 across species shows conservation of transmembrane domains. (A) TMEM33 predicted protein structure, with an N-terminal and C-terminal tails located on either side of the membrane. **(B)** TMEM33 protein sequence alignments demonstrate a high degree of conservation between teleost fish, medaka (*O. latipes*) and zebrafish (*D. rerio*), amphibians (*X. tropicalis*), birds (*G. gallus*), mice (*M. musculus*) and humans (*H. sapiens*). Blue boxes indicate transmembrane domains.

3.2 *tmem33* mRNA is expressed in the developing kidney and vasculature.

Previous work by Dr. Robert Wilkinson had shown that *tmem33* was expressed in the developing kidney (Figure 1.2). I observed that *tmem33* expression was ubiquitous consistent with earlier experiments (see Figure 1.2), but its expression was enriched within the pronephric tubule (Figure 3.2 B, yellow arrowhead). Developing SeAs labelled by *fli1a:eGFP* fluorescence (Figure 3.2 A, white arrowheads) displayed colocalisation of expression with *tmem33* (Figure 3.2 A-C, white arrowheads), suggesting *tmem33* is expressed in endothelial cells.

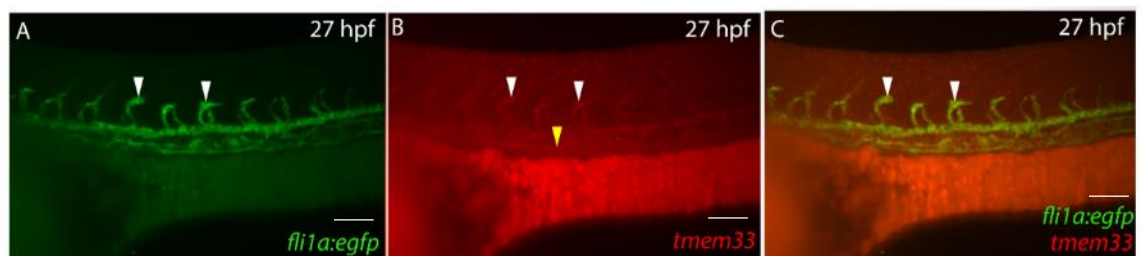


Figure 3.2 *tmem33* is expressed in the endothelium during zebrafish embryonic development. (A-C) 27 hpf *Tg(fli1a:EGFP)y1* embryo stained using an anti-GFP antibody. GFP is expressed in developing blood vessels (white arrowheads). Fluorescent tyramide *in situ* hybridisation has been performed for *tmem33* expression, which is observed in developing blood vessels (white arrowheads) and in the developing kidney (yellow arrowhead).

3.3 *tmem33-eGFP* mRNA localises to the endoplasmic reticulum and nuclear pore within zebrafish endothelial cells.

TMEM33 protein has been shown to localise to the ER membrane in MCF-7 and HeLa cells (Chadrin et al., 2010; Floch et al., 2015; Sakabe et al., 2015). I therefore overexpressed *tmem33-eGFP* mRNA (See Chapter 2.1.5) in *Tg(fli1a:DsRedEx2)* (See Chapter 2.2.1.4) to determine the subcellular localisation of *tmem33* in zebrafish ECs.

Following injection of *tmem33-eGFP*, the reporter was expressed in locations strongly suggestive of the ER (Figure 3.3 A-C, white arrowheads) and nuclear envelope (Figure 3.3 A-C, blue arrowheads). When co-expressed in an endothelial reporter that expresses DsRed, this pattern of expression was observed in both non-endothelial (*ds-Red* -ve) (Figure 3.3 A-C) and endothelial (*ds-Red* +ve) cells (Figure 3.3 D-F). These data therefore suggest zebrafish *tmem33* localises to the ER membrane and nuclear envelope, as in other systems (Chadrin et al., 2010; Floch et al., 2015; Sakabe et al., 2015).

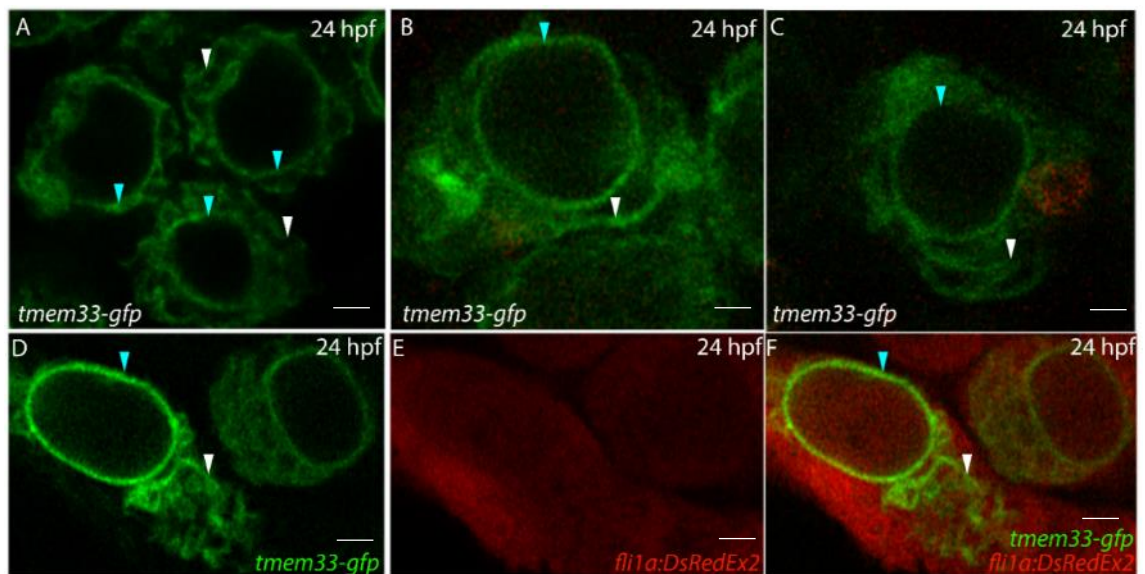


Figure 3.3 *tmem33-eGFP* appears to be expressed in the ER and nuclear envelope. **(A-C)** *tmem33-gfp* localised to the ER (white arrowheads) and nuclear envelope (blue arrowheads) in non-endothelial cells at 24 hpf in *Tg(fli1aDsRedEx2)* embryos. **(D-F)** *Tg(fli1aDsRedEx2)* positive endothelial cells displayed *tmem33-gfp* expression in the nuclear envelope (blue arrowheads) and ER (white arrowheads).

3.4 *Tg(fli1a:gff)ubs3;Tg(uas-GCaMP7a)sh392* is a genetically encoded calcium indicator (GECI), allowing visualisation of calcium signalling in endothelial cells in real-time and modulation of calcium signalling induces changes in *Tg(fli1a:gff)ubs3;Tg(uas:GCaMP7a)sh392* fluorescence levels.

tmem33 localises to the endoplasmic reticulum (Figure 3.3). The ER is the main site of intracellular Ca²⁺ storage, via which calcium signalling occurs (Bootman et al., 2002a). I hypothesised that *tmem33* may regulate calcium signalling during angiogenesis. The *Tg(fli1a:gff)ubs3;Tg(uas:GCaMP7a)sh392* and *Tg(fli1a:gff)ubs3;Tg(uas:GCaMP7a)sh393* lines generated by Dr. Wilkinson utilise a modified version of the Gal4-UAS system (Brand and Perrimon, 1993). The GCaMP7a module is a circularly permuted modified GFP, which makes use of calmodulin (CaM) and M13 molecules (Nakai et al., 2001). Under normal cellular conditions, the *Tg(fli1a:gff)ubs3;Tg(uas:GCaMP7a)sh392* and *Tg(fli1a:gff)ubs3;Tg(uas:GCaMP7a)sh393* lines fluoresce with low-level endothelial GCaMP, which increases in fluorescence intensity transiently in the presence of Ca²⁺ ions. During my work a similar transgenic line was published and shown to function in the same manner (Yokota et al., 2015). *Tg(fli1a:gff)ubs3;Tg(uas:GCaMP7a)sh392* embryos displayed greater GCaMP7a fluorescence intensity than *Tg(fli1a:gff)ubs3;Tg(uas:GCaMP7a)sh393* embryos, and were therefore used (unless otherwise stated) in this thesis. I observed transient changes in GCaMP fluorophore fluorescence in real time during angiogenesis, similarly to those reported previously (Yokota et al., 2015), which I termed calcium oscillations.

To determine whether the *Tg(fi1a:gff)ubs3;Tg(uas:GCaMP7a)sh392* transgenic line reports changes in cytosolic Ca²⁺ concentration within endothelial cells, I treated *Tg(fi1a:gff)ubs3;Tg(uas:GCaMP7a)sh392* embryos with small molecule modulators of calcium signalling. Thapsigargin, a SERCA ATPase pump inhibitor (Jones, 1994), was used to induce calcium release from the ER, and 2-aminoethoxydiphenyl borate (2-APB) was used to reduce calcium release from the ER. 2-APB blocks IP₃ receptors and inhibits TRP channel family members (Bootman et al., 2002b; Diver et al., 2001).

Thapsigargin increased GCaMP fluorescence levels in *Tg(fi1a:gff)ubs3;Tg(uas:GCaMP7a)sh392* embryos (Figure 3.4 B, D), indicating an increase in cytosolic Ca²⁺ concentration. However, Thapsigargin induces Ca²⁺ release from the ER while simultaneously blocking uptake and this reduced EC calcium oscillations (Figure 3.4 E). 2-APB treatment decreased both overall fluorescence levels (Figure 3.4 C, D) and the number of calcium oscillations (Figure 3.4 E). Furthermore, while 2-APB treatment reduced calcium oscillations, it also reduced the intensity change per oscillation, suggesting that fewer calcium ions were released from the ER compared to controls (Figure 3.4 F). These data suggest that *Tg(fi1a:gff)ubs3;Tg(uas:GCaMP7a)sh392* transgenic embryos accurately report fluctuations in endothelial calcium signalling induced by small molecule modulators of calcium signalling.

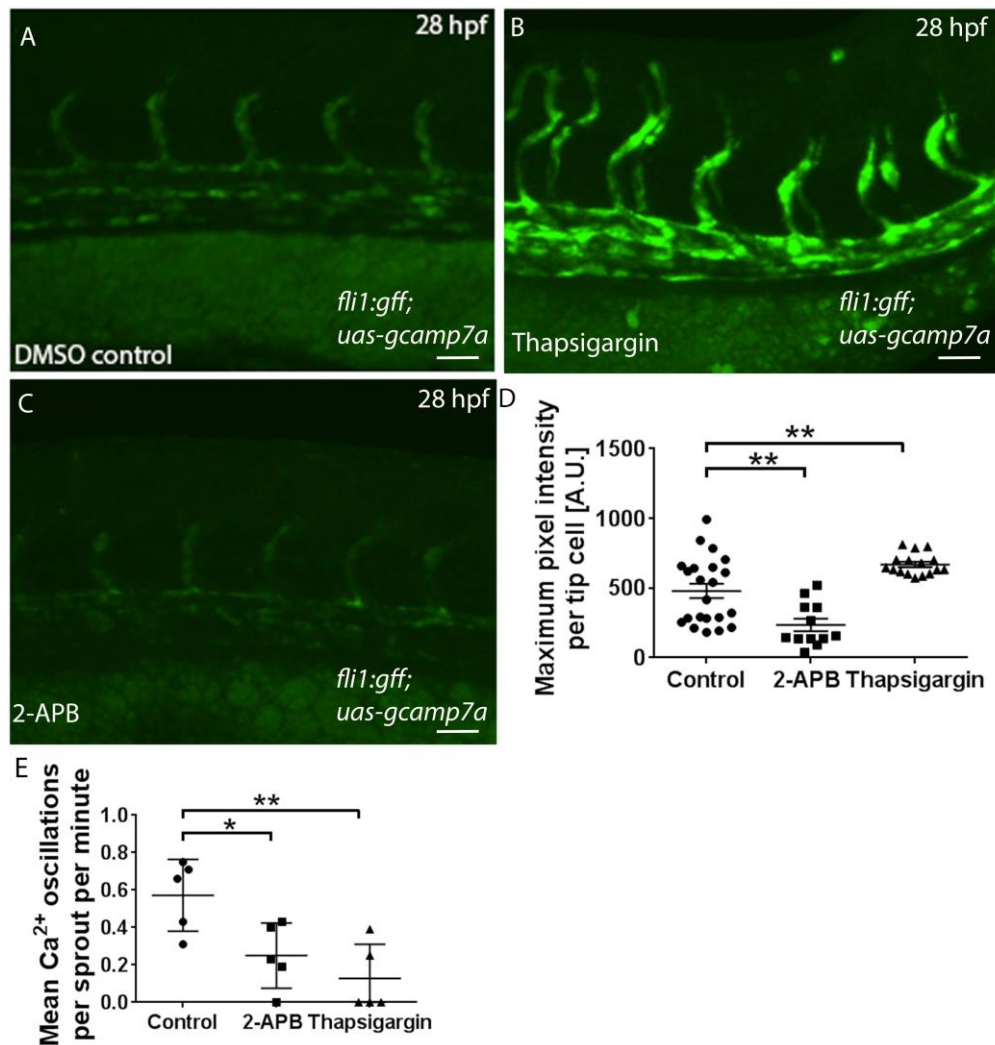


Figure 3.4 *Tg(fi1a:gff)ubs3;Tg(uas:GCaMP7a)sh392* fluorescence can be modulated by modulating calcium signalling. **(A)** *Tg(fi1a:gff)ubs3;Tg(uas:GCaMP7a)sh392* embryos display EC GCaMP7a fluorescence. **(B)** Thapsigargin treatment increased EC GCaMP7a fluorescence in *Tg(fi1a:gff)ubs3;Tg(uas:GCaMP7a)sh392* embryos. **(C)** 2-APB decreased GCaMP7a fluorescence in *Tg(fi1a:gff)ubs3;Tg(uas:GCaMP7a)sh392* embryos. **(D)** 2-APB and Thapsigargin modulated GCaMP7a fluorescence in endothelial cells, with 2-APB reducing GCaMP7a fluorescence and Thapsigargin increasing fluorescence (One-way ANOVA ** $p < 0.01$). **(E)** 2-APB and Thapsigargin negatively modulated Ca²⁺ oscillation frequency in endothelial cells (One-way ANOVA with *post-hoc* Dunnett's test * $p < 0.05$, ** $p < 0.01$). **(F)** 2-APB treatment reduced the mean change in GCaMP fluorescence per oscillation per embryo (unpaired t-test, *** $p < 0.001$).

3.5 VEGF signalling is required for endothelial calcium oscillations.

VEGF signalling induces downstream calcium oscillations (Yokota et al., 2015; Zadeh et al., 2009) and Notch signalling (Siekmann and Lawson, 2007; Williams et al., 2005) in tip cells during angiogenesis. I therefore examined the effect of modulating VEGF and Notch signalling on calcium signalling. Tivozanib (AV-951) is a VEGF inhibitor which antagonises the receptor tyrosine kinase activity of all VEGF receptors (Kang et al., 2013). I treated 26hpf embryos with AV951 or control and quantified GCaMP fluorescence in *Tg(fi1a:gff)ubs3;Tg(uas:GCaMP7a)sh392* embryos. AV951 caused a cessation of angiogenesis within 30 minutes of treatment, causing SeAs to halt mid-migration (Figure 3.5 C). Furthermore I observed a reduction of calcium oscillations (Figure 3.5 C, D). DAPT (N-[N-(3,5-Difluorophenacetyl)-L-alanyl]-S-phenylglycine t-butyl ester) is a γ -secretase inhibitor, which inhibits Notch signalling (Geling et al., 2002). DAPT treatment did not disrupt primary sprouting angiogenesis but caused an increase in both frequency and amplitude of calcium oscillations (Figure 3.5 E, F, I). Similarly, overexpression of *vegfr-165* mRNA increased calcium oscillation frequency (Figure 3.5 G, H, J).

These data suggest that calcium oscillations during SeA formation are dependent on VEGF signalling. Consistent with this, inhibition of Notch signalling, which normally antagonises VEGF signalling within angiogenic tip cells (Hellström et al., 2007; Suchting et al., 2007), increased calcium oscillation frequency (Figure 3.5).

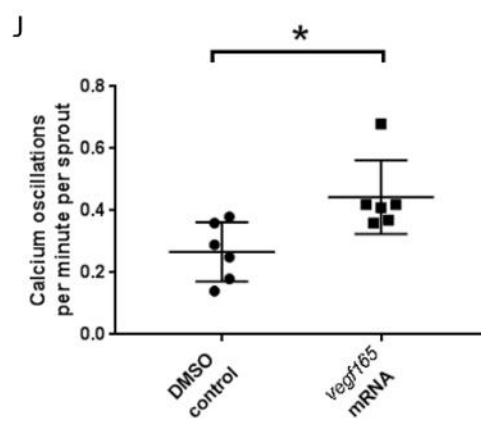
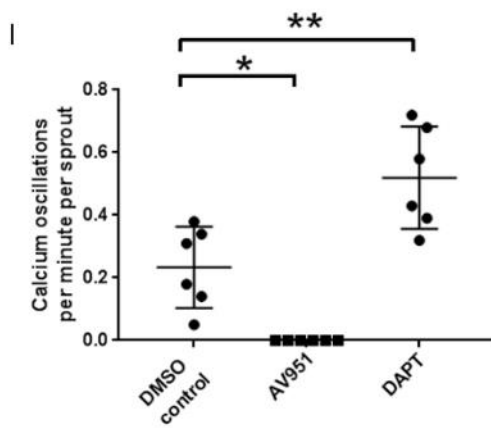
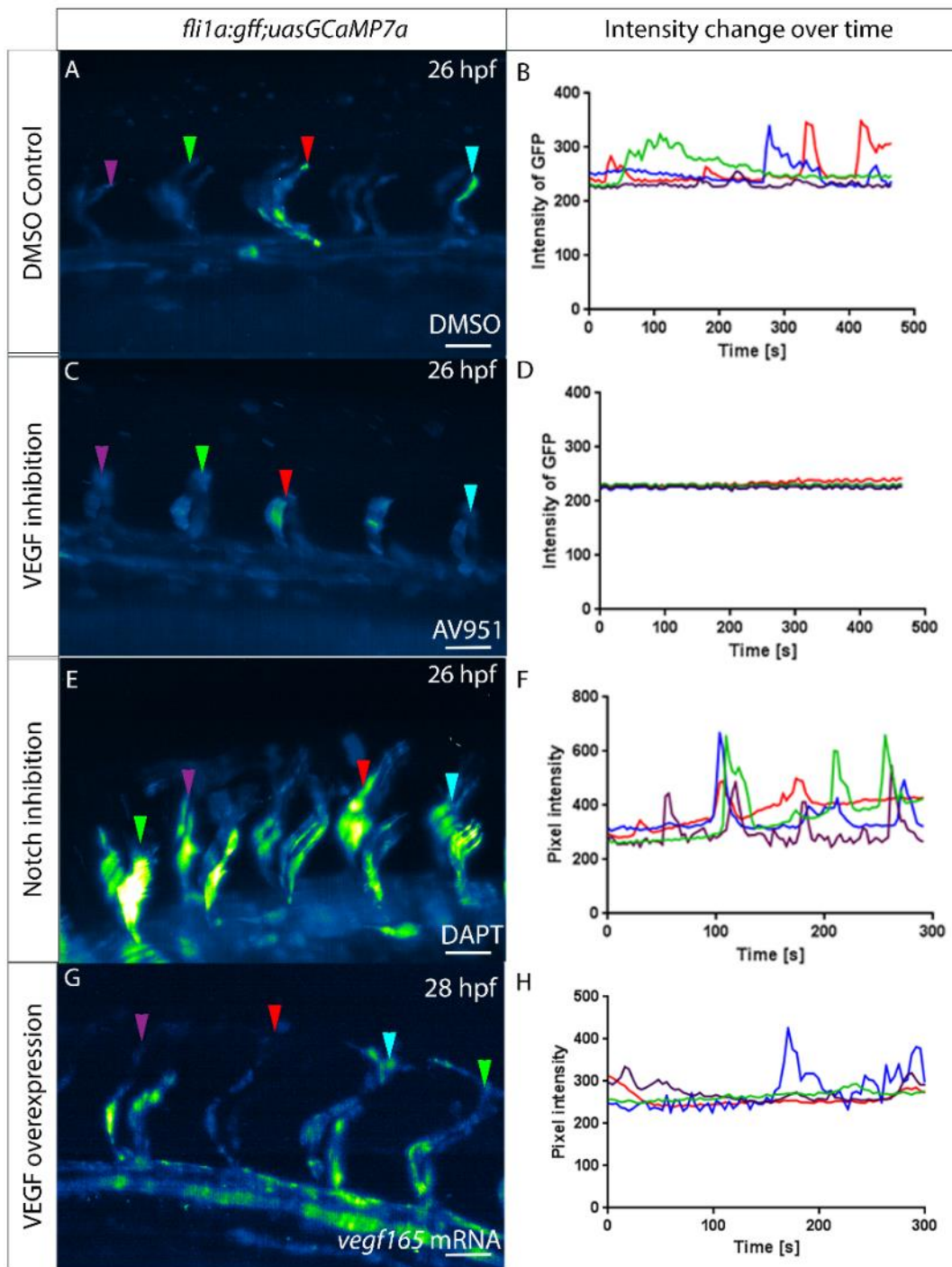


Figure 3.5. Modulation of VEGF and Notch signalling modify frequency of endothelial Ca²⁺ oscillations. (A) Intensity projection over time are shown. Control *Tg(fi1a:gff)ubs3;Tg(uas:GCaMP7a)sh392* embryos display changes in GCaMP7a fluorescence intensity over time in ECs. Scale bars 50 μ m. (B) Change in fluorescence plotted against time in n=4 EC tip cells in control embryos. Coloured traces correspond to arrowheads in (A). (C) *Tg(fi1a:gff)ubs3;Tg(uas:GCaMP7a)sh392* embryos treated with 500nM AV951 treatment abrogates Ca²⁺ oscillations in EC tip cells in representative *Tg(fi1a:gff)ubs3;Tg(uas:GCaMP7a)sh392* embryo. Scale bars 50 μ m. (D) Change in GCaMP7a fluorescence intensity over time in n=4 EC tip cells in representative AV951-treated embryo. Coloured traces correspond to arrowheads in (C). (E) DAPT treatment increases GCaMP7a fluorescence intensity over time and induces ectopic Ca²⁺ oscillations in stalk cells. Scale bars 50 μ m. (F) Change in GCaMP7a fluorescence over time in n=4 EC tip cells in representative DAPT-treated embryo. Coloured traces correspond to arrowheads in (E). (G) Overexpression of *vegfa*₁₆₅ mRNA (400pg) increases GCaMP7a fluorescence intensity and ectopic Ca²⁺ oscillations in stalk cells and the DA in *Tg(fi1a:gff)ubs3;Tg(uas:GCaMP7a)sh392* embryos. Scale bars 50 μ m. (H) Change in fluorescence over time in n=4 EC tip cells in representative following *vegfa*₁₆₅ overexpression. Coloured traces correspond to arrowheads in (G). (I) Frequency of Ca²⁺ oscillations per sprout per minute is significantly decreased by AV951 treatment and significantly increased by DAPT treatment (One-Way ANOVA with *post-hoc* Dunnett's test, *p<0.05, **p<0.01). (J) Overexpression of *vegfa*₁₆₅ significantly increases Ca²⁺ oscillation frequency per sprout per minute (unpaired t-test, *p<0.05).

3.6 *tmem33* morphants display impaired angiogenesis and reduced endothelial calcium oscillations.

Since Dr. Robert Wilkinson had previously undertaken experiments which showed that *tmem33* knockdown impaired vascular development (Figure 1.4), I sought to quantify this. Therefore, I repeated the experiment and analysed SeA length at 30 hpf and the percentage of anastomosis within the DLAV at 53 hpf. I observed a significant reduction in SeA length in morphants compared to controls at 30 hpf (Figure 3.6 A) and a significant reduction in DLAV anastomosis, indicating impaired angiogenesis, at 53 hpf (Figure 3.6 B).

tmem33 morphants display reduced angiogenesis (Figure 1.4; Figure 3.6). Calcium signalling functions downstream of VEGF signalling *in vitro* (Oike et al., 1994; Vaca and Kunze, 1994; Zadeh et al., 2009) and during angiogenesis in zebrafish (Figure 3.5) (Yokota et al., 2015) and *tmem33* is localised to the ER (Figure 3.3) (Sakabe et al., 2015). I therefore knocked down *tmem33* using morpholinos in *Tg(fi1a:gff)ubs3;Tg(uas:GCaMP7a)sh392* embryos and quantified calcium oscillations. Control embryos displayed transient regions of increased GCaMP intensity over the course of the time-lapse which were reduced in *tmem33* morphants (Figure 3.7 A-D). I quantified the number of calcium oscillations and observed significantly reduced calcium transient frequency in *tmem33* morphants (Figure 3.7 E). Collectively, these observations indicate that *tmem33* knockdown reduces calcium oscillations within endothelial cells, suggesting *tmem33* may promote endothelial calcium signalling through regulation of ER calcium efflux.

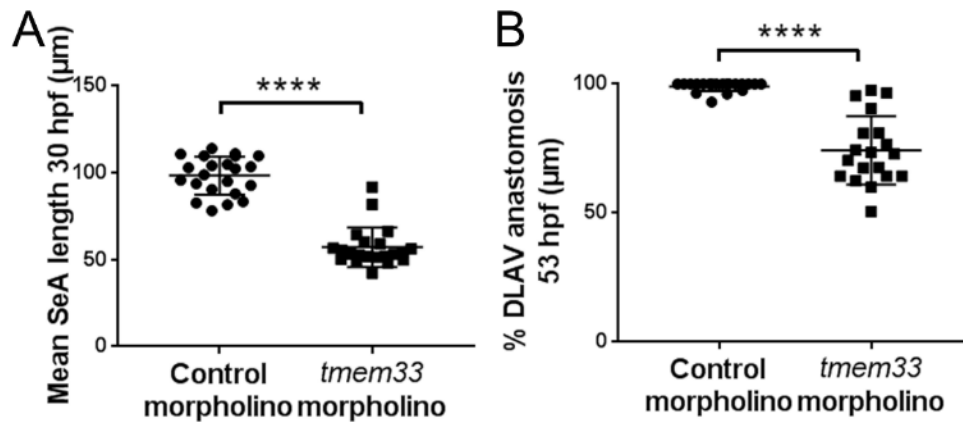


Figure 3.6. *tmem33* knockdown impairs EC migration. (A) *tmem33* morphants display significantly reduced SeA length at 30 hpf (t-test **** $p < 0.0001$. $n = 3$ repeats, 30 embryos total) and **(B)** significantly reduced DLAV continuity at 53 hpf (unpaired t-test **** $p < 0.0001$. $n = 3$ repeats, 27 embryos total).

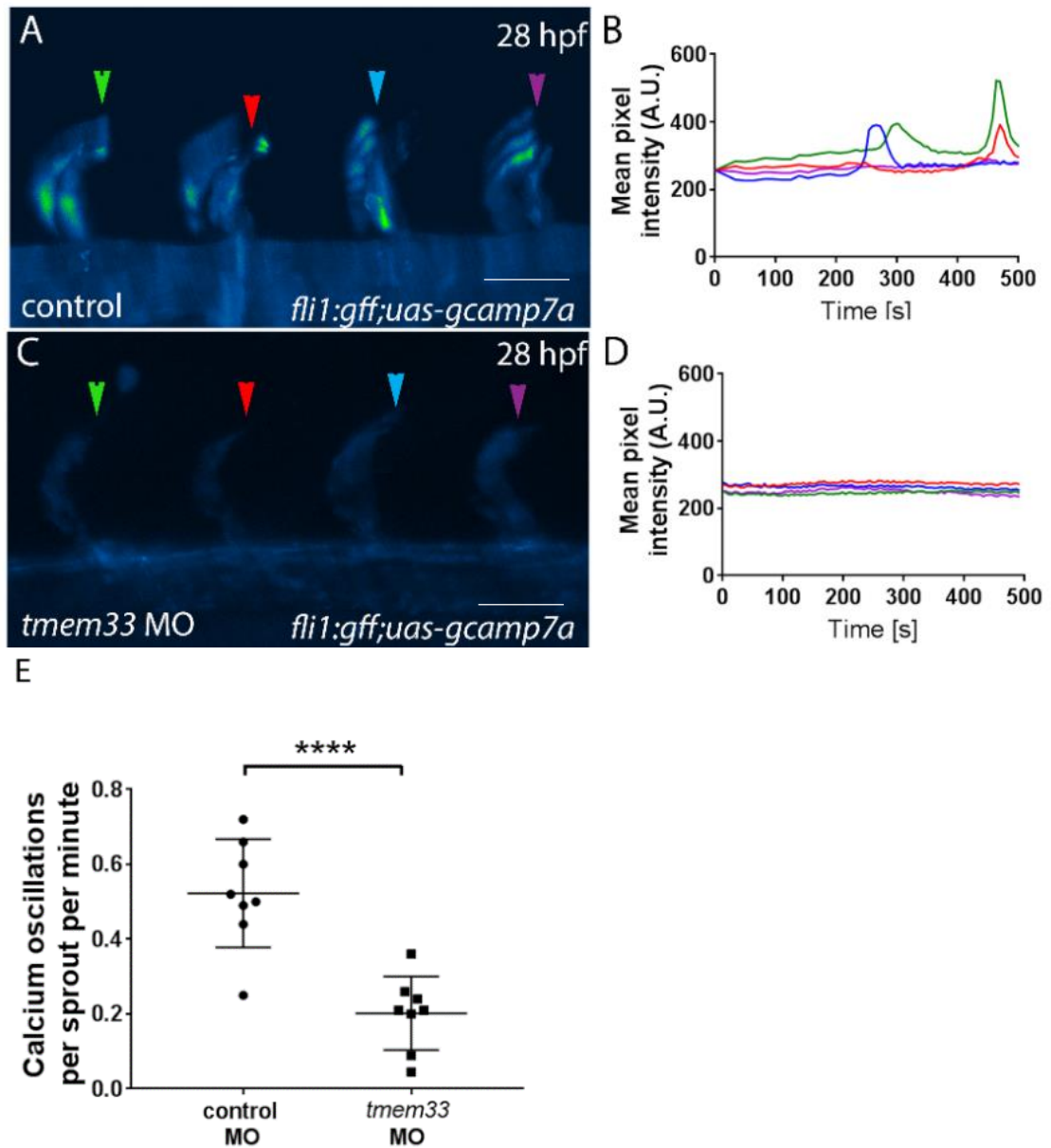


Figure 3.7. *tmem33* knockdown reduces Ca^{2+} oscillations in endothelial tip cells. (A-D) *tmem33* morphants display reduced endothelial Ca^{2+} oscillations. Intensity projections show Ca^{2+} oscillations in both control and *tmem33* morphants, highlighting intensity over duration of the time-lapse. Change in fluorescence over 500s for four SeAs, peak colours correspond to equivalent arrowheads. **(E)** *tmem33* morphants display a significant reduction in Ca^{2+} oscillations when compared to control morphants (unpaired t-test, **** $p < 0.0001$).

3.6.1 Thapsigargin-mediated elevations in cytosolic Ca²⁺ are reduced in *tmem33* morphants

Incubation with Thapsigargin increases cytosolic Ca²⁺ concentration in zebrafish ECs (Figure 3.5). To determine whether reduced calcium signalling observed in *tmem33* morphants was due to reduced calcium efflux from the ER, I treated *tmem33* morphants with Thapsigargin and quantified GCaMP7a fluorescence. In control embryos, Thapsigargin treatment increased displayed a trend towards an increase in GCaMP7a fluorescence intensity in tip cells, but this was not statistically significant (Figure 3.8 A, C). However, Thapsigargin treated controls displayed significantly greater EC tip cell fluorescence intensity compared to *tmem33* morphants treated with Thapsigargin (Figure 3.8 B, C). This indicates that cytosolic Ca²⁺ accumulation did not occur following *tmem33* knockdown, suggesting *tmem33* may promote ER Ca²⁺ release.

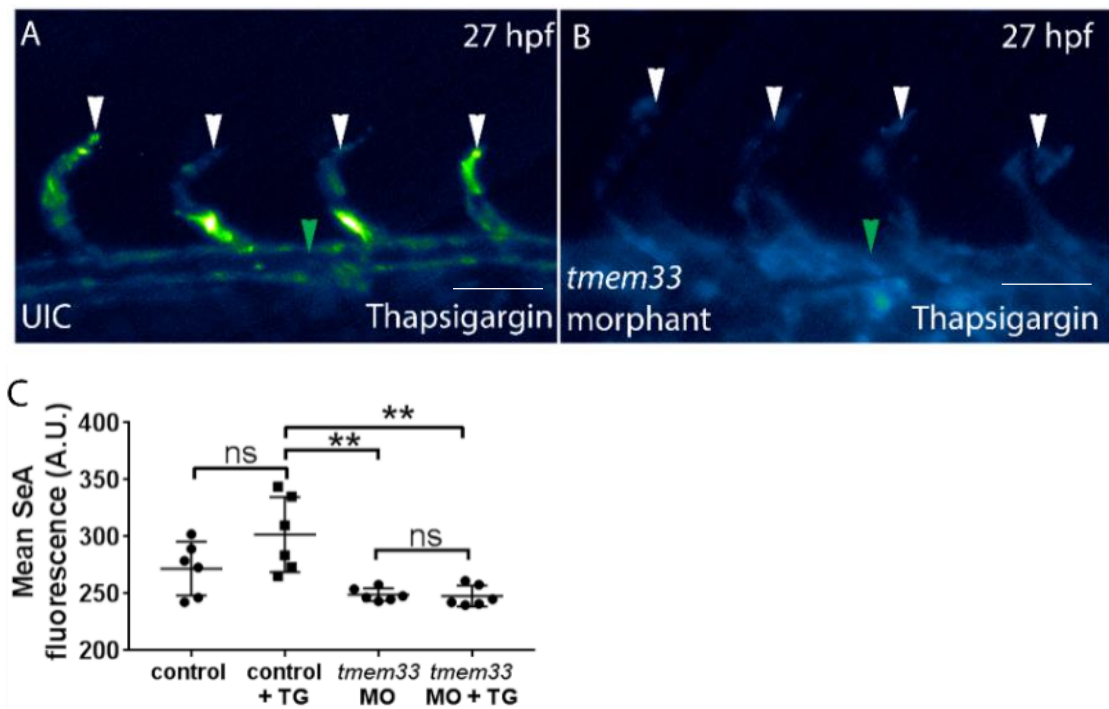


Figure 3.8 *tmem33* morphants do not display Thapsigargin-mediated increases in cytosolic Ca^{2+} . (A-B) *tmem33* knockdown reduces Thapsigargin-mediated Ca^{2+} intensity increase. Intensity projection showing 5 μM Thapsigargin-treated control and *tmem33* morphant embryos. Treatment increases GCaMP7a fluorescence in SeAs (white arrowheads) and the DA (green arrowhead) in uninjected controls, but not in morphants. (C) Thapsigargin increases SeA GCaMP7a fluorescence in controls compared to *tmem33* morphants (One-way ANOVA with *post hoc* Tukey's comparison test $**p < 0.01$).

3.7 *tmem33* morphants display reduced pronephric calcium signalling.

tmem33 is expressed in both the developing vasculature and the developing kidney (Figure 1.2; Figure 3.4) and *tmem33* knockdown induces abnormal glomerular development (Figure 1.5). I therefore examined whether *tmem33* is required for calcium oscillations in the developing kidney.

To analyse kidney calcium oscillations, the entire pronephric tubule was imaged over 8 hours. I measured the total number of calcium oscillations and observed

regions in which recurrent calcium oscillations occurred, similar to previous analysis (Aylin Metzner, PhD Thesis, 2016). I knocked *tmem33* down in *Tg(enpep:gff)ubs3;Tg(uas:GCaMP7a)* embryos (Aylin Metzner, PhD Thesis, 2016), where GCaMP7a is driven by a kidney specific promoter (Seiler and Pack, 2011) and observed that pronephric GCaMP7a fluorescence was significantly reduced in *tmem33* morphants (Figure 3.9 A, B). Calcium oscillations in the Kidney were less frequent than in the developing SeAs (Aylin Metzner, PhD Thesis, 2016). *tmem33* morphants displayed reduced oscillation frequency per hour (Figure 3.9 C) and a reduction in the number of clusters of cells which displayed recurrent oscillations (Figure 3.9 D), suggesting that *tmem33* is required for calcium oscillations in both endothelial and kidney cells.

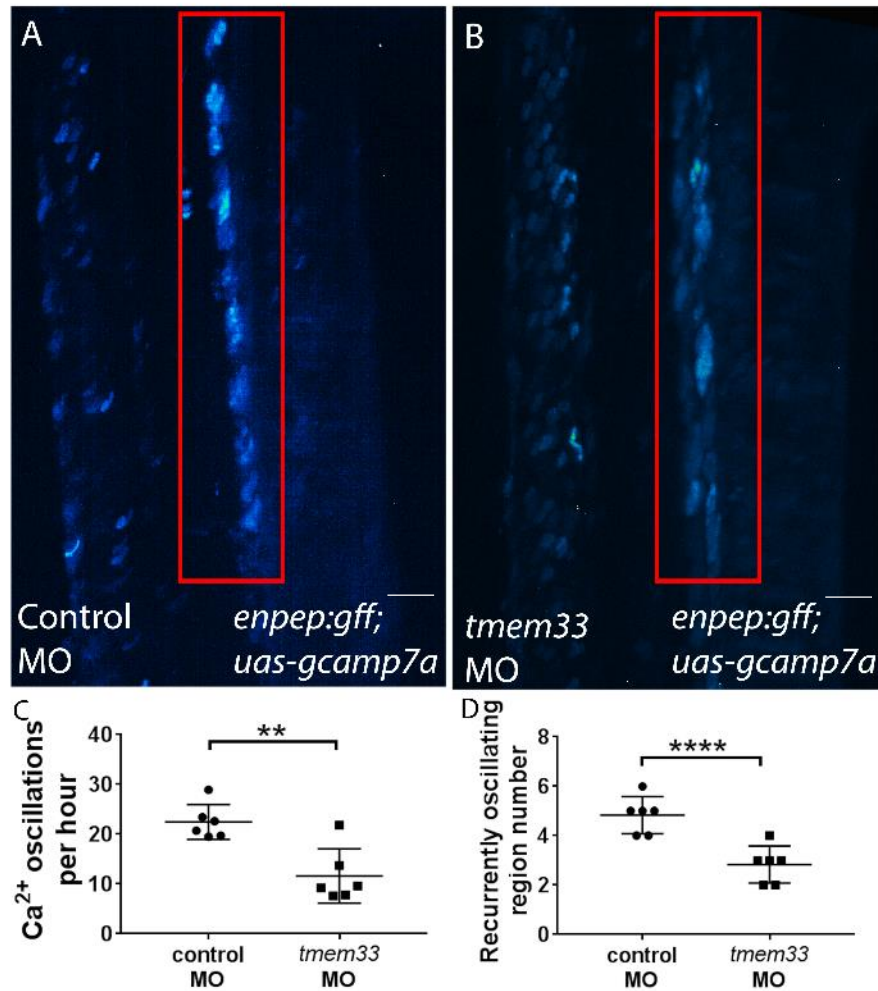


Figure 3.9 *tmem33* knockdown by morpholino reduces calcium signalling within the developing kidney. **(A-B)** Maximum projection over time, displaying regions of calcium signalling. Regions of the highest levels of calcium signalling are represented in white-green, while lower level calcium signalling are shown in dark blue. *tmem33* morphants display reduced GCaMP fluorescence throughout the pronephric tubules (red box) compared to controls. **(C-D)** Both pronephric calcium signalling oscillation frequency per embryo and number of recurrently oscillating regions are significantly reduced in *tmem33* morphants, compared to controls (unpaired t-tests ** $p < 0.01$, **** $p < 0.0001$).

3.8 Development of an endothelial F-actin reporter line to quantify filopodia dynamics during angiogenesis.

tmem33 morphants display angiogenic delays (Figure 1.4; Figure 3.6) and reduced calcium signalling, which has been shown to regulate the actin cytoskeleton *in vitro* in Jurkat T-cells and murine embryonic fibroblast cells (Hartzell et al., 2016; van Vliet et al., 2017). Therefore, impaired angiogenesis following *tmem33* knockdown could be due to abnormal filopodia formation. To quantify F-actin dynamics during angiogenesis I generated an endothelial F-actin reporter line, *Tg(fli1a:LifeACT-mClover)sh467* (chapter 2.1.2). I performed an intercross of *Tg(fli1a:DsRedEx2)sh511* and *Tg(fli1a:LifeACT-mClover)sh467* transgenic lines (see Chapter 2.1.2) and observed distinct fluorophore expression within endothelial cells. *Tg(fli1a:LifeACT-mClover)sh467* labels F-actin, while *Tg(fli1a:DsRedEx2)sh511* is cytoplasmic. In double positive transgenic embryos, endothelial F-actin was observed at 488nm emission wavelength (Figure 3.10 A, C, white arrowheads), while, no filopodial extensions could be observed at 561nm emission wavelength, (Figure 3.10 B, white arrowheads). *Tg(fli1a:DsRedEx2)sh511* positive endothelial cells displayed nuclear and plasma membrane exclusion (Figure 3.10 B, C, blue arrowheads), when compared to the *fli1a:lifeACT-mClover* transgene (Figure 3.10 C). This suggests increased regions of fluorescence in *Tg(fli1a:lifeACT-mClover)sh467* embryos are likely to be F-actin dense regions of the cell and not cytoplasm.

I next performed time-lapse imaging of *Tg(fli1a:LifeACT-mclover)sh467* embryos over 12 hours, during SeA formation. I observed numerous filopodia and F-Actin rich foci per SeA during the first 6 hours of development, corresponding to between 24 and 30 hpf (Figure 3.10 D-F). Beginning at around 30 hpf,

lumenisation of the sprouting SeA and DLAV occurs and filopodia activity began to decrease, suggesting filopodial activity is important during EC migration but less so once vessels lumenise (Figure 3.10 G-I), suggesting a reduced requirement for filopodia at this time point.

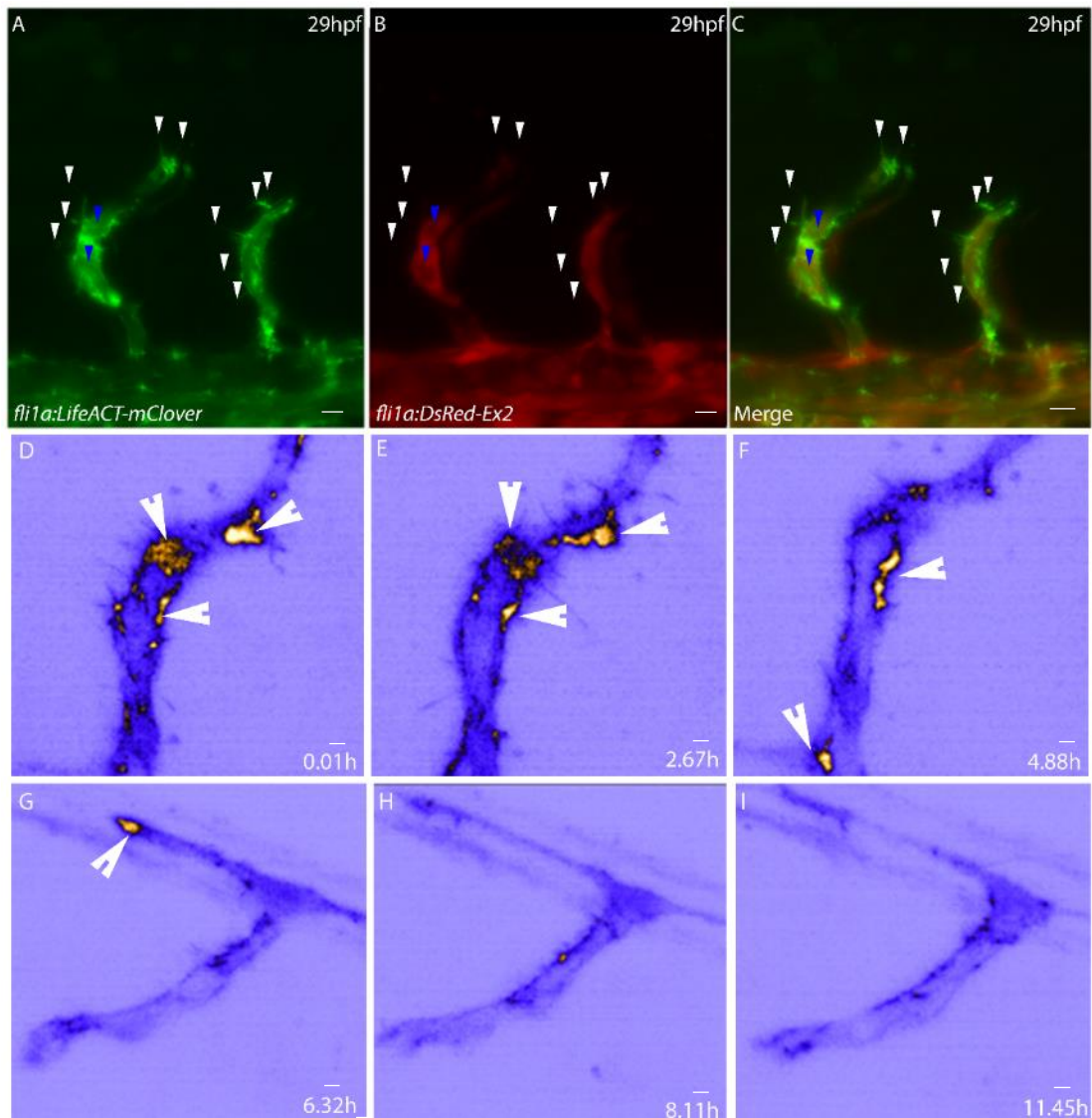


Figure 3.10 *Tg(fli1a:LifeACT-mClover)sh467;Tg(fli1a:DsRedEx2)sh511* embryos display spatially distinct fluorophores and *Tg(fli1a:LifeACT-mClover)sh467* highlights endothelial filopodia. **(A-C)** An intercross of *Tg(fli1a:LifeACT-mClover)sh467* and *Tg(fli1a:DsRedEx2)* embryos reveals spatially distinct expression. The LifeACT-mClover transgene is restricted to F-actin positive regions of ECs, including filopodia (white arrowheads), while the DsRedEx2 transgene displays cytoplasmic restriction, with possible nuclear exclusion (blue arrowheads). **(D-I)** A 12 hour time-lapse with embryos imaged from 27hpf to 39 hpf. Maximum projection over time, displaying regions of increased F-actin density. Regions of the highest levels of F-actin density are shown in orange (and indicated by white arrowheads), while regions of low F-actin density are in light blue. Endothelial cells display a greater density of F-actin before the onset of flow and before lumenisation begins.

3.9 Latrunculin B inhibits formation of endothelial filopodia but does not alter endothelial calcium oscillation frequency.

I next treated *Tg(fli1a:lifeACT-mClover)sh467* embryos with 397nM Latrunculin B, which binds G-actin and prevents F-actin polymerisation (Phng et al., 2013), for 5 hours beginning at 24 hpf. Latrunculin B treatment delayed SeA sprouting in *Tg(fli1a:lifeACT-mClover)sh467* embryos and altered endothelial cell morphology, with SeAs displaying aberrant tip cell morphology (Figure 3.11 B), by 29 hpf. ECs treated with Latrunculin B displayed no detectable filopodia or cortical F-actin. Instead, intense transient foci were detected, suggesting an inability of F-actin to properly polymerise into filaments (Figure 3.11 B, C). In contrast, filopodia extended from all ECs in control embryos (Figure 3.11 A, C). This is consistent with published data (Phng et al., 2013).

Regulation of calcium signalling and the actin cytoskeleton is tightly linked; cytosolic free Ca^{2+} ions are essential for actin cytoskeletal remodelling which is required to translocate the ER to the plasma membrane to resolve store operated calcium entry (van Vliet et al., 2017). Therefore, I examined whether F-actin polymerisation modified calcium oscillations. I treated *Tg(fi1a:gff)ubs3; Tg(uas:GCaMP7a)sh392* embryos with 397 nM Latrunculin B for 5 hours beginning at 23 hpf and observed no significant alteration in frequency of calcium oscillations by 28 hpf (Figure 3.11 D, E, F). This indicates that, while calcium signalling is essential for actin cytoskeleton remodelling (Hartzell et al., 2016; van Vliet et al., 2017), the presence of an active actin cytoskeleton is not essential for calcium oscillations in ECs. This is consistent with observations in mouse neuronal cell explants (Martini and Valdeolmillos, 2010).

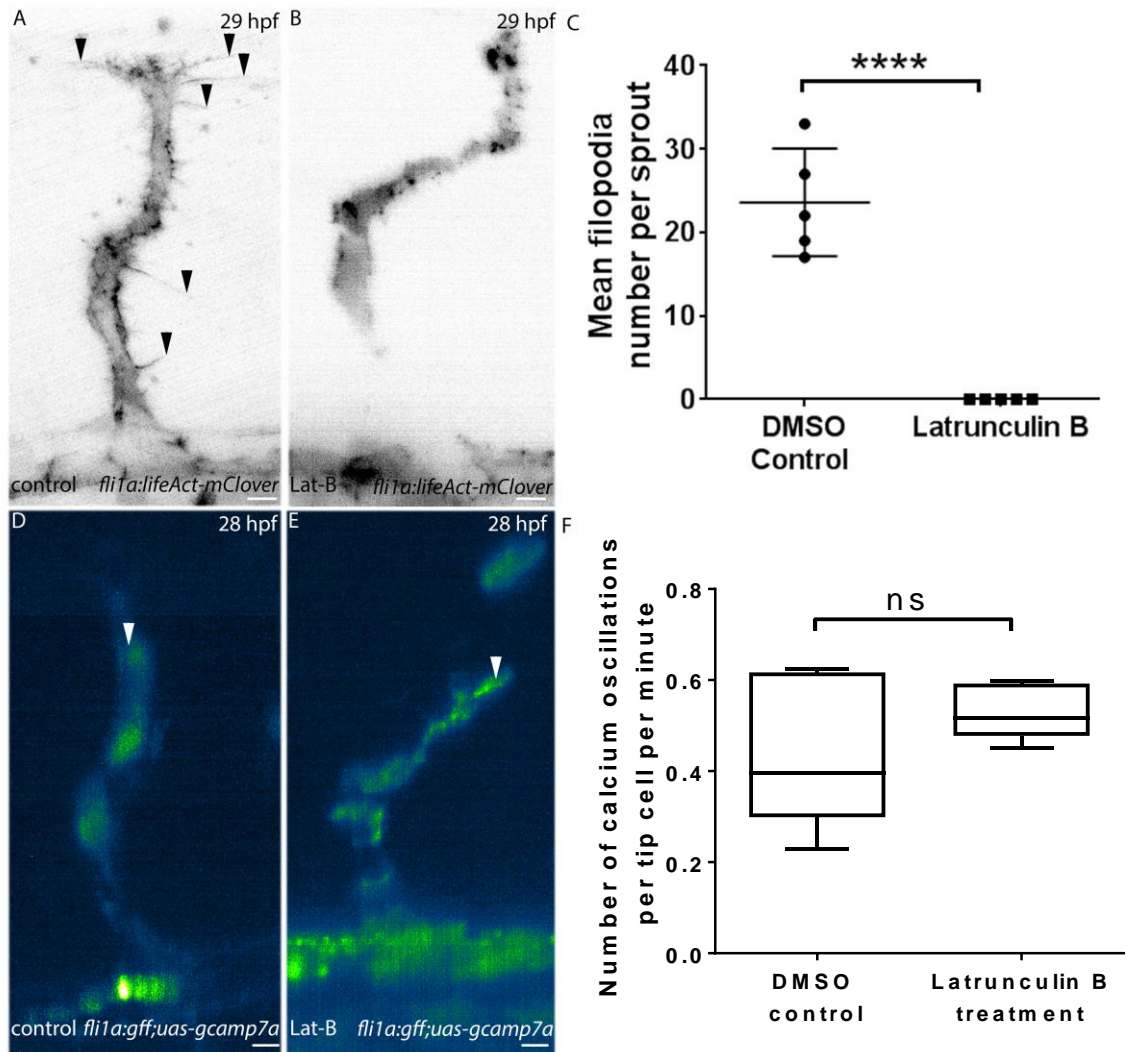


Figure 3.11 Endothelial Ca^{2+} oscillations within tip cells are not disrupted following loss of filopodia. (A-B) Latrunculin B treatment reduces endothelial filopodia number in *Tg(fli1a:LifeACT-mClover)sh467* embryos (black arrowheads). (C) Latrunculin B treated *Tg(fli1a:lifeact-mClover)sh467* embryos display significant reductions of filopodia number per SeA (unpaired t-test **** $p < 0.0001$). (D-F) Frequency of Ca^{2+} oscillations are not significantly altered by Latrunculin B treatment in *Tg(fli1a:gff)ubs3;Tg(uas:GCaMP7a)sh392* embryos (Mann-Whitney U-test, non-significant.).

3.10 *tmem33* knockdown inhibits endothelial filopodia formation.

Filopodia are present on many migratory cell types, including angiogenic endothelial cells (Gerhardt et al., 2003), yet, upon ablation of filopodia, endothelial

migration still occurs, albeit slower (Phng et al., 2013). *tmem33* knockdown delays angiogenesis (Figure 1.4), which may be due to impaired filopodia formation. I therefore next analysed filopodia formation in *Tg(fli1a:lifeACT-mClover)sh467* positive embryos following *tmem33* knockdown using morpholinos and analysed delayed endothelial tip cells, since these are indicative of *tmem33* knockdown (Figure 1.4). Endothelial tip cells with abnormal morphology (as previously observed in Figure 1.4) displayed reduced mClover fluorescence, in comparison to controls (Figure 3.12 A, B, black arrowheads) suggesting *tmem33* knockdown reduces F-actin formation. Furthermore, similar to treatment with Latrunculin B (Figure 3.11), *tmem33* knockdown significantly reduced both length of cellular extensions observed per tip cell (Figure 3.11 C) and number of filopodia per tip cell (Figure 3.11 D). This suggests that *tmem33* knockdown inhibits formation of endothelial filopodia which may be responsible for reduced endothelial migration in *tmem33* morphants.

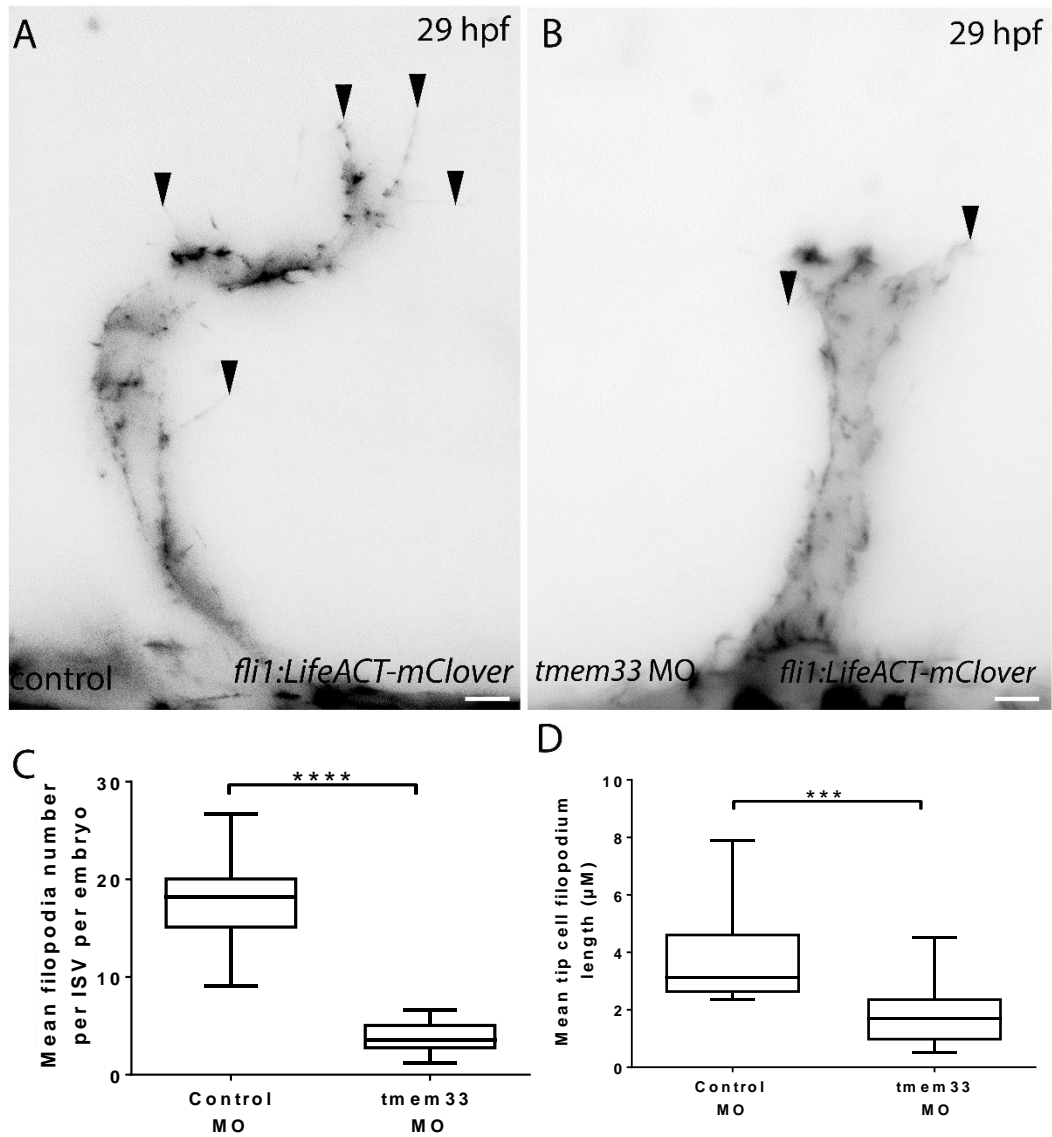


Figure 3.12 *tmem33* knockdown by morpholino reduces endothelial filopodia activity. (A-B) *tmem33* morphants display delayed migration of SeAs which extend fewer filopodia, compared to controls (black arrowheads. **(C)** *tmem33* morphants display significantly fewer filopodia per SeA compared to controls. Measurements taken from n=4 SeAs from n=13 embryos in each case. Mann-Whitney U test, ****p<0.0001). **(D)** *tmem33* morphants display reduced filopodia length compared to controls, measurements taken from n=4 SeAs from n=13 embryos. Mann-Whitney U test, *** p<0.0005).

3.11 *tmem33*^{sh443} mutants exhibit nonsense mediated decay but normal angiogenesis.

Since morpholino knockdown is transient and may induce off target effects (Kok et al., 2015; Robu et al., 2007), I next examined vascular development in a *tmem33* stable mutant. The *tmem33*^{sh443} allele was generated via TALEN mutagenesis by Dr. Robert Wilkinson (see methods) (Cermak et al., 2011b) and contains a 2bp deletion in exon 3 (Figure 3.13 A). The mutation is predicted to cause a frameshift from exon 3, leading to a premature stop codon in exon 4. Exons 3-5 contain the sequence which makes up the conserved 3-transmembrane domain (Figure 3.13 B). therefore, this mutation is predicted to cause loss of two of the three conserved transmembrane domains.

Nonsense mediated decay (NMD) occurs when a functional transcript is not viable and NMD is activated by RNA surveillance mechanisms within the ER which detect improperly formed mRNA transcripts (reviewed in Lykke-Andersen and Jensen, 2015). Recent analysis has suggested that NMD occurs most effectively when a mutation causes a premature termination codon (PTC) at least 350 bp downstream of the start codon and upstream of the last 50 bp of the penultimate exon (Lindeboom et al., 2016). Furthermore, it has been reported that truncated sequences at least 20-24 nt from exon-exon mRNA boundaries retain binding of exon-exon junction proteins, which contribute to recognition of NMD on such transcripts (Le Hir et al., 2001). *tmem33*^{sh443} occurs within the third exon, 74 nt away from the nearest exon-exon junction, suggesting NMD could be induced. To examine this possibility, *in situ* hybridisation for *tmem33* was performed in mutant and wild type embryos. Wild type embryos displayed *tmem33* expression as described earlier (Figure 3.13 C), while expression of

tmem33 was greatly reduced in *tmem33^{sh443}* mutants (Figure 3.13 D). I quantified *tmem33* expression by qPCR and found this was significantly reduced in heterozygotes and abrogated in homozygous *tmem33^{sh443}* mutants (Figure 3.13 E). Collectively, these data indicate that the *tmem33^{sh443}* mutant allele is likely to represent a loss-of-function or null and activates NMD.

To examine angiogenesis in *tmem33^{sh443}* mutants these were crossed with *Tg(fli1a:EGFP)* transgenics and the effect of the mutation on vascular development assessed as in the morphants. Despite the evidence suggesting the *tmem33^{sh443}* mutation induces a loss-of-function, I found no difference in angiogenesis between controls or *tmem33^{sh443}* mutants at 52 hpf (Figure 3.13 F, G). In addition, homozygous *tmem33^{sh443}* mutants are viable and survive to adulthood, suggesting vascular patterning and maintenance is not affected at later stages.

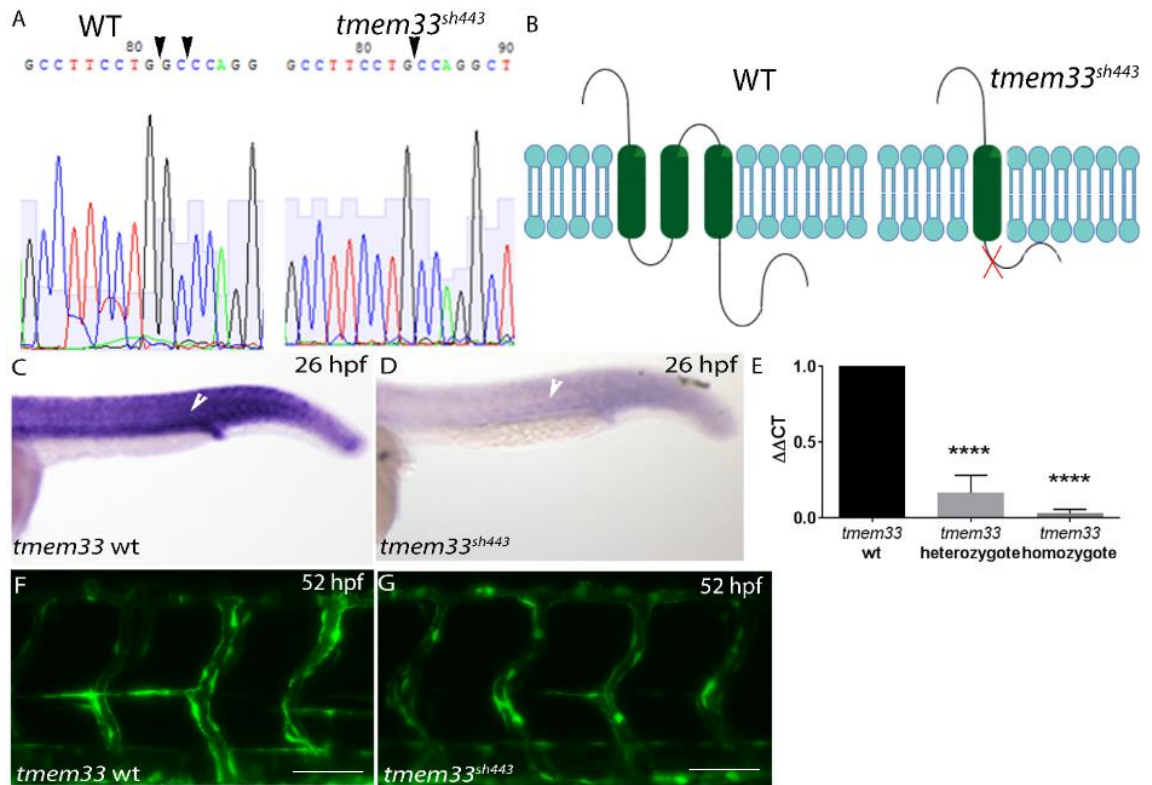


Figure 3.13 *tmem33^{sh443}* mutants are predicted loss of function and display nonsense-mediated decay but normal angiogenesis. **(A)** *tmem33^{sh443}* consists of a 2 bp deletion within exon 3, deleting a guanine and a cytosine. **(B)** The mutation leads to a frameshift, resulting in a premature stop codon in exon 4, within the first ER-lumenal loop of TMEM33. The predicted protein loses the final two conserved transmembrane domains. **(C-E)** Both *tmem33^{sh443}* heterozygous and homozygous mutants display a significant reduction in *tmem33* expression, as visualised by *in situ* hybridisation and qRT-PCR gene expression analyses (One-way ANOVA with *post-hoc* Dunnet's test **** $p < 0.001$). **(F, G)** *tmem33^{sh443}* mutants display no difference in segmental artery or lymphatic vasculature by 52 hpf, compared to controls.

3.12 *tmem33^{sh448}* mutants are protected from the effects of *tmem33* morpholinos

The discrepancy between the vascular defects observed in *tmem33* morphants and the normal vascular development of *tmem33^{sh443}* mutants raised the possibility that the *tmem33^{sh443}* mutation induces genetic compensation as described previously (Rossi et al., 2015). This possibility can be assessed by

examining the effect of morpholino knockdown in the mutant background. I therefore injected *tmem33* morpholinos into embryos generated from a *tmem33^{sh448/+}* incross and examined the effect on vascular development. *tmem33* morphants were observed for evidence of vascular defects at 50 hpf and subsequently genotyped for the *tmem33^{sh443}* mutation. Morphants were ranked into three categories: no phenotype (Figure 3.14 B), mild phenotype (<3 vascular branching defects) (Figure 3.14 C) and severe phenotype (>3 branching defects) (Figure 3.14 D). Vascular branching defects were defined as stunted SeAs, incomplete anastomosis or misbranched vessels. Homozygous *tmem33^{sh443}* mutants displayed significantly fewer vascular defects than either wild type or heterozygotes injected with the *tmem33* morpholino (Figure 3.14 A). This indicates that the *tmem33^{sh443}* mutation probably induces genetic compensation which partially protects against the morphant phenotype.

Having shown that *tmem33* mutants display protection from angiogenic defects, a similar experiment was performed using a *Tg(-26wt1b:eGFP)li1;tmem33^{sh448+/-}* heterozygous incross, to determine whether *tmem33^{sh443}* mutants were protected from the effects of *tmem33* morpholino knockdown on glomerular size. As expected, the *tmem33* morpholino induced abnormally large glomeruli (Figure 3.14 F) in 67% of wildtype and 63% of heterozygous *tmem33^{sh443}* mutant embryos. However, homozygous *tmem33^{sh443}* mutants were partially protected against this effect (Figure 3.14 E), with significantly fewer embryos developing expanded glomeruli (Figure 3.14 G).

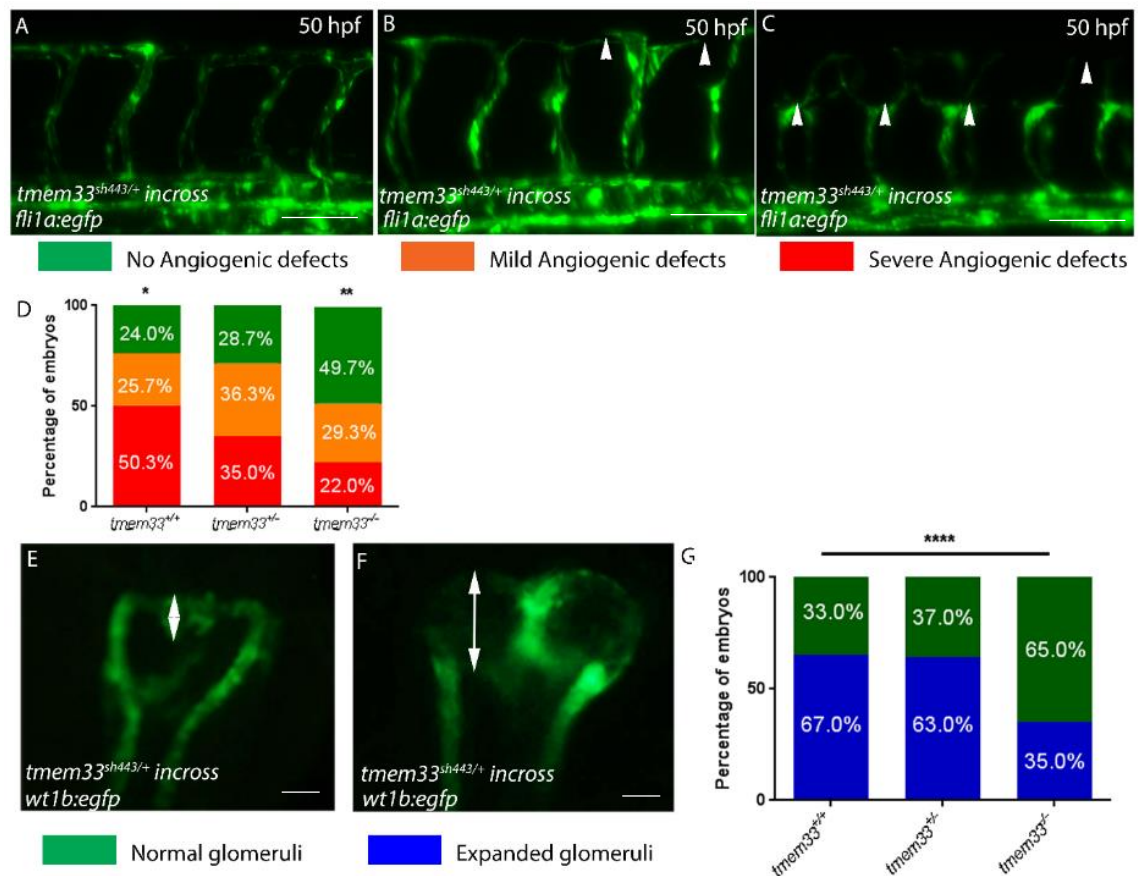


Figure 3.14 *tmem33^{sh443}* mutants are partially protected from morpholino-induced angiogenic and glomerular defects. **(A)** *Tg(fli1a:eGFP)y1; tmem33^{sh443/+}* heterozygous incross injected with *tmem33* morpholinos, blindly ranked for phenotype and retrospectively genotyped. *tmem33^{sh443}* embryos display protection from morphant phenotype (2-way ANOVA using Tukey's multiple corrections: ***p*=0.005; **p*=0.05; *F*=4.435 *DF*=4. 3 technical repeats, *tmem33^{+/+}* *n*=42, *tmem33^{+/-}* *n*=67, *tmem33^{-/-}* *n*=41) **(B)** Representative *Tg(fli1a:eGFP)y1; tmem33^{sh443/+}* embryo displaying normal angiogenesis. **(C)** Representative *Tg(fli1a:eGFP)y1; tmem33^{sh443/+}* embryo displaying mild angiogenic defects (<3 discontinuous DLAV, SeA misbranching events). **(D)** Representative *Tg(fli1a:eGFP)y1; tmem33^{sh443/+}* embryo displaying severe angiogenic defects (*n*=>3 discontinuous DLAV, SeA misbranching events). **(E)** Representative *Tg(-26wt1b:eGFP)li1* embryo displaying normal pronephric development. **(F)** Representative *Tg(-26wt1b:eGFP)li1* embryo displaying distended glomeruli. **(G)** *tmem33^{sh443/+} Tg(-26wt1b:eGFP)li1* heterozygous incross injected with *tmem33* morpholinos, blindly ranked for phenotype and retrospectively genotyped (2-way ANOVA, Sidak's multiple corrections *****p*<0.0001; *F*=81.78 *DF*=2. 3 technical repeats, *tmem33^{+/+}* *n*=31 *tmem33^{+/-}* *n*=48, *tmem33^{-/-}* *n*=27).

3.13 Discussion

3.13.1 Overview

In this chapter, I have identified novel functions for *tmem33*. No previous work has examined the role of *tmem33* in any multicellular organism *in vivo* but my data shows it plays central roles in actin cytoskeleton organisation and calcium signalling.

I therefore suggest that *tmem33* may function to regulate calcium efflux from the ER which is important for normal F-actin mobilisation, including filopodia formation (Figure 3.15).

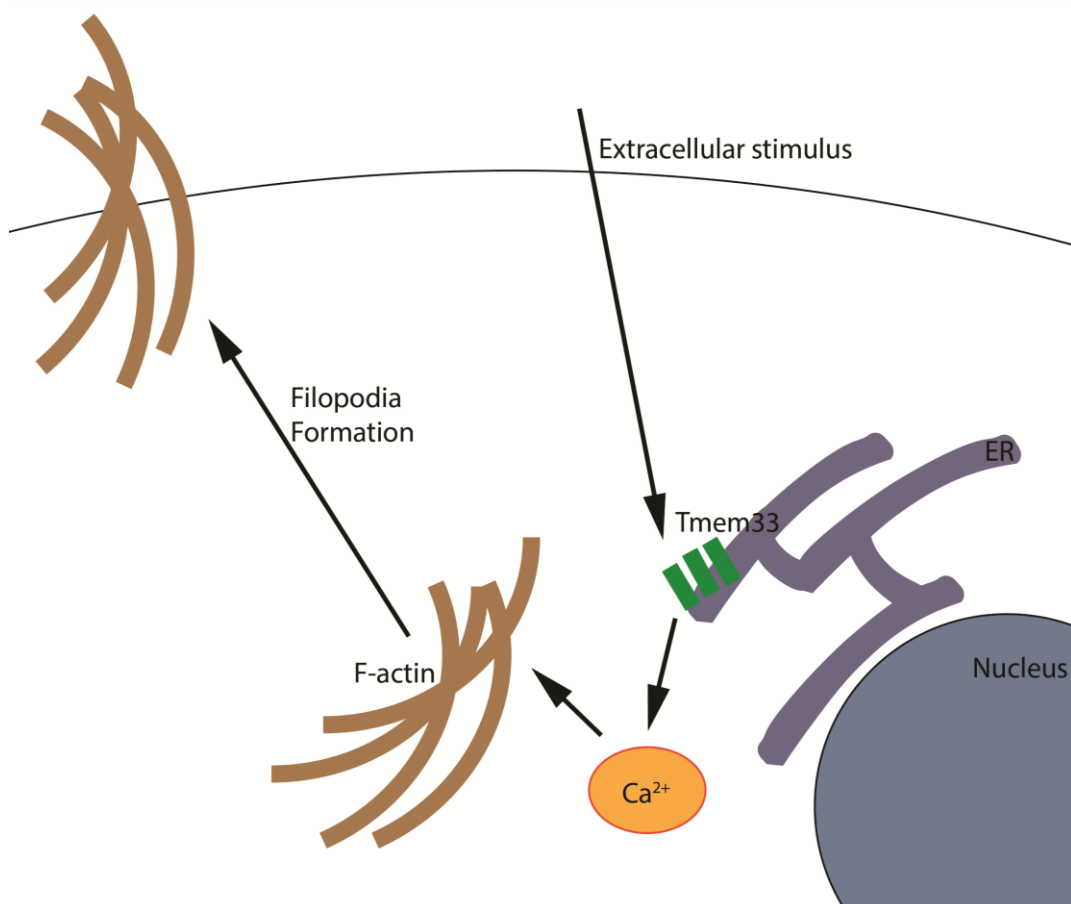


Figure 3.15 *tmem33* functions to regulate calcium efflux from the ER, which is essential for normal F-actin mobilisation, including filopodia formation.

3.13.2 *tmem33* is expressed ubiquitously early in development, and is expressed in both pronephros and endothelial cells later in development, probably localising to the ER

When I examined expression of *tmem33* during embryonic development, this was ubiquitous at early stages, although more restricted in later stages particularly to the pronephros. I found evidence that *tmem33* is co-expressed with vascular reporters, confirming that it is expressed in endothelial cells as well as other cell types. However, expression of *tmem33* is clearly not endothelial or kidney-specific, yet the only phenotypes I observed in *tmem33* morphants were vascular and renal. I did not observe any evidence of abnormalities of body plan, or brain development even though *tmem33* was expressed in these regions. Phenotypes were only observed during kidney and vascular development; regions in which *tmem33* expression is enriched. However, the exact reason for *tmem33* knockdown affecting these organs preferentially is unknown.

I found that *tmem33* appears to localise to the endoplasmic reticulum and nuclear membrane in both endothelial and non-endothelial cells (Figure 3.4). This is compatible with a role in ER homeostasis, as has been reported in other studies in cell culture and yeast, including during cell division (Sakabe et al., 2015; Zhang and Oliferenko, 2014; Zhang et al., 2010). This localisation places it in the correct subcellular organelle to influence calcium release and signalling (Berridge et al., 2003). Interestingly, however, while current studies have implicated *tmem33* in regulation of ER homeostasis, no study has, thus far, directly linked *tmem33* function to the regulation of calcium signalling. In this thesis, I showed *tmem33*

functions during calcium signalling in endothelial and kidney cells, which has previously not been described.

3.13.3 *tmem33* knockdown impairs angiogenesis

tmem33 morphants display a pronounced impairment of angiogenesis. The phenotype observed is similar to loss-of-function VEGF signalling phenotypes previously described. For example, morpholino knockdown of *vegfab* impairs, but does not abolish angiogenesis in the trunk, head and subintestinal vein (SIV) (Bahary et al., 2007). Moreover, *kdr* morphants display mild trunk angiogenic defects by 4 dpf, indicating a small loss of VEGF response, while angiogenesis is abrogated in *kdr/kdr1* double morphants by 28 hpf (Bahary et al., 2007). *kdr1* zebrafish mutants also fail to develop normal vasculature (Covassin et al., 2006, 2009; Habeck et al., 2002). *tmem33* morphants display impaired angiogenic migration and reduced secondary angiogenesis (Figure 1.4), suggesting *kdr/kdr1* function is not impaired. Furthermore, I observed no ectopic angiogenesis, which would suggest a downregulation of *flt1*, but not other receptors (Krueger et al., 2011). *Tmem33* knockdown also impairs lymphatic vascular development (Figure 1.4), which requires *vegfc/flt4* signalling (Le Guen et al., 2014; Joukov et al., 1996). Therefore, the *tmem33* morphant phenotype suggests an impaired overall response to VEGF signalling, as opposed to differential regulation of VEGF receptors. Interestingly, *plcg1* mutants display a complete loss of angiogenesis (Covassin et al., 2006, 2009; Wilkinson et al., 2012). *Plcg1* functions downstream of VEGF signalling to regulate angiogenesis, including the induction of calcium signalling (Jones et al., 2005b; Lawson et al., 2003).

Consistent with the suggestion that *tmem33* morphants display a mild loss-of-VEGF signalling phenotype, I showed a requirement for VEGF signalling during sprouting angiogenesis. Tivozanb/AV951, which acts as a pan-VEGF receptor inhibitor (Nakamura et al., 2006), significantly reduced angiogenesis (Figure 3.5) and produced a more severe phenotype than *tmem33* morphants.

3.13.4 The role of calcium signalling in angiogenesis and angiogenic signalling pathways

In this chapter I characterise a novel transgenic line *Tg(fi1a:gff)ubs3;Tg(uas:GCaMP7a)sh392* which expresses a genetically encoded calcium indicator specifically in endothelial cells. Consistent with other work published during my PhD (Yokota et al., 2015), this reveals alterations in endothelial calcium levels during embryonic vascular development. During normal sprouting angiogenesis, endothelial cells displayed periodic oscillations in calcium levels, but VEGF inhibition completely abolished these (Figure 3.5). Conversely, Notch inhibition appeared to increase the number and amplitude of such oscillations above baseline, confirming that calcium reporter levels are a surrogate of VEGF signalling in vivo (Figure 3.5). Previous studies have also shown that calcium signalling is induced downstream of VEGF signalling (Oike et al., 1994; Vaca and Kunze, 1994; Yokota et al., 2015; Zadeh et al., 2009), suggesting it may play an important role during angiogenesis. Furthermore, calcium signalling is induced downstream of *plcg1* signalling (Jones et al., 2005b), which is known to be important during angiogenesis in zebrafish (Covassin et al., 2009; Lawson et al., 2003). Phosphorylated PLCG1 has been shown to be required for MAP kinase signalling in endothelial cells (Takahashi

and Shibuya, 1997; Takahashi et al., 2001), which suggests that both MAP kinase signalling and calcium signalling function downstream of PLCG1.

Interestingly, *tmem33* morphants lack lymphatic vasculature, which forms during secondary angiogenic sprouting, primarily as a result of *vegfc/flt4* signalling (Le Guen et al., 2014; Joukov et al., 1996). This suggests that *tmem33*-mediated calcium signalling may be required during secondary angiogenesis as well as primary angiogenesis. However, no study to date has shown a requirement for calcium signalling in lymphatic endothelial cells during development *in vivo*. However calcium signalling, including SOCE, has been studied in lymphatic cell culture (Choi et al., 2017; Outeda et al., 2012). It may, therefore, be interesting to study *tmem33* function in calcium signalling during lymphatic development by generating a *prox1a*-driven GCaMP7a transgenic line (Dunworth et al., 2014).

3.13.5 *tmem33* knockdown impairs calcium signalling and actin cytoskeleton regulation.

My data implicate *tmem33* in regulation of calcium signalling in endothelial cells, therefore identifying a novel component of calcium signalling. Furthermore, *tmem33* knockdown induces aberrant angiogenesis, including delayed SeA migration and defective anastomosis (Figure 1.9), suggesting *tmem33*-mediated calcium signalling is required for normal angiogenesis.

Calcium signalling in endothelial cells, which are non-excitabile, primarily occurs via store operated calcium entry (SOCE). SOCE utilises, at least in part, the

CRAC channel STIM (Jones et al., 2005a; Roos et al., 2005; Zhou et al., 2013, Feske et al., 2006; Vig et al., 2006a; Zhou et al., 2010). Recently, signalling via the CRAC channel has been shown to regulate changes in actin cytoskeleton organisation in T-cells (Hartzell et al., 2016) while a calcium-dependent mechanism has been proposed for organisation of actin during cell migration in zebrafish neural explants (Martini and Valdeolmillos, 2010). Similarly, calcium-dependent re-organisation of cellular actin has been reported, in which cytoskeletal rearrangement is required to allow SOCE to occur, by bringing the ER into contact with the plasma membrane (van Vliet et al., 2017). I have shown that *tmem33* knockdown reduces both calcium signalling and actin cytoskeleton organisation in endothelial cells (Figure 3.7; Figure 3.12). Given that endothelial cells are non-excitable and therefore utilise SOCE (Oike et al., 1994; Vaca and Kunze, 1994), it is possible that reduced calcium signalling observed in *tmem33* morphants impairs the cells ability to regulate actin cytoskeletal dynamics which are required for the ER-PM contact essential for SOCE to take place. This, in turn, would reduce EC Ca^{2+} replenishment essential for rapid reorganisation of the actin cytoskeleton. Alternatively, *tmem33* may directly regulate actin cytoskeletal rearrangement by interacting with genes such as *filamin a* (van Vliet et al., 2017). In order to test this, *filamin a* could be overexpressed in *tmem33* morphants to determine whether actin cytoskeleton function could be restored.

Filopodia project from the cell during migration through cytoskeletal rearrangement. Filopodia are F-actin rich, yet have been shown to be dispensable during migration (Gerhardt et al., 2003; Phng et al., 2013). Both blebbing and lamellipodia are also utilised by migratory cell types (reviewed in Ridley, 2011). While lamellipodia also utilise F-actin, blebs do not. Since *tmem33*

morphants appear to be unable to properly regulate F-actin polymerisation (Figure 3.12), ECs may instead undergo membrane blebbing to migrate in these embryos (Ridley, 2011).

3.13.6 *tmem33* is required for normal calcium signalling in both developing endothelial and kidney cells, suggesting a wider function than just during VEGF-mediated calcium signalling.

tmem33 knockdown reduces GCaMP oscillation frequency in both endothelial cells and kidney cells (Figure 3.7; Figure 3.9). While endothelial calcium signalling appears to rely mainly on VEGF signalling (Figure 3.5) (Oike et al., 1994; Vaca and Kunze, 1994; Yokota et al., 2015), renal calcium signalling appears to be regulated by purinogenic signalling, though this has mostly been studied within the context of autosomal dominant polycystic kidney disease (ADPKD) (reviewed in Chebib et al., 2015). *Wnt5a* signalling has also been suggested to regulate calcium signalling via regulation of calmodulin/calcineurin in diabetic mice (Ando et al., 2016). VEGF signalling in the kidney has been studied in the contexts of glomerular capillary development (reviewed in Robert and Abrahamson, 2001) and disease (reviewed in Schrijvers et al., 2004), suggesting VEGF does not function in pronephric tubule development.

Since I observed reduced pronephric calcium signalling in *tmem33* morphants (Figure 3.7), this suggests that *tmem33* may function as a general regulator of calcium signalling. Furthermore, since Thapsigargin treatment was not sufficient to rescue *tmem33*-mediated reductions in cytosolic Ca^{2+} (Figure 3.8), this may suggest that *tmem33* functions to regulate ER calcium homeostasis. However,

since endothelial calcium signalling is ablated in the absence of VEGF signalling (Figure 3.5), *tmem33* is likely to function downstream of VEGF signalling within the context of angiogenesis.

3.13.7 *tmem33* mutants appear to display genetic compensation.

Concerns regarding the use of morpholino knockdown as an approach to study gene function have arisen, particularly in light of CRISPR/Cas9 and TALEN technology and their relatively straight-forward practice (Kok et al., 2014; Schulte-Merker and Stainier, 2014). Indeed, before even TALENs were available, misinterpretation of morpholino phenotypes was abundant; common off-target effects, such as an expanded hindbrain were cited as phenotypes. However, often these could not be reproduced (Eisen and Smith, 2008). Recently, morpholinos were shown to be capable of causing severe off-target phenotypes, even in genes in which the target locus had been deleted and the suggested proportion of genes in which morpholino phenotypes translated into mutant phenotypes was low (Kok et al., 2014). Recently a study involving an *egfl7* mutant line with no phenotype was conducted, in which mutants exhibited reduced morphant phenotype compared to wild type or heterozygous embryos. In this study, genetic compensation was suggested to occur in the *egfl7* mutants, negating the effects of genetic knockdown. Indeed, *emilin2* was found to be upregulated and was able to rescue the morphant phenotype (Rossi et al., 2015). Furthermore, genetic compensation via transcriptional adaptation has been suggested due to the frequency in which either compensation is found, or the frequency of disparity between knockdown and knockout phenotypes, though the mechanism by which this acts as yet remains unclear (El-Brolosy and Stainier, 2017).

I sought to address whether *tmem33* mutants may display compensation, and so conducted a similar series of experiments. *tmem33* morpholino knockdown induces endothelial and renal developmental defects, yet *tmem33^{sh443}* mutants do not display any phenotypes, despite displaying a reduction in *tmem33* expression (Figure 3.13). I found that injection of the morpholino into *tmem33^{sh443}* mutants does induce a phenotype in significantly fewer embryos than wild type or heterozygous mutants (Figure 3.14), suggesting that, although *tmem33* morpholinos may induce some off-target effects, mutants are protected from morpholino-induced phenotypes. This does not, however, confirm that *tmem33* mutants display compensation, and only suggests it may be the case. *tmem33* embryos display a significant reduction in *tmem33* expression (Figure 3.13) which may suggest that NMD takes place, since a prematurely truncated protein is predicted to be produced (reviewed in Lykke-Andersen and Jensen, 2015). Interestingly, a recent study has suggested a link between NMD and genetic compensation, whereby knockdown of components of the NMD machinery induced a phenotype in a greater number of embryos (Schuermann et al., 2015). Given the recent studies in which knockdown and knockout have been compared (Kok et al., 2015; Rossi et al., 2015), I suggest that *tmem33^{sh443}* mutants display genetic compensation. I show that expression of the *tmem33* mRNA transcript is reduced, suggesting that the transcript may undergo nonsense-mediated decay. However, the *tmem33 in situ* probe used targets the entire mRNA transcript, and might not be able to properly target a truncated mRNA transcript. Furthermore, the *tmem33* Taqman probe may not also bind well to a truncated transcript, given that it targets exons 3-4. This may suggest that the methods employed herein are not entirely appropriate. Therefore, a shorter *in situ* probe and a custom-designed

Taqman probe may be necessary to confirm these findings. Furthermore, alternative knockdown approaches may be necessary to determine whether the morphant or mutant phenotype is representative of loss of *tmem33*. To entirely conclude that genetic compensation occurs in *tmem33^{sh443}* mutants, a whole genome RNA-seq would need to be performed to identify genes upregulated in *tmem33^{sh443}* mutants.

However, despite the fact that *tmem33* mutants display nonsense mediated decay of *tmem33* transcripts they do not display abnormal angiogenesis, although my data suggest this may be due to genetic compensation. Furthermore, phenotypes observed in *tmem33* morphants and *tmem33^{sh443}* mutants do not correlate. Therefore alternative approaches are required to address this. I further explore this in chapter IV, in which I develop tissue-specific CRISPR interference to study *tmem33* function conditionally.

4 Development of a strategy for conditional knockdown of genes via CRISPR interference to validate and extend functional analysis of *tmem33*

4.1 Introduction

In this chapter, I describe the optimisation of CRISPR interference and development of tissue-specific CRISPR interference as a means to knock down gene expression globally or tissue-specifically in zebrafish embryos. Using these techniques, I am able to verify the *tmem33* morphant phenotype established in Chapter 3. Furthermore, I establish a cell-specific requirement for *tmem33* during endothelial and renal development. I also characterise *tmem33* function in greater detail and show that *tmem33* is required for cytosolic calcium oscillations in response to Vegfa in a series of epistasis experiments. I show that *tmem33*-mediated endothelial calcium signalling is required for normal downstream responses to VEGF signalling including ERK phosphorylation and Notch signalling, implicating a novel function for *tmem33* during angiogenesis. This suggests that *tmem33*-mediated calcium oscillations regulate signalling pathways downstream of VEGF signalling and promote angiogenesis.

4.1.1 VHL and Hypoxia-induced angiogenesis.

In conditions in which oxygen levels are low, the hypoxia signalling pathway is induced. This is regulated by several genes, including hypoxia-inducible factors (HIFs), VHL protein (pVHL) and regulators of pVHL including prolyl hydroxylase enzymes (PHDs). Under normoxia, the hypoxia signalling pathway is inactivated. PHD proteins hydroxylate HIF-1 α on two conserved proline residues in an

oxygen-dependent manner, targeting HIF-1 α for proteasomal degradation (Ivan et al., 2001; Jaakkola et al., 2001; Masson et al., 2001; Maxwell et al., 1997; Yu et al., 2001). Additionally, the Factor Inhibiting HIF-1 α (FIH) hydroxylates a conserved asparagine residue on HIF-1 α , preventing HIF-1 α from binding p300, which is necessary for downstream transcriptional activation during hypoxia (Lando et al., 2002). Proteasomal degradation of HIF-1 α prevents formation of the HIF-1 α -HIF-1 β complex required for hypoxic signalling.

PHD and FIH post-translationally modify HIF-1 α in an O₂-dependent manner (Hewitson et al., 2002; McNeill et al., 2002). Therefore, during hypoxia, insufficient levels of O₂ impair proteasomal targeting. HIF-1 α is therefore free to bind HIF-1 β (Jiang et al., 1996), which together translocate to the nucleus, wherein the HIF-1 α -HIF-1 β complex binds p300 and other co-factors required to activate transcription of downstream HIF-responsive genes via the HIF-responsive element (Arany et al., 1996; Ema, 1999; Freedman et al., 2002; J.Kallio et al., 1998; Kimura et al., 2000, 2001). Transcriptionally activated genes include VEGF, PHD3 and erythropoietin (EPO) (Jiang et al., 1996; Kimura et al., 2000; Pescador et al., 2005). Increased VEGF signalling induces ectopic angiogenesis, which is required during tumour angiogenesis for vascularisation of the tumour (Maxwell et al., 1997). Furthermore, genes associated with the regulation of oxygen transport such as EPO are upregulated (Jiang et al., 1996). Interestingly, PHD3 is upregulated, indicating negative feedback regulation of HIF-1 α .

Hypoxia-induced angiogenesis has primarily been studied *in vitro* (DelNero et al., 2016; Maxwell et al., 1997; Rofstad and Danielsen, 1998; Shweiki et al., 1992). However, recent studies used zebrafish to study von Hippel-Lindau disease (Rooijen et al., 2009; van Rooijen et al., 2010; Santhakumar et al., 2012). Zebrafish *vhl* mutants display upregulation of PHD3 (Santhakumar et al., 2012), ectopic angiogenesis (Rooijen et al., 2009) and poor kidney filtration associated with clear cell renal cell carcinoma (Noonan et al., 2016).

4.2 Development of *vhl-phd3* pathway as a novel test-bed for CRISPRi.

Since CRISPR interference was a new technique in zebrafish, it was necessary to first optimise the technique for application on *tmem33*. I therefore employed the Von Hippel-Lindau gene (*vhl*) as a positive control to optimise CRISPR interference, due to the ease of identifying successful knockdown using an established transgenic reporter of hypoxic signalling, *Tg(phd3:egfp)*, which expresses GFP under the control of the *phd3* promoter (Santhakumar et al., 2012; van Rooijen et al., 2009). Loss of VHL protein (pVHL) induces activation of the hypoxia pathway (Santhakumar et al., 2012; van Rooijen et al., 2009) and previous studies have shown an induction of *phd3:egfp* fluorescence using *vhl* morpholino knockdown (Santhakumar et al., 2012; van Rooijen et al., 2009). The von-Hippel Lindau protein (pVHL) regulates the physiological response to hypoxia. In normoxic conditions, it binds to the hypoxia inducible factor-1 alpha subunit (HIF-1 α), ubiquitinating it and tagging it for degradation. In hypoxic conditions, pVHL does not bind HIF-1 α , which then forms a complex with HIF-1 β and activates target gene expression.

A *vhl* gRNA (designed by Dr. Freek van Eeden and hereafter termed *vhl*-gRNA-1) targets exon 1 of *vhl*. Injection of *vhl*-gRNA-1 alongside the Cas9 endonuclease results in mutagenesis within the coding region of *vhl*. *Vhl*-gRNA-1 was targeted to a region which contains the sequence for the restriction enzyme, BslI. Co-injection of *vhl*-gRNA-1 and Cas9 induces genomic mutation at high efficiency, which is tested for by performing a PCR amplification of the surrounding genomic region and performing restriction digestion using BslI (data not shown). If BslI does not cut the DNA, a mutation has taken place. While CRISPRi gRNA design guidelines in zebrafish were unclear, it has been suggested that gRNAs designed less than 400 bp downstream of the transcriptional start site function the most effectively, *in vitro* (Mohr et al., 2016; Radzishchenskaya et al., 2016). The target sequence for *vhl*-gRNA-1 resided within the first exon and was fewer than 350bp downstream of the transcriptional start site (Figure 4.1 A). I therefore tested *vhl*-gRNA-1 for use in CRISPR interference.

A

```

AAATAATTGCTTTATTGCATGACAAATGCTACAAATGTATTGCTAAAGCATTAGAAAAGTTACATTAAAAAAAAAACATACACACATATAATTAAAAAACAGCAAGTAGTAGTCTCTCTCTCACACACAC
ACAAAACATACACACACGCGCGCGGTTTTCAATACCAACCAAAGCACTAGAGGGAGCTGTTATCATCTCTCTCTCTCACCGACTCTCACAGGATTACGCAATCAAAAACAAACGACGCCAGCAGCACGGACGTATGTG
GACAGTCACGTACACAGTCTTTCTCTCCGTTTCGGTAAATTTTcagggttaaatcagatcattgctTCTTAAAGGGCTTAGCGCATGTTTATTATAATTAAGAGAGAGCTTTAACATTTCTAGTTTGTGATTTATGTTTT
GTTGGGCTTTTTAAAAACGATTAACGTTGAAGCTTTAGTCTAACTCGGTGGAGGAGCAAGCACTGTCCTGCTTTGACGATGCCCCAGGACTCTCAGGAGGGGCGAGCGCCGCTCCCGCTGGTCCGCTCTCTGATCAGCCC
GATACAGGICAAAGTCTGTTCTGTAAGTGCAGCCCGCGCTCGTCAAGCCCGCTGGATCACTTCTCGGAGAGCCGCGAGCCGTACGTTGAACATTGAGCCGTACCCGGACGGAAGAATAACAACCTTTTGTGGTTCCG
TGAATTTATGCTGAATTAATGTTGATTAATTAATTTGGTGAATTTGCTATCTACCGGCTTTAACTCGTCTGAAAATAGATATAAAACAAAGTATTTTAAcaaatacaacaataagcaataaggtAAAATTTGGCTTTAAATTT
ATATTGACAGCATTATAATCAGTTTCAGAAAAGTATTAATTTGCGAATTTCTAAATCATATTAACAGTCAATGATTATCAAATAACAACATTTGCCAGTCAATTAATGATGATTATGCTGTTTGAAGTCATACTTAT
AATAAACAAATATAACCAAGTGTGGGGTAATGGATACAAAGTAACGCGAGTTATCTAATAATATTAATTTCTAAGTAACGAGTAAGCAACTCATTACTTAAAAACGTCAGTAATAATATTTGAGTTACTTTAAAAAAA
TTTAAGTGTAGTTACTTTTTAAATTTAAATTTGCTTTAAAAAATGCTGAATTAATAATGATTCAGTCAATGTTAAATCTCACAAATAAGAGAATGCAGGAACAAACAGAAATGGAGAGTCAAGCCCTTACATTTCTGCAATA
TTCTTATTAATTTTGAACACATGGAAGAGATGATTATCTGAATGGACAGTGAATTTACTTCACTCCTCTTTAAAAAAGCGAAGAAAAAACCCCTCTTGAAGTTCTGAAAAAGATAAAGAGACCAAGCCCTCAGCCAGGT
CAGAAAAACGCAAAAGTAACTCAATGTAACATAACGCATCACTTACCATAAAAGTAACTAGGTAATGCAACTAGTTACTTTTTTGGAGAGTAACTCACTGTTGTAATGCATTACTCATTCAATTTCTTTCTTT
TCGGCTTAGTCCCTTTAATACTGCGGGTCCGCATAGCAGAATGAAGTCCCAACTTATTGACATATGTTTATGACGCGGATGCCCTTCCAGTTGCAACCTTACTGGAACACCCCATACACACTCATTACACAC
ACATAAACTACAGAAAATGAGCCTACCCAAATCACCTGTAGTACATGCTTTGGACTGTGGGGAAACCGGAGCACTCGGAGGAACCCAGCAGATGCGGGGAGAACATGCAAACTCCACAAAAGACACGCCAACTGA
CCCATCCGAGGCTCAARCCAGCAACCTTTTTGCTGTGAGGCGACAGCACTACTACTGCGGCACCGCGTCAACCCTGTAATGCATTACTTTTTAAATGTAACCTTTACCCGACACTAATACAAAACCGTTAATGAAACAAAT
GTTTAAATATAAAACCAACTTTACCTCCATACAAAAGCATGTAGCTTGACTCATTATCTCAGATTTGTGATTTAGTCTTAGAAGGAATCGCTTACTGTAATATGAAGTCTGACTCCAAATGTGAGTTAATTAACCTI
ACTTTTCAGTTTAGTTTGTAGTGGCTTTAAAAATAAAATAAAGGATTTGTCATTTGTGTTATCAACTATTTTATGATATTTTTATTTGCTGTTTTTCTGTTTCTGTCAGGACATCCATGGATGTTTCGGGATGC
AGAAACTGATGATCCAATGGTAGTCAACAATAAAGAGATGTAATTTGCCAGCATCTTTGAAAATGGGCAAGTCGCAAAATGCCAAGATCACATTCGCTGGTATGCATATTTCACTTCAATTTCAATCACACATCTTGTG
CTAATATTGAATTCAGTGTGATACTACAATATAAGTGTGCATTTAAAGGGTTAGCAACCTAAAAAAACCCTAAGACCTTCACTTATTTTGGAAACACAAATTAAGATATGTTAGCTTAAACCTGAAGGAGCTCAT
TCGTATACAGCAACAGTCTGTGATGTTCAAAAGTTGAGAAAAGGAACCAATCCATGTGACTTTAGTGATTCATTTATACAAATTTAATAATATAAAGACACAAGAACATTTTTGTGTGCCAAAAAATGCCTTTAATAA
ATAAATATATATAGTTATAGTATAAATATAACAAGGTTAATGGAAGACAATATGATCTGTGTGAACAAGATAAAACAAGAACTAGTATATATAGTCTTTTGGAGCATGAAAAAATTTGTTGGAACATTTT
TCATGCTGTACTTATGAGTGTTCGCAAGTGTGTAATTCGGTATGGTACTGTATGAGTCTGTCCGCTGTTTCTAAAAACAAAGTTGATGAACAGATTAAAAATCTGTTCAAAAATAGTAGGAAAGCCCTTTGAGAAA
TTATATGACCAATTTATATACAAGAACTTCACAAGGCTGGCAAGAAACATCATTTCAAACCCAGTCTTGAACATTAATTTATACCAITAAAGTCTTACCCTCGATTTAGAGTCCAGGTTTTAATAAATGCAATTT
AAAAAGTCATTTGTACATCAGGCTGTCTTGGAGCTGAATAAGTCTTTTAAAGTGTTTTTTTTTTATTAGTCTGTAGTTTATTATGCTGTGATGCAAGAAAATTTTCCAGTACAGTCTGACAAATAAAGTATTGTA
TTGTTATTGATATATATTAACAATAAAAAAACTAATAAGTATCAAAAAACACAGCAGAACTACTTTAATAAACTAAATCAGAATTAGAAATTAACACTAATCATTITGCAAGTATACAAAAATTAACACTGTTG
ATGTTGTTTAAATAACAAAATTTGCAATTTGCAAAACACACTGTAAAATTTGTTCAAAAATAAAATGGAGCTCATGAATCAAACTCGAGTTGAGTCTGAAAATTTTTTTGCAATGTTGTGTTTGTGTTTACCAGTGTCTGA
CGTTGCGAGATCGCTGTCTGCAAGTTGTGAGACGGTTGGTGGCAGGGAAGATGTCCGCTGTCTGGAGATTGCCCGCTGCTTCAAGAGGATCTAGCTCAGAGACCCAGCATTGAGGCTGATCTACAACGCATTAGCCA
GCGGGTGGAAACAGAAGTTACTGGAGAACAGAGAAGTCAAAAACAGACGAAAACATCAACATTAACCTGGACTGTGCATATGTAAGTCAACCAACAATATAAAAACAACTATATACTATAGTGC
TGTATAACACACAGGGCTGACAAAACAGAGACTGTTTTCTTAATCAGATGGACACTAGATGTTTTAGCTGTTATGATTCATTGACAGGCAGAGACTTGAGAATGCGCAGAGGGAACCTCAGGAAATAGASTTTTTGT
GGTTGTCTGTGTGGCGCCCTACCAATAGATGAGGACAGAAATCTTTTTGGTTAATTTATCTGCATACTTTTACTCAATTACTTTCCATTTGTTTTAAATAATGTTAATAAATAATGTTACTATATTTTTATGTTA
ATAATATAA

```

B

```

AAAGCACCAGACTCGGTGCCACTTTTTCAAGTTGATAACGGACTAGCCCTATTTTAACTTGTATTTCTAGCTCTAAAAAGTATCCGGCTGATCAGAGACTATAGTGAGTCTGATTACGC

```

Figure 4.1. Schematic representation of *vhI* gRNA superimposed on *vhI* genomic sequence (A) *vhI*-gRNA-1 targets the first exon of *vhI*. Text highlighted in red represents untranslated regions, blue represents exons, grey represents introns and green highlights the *vhI*-GNRA-1 binding site. (B) *vhI*-gRNA-1 sequence. Green highlighted text represents the *vhI* target sequence (Target sequence: CGTATCCGGCTGATCAGAGAC).

4.1.1. Using *vh1* loss-of-function to optimise CRISPRi.

To begin utilising CRISPRi as a technique for global gene knockdown, I first established the effective, non-toxic concentration of both gRNA and dCas9. I injected dCas9 into embryos from 250pg/nl through to 1ng/nl and determined the proportion of embryonic lethality (Figure 4.2 A). At 250pg/nl over 80% of embryos survived, while the number of embryos which survived dropped at each successive dose tested. Therefore, 250pg/nl was selected as the optimal concentration, which is similar to concentrations used previously (Rossi et al., 2015). Next, the *vh1* gRNA was injected alone into wild type embryos. Around 60% of embryos survived at 500pg/nl, 1ng/nl and 1.5ng/nl (Figure 4.2 B). I therefore selected 1ng/nl of gRNA.

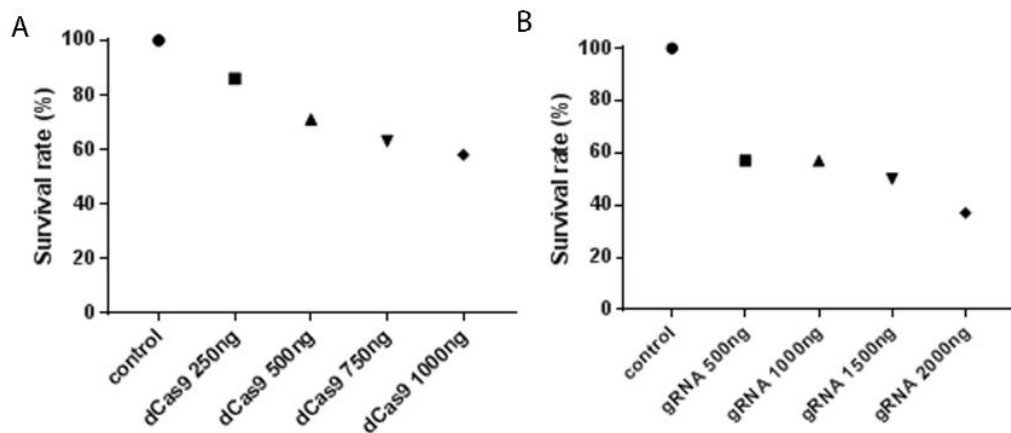


Figure 4.2 Embryonic survival is reduced at by injection of high concentrations of dCas9 or gRNA. (A) Injection of dCas9 mRNA alone causes a dose-dependent increase in embryo death from 250pg/nl to 1ng/nl. **(B)** Injection of *vh1*-gRNA-1 alone also causes a dose-dependent increase in embryo death from 500pg/nl to 2ng/nl.

4.1.2. *vhl* CRISPRi efficiently activates hypoxic signalling

Having established non-lethal concentrations of gRNA and dCas9 mRNA, I sought to ensure that dCas9 was catalytically inactive and therefore did not induce double strand breaks at these doses. CRISPRi knockdown using dCas9 and *vhl*-gRNA-1 was performed alongside mutagenesis using active Cas9, which destroys a *Bs*II restriction site. Amplification of the *vhl* target region by PCR followed by digestion with *Bs*II confirmed that dCas9 is unable to cause DNA double strand breaks and functions as described previously (Rossi et al., 2015) (Figure 4.3).

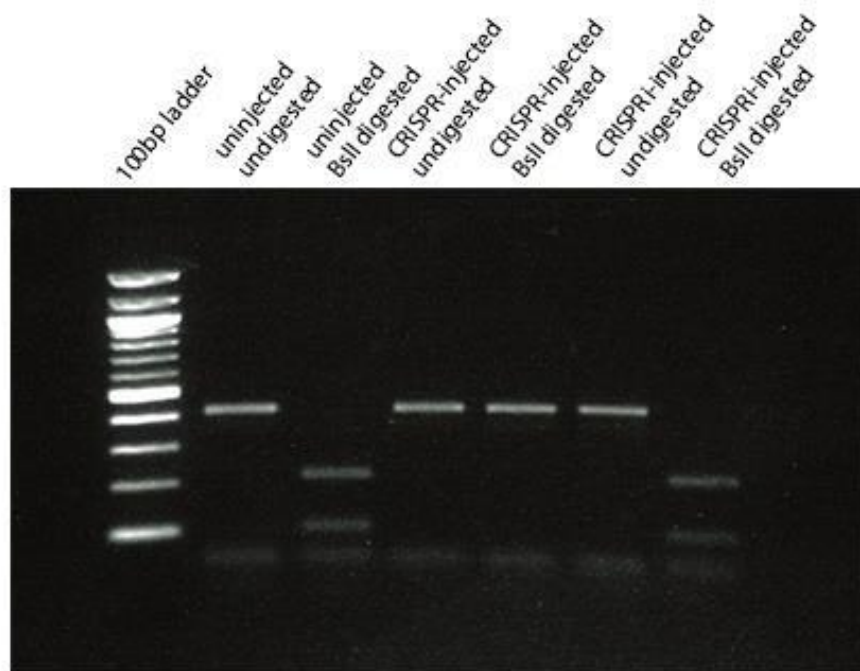


Figure 4.3 *vhl*-gRNA-1 induces double strand breaks when co-injected with active Cas9, but not with dCas9. *vhl*-gRNA-1 targets a *Bs*II restriction enzyme site. Co-injection of *vhl*-gRNA-1 with active Cas9 endonuclease mutates the restriction site. Co-injection with dCas9 does not destroy the restriction site, confirming that dCas9 does not induce double strand DNA breaks in zebrafish embryos.

I employed *Tg(phd3:eGFP)* larvae to determine the efficacy of *vhl* knockdown by CRISPRi compared to *de novo* mutation of *vhl* by co-injection of *vhl*-gRNA1 with Cas9 protein. Ubiquitous activation of GFP was observed in *Tg(phd3:eGFP)* embryos following co-injection of *vhl*-gRNA1 with either dCas9 mRNA or Cas9 protein (Figure 4.4 A-C). Embryos displayed varying levels of GFP fluorescence and were broadly grouped into three categories: GFP high, GFP low and GFP negative (Figure 4.4 A-C). I quantified the frequency of GFP negative, GFP low and GFP high embryos in uninjected controls, embryos injected with *vhl* gRNA1 (hereafter, embryos in which CRISPRi has been performed will be termed “crispants”, while injected mutagenized embryos will be termed “*de novo*” mutants.) and dCas9 and embryos injected with *vhl* gRNA1 and Cas9 protein between embryonic days 1-3 (Figure 4.4 D-F). While a small number of embryos (<5%) showed increased GFP expression in uninjected controls, in both CRISPR knockout and CRISPRi knockdown more than half of injected embryos which carried the *Tg(phd3:eGFP)* transgene displayed increased GFP expression between days 1-3 (Figure 4.4 D-F). However, compared to *vhl*gRNA + Cas9 protein, for which the proportion of GFP high and GFP low embryos remained consistent throughout the three days analysed, CRISPRi embryos displayed an increase in the proportion of embryos which displayed high levels of GFP fluorescence between day 1 and day 2 (Figure 4.4 D, E), and this began to decrease from day 3 to day 5 (Figure 4.4, F-G). This suggests CRISPRi acts transiently before gRNAs degrade, or become too diffuse through subsequent rounds of cell division to effectively knockdown gene expression.

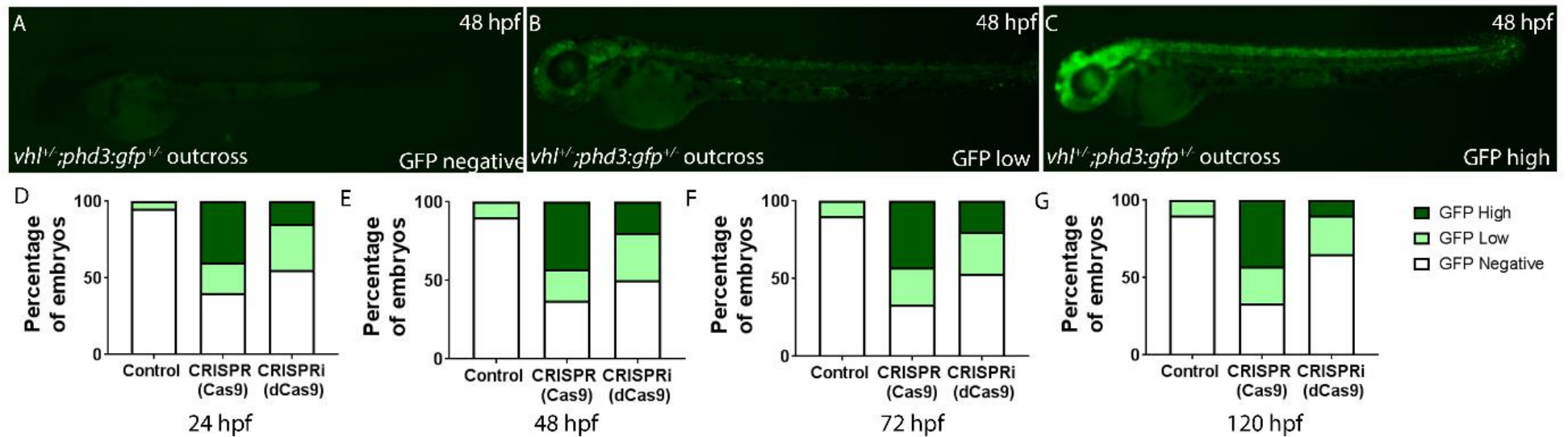


Figure 4.4 *vhl* CRISPRi knockdown transiently activates *phd3:eGFP* expression. (A-C) CRISPRi knockdown of *vhl* increases GFP fluorescence in *Tg(phd3:GFP)* embryos. Examples are shown at 48 hpf and reflect GFP negative (A), GFP low (B) and GFP high (C) categories. All three examples were taken from embryos following CRISPRi knockdown and comparable embryos were observed using CRISPR-Cas9 *de novo* mutagenesis. (D-F) Activation of fluorescent *phd3:GFP* reporter increases in efficiency between 24 and 48 hpf, but begins to decrease in efficiency between 48 hpf and 120 hpf. CRISPR/Cas9 *de novo* knockout remains consistent for all five days.

4.3 Knockdown of *vhl* induces angiogenic branching defects and kidney filtration defects

Vhl^{hu2117} mutants display excessive angiogenesis from 3 dpf onwards, due to increased VEGF signalling (van Rooijen et al., 2010), which can be rescued by inhibiting blood flow (Watson et al., 2013). Recent observations in *vhl* mutant embryos described kidney filtration defects (Noonan et al., 2016). Having established activation of the *phd3:eGFP* reporter, I next examined whether well established *vhl* loss of function phenotypes were induced by CRISPRi. To determine whether *vhl* knockdown could induce increased angiogenesis as observed in *vhl^{hu2117}* mutants (van Rooijen et al., 2010), I performed *vhl* CRISPRi in *Tg(fli1a:EGFP)y1* embryos alongside both *vhl* mutagenesis using Cas9 protein and observation of mutants from a *Tg(fli1a:EGFP)y1;vhl^{hu2117/+}* heterozygous incross.

Tg(fli1a:EGFP)y1;vhl^{hu2117/+} embryos were observed at 5 dpf and imaged above the cloaca. While *vhl* mutants clearly displayed clear excessive angiogenesis around the DLAV, compared to controls (Figure 4.5 A, B, E), the phenotype was less pronounced in both *de novo vhl* mutants and in *vhl* CRISPRi knockdown (Figure 4.5 C, D, E). *vhl* CRISPRi moderately induced ectopic angiogenesis at the site at which ISVs form the DLAV and which was more pronounced in *de novo* mutants. Proportionally, fewer embryos displayed a phenotype using CRISPRi (Figure 4.5 E), in keeping with indications that CRISPRi efficiency decreases beyond 3 dpf (Figure 4.4).

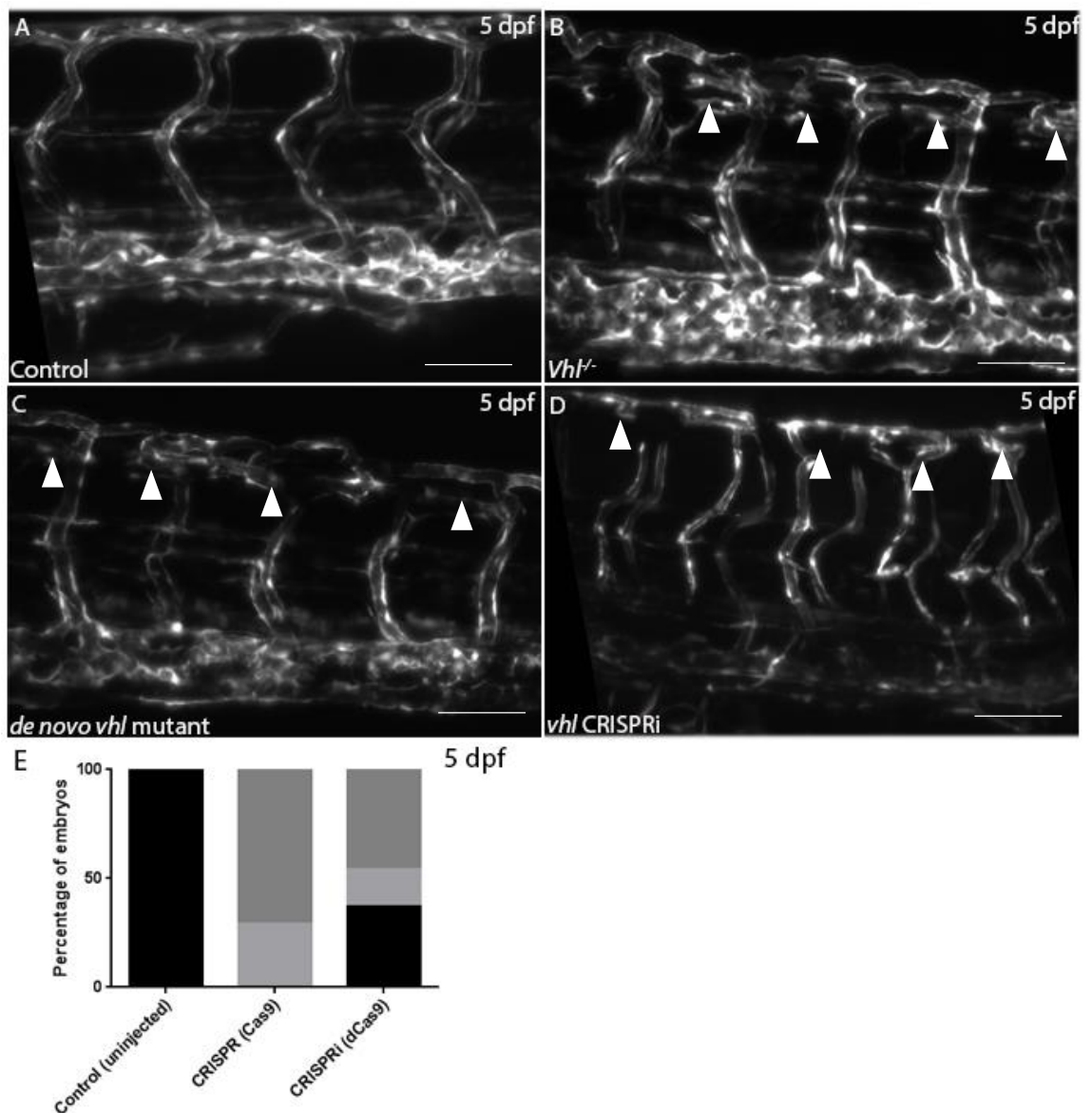


Figure 4.5 *vhl* CRISPRi knockdown induces mild ectopic angiogenesis at 120 hpf. (A-D) *vhl* CRISPRi knockdown causes ectopic angiogenesis around the DLAV (D), which is less pronounced than both *vhl* mutants (B) and *de novo vhl* mutants (C). (E) Compared to controls, both *de novo* mutants and CRISPRi knockdown embryos display more embryos with mild or severe phenotypes. Black represents no phenotype, dark grey represents a mild phenotype and light grey represents a severe phenotype.

In *vhl* mutants, impaired kidney filtration has been demonstrated using the lipophilic fluorescent dye, BODIPY 493/503, to quantify lipid density within the pronephric tubules. *Vhl* mutants display increased pronephric lipid density compared to controls, as indicated by increased BODIPY fluorescence (Noonan

et al., 2016). I applied this approach to *vhl* CRISPRi, using *vhl* mutants and uninjected embryos as controls.

Fluorescence was measured in each embryo and groups were compared. Both *vhl^{hu2117}* mutants and *vhl* CRISPRi showed significant increases in mean fluorescence intensity (Figure 4.6 B-D), compared to uninjected controls (Figure 4.6 A, D). Mean pronephric fluorescence intensity was greater in *vhl^{hu2117}* mutants, indicating increased Vhl function *vhl* CRISPRi embryos than in *vhl^{hu2117}* mutants, as previously shown (Figure 4.4; Figure 4.5). Taken together these data indicate that CRISPRi reliably inhibits gene function in zebrafish embryos.

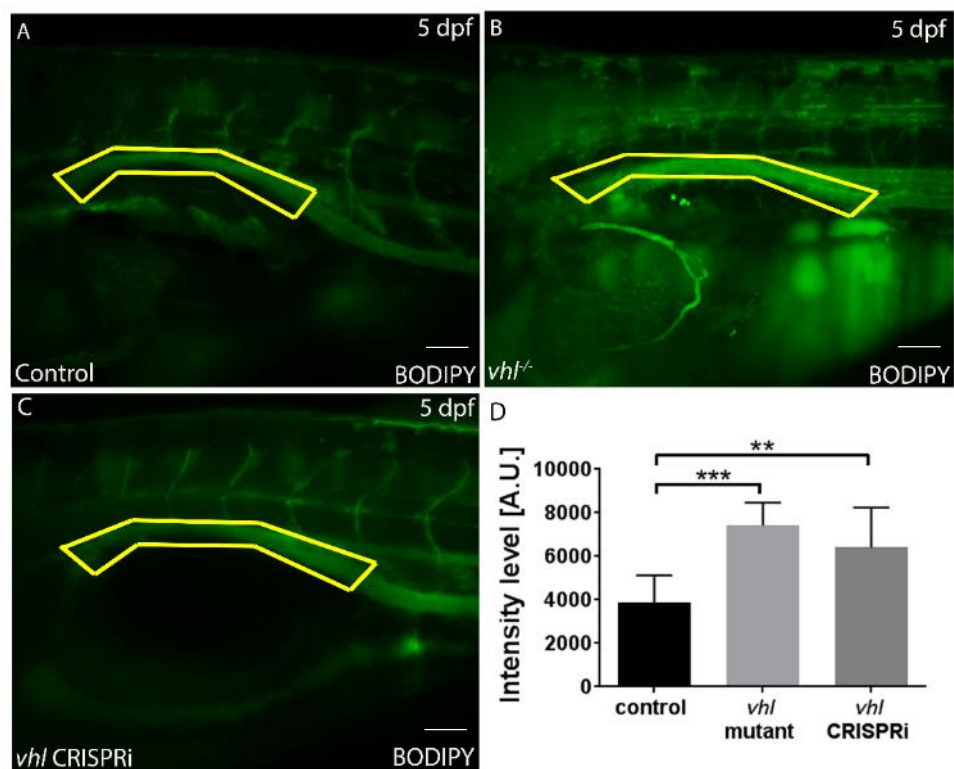


Figure 4.6 *vhl* CRISPRi knockdown induces kidney filtration defects comparable with *vhl* mutants. (A-D) *vhl* CRISPRi knockdown causes kidney filtration defects comparable to *vhl^{hu2117/hu2117}* mutants. Both mutants and knockdown embryos display significantly increased fluorescence intensity compared to controls. Yellow boxes indicate region of interest which was quantified.

4.4 Development of tissue-specific CRISPRi as a tool to conditionally modulate gene expression.

Conditional gene knockout has recently been achieved in zebrafish using tissue specific expression of active Cas9 (Ablain et al., 2015). However, this approach generates highly mosaic embryos harbouring distinct mutations, harmful or otherwise, in different cells of the embryo. I therefore hypothesised that by utilising a similar approach and expressing dCas9 under the control of tissue specific promoters, I could, achieve tissue-specific knockdown. Since knockdown of *vhl* or *tmem33* induce abnormal kidney and vascular development, I generated transgenic constructs to drive dCas9 expression from under the control of the endothelial specific *fli1a* (Villefranc et al., 2007) and kidney specific *enpep* (Seiler and Pack, 2011) promoters. I hypothesised that by using this approach, I would be able to determine whether the observed vascular and kidney phenotypes in *vhl* and *tmem33* knockdown arise due to loss of gene function within those tissues.

Initial attempts to label dCas9 by fusion to a fluorophore were unsuccessful and reduced knockdown efficacy or low fluorescence were encountered (data not shown). Therefore I employed a dominant marker for transgenesis. Since endothelial cells and kidney cells were under study I selected, *cryaa:CFP* to allow visualisation of transgene integration since this labels the lens with CFP (Durdu et al., 2014; Zou et al., 2015) (Figure 4.7).

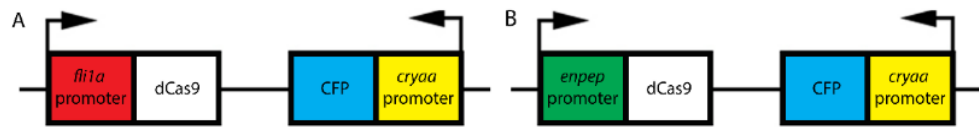


Figure 4.7 Schematic representation of tissue-specific CRISPRi constructs. (A) Construct to drive dCas9 expression in endothelial cells under the control of the *fli1a* promoter. **(B)** Construct to drive dCas9 expression in kidney cells under the control of the *enpep* promoter. In each construct the *cryaa* promoter drives CFP in the eye as a positive control for transgenesis.

4.4.1 Developing kidney specific gene knockdown by CRISPRi: *vhl* is required in a tissue specific manner for normal kidney function

To determine whether my *enpep:dCas9* construct facilitated transient knockdown of *vhl* within the kidney, I exploited the *Tg(phd3:GFP)* transgenic reporter. Embryos were injected with the *enpep:dCas9* construct alongside Tol2 transposase mRNA to facilitate transgenesis, and *vhl*-gRNA-1 or a control gRNA. Control gRNA was designed using the targeting sequence for *vhl*-gRNA-1, but lacked the Cas9 binding element of the RNA (see Table 2.3). Embryos injected with the *enpep:dCas9* plasmid and *vhl*-gRNA-1 displayed clear upregulation of GFP in the pronephric tubules (Figure 4.8 B, D white arrowheads) and developing glomeruli (Figure 4.8 D red arrowheads). GFP expression was also observed in the neural tube, suggesting the promoter is not entirely specific to the kidney (Figure 4.8 B blue arrowhead). However, the clearest upregulation of *phd3:GFP* occurred in the kidney, suggesting the kidney was the tissue in which *vhl* knockdown was most effective.

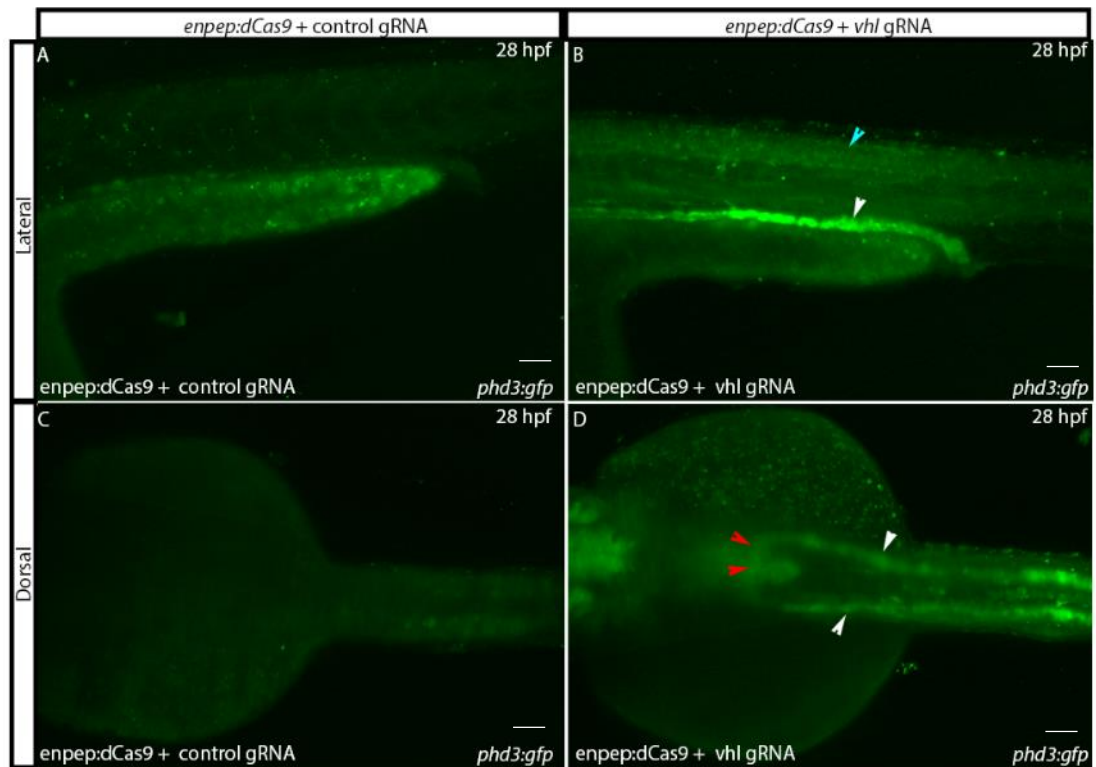


Figure 4.8 Tissue-specific knockdown of *vhl* by CRISPRi increases GFP in the kidney of *Tg(phd3:GFP)* embryos. (A-D) Kidney-specific *vhl* CRISPRi upregulates *phd3:gfp* fluorescence in the pronephros (blue arrowheads) and developing glomeruli (red arrowheads). Embryos also display ectopic upregulation of *phd3:gfp*, particularly in neural tissues (blue arrowhead).

Having shown that it was possible to upregulate GFP in a kidney-specific manner via CRISPRi in *Tg(phd3:GFP)* embryos, I applied kidney-specific CRISPRi knockdown to examine whether the kidney filtration defect observed in both *vhl* mutants and following global knockdown of *vhl* by CRISPRi occurred cell autonomously. Fertilised eggs were injected with the *enpep:dCas9* plasmid and *vhl*-gRNA-1 before incubation with BODIPY 493/503 dye. Embryos displayed a dose-dependent increase in BODIPY fluorescence (Figure 4.9 A-C), with embryos injected with 2nl of 25pg/nl plasmid, 250pg/nl Tol2 and 1ng/nl *vhl*-gRNA-

1 displaying significantly greater fluorescence than controls, while 1nl injections were not sufficient to cause a significant increase in fluorescence (Figure 4.9 D).

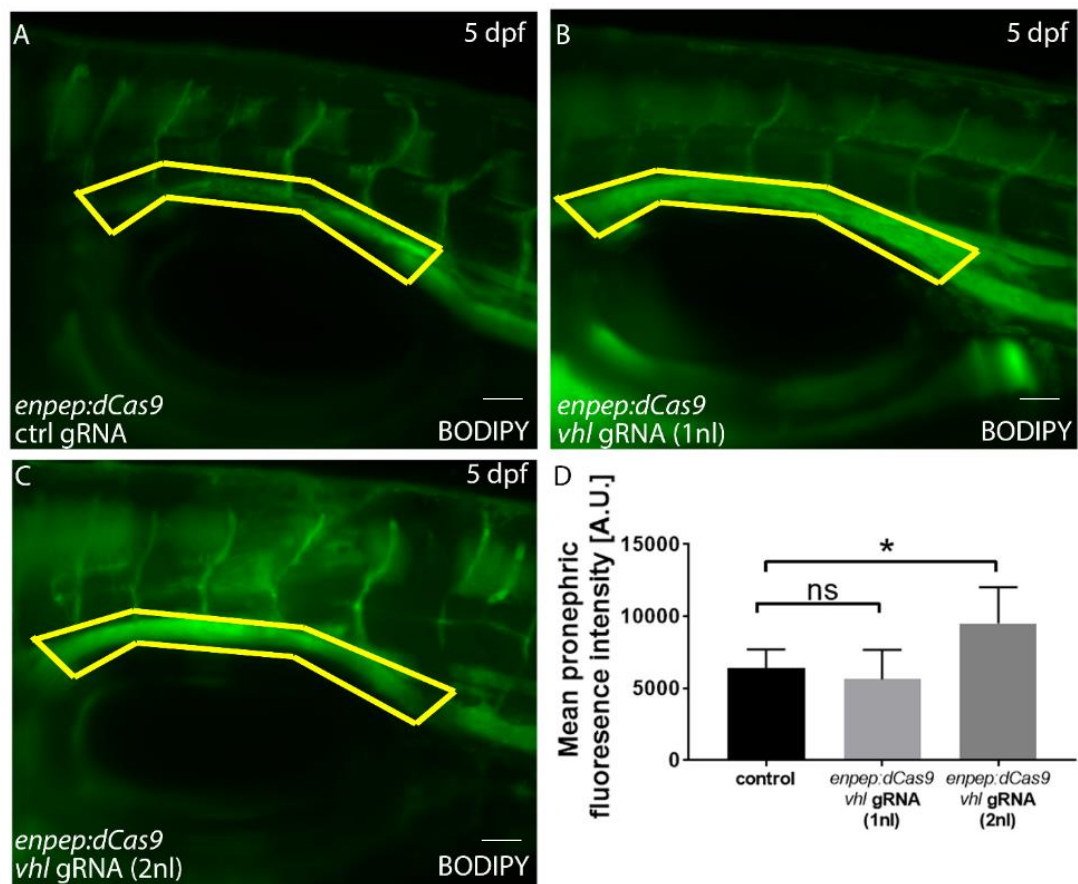


Figure 4.9 Kidney-specific knockdown of *vhl* by CRISPRi is sufficient to induce kidney filtration defects observed following global knockdown of *vhl* by CRISPRi. (A-D) Kidney-specific *vhl* CRISPRi induces a dosage dependent increase in BODIPY 493/503 fluorescence intensity, with the highest dose being significant.

4.5 Knockdown of *tmem33* using CRISPR interference reduces *tmem33* mRNA expression and induces vascular and kidney defects.

I established CRISPRi and tissue-specific CRISPRi as an effective means of knockdown, using *vhl* as a test bed. I next sought to apply the same approaches to *tmem33*, to determine whether CRISPRi knockdown could recapitulate the vascular and kidney abnormalities induced by morpholino knockdown. Guide

RNAs were designed to target *tmem33* before and after the translation start site to enable them to be used in tandem. One guide targeted the 5'UTR, while the second targeted the coding sequence just downstream of the translation start site (Figure 4.10).

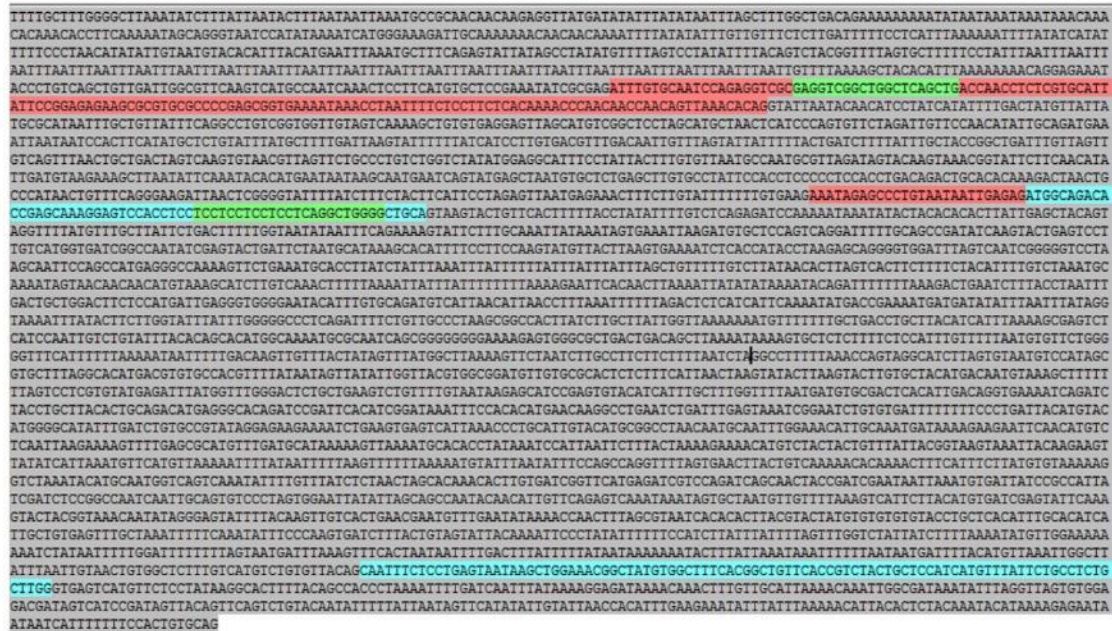


Figure 4.10 Guide RNA design for *tmem33*. *tmem33* exon 1-3 are shown in blue for coding sequence and red for untranslated regions. Grey represents intronic DNA and green represents gRNA target sequences.

To confirm that the gRNAs designed for *tmem33* functioned as expected, I injected embryos with dCas9 and *tmem33* gRNAs. These were then fixed and *in situ* hybridisation for *tmem33* mRNA was performed. Embryos subject to *tmem33* CRISPRi displayed a reduction in staining for *tmem33*, suggesting CRISPRi reduces transcription and the gRNAs function as expected (Figure 4.11). Although embryos displayed a reduction in mRNA (Figure 4.11 B), a complete loss of mRNA was not observed, indicating a reduction, but not abrogation of expression. This was present in roughly 60% of embryos, which is comparable to

the proportion of embryos displaying *vhl* knockdown, shown previously (Figure 4.4). Knockdown of *tmem33* by CRISPRi was confirmed by qPCR and a mean knockdown of around 70% observed, indicating this was a robust procedure to knockdown *tmem33* expression (Figure 4.13 C).

Recent studies have suggested that morpholino knockdown causes off-target effects, including the upregulation of *p53* expression (Kok et al., 2014; Rossi et al., 2015). To determine whether *tmem33* knockdown by both morpholino and CRISPRi induce *p53*, I performed qRT-PCR on batches of embryos in which *tmem33* had been knocked down by either morpholino or CRISPRi. While *tmem33* morphants displayed a significant increase in *p53* expression, *tmem33* crispants did not (Figure 4.11 D), indicating that *tmem33* CRISPRi induces fewer off-target effects than morpholinos.

I next analysed the effects of *tmem33* CRISPRi knockdown on endothelial and kidney development. *tmem33* was knocked down in *Tg(fli1a:AC-TagRFP)sh511* embryos. Injected embryos were analysed at 52 hpf, to determine whether DLAV formation was compromised. Embryos displayed vascular branching defects including poorly developed ISVs and DLAV malformations (Figure 4.11 E-G), recapitulating the morpholino phenotype observed previously (Figure 1.2). *tmem33* morphants develop glomerular distension from 52 hpf onwards (Figure 3.9). Furthermore, comparably to morphant kidney phenotypes, *tmem33* crispants displayed glomerular expansion at 52 hpf (Figure 4.11 H-J).

These data indicate that CRISPRi knockdown of *tmem33* is sufficient to induce development of glomerular and vascular defects, similarly to morpholino

knockdown, while at the same time, *tmem33* knockdown does not induce *p53* upregulation, suggesting fewer off-target effects take place.

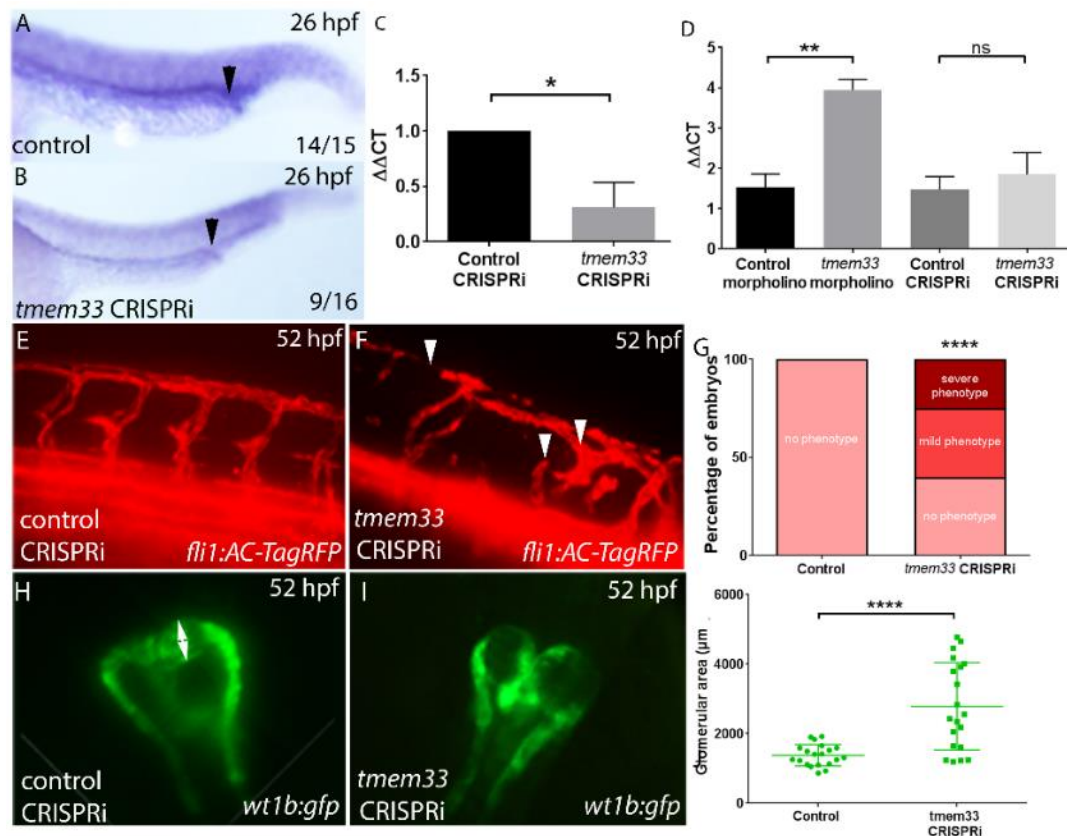


Figure 4.11 *tmem33* CRISPRi recapitulates *tmem33* morpholino phenotypes (A-B) *tmem33* CRISPRi injected embryos display reduced *tmem33* expression by *in situ* hybridisation (black arrowhead indicates developing pronephros). (C) *tmem33* expression is significantly reduced following CRISPRi (unpaired t-test * $p < 0.05$). (D) Induction of *p53* expression is reduced in *tmem33* crispants in comparison to *tmem33* morphants (one-way ANOVA ** $p < 0.01$). (E-G) *tmem33* CRISPRi injected *Tg(fli1a:AC-TagRFP)sh511* embryos display angiogenic defects (white arrowheads) at 52 hpf, compared to controls (mild phenotype = <3 angiogenic defects; severe ≥ 3 angiogenic defects; unpaired t-test **** $p < 0.0001$). (H-J) *tmem33* CRISPRi increases glomerular size similar in *tmem33* crispants (white arrowheads) in *Tg(-26wt1b:eGFP)li1* embryos (unpaired t-test **** $P < 0.0001$).

4.6 *tmem33* overexpression rescues *tmem33* crispant phenotype.

To confirm that the vascular phenotype observed in *tmem33* crispants was due to loss of *tmem33* function, I simultaneously overexpressed *tmem33* in *tmem33* crispants to determine whether it was able to rescue the CRISPRi phenotype. While *tmem33* knockdown alone significantly increased angiogenic abnormalities, overexpression of *tmem33* alone did not (Figure 4.12, B, C, E). Furthermore, simultaneous knockdown and overexpression did not significantly increase the frequency of angiogenic defects, compared to controls (Figure 4.12 A, E). Significantly fewer angiogenesis defects were observed in simultaneous knockdown and overexpression compared to knockdown alone (Figure 4.12 D, E). Collectively this demonstrates that aberrant angiogenesis observed following *tmem33* knockdown is not due to off-target effects, but loss of *tmem33* function.

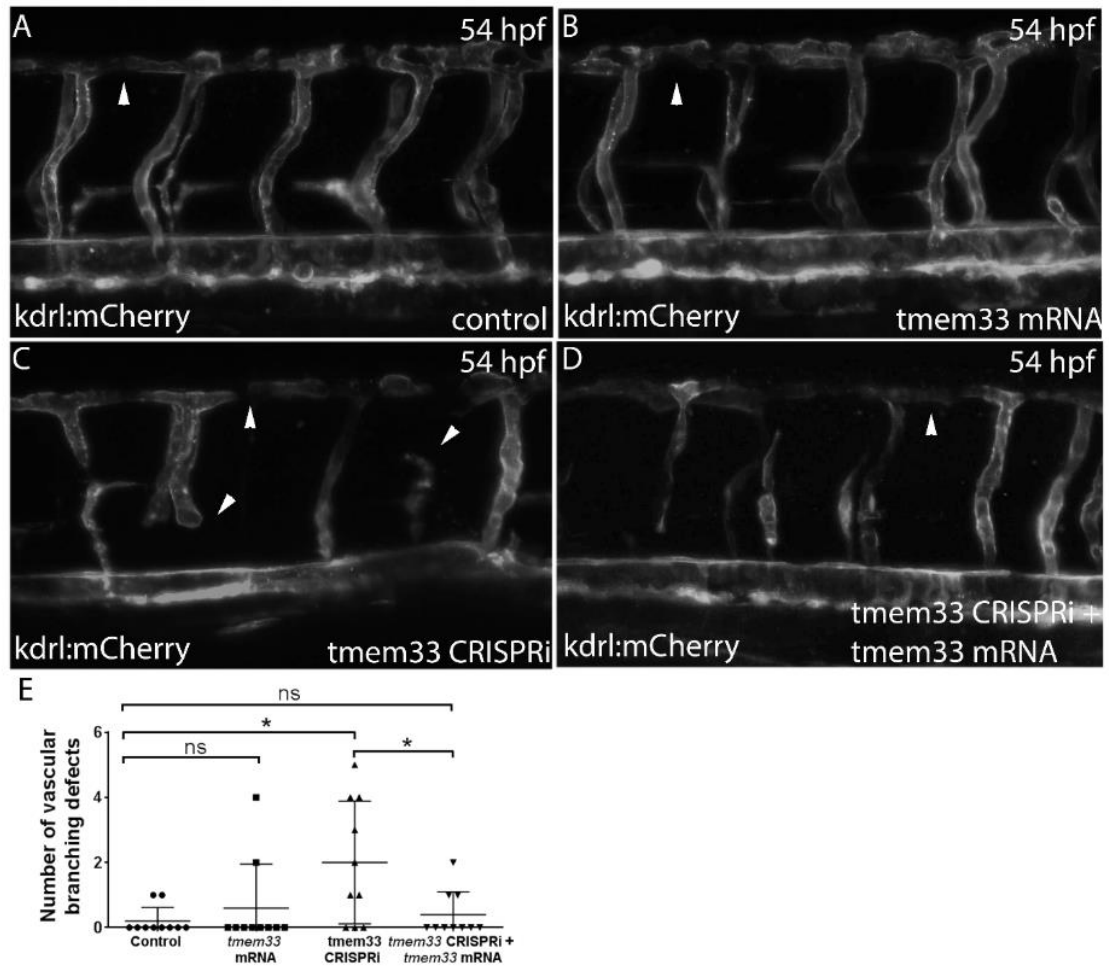


Figure 4.12 *tmem33* CRISPRi-induced defects can be rescued by overexpression of full-length *tmem33* mRNA (A-D) *tmem33* CRISPRi-induced angiogenic defects (C) are reduced when full-length *tmem33* mRNA is simultaneously overexpressed (D) (white arrowheads). *tmem33* overexpression alone is not sufficient to cause angiogenic defects (B). (E) Angiogenic defects observed in *tmem33* overexpression and simultaneous overexpression and knockdown are not significantly increased compared to controls, while *tmem33* knockdown alone is significantly increased. (One-way ANOVA with *post-hoc* Dunnett's test, * $p < 0.05$).

4.7 *tmem33* knockdown by CRISPRi attenuates endothelial calcium oscillations.

I next performed *tmem33* CRISPRi knockdown on *Tg(fi1a:gff)ubs3;Tg(uas:GCaMP7a)sh392* embryos to determine whether CRISPRi was sufficient to impair calcium signalling, as observed in morpholino knockdown. *tmem33* crispants displayed reduced endothelial calcium oscillations, with fewer regions of intensity observed in sprouting SeAs compared to controls (Figure 4.13 A, C). This correlated with observed changes in fluorescence over time and the overall frequency of calcium oscillations (Figure 4.13 B, D, E). Therefore *tmem33* CRISPRi is sufficient to recapitulate reduced calcium oscillations induced by morpholino knockdown. These data further indicate that *tmem33* is required for endothelial calcium signalling during sprouting angiogenesis.

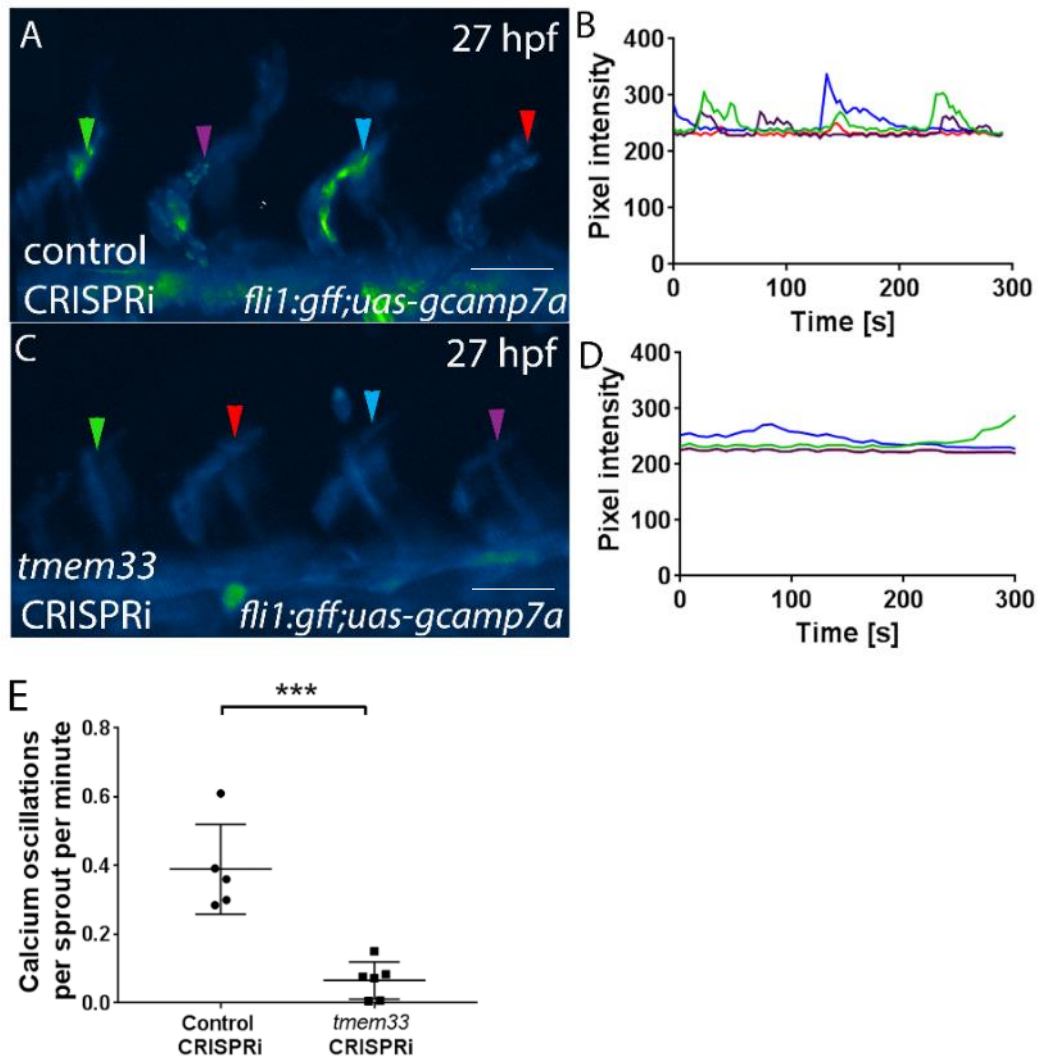


Figure 4.13 *tmem33* CRISPRi reduces endothelial calcium signalling frequency. (A-D) (A, C) Maximum projection over time, displaying regions of increased calcium signalling. Regions of the highest levels of calcium signalling are in yellow, while regions of low calcium signalling are in dark blue. *tmem33* crispants display reduced calcium signalling in endothelial tip cells (arrowheads). (B, D) Intensity trace peak colours correspond to coloured arrowheads in (A) and (C). (D) *tmem33* crispants display a significant decrease in calcium oscillation frequency per embryo overall (unpaired t-test, *** $p < 0.001$).

4.8 *tmem33* knockdown by CRISPRi reduces endothelial filopodia dynamics and number

tmem33 morphants display delayed angiogenesis and reduced endothelial filopodia numbers (Figure 1.8 and Figure 3.12). To determine whether endothelial malformations observed in *tmem33* crispants were due to reduced F-actin dynamics, and whether crispants fully recapitulate the morphant phenotype, I performed *tmem33* CRISPRi in *Tg(fli1a:LifeACT-mClover)sh467* embryos. *tmem33* crispants displayed reduced endothelial filopodia compared to controls (Figure 4.14 A-B, black arrowheads, C). Furthermore, filopodial length was significantly reduced, indicating a reduction in F-actin-dependent cellular extensions (Figure 4.14 D). These data confirm that *tmem33* is required for endothelial filopodia formation, as previously observed following morpholino knockdown.

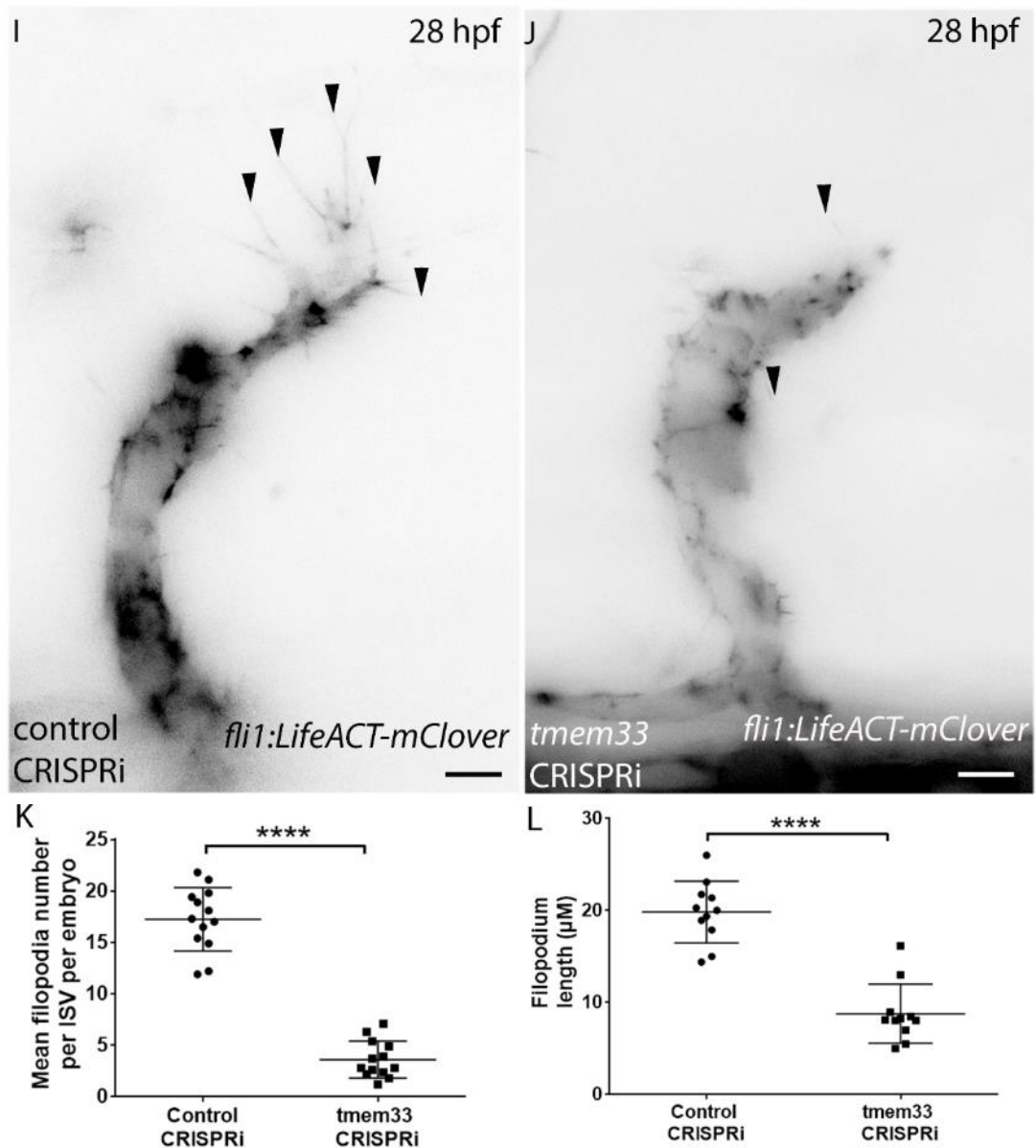


Figure 4.14 *tmem33* CRISPRi reduces endothelial filopodia numbers during sprouting angiogenesis (A-B) *tmem33* CRISPRi causes angiogenic delays and a reduction in endothelial filopodia in *Tg(fli1a:LifeACT-mClover)sh467* embryos (black arrowheads). (C-D) Significantly fewer filopodia are observed and observed cellular extensions are reduced in length (unpaired t-tests, ** $p < 0.01$, **** $p < 0.0001$).

4.9 Transient knockdown of *tmem33* by tissue-specific CRISPRi can uncouple kidney and vascular defects.

I next sought to determine whether *tmem33* is required specifically in endothelium and kidney during development. I therefore performed transient tissue-specific knockdown in endothelial and kidney cells using constructs driving dCas9 expression under the control of the *fli1a* and *enpep* promoters, respectively (Figure 4.7). An intercross of *Tg(fli1a:AC-TagRFP)sh511* and *Tg(-26wt1b:eGFP)li1* lines was performed and progeny with RFP positive vasculature and GFP positive kidney were injected with plasmids driving dCas9 within endothelial or kidney cells (Figure 4.7) alongside either control gRNA or *tmem33* gRNAs. Embryos were imaged at 55 hpf.

While embryos injected with *tmem33* control gRNAs were morphologically normal (Figure 4.15 A, C, E, G), endothelial-specific *tmem33* knockdown induced angiogenic patterning defects but not glomerular expansion (Figure 4.15 B, F) and kidney-specific knockdown caused glomerular expansion, but not vascular malformations (Figure 4.15 D, H). When vascular abnormality was quantified, transient *tmem33* EC-specific knockdown induced a significant number of mild or severe vascular defects (Figure 4.15 I). Conversely, transient *tmem33* kidney-specific knockdown displayed expanded glomeruli (Figure 4.15 J). These data indicate that *tmem33* is required within endothelial cells for normal angiogenesis and kidney cells for normal pronephric development

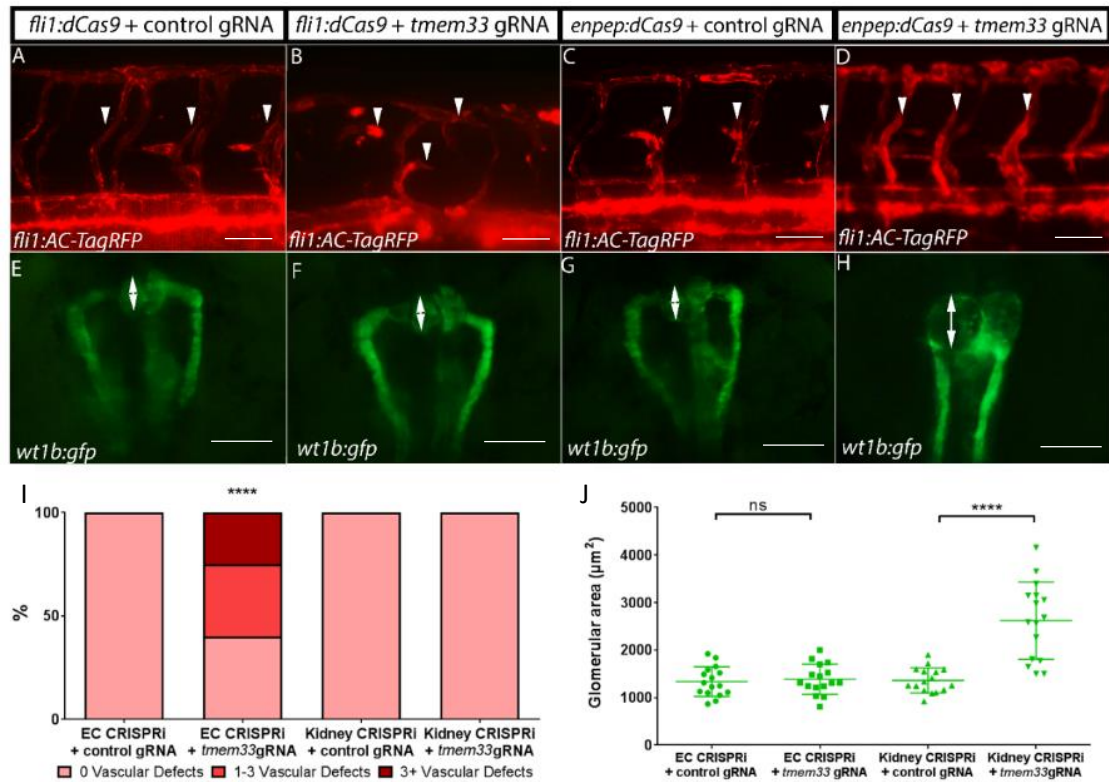


Figure 4.15 Transient tissue-specific *tmem33* CRISPRi induces defects during angiogenesis and kidney development independently at 55 hpf (A-H) (A, C, E, G) Transient endothelial and kidney dCas9 expression does not cause vascular or glomerular defects when co-injected with control gRNAs. (B, F) Endothelial-specific *tmem33* knockdown induces vascular defects, but not kidney defects. (D, H) Kidney-specific *tmem33* knockdown causes glomerular expansion but does not affect vascular patterning. **(I)** Only endothelial-specific *tmem33* knockdown induces vascular defects (Two-way ANOVA **** $p < 0.0001$). **(J)** Only kidney-specific *tmem33* knockdown causes glomerular expansion (One-way ANOVA with *post-hoc* Dunnett's test **** $p < 0.0001$).

4.10 Transient knockdown of *tmem33* using tissue specific CRISPRi is comparable to global *tmem33* knockdown by morpholinos or global CRISPRi.

To determine whether tissue-specific knockdown was as effective as global knockdown, I compared phenotypes induced by transient knockdown to both

global *tmem33* CRISPRi and global knockdown via morpholinos. Again, an intercross of *Tg(fli1a:AC-TagRFP)sh511* and *Tg(-26wt1b:eGFP)li1* lines was performed to differentially label the developing vasculature and kidney and embryos were injected with either global control CRISPRi, *tmem33* morpholinos, global *tmem33* CRISPRi, EC-specific *tmem33* CRISPRi or kidney-specific *tmem33* CRISPRi. At 55 hpf, frequency of abnormal vascular branching events and glomerular area were quantified.

Knockdown of *tmem33* by morpholino induced both the greatest number of vascular defects and the greatest increase in glomerular area, while global CRISPRi and tissue specific CRISPRi induced comparable vascular defects and glomerular expansion (Figure 4.16 A-B). The greater phenotypic severity of morphants may in part be due to the increased off-target effects of morpholinos in comparison to CRISPRi (Figure 4.11). These data suggest that tissue-specific knockdown is comparable to global knockdown with regards to efficacy and reinforces my data indicating that the vascular and kidney phenotypes induced by global *tmem33* knockdown are caused by loss-of-function of *tmem33* in these tissues.

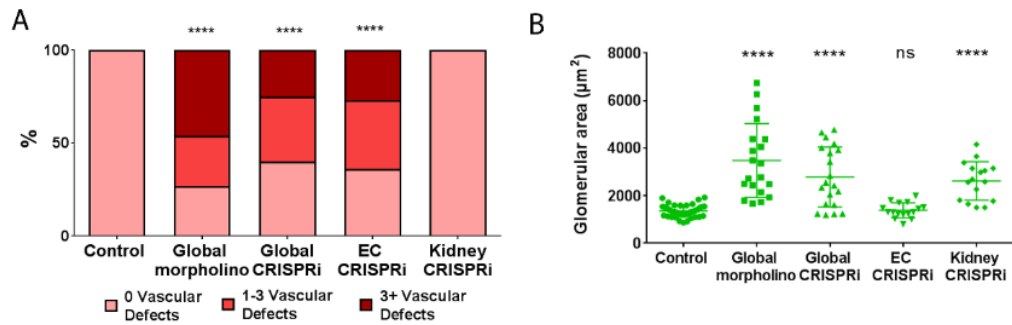


Figure 4.16 Transient tissue-specific *mem33* CRISPRi induces both vascular and kidney developmental defects comparable to global knockdown. (A) Global knockdown by morpholino and CRISPRi, as well as endothelial-specific *mem33* knockdown induce vascular defects, while control CRISPRi and kidney-specific CRISPRi do not (Two-way ANOVA **** $p < 0.0001$). **(B)** Global knockdown by morpholino and CRISPRi, as well as kidney-specific *mem33* knockdown induce glomerular expansion, while control CRISPRi and endothelial-specific CRISPRi do not (One-way ANOVA **** $p < 0.0001$).

4.11 Generation of a stable *Tg(fli1a:dCas9,cryaa:CFP)sh512* transgenic zebrafish line

Transient tissue-specific knockdown can be used to determine whether a gene is required during development in a tissue-specific manner. However, transient knockdown relies on mosaic integration of plasmids into the host embryo genome. If transgene integration occurs after the single-cell stage, embryos mosaically express transgenes, leading to the possibility that neighbouring cells may not express the same transgene, or express it at the same level. Therefore, to overcome this variability and control the level of dCas9 expression, I raised *cryaa:CFP*⁺ embryos injected with the *fli1a:dCas9;cryaa:CFP* plasmid to adulthood. Embryos were raised in *Tg(kdrl:HRAS-mCherry-CAAX)s916* and *Tg(fli1a:EGFP)y1* transgenic backgrounds to label the developing endothelium

with different fluorophores, in addition to a non-transgenic background to facilitate intercrosses with other transgenic reporters.

Following the establishment of transgenic lines expressing the *fli1:dCas9* transgene, I screened the F1 progeny using *in situ* hybridisation to determine whether dCas9 was expressed specifically in endothelial cells. An outcross was performed and embryos were selected according to the presence or absence of *cryaa:CFP* fluorescence. Founders were identified whose progeny expressed dCas9 in endothelial cells, in both SeAs (Figure 4.17 A, black arrowheads) and the dorsal aorta (Figure 4.17 A, red arrowhead). At this time point, *cryaa* is not expressed, meaning selection by eye colour is impossible. However, around 50% of embryos selected displayed endothelial enrichment, suggesting a single copy was transmitted. At 50 hpf, expression within the endothelium was maintained in *cryaa:CFP⁺* embryos (Figure 4.17 C), but not in *cryaa:CFP⁻* embryos (Figure 4.17 B), confirming that the presence of *cryaa:CFP* fluorescence is an indicator of *fli1a:dCas9* expression. This transgenic line was designated *Tg(fli1a:dcas9;cryaa:CFP)^{sh512}*.



Figure 4.17 *Tg(fli1a:dCas9,cryaa:CFP)sh512* embryos express dCas9 in endothelial cells.

(A) dCas9 expressed is enriched in endothelial cells in *Tg(fli1a:dCas9,cryaa:CFP)sh512* embryos at 26 hpf in the dorsal aorta (red arrowhead) and SeAs (black arrowheads). (B) In 50 hpf *Tg(fli1a:dCas9;cryaa:CFP)sh512*, *cryaa:CFP*⁻ embryos, no expression is observed in the dorsal aorta or ISVs. However trapping is observed in the notochord (blue arrowhead). (C) dCas9 expressed is enriched in endothelial cells in *Tg(fli1a:dCas9;cryaa:CFP)sh512*, *CFP*⁺ embryos at 50 hpf in the dorsal aorta (red arrowhead) and ISVs (black arrowheads). Trapping in the notochord is observed at this stage (blue arrowhead).

4.12 Endothelial specific *dll4* knockdown by CRISPRi in stable *Tg(fli1a:dcas9;craa:CFP)sh512* transgenics induces aberrant DLAV patterning.

Having identified stable dCas9 expression in *Tg(fli1a:dCas9,cryaa:CFP)sh512* embryos, I next sought to perform EC-specific *dll4* knockdown, since the *dll4* loss of function phenotype is well-characterised in zebrafish and this would serve as a positive control as to whether the transgenic functions as expected (Suchting et al., 2007; [CSL STYLE ERROR: reference with no printed form.]). I performed EC-specific *dll4* knockdown by CRISPRi in an intercross between *Tg(fli1a:dCas9,cryaa:CFP)sh512* and *Tg(fli1a:EGFP)y1* transgenic lines and raised embryos until 3 dpf to analyse vascularisation around the DLAV. At 48 hpf, I separated *cryaa:CFP*⁺ and *cryaa:CFP*⁻ embryos. I observed an increased DLAV diameter in *cryaa:CFP*⁺ embryos at 3 dpf (Figure 4.18 B, white arrowheads), whereas *cryaa:CFP*⁻ embryos did not display this (Figure 4.18 A, white

arrowheads). I measured the diameter of the DLAV at the widest point and found that *cryaa:CFP*⁺ embryos displayed a significant increase in DLAV diameter compared to *cryaa:CFP*⁻ embryos (Figure 4.18 C).

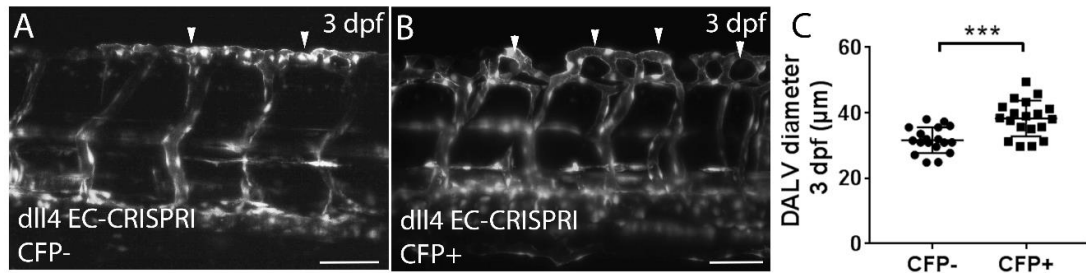


Figure 4.18 Tissue-specific *dlla4* CRISPRi increases DLAV vascularisation (A-B) *dlla4* EC-specific crisprants display increased vascularisation around the DLAV from 3 dpf (white arrowheads), indicating increased angiogenesis. **(C)** DLAV area is significantly increased in *dlla4* EC-specific crisprants (unpaired t-test, *** $p < 0.001$).

4.13 Endothelial specific knockdown of *tmem33* by CRISPRi in stable *Tg(fli1a:dcas9;craa:CFP)^{sh512}* transgenics induces vascular branching defects but not glomerular expansion.

To determine whether sufficient knockdown could be performed in stable *Tg(fli1a:dcas9,cryaa:CFP)^{sh512}* transgenic zebrafish, I injected *tmem33* gRNAs into *Tg(fli1a:dcas9,cryaa:CFP);Tg(fli1a:EGFP)y1* embryos. Embryos did not display *cryaa:CFP* expression by 30 hpf since this promoter is active from 48 hpf. Therefore embryos were selected blindly and ISV length was quantified, before separating the fish to determine genotype by *cryaa:CFP* fluorescence retrospectively after 48 hpf. *tmem33* crisprants displayed significantly reduced SeA length (Figure 4.19, white arrowheads, C), indicating reduced EC migration compared to controls, in which more SeAs had completed dorsal migration

(Figure 4.19 A-B, yellow arrowheads; C). At 53 hpf, embryos were selected for the presence or absence of *cryaa:CFP* fluorescence. *cryaa:CFP⁻* embryos displayed no angiogenic defects and had completed DLAV anastomosis, with a continuous DLAV (Figure 4.19 D, yellow arrowhead). *Cryaa:CFP⁻* embryos also displayed normal development of parachordal lymphangioblasts (Figure 4.19 D, red arrowhead). In contrast, *cryaa:CFP⁺* embryos displayed incomplete anastomosis (Figure 4.19 E, yellow arrowhead), misbranched ISVs (Figure 4.19 E, white arrowhead) and an absence of parachordal lymphangioblasts (Figure 4.19 E, red arrowhead), as previously demonstrated in *tmem33* morphants (Figure 1.9). Quantification of total DLAV length revealed a significant reduction in *CFP⁺* embryos (Figure 4.19 F). Next, to determine whether knockdown occurred within non-endothelial cells in *Tg(fli1a:dCas9,cryaa:CFP)sh512* embryos, I injected *tmem33* gRNAs into progeny from an intercross of *Tg(fli1a:dCas9,cryaa:CFP)sh512* x *Tg(-26wt1b:EGFP)li1* zebrafish to label the developing kidney. Embryos were raised to 55 hpf and selected for the presence or absence of *cryaa:CFP* expression. Glomeruli were imaged and quantified and no significant difference in glomerular area was observed between *cryaa:CFP⁺* or *cryaa:CFP⁻* embryos (Figure 4.19 G-I), indicating that *tmem33* knockdown within *Tg(fli1a:dCas9,cryaa:CFP)sh512* embryos is sufficient only to induce vascular defects. Collectively this demonstrates that generation of stable transgenic lines in which dCas9 expression is driven under control of tissue type-specific promoters is a viable method by which to conditionally abrogate gene function.

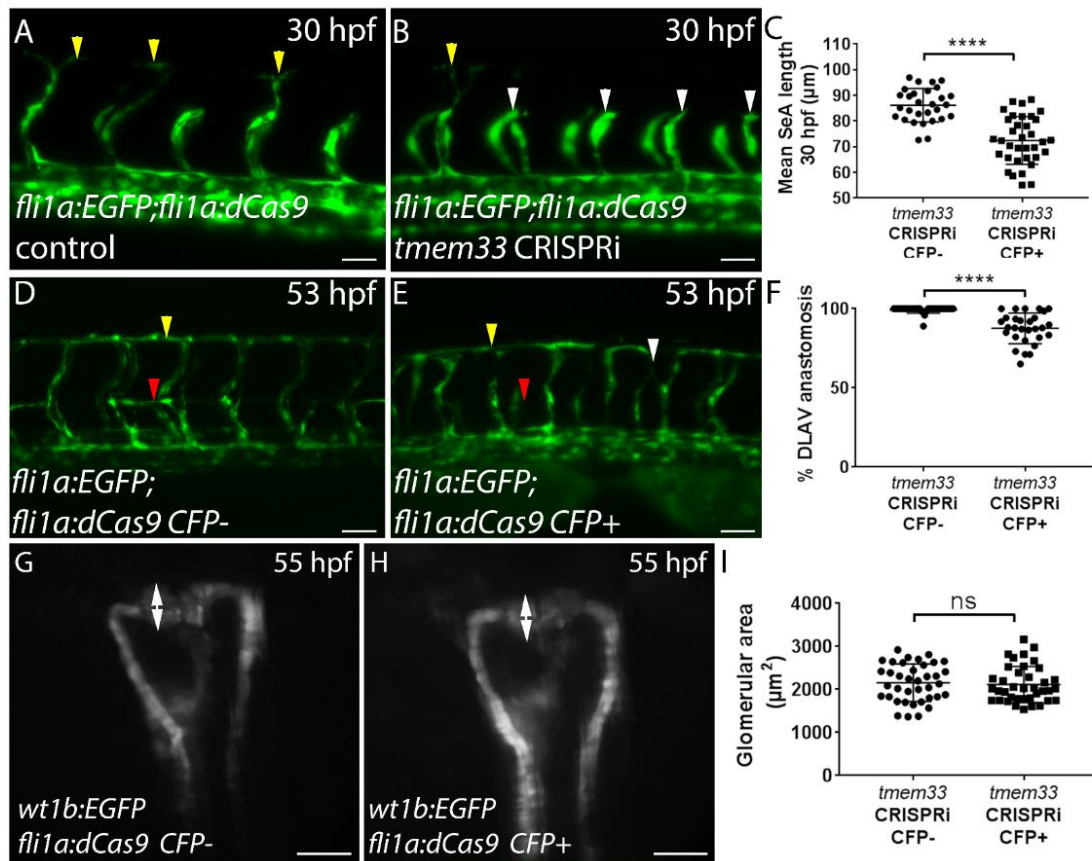


Figure 4.19 Tissue-specific *tmem33* CRISPRi induces vascular developmental defects but not glomerular expansion. (A-B) *tmem33* crispants display more delayed SeAs (white arrowheads) than SeAs beginning anastomosis (yellow arrowheads) than control embryos. (C) *tmem33* crispant mean SeA length is significantly lower than controls (unpaired t-test *p=<0.001). (D-E) *tmem33* crispants display impaired anastomosis (yellow arrowheads), collateral vessel formation (white arrowheads) and a lack of lymphatic vasculature (red arrowhead). (F) *tmem33* crispant percentage DLAV anastomosis is significantly lower than controls (unpaired t-test *p=<0.05). (G-H) EC-specific *tmem33* does not induce an increase in glomerular area in *cryaa:CFP+* or *cryaa:CFP-* embryos. (I) No significant difference in *tmem33* crispant glomerular area is observed between CFP+ and CFP- embryos (unpaired t-test P, non-significant).**

4.14 *tmem33* functions downstream of VEGF signalling during angiogenesis.

To determine whether *tmem33* may function downstream of VEGF signalling during angiogenesis, I first asked whether *tmem33* knockdown could suppress *vegfa*-mediated calcium signalling in developing SeAs. Calcium signalling is known to be activated downstream of VEGF signalling both in cell culture and *in vivo* (Yokota et al., 2015; Zadeh et al., 2009). *Tmem33* localises to the ER (Figure 3.3) and I have demonstrated that knockdown of *tmem33* disrupts endothelial calcium signalling (Figure 3.7, Figure 4.13), suggesting *tmem33* promotes endothelium calcium oscillations during angiogenesis. Furthermore, I have shown that overexpression of *vegf165* mRNA increases calcium oscillation frequency (Figure 3.5). I therefore selected calcium signalling frequency as a metric to establish epistasis between VEGF signalling and *tmem33*. *Tg(fi1a:gff)ubs3;Tg(uas:GCaMP7a)sh392* embryos were injected with *vegf165* mRNA, *tmem33* CRISPRi or both *vegf165* mRNA and *tmem33* CRISPRi simultaneously and imaged at 26 hpf continuously for five minutes to quantify calcium signalling frequency. Embryos injected with *vegf165* mRNA alone displayed an increase in calcium signalling frequency, compared to controls (Figure 4.20 A, B, I) and increased calcium signalling in stalk and dorsal aorta cells (Figure 4.20 B, white arrowheads), which do not display high levels of calcium signalling in control embryos (Figure 4.20 A). As previously shown (Figure 3.7; Figure 4.13), *tmem33* knockdown reduced calcium signalling frequency (Figure 4.20 C, I) and reduced overall GCaMP fluorescence (Figure 4.20 C). Overexpression of *vegf165* mRNA in the presence of *tmem33* knockdown by CRISPRi reduced calcium oscillations similar to *tmem33* knockdown alone (Figure 4.20 C, D, I). These data suggest *Tmem33* functions downstream of

VEGF signalling and promotes VEGF-mediated calcium oscillations during angiogenesis.

I next asked whether *tmem33* knockdown could suppress *vegfa*-mediated proliferation of ECs within developing ISVs. Since VEGF functions as a mitogen, increased VEGF signalling increases EC proliferation. To determine whether *Tmem33* functions downstream of VEGF signalling during EC proliferation in angiogenesis, I injected *Tg(flk1:EGFP-NLS)zf109;Tg(kdrl:HRAS-mCherry-CAAX)s916* embryos which label endothelial membrane with RFP and endothelial nuclei with GFP, with *vegf₁₆₅* mRNA, *tmem33* morpholinos or both *vegf₁₆₅* mRNA and *tmem33* morpholinos simultaneously. Embryos were imaged at 55 hpf and the mean number of ECs was quantified in 10 pairs of ISVs along the yolk cell extension. Control embryos displayed an average of 3 ECs per ISV (Figure 4.20 E, J), while embryos injected with *vegf₁₆₅* mRNA alone displayed a significant increase, to an average of 3.5 ECs per ISV (Figure 4.20 F, J). However, *tmem33* knockdown in the presence or absence of *vegf₁₆₅* mRNA overexpression reduced EC numbers to an average of 2.5 ECs per ISV (Figure 4.20 G, H, J), suggesting *tmem33* functions downstream of VEGF signalling during EC proliferation. Furthermore, these data suggest that *tmem33* mediates the effect of VEGF during EC proliferation within forming ISVs.

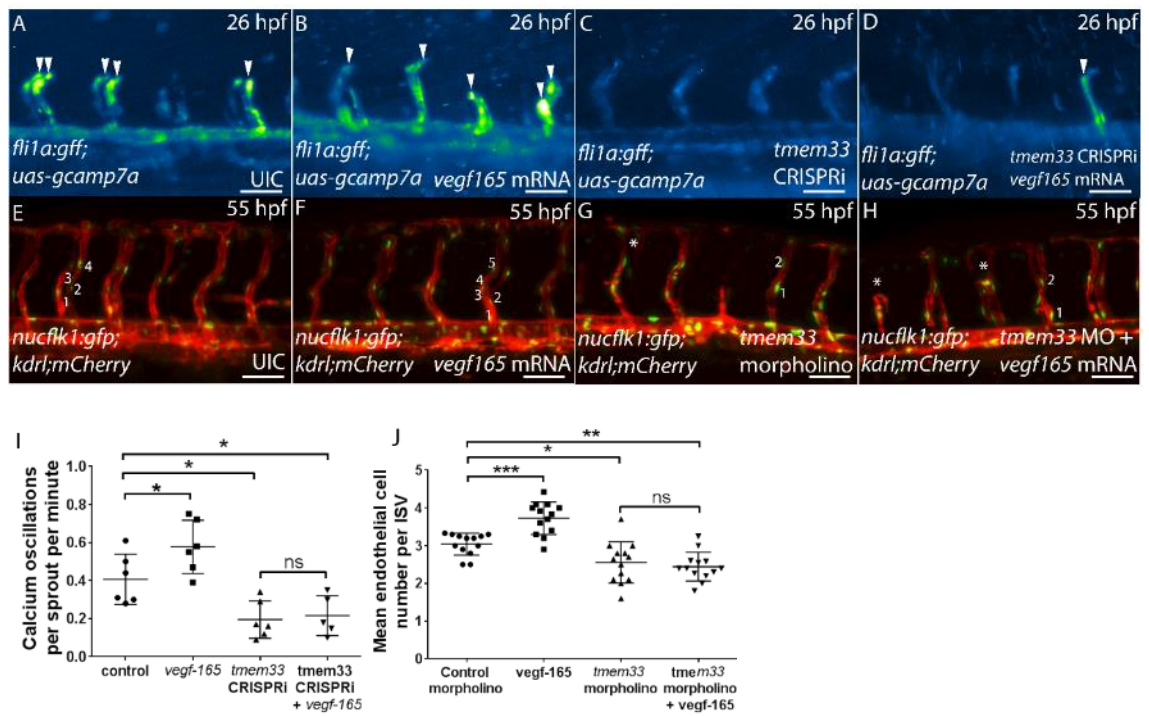


Figure 4.20 *tmem33* functions downstream of VEGF during endothelial proliferation and the regulation of calcium signalling. **(A-D)** Overexpression of *veg165* mRNA causes increased endothelial calcium signalling, including ectopic stalk cell calcium signalling (B, white arrowheads), while *tmem33* knockdown reduces endothelial calcium signalling (C). Reduced calcium signalling is also observed following simultaneous *tmem33* knockdown and *veg165* overexpression (D). **(E-H)** Overexpression of *veg165* mRNA increases ISV EC number (F, white numbers), while both *tmem33* knockdown and simultaneous *tmem33* knockdown and *veg165* overexpression reduce EC number (G, H). **(I)** *veg165* overexpression causes a significant increase in calcium oscillation frequency compared to controls, while both simultaneous *tmem33* knockdown and simultaneous *tmem33* knockdown and *veg165* overexpression significantly reduce calcium oscillation frequency (One-way ANOVA with Holm-Sidak's corrections * $p < 0.05$). **(J)** EC number is significantly increased by *veg165* overexpression and significantly decreased by both simultaneous *tmem33* knockdown and simultaneous *tmem33* knockdown and *veg165* overexpression significantly (One-way ANOVA with Holm-Sidak's corrections * $p < 0.05$, ** $p < 0.01$, *** $p < 0.001$).

To determine whether *tmem33* knockdown affects transcription of the VEGF signalling machinery, I analysed expression of the four zebrafish VEGF receptors

vegfr1/flt1, *vegfr2/kdr*, *vegfr3/flt4* and *vegfr4/kdr1* by *in situ* hybridisation on both control embryos and embryos in which *tmem33* had been knocked down by CRISPRi. No obvious difference was observed in expression of *mflt1*, *sflt1*, *kdr* or *kdr1*, suggesting that expression of these receptors are not affected by *tmem33* knockdown (Figure 4.21 A-F, I, J). However, *flt4* displayed a clear reduction in staining (Figure 4.21 G, H), suggesting that *tmem33* knockdown reduces *flt4* transcription. To further confirm that *flt4* transcription, but not transcription of other VEGF receptors, was reduced following *tmem33* knockdown, I performed qRT-PCR on *tmem33* morphants and crispants. Only *flt4* displayed a significant reduction in transcription, when knocked down by morpholino, but not CRISPRi (Figure 4.21 K). These data suggest that *tmem33* knockdown reduce expression of *flt4*. Since *flt4* is essential for development of lymphatic vasculature (Joukov et al., 1996), this may explain why *tmem33* knockdown inhibits formation of lymphatic vessels in zebrafish. Furthermore, *flt4* is dispensable for SeA formation and therefore unlikely to account for primary angiogenic defects observed (Hogan et al., 2009).

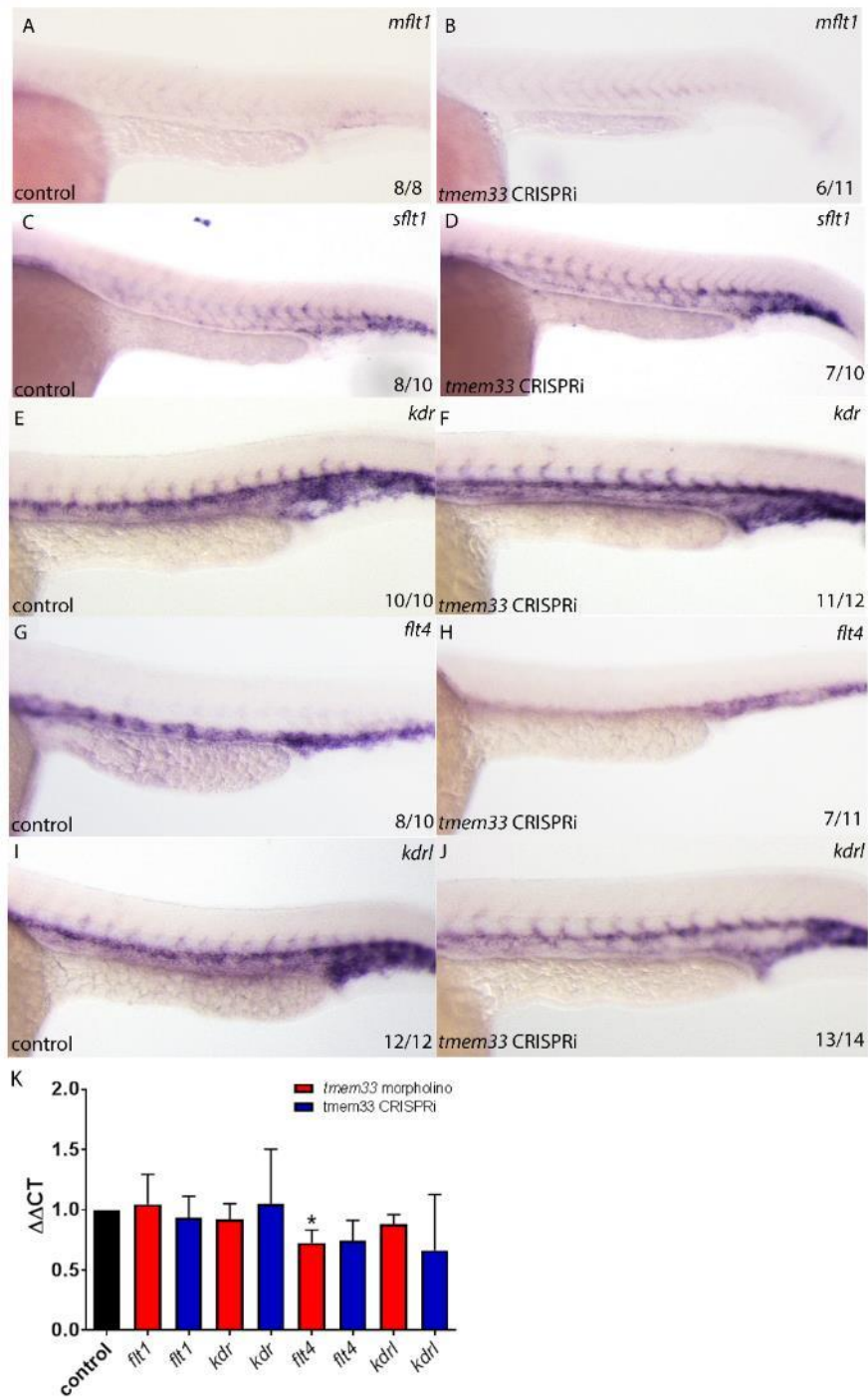


Figure 4.21 *tmem33* CRISPRi reduces expression of *flt4*, but not other VEGF receptors. (A-J) *In situ* hybridisation shows that *flt4* expression is downregulated within the PCV following *tmem33* CRISPRi knockdown (H), but no other gene displays any clear change in expression compared to controls. (K) *tmem33* knockdown does not significantly alter *flt1*, *kdr* or *kdrl* mRNA expression levels. However, *flt4* expression is significantly reduced following *tmem33* morpholino knockdown, but interestingly not by CRISPRi (Two-way ANOVA * $P < 0.05$). Numbers indicate proportion of embryos which displayed expression pattern.

4.15 *tmem33* promotes Notch signalling during angiogenesis

Given that *tmem33* mediates the response to VEGF and VEGF induces Notch signalling during angiogenesis (Phng and Gerhardt, 2009), I sought to determine epistasis between *tmem33* and Notch signalling. I employed the *Tg(CSLBS:Venus)qmc61* reporter, which accurately reports Notch signalling using expression Venus fluorescent protein driven by concatemers of a binding site of the Notch target, CSL (Gray et al., 2013).

At 28 hpf, no difference in the expression of Venus was observed in the notochord (Figure 4.22 A, B blue asterisk), neural tube (Figure 4.22 A, B blue arrowhead) and dorsal aorta (Figure 4.22 A, B red arrowhead) of control or *tmem33* morphants. This was verified by measuring mean pixel intensity of dorsal aortas, normalised to the yolk cell extension background fluorescence (Figure 4.22 C). However, by 48 hpf, reduced Venus expression in endothelial cells of *tmem33* morphants were observed compared to controls, both in the dorsal aorta (Figure 4.22 D, E red arrowhead) and ISVs (Figure 4.22 D, E white arrowheads). Furthermore, reduced Venus expression was observed in the notochord and neural tube (Figure 4.22 D, E blue asterisk and blue arrowheads, respectively) of *tmem33* morphants. This was also verified by quantification of mean aortic pixel intensity (Figure 4.22 F)

To verify observed changes in Notch reporter fluorescence I assayed expression of components of Notch signalling using qPCR following *tmem33* knockdown. I found that expression of multiple Notch ligands (*notch1a*, *notch1b* and *notch3*), receptors (*dll4*) and targets (*hey1*, *hey2* and *her12*) were reduced by *tmem33*

knockdown using morpholino or CRISPRi (Figure 4.22 G-H). No significant difference in expression of Notch signalling components was observed at 26 hpf between control and *tmem33* knockdown embryos (Figure 4.22 G-H), consistent with Notch reporter data (Figure 4.22 A-C). However, in accordance with observations in the Notch reporter, (Figure 4.22 D-F), components of Notch signalling were reduced at 48 hpf, via both CRISPRi and morpholino knockdown. This showed that *tmem33* knockdown impaired expression of Notch signalling genes known to regulate angiogenesis, such as *dll4*, by 48 hpf (Suchting et al., 2007; [CSL STYLE ERROR: reference with no printed form.]) (Figure 4.22 G-H). These data suggest that *tmem33* promotes induction of Notch signalling in endothelial cells.

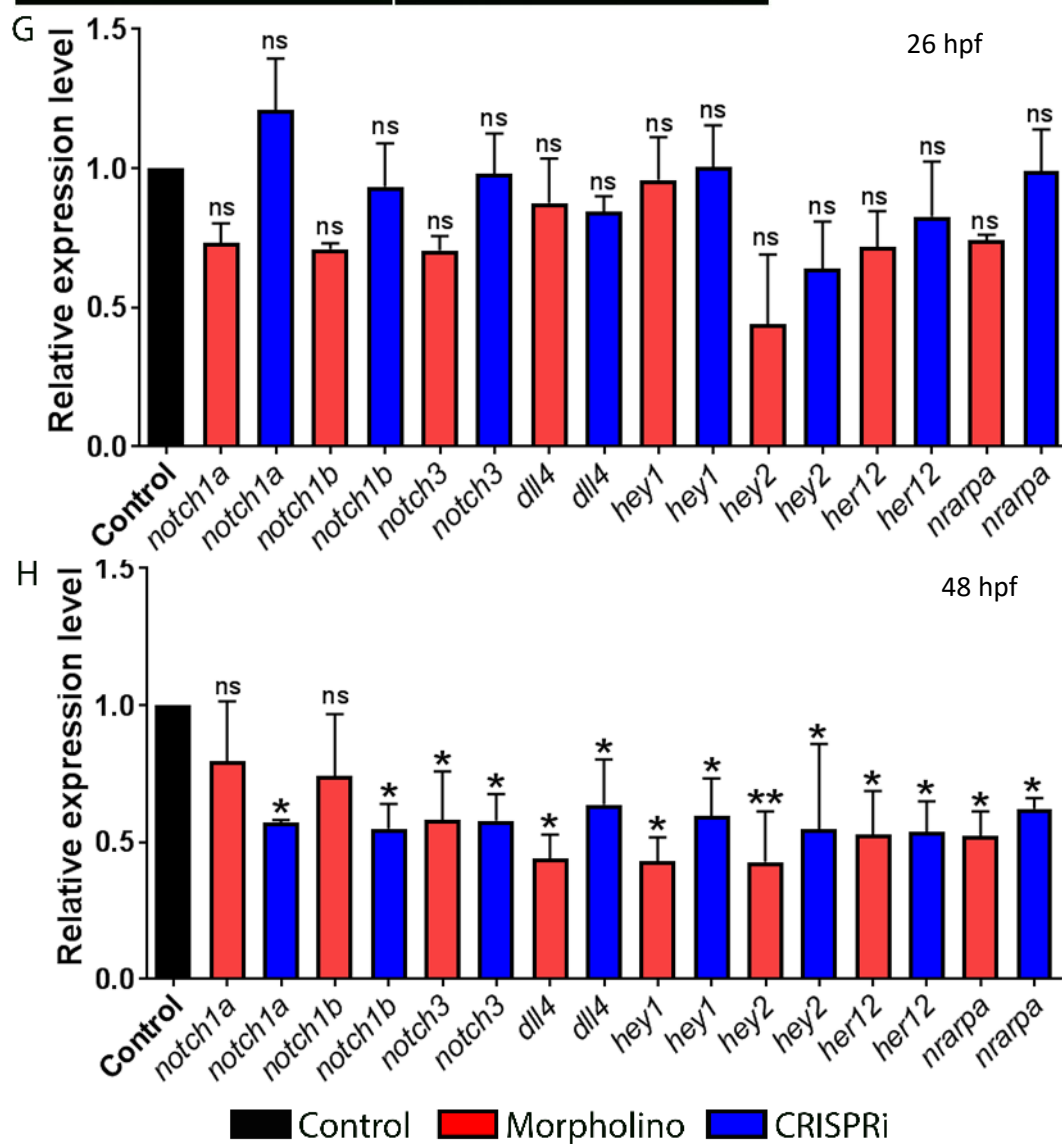
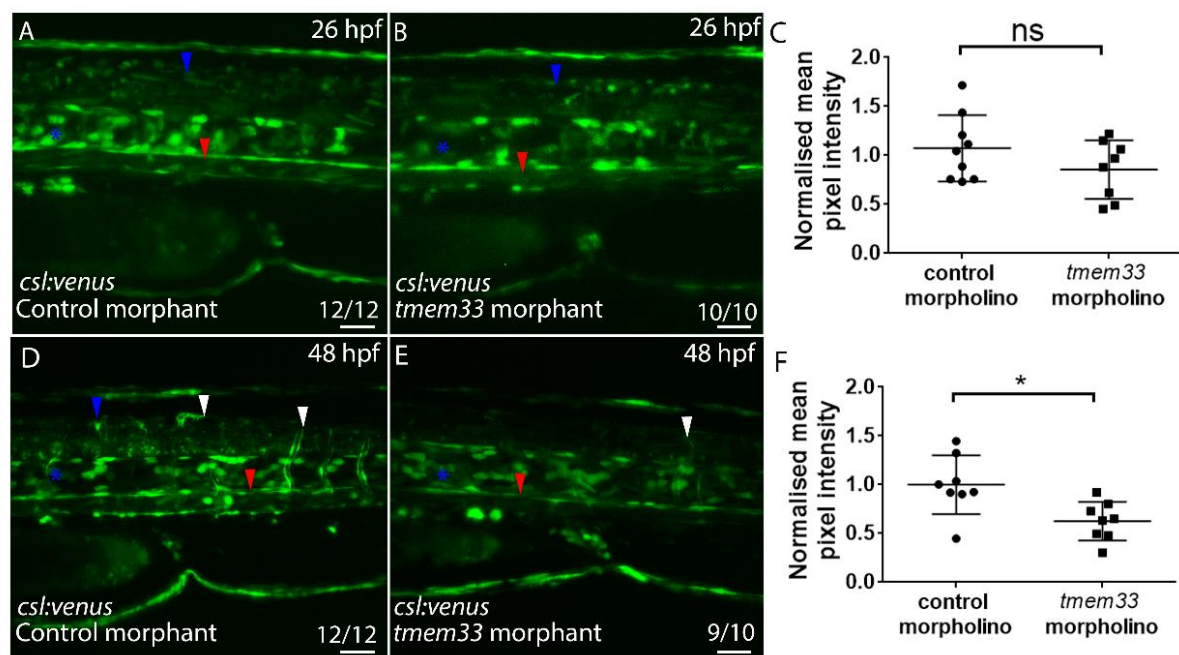


Figure 4.22 *tmem33* knockdown reduces Notch signalling in the endothelium (A-B) At 28 hpf, *CSL:Venus* fluorescence is observed in the neural tube (blue arrowhead), notochord (blue asterisk) and dorsal aorta (red arrowhead) in both control and *tmem33* morphants. **(C)** Mean normalised aortic pixel intensity is not significantly affected at 28 hpf (unpaired t-test, ns=non significant). **(D-E)** At 48 hpf, fluorescence is observed in the neural tube (blue arrowhead), notochord (blue asterisk), ISVs (white arrowheads) and dorsal aorta (red arrowhead) in control morphants. In *tmem33* morphant, fluorescence is reduced in the dorsal aorta (red arrowhead) and ISVs (white arrowhead). **(F)** Mean normalised aortic pixel intensity is significantly reduced at 48 hpf (unpaired t-test, * $p < 0.05$) (G-H) At 28 hpf, vasculature-enriched genes do not display significant changes in expression levels following *tmem33* knockdown, either by CRISPRi or morpholino, but do display significantly decreased expression by 48 hpf (Two-way ANOVA * $p < 0.05$).

4.16 *tmem33* promotes endothelial MAPK/ERK signalling during angiogenesis

The MAP Kinase signalling cascade is activated downstream of VEGF signalling (Deng et al., 2013b; Hong et al., 2006; Murakami et al., 2011; Shin et al., 2016) and regulates many aspects of EC physiology during angiogenesis, including EC proliferation and migration (McMullen et al., 2005; Meadows et al., 2001). ERK signalling induces expression of *dll4* and *flt4* in ECs (Shin et al., 2016). Since *tmem33* functions downstream of VEGF and promotes Notch signalling, I examined whether induction of ERK was dependent upon *tmem33* function. I knocked down *tmem33* in *Tg(fli1a:EGFP)y1* embryos using by CRISPRi and quantified phosphorylated ERK activity using whole-mount immunofluorescence. *tmem33* crispants displayed reduced endothelial pERK staining (Figure 4.23 A). ECs displayed a significant reduction in normalised pERK fluorescence, indicating that MAP kinase signalling is reduced in ECs *tmem33* knockdown

(Figure 4.23 B). This suggests that at least a partial requirement for calcium signalling exists upstream of ERK signalling.

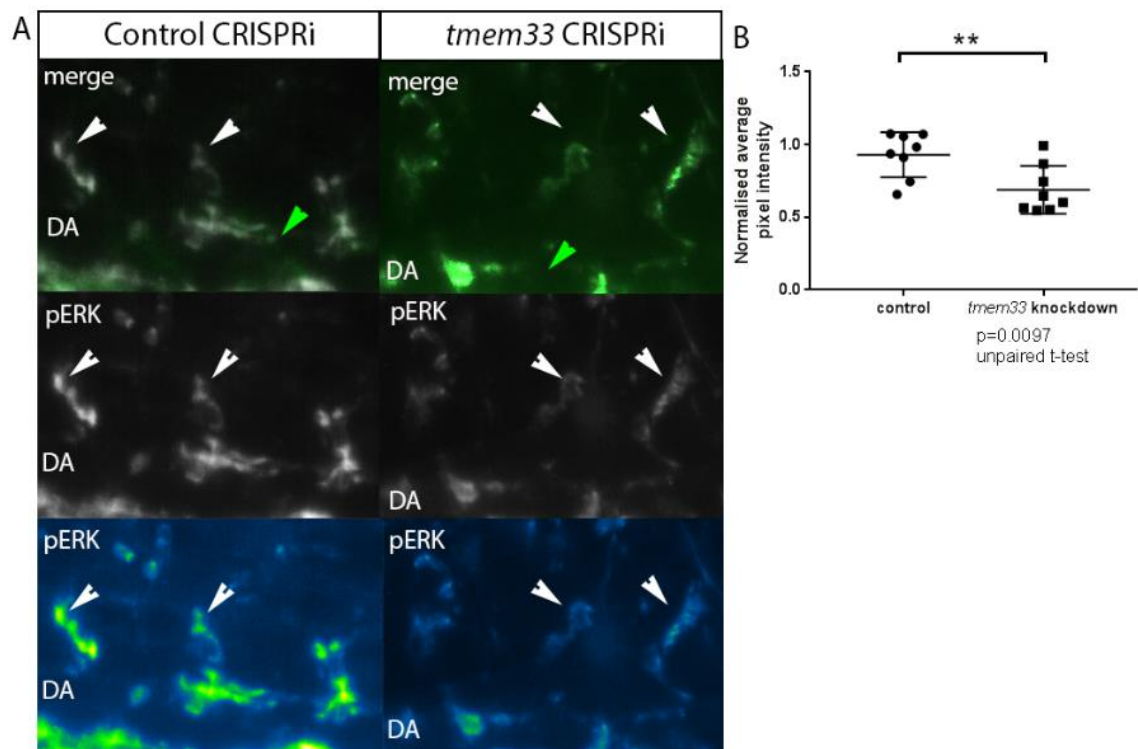


Figure 4.23 *tmem33* CRISPRi reduces endothelial ERK phosphorylation. (A) *tmem33* CRISPRi knockdown reduces vascular pERK staining in *Tg(fli1a:eGFP)y1* embryos. Top panels display *fli1a:EGFP* in green and pERK in grey. Middle panels display pERK in grey alone and bottom panels display pERK staining intensity using a lookup table in which regions of the highest levels intensity are yellow, while regions of low intensity are dark blue. (B) *tmem33* CRISPRi significantly reduces normalised vascular pERK fluorescence intensity compared to controls (unpaired t-test $**p < 0.01$).

4.17 Both *flt4* and *dll4* function downstream of calcium signalling

Transcription of *flt4* is upregulated downstream of ERK signalling (Shin et al., 2016). *Tmem33* knockdown reduces both endothelial calcium oscillations and

ERK phosphorylation (Figure 3.7; Figure 4.13; Figure 4.23). To exclude that *flt4* functions during primary sprouting angiogenesis, *flt4* was knocked down in *Tg(fi1a:gff)ubs3;Tg(uas:GCaMP7a)sh392* embryos. Time-lapse imaging was performed for 5 minutes and the frequency of calcium oscillations was quantified.

I measured calcium oscillation frequency, averaged over 4 independent tip cells per embryo (Figure 4.24 A-B). I found that *flt4* knockdown did not induce a significant change in calcium oscillation frequency (Figure 4.24 C). These data therefore suggest that *flt4* does not function downstream of VEGF in calcium signalling during primary sprouting angiogenesis. This is consistent with data suggesting endothelial cells in which high levels of Notch signalling are present downregulate *flt4* (Siekman and Lawson, 2007).

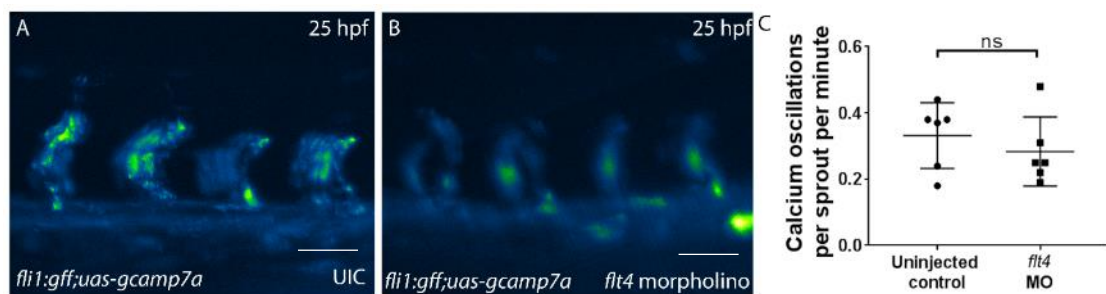


Figure 4.24 *flt4* knockdown does not significantly affect calcium oscillation frequency. (A-C) Control embryos display normal endothelial GCaMP7a fluorescence (A). Morpholino knockdown of *flt4* (B) does not cause a significant change in calcium oscillation frequency (unpaired t-test, non-significant) (C).

4.18 Inhibition of Store Operated Calcium Entry (SOCE) delays angiogenesis.

I have demonstrated that *tmem33* promotes VEGF-mediated endothelial calcium oscillations and angiogenesis in zebrafish embryos and induces ERK and Notch signalling during angiogenesis. While elevations of intracellular Ca^{2+} are the immediate response when an EC responds to VEGF (Oike et al., 1994; Vacaru et al., 2014; Yokota et al., 2015; Zadeh et al., 2009), it remained unclear whether Ca^{2+} oscillations were required during angiogenesis, or whether these were a secondary effect induced by VEGF signalling. Since endothelial cells are non-excitabile and primarily undergo store-operated calcium entry (SOCE), I therefore examined whether direct inhibition of SOCE disrupted angiogenesis *in vivo*. I employed the SOCE inhibitor SKF96365, which is known to inhibit the function of STIM1 and TRP channels (Singh et al., 2010).

Tg(flia:EGFP) γ 1 embryos were treated with SKF96365 for 6 hours, from 21 hpf to 27 hpf, at which point they were imaged and compared to control embryos. SOCE-inhibited embryos displayed clear angiogenic delays (Figure 4.25 B, C) compared to control embryos (Figure 4.25 A, C), similar to those induced by *tmem33* knockdown (Figure 1.3; Figure 4.11; Figure 4.19). Indeed, several SeAs displayed a spade-shaped morphology, highly similar to that observed following *tmem33* knockdown (Figure 4.36 B white asterisks). To observe the effects of long-term SOCE inhibition, *Tg(fli1a:eGFP) γ 1* embryos were treated with SKF96365 between 24-50 hpf. SKF96365 treated embryos displayed severe branching abnormalities and impaired DLAV formation (Figure 4.25 E, F, white asterisks), demonstrating a more severe phenotype than *tmem33* knockdown at

50 hpf. Given that SOCE inhibition causes angiogenic delays, and that inhibition of *tmem33* induces a very similar phenotype, this suggests that inhibition of calcium signalling inhibits endothelial migration during angiogenesis.

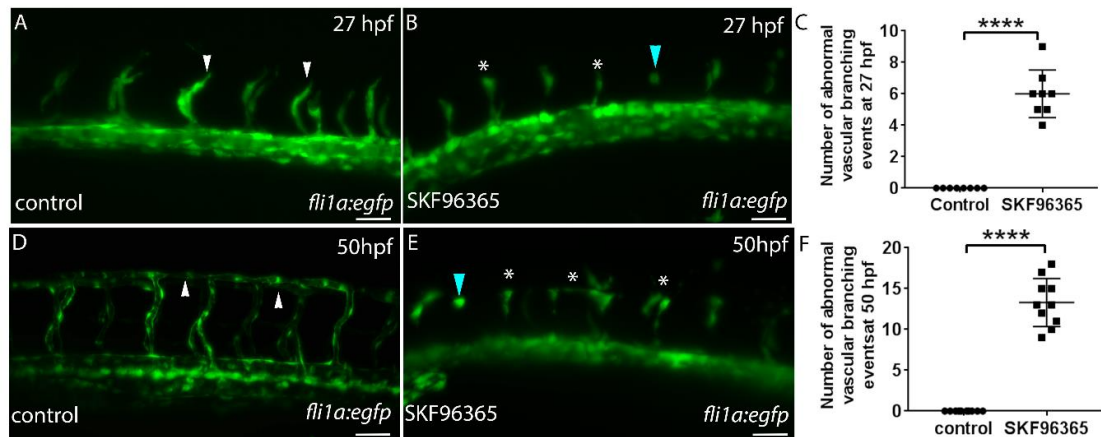


Figure 4.25 SKf96365 treatment induces angiogenic delays. (A-C) SKf96365 treated embryos display a significant number of delayed SeAs (white asterisks) compared to control embryos (white arrowheads) at 27 hpf (unpaired t-test, ****p=<0.0001). **(D-F)** SKf96365 treated embryos display a significant number of vascular defects, including delayed vessels and failure to form the DLAV (white asterisks) compared to control embryos (white arrowheads) at 50hpf (unpaired t-test, ****p=<0.0001).

4.19 Inhibition of SOCE via SKf96365 reduces frequency of endothelial calcium oscillations.

To confirm that SKf96365 was sufficient to inhibit calcium oscillations, I treated *Tg(fi1a:gff)ubs3;Tg(uas:GCaMP7a)sh392* embryos for 3 hours and performed time-lapse lightsheet microscopy for five minutes at a time to quantify frequency of calcium oscillations. Similar to *tmem33* CRISPRi knockdown (Figure 4.20), SKf96365 treatment significantly reduced calcium oscillation frequency (Figure 4.26). This suggests that acute inhibition of SOCE is sufficient to reduce

endothelial calcium oscillations. Furthermore, this suggests that angiogenic delays induced by SKF96365 treatment, (Figure 4.25) may be associated with reduced endothelial calcium oscillations.

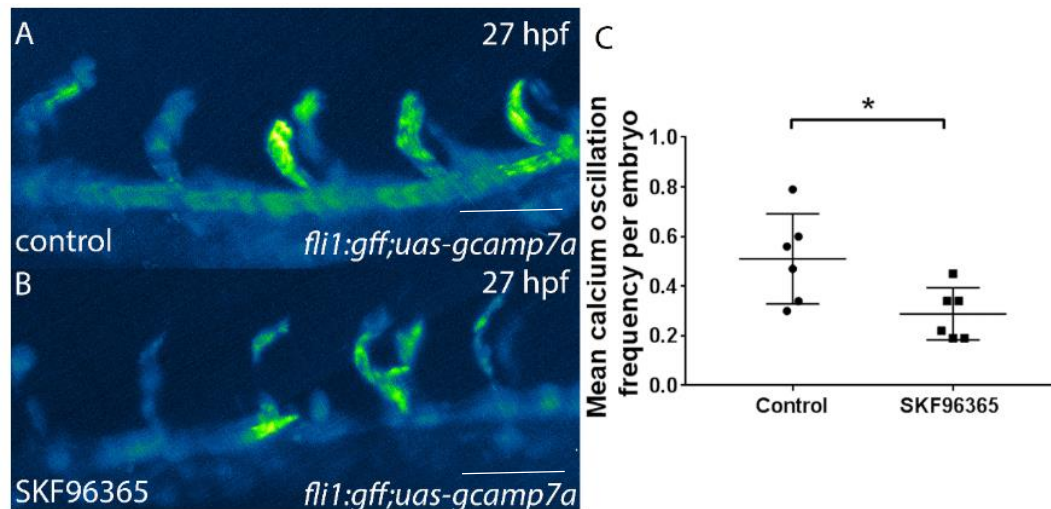


Figure 4.26 Inhibition of SOCE reduces frequency of endothelial calcium oscillations. (A-C) Acute (3 hour treatment) inhibition of SOCE by SKF96365 causes decreased endothelial GCaMP fluorescence and decreased endothelial calcium signalling frequency (unpaired t-test, $*p < 0.05$).

4.20 Inhibition of SOCE reduces endothelial Notch signalling and filopodia dynamics.

To further examine whether changes in EC physiology induced by *tmem33* knockdown are reproduced by SOCE inhibition, I quantified Notch activity in *Tg(CSLBS:Venus)qmc61* embryos treated with SKF96365 between 24 -50 hpf.

SKF96365-treated embryos displayed reduced Venus fluorescence in ISVs (Figure 4.27 A, B, white arrowheads) and the dorsal aorta (Figure 4.27 A, B, red

arrowheads), similar to *tmem33* knockdown indicating that inhibition of SOCE reduces endothelial Notch signalling.

SOCE inhibition induces EC migratory delays and misdirection during angiogenesis (Figure 4.25) and I have previously shown that migratory delays associated with *tmem33* knockdown may be due to impaired actin cytoskeleton reorganisation and filopodia formation (Figure 3.12; Figure 4.17). It has also recently been shown that SOCE and actin cytoskeleton reorganisation are closely linked (Hartzell et al., 2016; van Vliet et al., 2017). I therefore examined the filopodia formation in *Tg(fli1a:LifeACT-mClover)sh467* embryos treated with SKF96365. Embryos were treated between 22 and 26 hpf. SOCE inhibition delayed angiogenic migration as previously observed and significantly reduced filopodia number (Figure 4.27 C-E, black arrowheads). Interestingly, in SKF96365 treated embryos, tip cells were observed to display a rounded morphology in which F-actin was enriched cortically (Figure 4.27 D, blue arrowhead). This was not observed in control embryos (Figure 4.27 C).

Taken together, these data indicate that inhibition of store operated calcium entry induces highly similar angiogenic defects to *tmem33* knockdown. Critically, SKF96365 treatment does not affect *tmem33* expression. This suggests that VEGF-mediated endothelial calcium oscillations, promoted by *Tmem33*, are essential for multiple aspects of endothelial cell physiology including induction of Notch signalling and formation of filopodia during migratory angiogenesis.

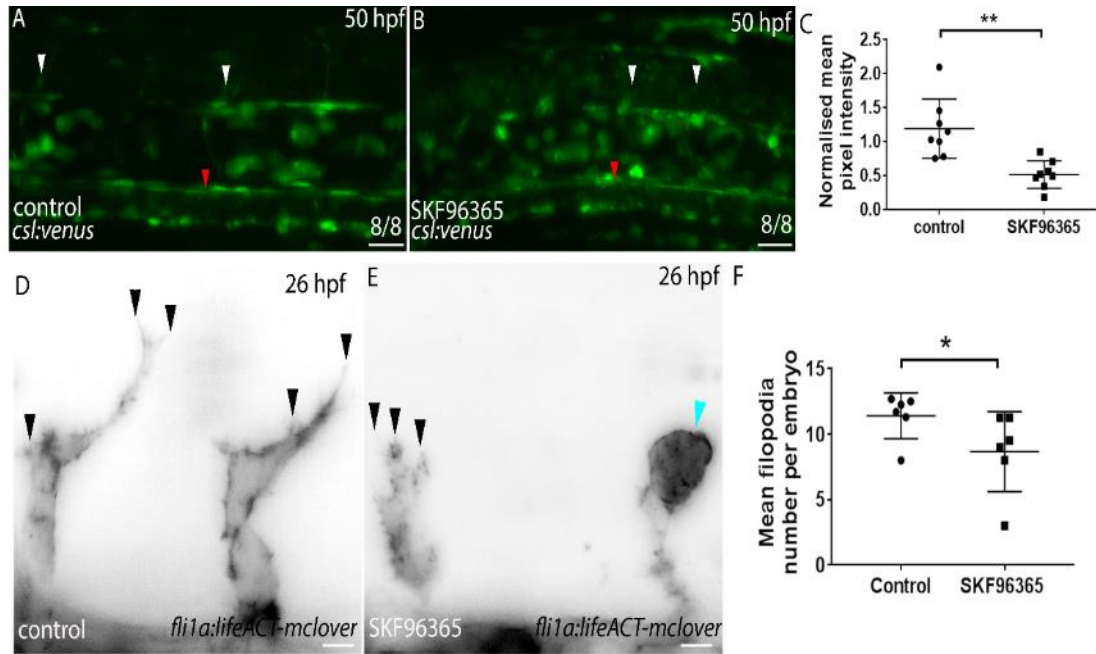


Figure 4.27 Endothelial Notch signalling and filopodia dynamics are reduced by SKF96365 treatment. (A-B) Inhibition of SOCE by SKF96365 reduces *CSL:Venus* fluorescence within ISVS (white arrowheads) and the dorsal aorta (red arrowheads) at 50 hpf. **(C)** Normalised mean aortic pixel intensity is significantly reduced in SKF9635 treated embryos compared to controls (unpaired t-test, $**p < 0.01$). **(D-F)** SKF96365 treatment significantly reduces the mean number of filopodia per embryo (black arrowheads). SKF96365-treated embryos display occasional rounded tip cell morphology (blue arrowhead).

To summarise the similarities between *tmem33* knockdown and calcium signalling inhibition via SKF96365 treatment, I have generated the following table:

Table 4.1 A summary and comparison of phenotypes observed following *tmem33* knockdown and SKF96365 treatment.

Phenotype	Present following <i>tmem33</i> knockdown?	Present following SKF96365 treatment?
Delayed angiogenesis by 30 hpf	Yes	Yes
Reduced anastomosis by 53 hpf	Yes	Yes – delays from 30 hpf never resolved
Reduced lymphatic development	Yes	Yes – Reduced vascularisation overall
Gomerular expansion	Yes	No
Reduced calcium oscillation frequency	Yes	Yes
Impaired filopodia formation	Yes	Yes
Reduced vascular Notch signalling	Yes	Yes
Reduced expression of downstream Notch targets/effectors	Yes	Unknown
Reduced ERK phosphorylation	Yes	Unknown
Tissue-specific capability	Yes	No

4.21 Discussion.

4.21.1 General discussion: development of tissue-specific CRISPRi as a strategy to conditionally modulate gene expression.

Until recently, loss-of-function approaches to study gene function in zebrafish have been limited to global techniques, such as morpholino knockdown (Nasevicius and Ekker, 2000) or mutagenesis using TALENs or the CRISPR/Cas9 system (Cermak et al., 2011b; Hwang et al., 2013). However, morpholinos are prone to off-target effects including induction of *p53* (Robu et al., 2007) and mutations often fail to yield a phenotype, leading to suggestions that compensatory machinery exists (El-Brolosy and Stainier, 2017; Kok et al., 2015; Rossi et al., 2015). Interestingly, I have demonstrated that knockdown via CRISPRi did not induce transcriptional upregulation of *p53*, in comparison to morpholinos which did induce *p53*, suggesting CRISPRi induces fewer off-target effects than morpholinos. However, both approaches induced a comparable phenotype (Figure 1.4; Figure 4.13). However, upregulation of *p53* is not the only marker for off-target defects, and others may be unaccounted for in this study. Furthermore, it has been suggested that CRISPR knockout mutants may be subject to further off target mutations, though further investigation is required (Schaefer et al., 2017). This may be similarly true for CRISPRi, whereby multiple genes may be knocked down by the same gRNA, leading to an unexpected phenotype. Since CRISPRi does not induce permanent genetic mutations, such phenotypes may be less severe. Furthermore, multiplexing gRNAs may improve specificity. Given, however, that *tmem33* knockdown by both morpholinos, targeting translation, and CRISPRi, targeting transcription, induce similar phenotypes, it is unlikely that off-target effects account for this.

To date, no technique to abrogate gene function in a cell- or tissue-specific manner consistently has been described in zebrafish. However, recent attempts to utilise the CRISPR/Cas9 system to generate mosaic tissue-specific knock out in zebrafish have been developed (Ablain et al., 2015). However, due to the nature of CRISPR/Cas9-induced mutations, such techniques may be subject to a degree of stochasticity, in that mutations generated in each cell may differ and may not necessarily lead to loss-of-function. I have developed an alternative approach, to successfully achieve tissue-specific perturbation of gene function. Tissue-specific CRISPRi is not without potential problems, since I have shown that gene knockdown is transient (Figure 4.5), which suggests that gene function is only temporarily reduced. Similarly, widely used knockdown techniques, such as morpholinos display transient knockdown (Schulte-Merker and Stainier, 2014). To generate a more stable knockdown, co-expression of target gRNAs using an appropriate promoter, alongside tissue-specific dCas9 expression would be preferred, in a similar manner to the recently described conditional mosaic knockout approach (Ablain et al., 2015). This confers upon the technique a distinct advantage over current knockdown approaches, such morpholinos, which cannot be relied upon for knockdown over long time scales. However, transient CRISPRi is suitable for screening large numbers of genes either globally or for tissue specific functions, whereas co-expression approaches would be unfeasible for these approaches. I have utilised the novelty of tissue-specific CRISPRi to determine that *tmem33* is required cell autonomously within developing blood vessels during angiogenesis and within the developing pronephros for normal kidney development.

Recently, the CRISPR/Cas9 system has been adapted to allow for increased transcriptional repression beyond steric hindrance via the addition of histone methylation domains such as the krüppel-associated box (KRAB) (Gilbert et al., 2014; Thakore et al., 2015). Such advances may prove invaluable in the study of gene function. It is therefore possible to generate transgenic lines in which a dCas9-KRAB fusion, similar to the *Tg(fli1a:dCas9,cryaa:CFP)sh512* transgenic line developed in this thesis. This would theoretically provide a tool with which long-term, conditional transcriptional repression could be observed. This may provide greater insight into gene function, particularly if it were coupled with transgenic expression of gRNAs (Ablain et al., 2015). With regards to *tmem33* function, this may be particularly interesting in studying secondary angiogenesis, given that repression is maintained for longer. dCas9 fusion proteins may therefore represent a method of introducing a greater level of transcriptional control to genes of interest, resulting in a greater understanding of gene function. This may be especially interesting within a tissue-specific context in comparison to global transcriptional control, enabling understanding of how gene function regulates cell behaviour within a specific cell type.

Alternatively, VP64 or p65-fused dCas9 proteins have been developed, which function to recruit transcriptional machinery to increase expression of the specified gene (Kearns et al., 2015; Konermann et al., 2015), termed CRISPR activation (CRISPRa). However, it has been suggested that such fusions may reduce the efficacy of the Cas9 enzyme (Choudhury et al., 2016). This may mean that transcriptional activator-dCas9 fusions are subject to reduced efficacy, since they rely on binding to introduce transcriptional machinery to the gene locus (Konermann et al., 2015). Efforts have been made to redress this and newer

transcriptional activation fusion proteins have been developed, such as SunTag (Gilbert et al., 2014; Horlbeck et al., 2016) and dCas9-VPR, dCas9 fused to the a combination of VP64, P65 and Rta (replication and transcription activator (Hong et al., 2011)) transcriptional activation domains (Chavez et al., 2015). It is therefore possible to generate transgenic lines which utilise transcriptional activation rather than transcriptional repression. This represents an interesting alternative, with regards to analysis of gene function, in that it is possible to regulate gene expression within different to analyse cell-autonomous or non cell-autonomous effects of overexpression. This is interesting in a developmental context, since complex genetic interaction between cells of not only the same tissue, but also neighbouring tissues occur to regulate growth and development.

4.21.2 EC-specific knockdown of *tmem33* using CRISPRi reveals *tmem33* is required in ECs for normal angiogenesis.

In this study, I demonstrate a requirement for *tmem33* within ECs during VEGF mediated angiogenesis for normal tip cell behaviour, including calcium signalling, filopodia formation and regulation of downstream signalling pathways including Notch and ERK signalling. Using EC-specific CRISPRi, I was able to show that *tmem33* functions within endothelial cells and is essential for normal primary sprouting angiogenesis (Figure 4.19). I observed delayed angiogenesis and impaired anastomosis in *Tg(fli1a:dCas9,cryaa:CFP)sh512* embryos in which *tmem33* was knocked down (Figure 4.19). Interestingly, I also found that, compared to global morpholino knockdown, EC-specific CRISPRi induced a milder phenotype (Figure 1.4; Figure 4.16; Figure 4.15; Figure 4.19). However, *tmem33* is expressed ubiquitously at low levels during early embryonic

development and is therefore likely to function in many tissues (Figure 1.2). I have shown in this thesis that *tmem33* functions during both vascular and kidney development. Therefore, when global knockdown is undertaken, non-cell autonomous effects may be observed in tissues studied. Another potential explanation for the difference in phenotypic severity is that when *tmem33* function is knocked down globally, knockdown begins earlier than tissue-specific knockdown. Using EC-specific knockdown, dCas9 only becomes expressed when *fli1a* is expressed, at approximately 10 hpf (Brown et al., 2000). Therefore *tmem33* knockdown will not occur until dCas9 protein is produced. Furthermore, *in situ* hybridisation revealed weak expression of dCas9 within the endothelium of *Tg(fli1a:dCas9,cryaa:CFP)sh512* (Figure 4.17), suggesting that *dCas9* may be expressed at low levels in my stable transgenic lines. This may mean that fewer molecules of dCas9 are present, accounting for reduced knockdown efficiency and a milder phenotype. This could be addressed by producing a Gal4-UAS driven transgenic line, which would be expressed at higher levels due to tandem UAS driver repeats (Scheer and Campos-Ortega, 1999).

One limitation of tissue-specific CRISPRi is that knockdown is transient, meaning that knockdown phenotypes beyond 96 hpf may be difficult to achieve (Figure 4.4). This is likely to be due to gRNA degradation or dilution. As previously discussed, a recent study utilised transgenic expression of gRNAs alongside active Cas9, to ensure continual transcription. While this study utilised tissue-specific control of the active, mutagenic form of Cas9 to introduce tissue-specific mutations, similar to the tissue-specific dCas9-mediated knockdown technique described herein (Ablain et al., 2015), a key advantage of tissue-specific knockdown is that it does not introduce mosaic genomic lesions as tissue-

specific Cas9. I therefore believe that tissue specific knockdown provides distinct advantages in the analysis of experimental outcomes over similar approaches.

To further understand *tmem33* function, development of transgenic lines in which greater repression (dCas9-KRAB fusions) or transcriptional activation (dCas9-VPR fusions) can be applied tissue-specifically may be useful (see 4.21.1).

4.21.3 TMEM33 maintains normal migrational endothelial cell biology via regulation of calcium signalling, integrating VEGF, ERK and Notch signalling pathways.

During angiogenesis, pro-migratory and -angiogenic VEGF signals direct migration of endothelial tip cells. MAP kinase and Notch signalling pathways are downstream of VEGF signalling (Lawson et al., 2002; Shin et al., 2016). I show that *tmem33* functions downstream of VEGF signalling in endothelial cells (Figure 4.25; Figure 4.27). I furthermore indicate that *tmem33* is a regulator of endothelial calcium signalling during SeA migrational angiogenesis (Figure 3.7; Figure 4.16). Calcium signalling has been shown to be induced upon VEGF stimulation of ECs, both *in vitro* and *in vivo* during angiogenesis, which can be blocked via inhibition of known calcium channels (Bates and Curry, 1997; Criscuolo et al., 1989; Hamdollah Zadeh, 2008; Yokota et al., 2015). I therefore suggest that following stimulation of endothelial cells by VEGF signalling, intracellular calcium oscillations are induced during flow-independent angiogenesis and that *tmem33* functions to regulate EC calcium signalling during this process.

Dll4/Notch signalling is induced downstream of VEGF signalling in ECs during angiogenesis. The Notch ligand, *dll4*, is upregulated downstream of VEGF signalling in endothelial tip cells, inducing Dll4/Notch signalling in neighbouring cells via lateral inhibition (Hellström et al., 2007; Leslie et al., 2007). I show in this thesis that inhibition of either *tmem33* or calcium signalling inhibits Notch signalling activity. Furthermore, recent studies have shown that ERK signalling functions to induce Dll4/Notch signalling during sprouting angiogenesis, and that ERK signalling induces both *dll4* and *flt4* transcription (Shin et al., 2016). My data show that pERK is reduced following *tmem33* knockdown, suggesting a role for calcium signalling upstream of ERK signalling. Protein kinase signalling has been shown to function upstream of the MAP kinase signalling family (Wong and Jin, 2005) and within zebrafish, both members of the protein kinase C and protein kinase D family have been shown to function during angiogenesis (Hollenbach et al., 2013; Oubaha et al., 2012).

Interestingly, protein kinase D is a member of the calcium/calmodulin-dependent family of protein kinases and inhibition of protein kinase D1 in zebrafish results in impaired DLAV anastomosis at 48 hpf (Hollenbach et al., 2013), strikingly similar to the phenotype observed following *tmem33* knockdown (Figure 3.7; Figure 4.14). Furthermore, inhibition of protein kinase C function by treatment via both morpholino knockdown and treatment with cinnamon extract has been shown to impair angiogenesis (Bansode et al., 2013; Oubaha et al., 2012). However cinnamon extract treatment inhibited VEGF receptor transcription, suggesting the phenotype could be attributed to VEGF receptor inhibition (Bansode et al., 2013). Furthermore, direct inhibition of protein kinase C induced no observable angiogenic defects (Oggier et al., 2011). This may suggest that calcium signalling

is important for protein kinase D function, which, in turn, regulates MAP kinase signalling. However, to further validate this, overexpression of protein kinase D1 following *tmem33* knockdown would be necessary to determine epistasis.

tmem33 crispants show reduced expression of genes within the Notch signalling pathway, including *notch3*, *dll4* and *hey2*, indicating that receptor, ligand and downstream target gene transcription are reduced by 48 hpf. Interestingly, although I see angiogenic defects at 26 hpf, I do not see a significant decrease in expression of Notch signalling genes at this time point. This suggests the angiogenic defect observed following *tmem33* knockdown at 26 hpf is not due to reduced Notch signalling, but rather other observable defects, such as reduced calcium signalling and reduced filopodia formation. Furthermore, reduced Notch signalling from 26 hpf would be predicted to induce more angiogenic sprouting, since inhibition of *dll4* function by both morpholino knockdown and mutagenesis results in ectopic angiogenesis and ectopic sprouting is observed in Notch-signalling deficient *mindbomb* mutants (Lawson et al., 2001). Furthermore inhibition of Notch signalling via DAPT treatment produces a similar effect. I did not observe ectopic angiogenesis following *tmem33* knockdown, which further suggests Notch signalling is not interrupted at 26 hpf.

4.21.4 Calcium signalling is required for normal endothelial cell behaviour.

In this thesis, I show that calcium signalling via *tmem33* regulates distinct aspects of endothelial cell biology during angiogenesis. Furthermore, I show that, by inhibiting calcium signalling independently of *tmem33* via SKF96365 treatment, I can impair endothelial cell behaviour in a similar manner to *tmem33* knockdown.

Calcium signalling has been shown to function downstream of VEGF signalling both *in vitro* and *in vivo* (Hamdollah Zadeh, 2008; Yokota et al., 2015). I have shown that *tmem33* regulates endothelial calcium signalling and knockdown reduces calcium transients and filopodia dynamics within endothelial tip cells. I have shown that SKF96365 treatment impairs developmental angiogenesis, leading to angiogenic delays, albeit more severely than *tmem33* knockdown at 30 hpf. Furthermore, angiogenesis continues to be impaired by 50 hpf, resulting in reduced DLAV anastomosis, similar to *tmem33* knockdown. This may be due to the fact that SKF96365 impairs calcium signalling globally and will likely have wider reaching impacts on calcium signalling than knockdown of *tmem33* alone.

Acute SOCE inhibition also reduced calcium oscillation frequency and endothelial tip cell filopodia number, similar to *tmem33* knockdown. Since, SOCE is the primary route of ER Ca²⁺ refilling in ECs, a reduction in calcium transients may be expected following acute treatment. Longer treatments may have induced further reductions in EC calcium transients, however I found long-term incubation with SKF96365 to be toxic to zebrafish embryos. Interestingly, I found that the reduction of filopodia number was more severe than observed in *tmem33* knockdown and phenotypically more akin to Latrunculin B treatment, which depolymerises F-Actin (Phng et al., 2013). Furthermore, I repeatedly observed tip cells with a rounded morphology, in which a greater density of cortical F-actin were observed. This may correlate with recent findings regarding the interaction between calcium signalling via SOCE and regulation of the actin cytoskeleton (Hartzell et al., 2016; van Vliet et al., 2017). For SOCE to take place, the ER and plasma membrane (PM) must come in contact, to allow STIM and ORAI proteins to form the CRAC channel (van Vliet et al., 2017). Recently it has been shown

that cytoskeletal rearrangement coordinated by Ca²⁺-dependent PERK (eif2ak3) and Filamin A is required for ER-PM contact and the induction of SOCE (van Vliet et al., 2017). Inhibition of SOCE may suggest that the cells are unable to complete ER Ca²⁺ replenishment and therefore both F-actin and the ER remain in close association with the PM. Furthermore, a reduction in calcium transients may mean that cytoskeletal rearrangements required to translocate the ER from the PM may not be possible.

I also observed a reduction in endothelial Notch signalling, as documented using the *Tg(CSLB:Venus)qmc61* Notch signalling reporter transgenic line (Figure 4.27). I found that ISVs displayed reduced CSL:Venus fluorescence compared to control treated embryos, similar to observations made during *tmem33* knockdown, suggesting reduced calcium signalling impairs Notch signalling. It is well established that both calcium signalling and Notch signalling are induced downstream of VEGF signalling. Furthermore, Notch signalling has been implicated downstream of the MAP kinase signalling pathway, which may function downstream of Ca²⁺-dependent protein kinase signalling.

I therefore suggest that VEGF-mediated calcium signalling is important during angiogenesis to promote normal EC migration, proliferation, filopodia formation, Notch and ERK signalling and that *tmem33* regulation of calcium signalling from within the ER is vital for this process. I have observed that calcium signalling is required for induction of signalling pathways downstream of VEGF and to control endothelial physiology, suggesting calcium signalling may serve to function in a general role, as well as a specialised one, dependent on cell type.

4.21.5 Much still remains unknown regarding TMEM33 function *in vivo*.

In this thesis I have presented novel functional understanding of *tmem33* primarily in the context of sprouting angiogenesis but I have also observed a role during renal development. However, much remains unknown regarding both *tmem33* function in other tissues and a deeper understanding of how the protein functions during cell homeostasis. Studies have predicted a 3-transmembrane structure for *tmem33* and shown that it localises to the ER, likely in the membrane (Sakabe et al., 2015; Urade et al., 2014). Furthermore, I have shown that *tmem33* localises to the ER in zebrafish (Figure 3.4). I have also shown potential interaction with the SERCA ATPase (*SERCA*), which localises to the ER membrane. Simultaneous *tmem33* knockdown and *SERCA* inhibition via Thapsigargin treatment phenocopies *tmem33* knockdown alone (Figure 3.12). It is therefore possible that *tmem33* may either be important for ER calcium release, or may function to inhibit *SERCA* activity. Therefore, when *tmem33* is knocked down, calcium uptake into the ER via *SERCA* may occur more rapidly. However, further testing would be required to ascertain this.

Alternatively, *tmem33* may function to regulate calcium re-uptake into the ER via interaction with the calcium release-activated calcium (CRAC) channel, made up of STIM and ORAI proteins (Feske et al., 2006; Jones et al., 2005; Roos et al., 2005; Vig, 2006). Recent studies have shown that reorganisation of the ER during calcium signalling is dependent upon regulation of the actin cytoskeleton; itself a Ca^{2+} -dependent phenomenon (Hartzell et al., 2016; van Vliet et al., 2017). This

is particularly important during store operated calcium entry (SOCE) in which ORAI proteins in the PM must interact with STIM proteins in the ER membrane (Zhou et al., 2010). I have shown that *tmem33* knockdown reduces cytosolic Ca^{2+} concentrations. This may be due to several factors. *tmem33* may regulate Ca^{2+} release from the ER, which is required for the ER-associated protein PERK to regulate F-actin structure via *filamin a* (van Vliet et al., 2017), or *tmem33* may regulate changes in ER 3-dimensional structure alongside actin cytoskeletal regulation. It has recently been suggested that *tmem33* interacts negatively with reticulon proteins to regulate ER shape, inhibiting the tubule forming capabilities of reticulons (Urade et al., 2014). *Tmem33* was shown to interact strongly with reticulon 4C (RTN4C), along with others, showing co-localisation within the ER (Urade et al., 2014). Interestingly, reticulon 4 (RTN4)-mediated ER-tubule formation has been shown to be important during SOCE via the CRAC channel in MEF cells, wherein RTN4 knockout reduced relative levels of ER tubules compared to ER sheets (Jozsef et al., 2014). However, if *tmem33* functioned to repress the function of RTN4, *tmem33* knockdown might be expected to result in increased ER tubule formation and therefore increased calcium signalling via SOCE. However, Urade *et al.* utilised an overexpression assay, in which both *tmem33* and RTN4C were overexpressed. Since overexpression assays rarely represent biology accurately, this may account for discrepancies between the two studies. Regardless, further study is required to better understand the proteins with which *tmem33* interacts *in vivo*.

I have shown a reduction in endothelial calcium oscillations following *tmem33* knockdown (Figure 3.11; Figure 4.16). Interestingly, I found a similar effect following *tmem33* knockdown when analysing calcium oscillation frequency in the

kidney, with pronephric tubule cells displaying reduced calcium signalling frequency compared to controls (Figure 3.14). This may therefore point to a more general role for *tmem33* in regulation of ER homeostasis and calcium signalling. Since calcium signalling machinery is highly conserved between cell types, it is likely that this could be the case, suggesting a wider importance for *tmem33* outside of angiogenesis.

Alternatively, Tmem33 may function in calcium signalling as part of a channel complex. Several known channel complexes exist, including TRP channels, which form a tetrameric complex with each component contributing two transmembrane domains to the central pore. TRP channels have been shown to form heterotetramers, two pairs of homodimers and mixed heterotetramers (Cheng et al., 2010; Hoenderop et al., 2003; Hofmann et al., 2002). Evidence from collaborators has suggested that human TMEM33 increases Ca²⁺ channel activity of PKD2 in lipid bilayer reconstitution assays (Eric Honore, data not shown). Interestingly, TRPC1 has already been implicated during angiogenesis in zebrafish (Yu et al., 2010) and studies in cell culture have shown that TRPC1 can form complexes with both TRPV4 and PKD2/TRPP2 (Du et al., 2014). Interactions between TRPV4 and PKD2 in various cell types have been observed (Köttgen et al., 2008; Zhang et al., 2013). Furthermore, recent evidence has implicated TRPV4 and PKD2 in endocardial calcium signalling. Both TRPV4 and PKD2 reduced endocardial calcium signalling within the arterio-venous canal (Heckel et al., 2015). Therefore, a role during calcium signalling in endothelial development cannot be excluded. Since TRP channels are known to form complexes, it is possible that *tmem33* may form part of a channel complex, given similarities in structure, including highly conserved transmembrane domains.

In Chapter V, I assess the function of TRP channels during calcium signalling in angiogenic endothelial cells and analyse potential interactions between *tmem33* and *pkd2*.

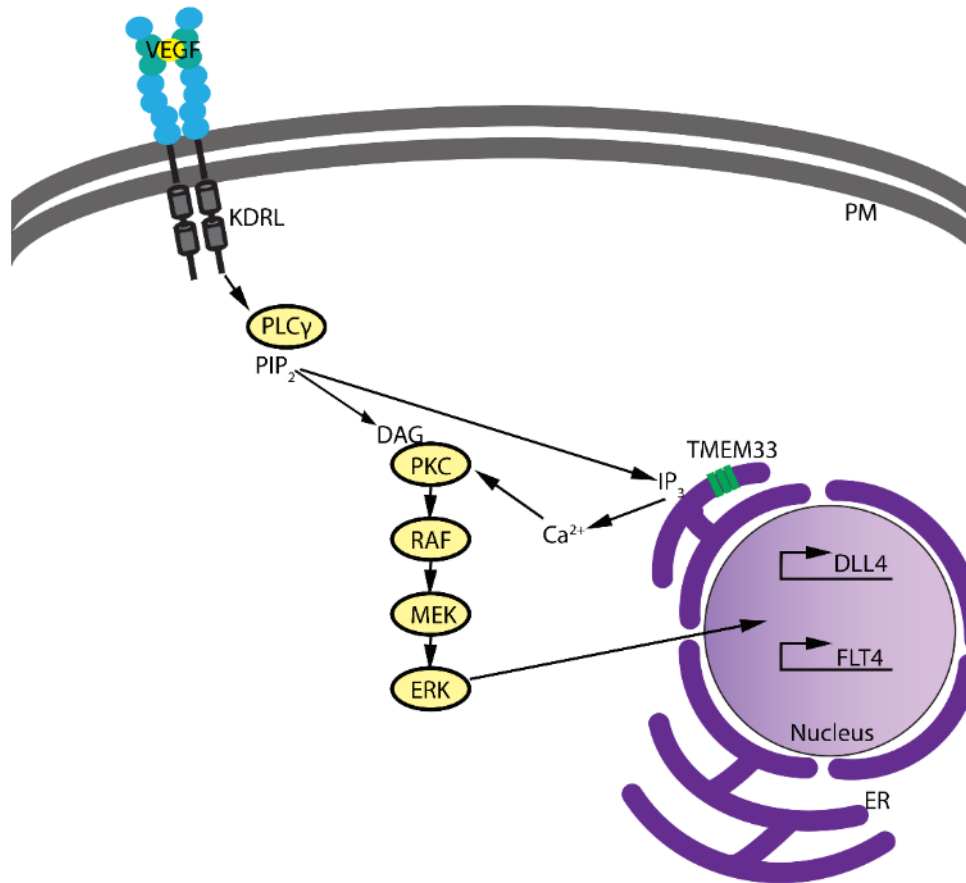


Figure 4.28 A proposed role for *tmem33* within the angiogenic hierarchy. *Tmem33* is located within the ER wherein it regulates the release of Ca²⁺ ions critical for downstream signalling pathways, including MAP kinase signalling

5 Investigation of putative genetic interactions of *tmem33* with TRP channels.

5.1 Introduction

TMEM33 was identified by my collaborators via pulldown experiments which showed it interacted with PKD1/TRPP1 in mice (Eric Honore, data not shown). Furthermore, when co-expressed with PKD2/TRPP2 in a lipid bilayer reconstitution assay, it increased the activity of the PKD2 Ca²⁺ channel (Eric Honore, data not shown). I have demonstrated that *tmem33* is essential for normal vascular and kidney development in the zebrafish. Following *tmem33* knockdown, angiogenesis becomes delayed and establishment of vascular patterning is impaired, suggesting an abnormal response to guidance cues from VEGF signalling. Both PKD1 and PKD2 are mutated in polycystic kidney disease (Hughes et al., 1995; Mochizuki et al., 1996). *tmem33* knockdown also induces glomerular expansion within the developing kidney, a phenotype also observed in *pkd1a/pkd1b* and *pkd2* morphants (Mangos et al., 2010; Sullivan-Brown et al., 2008; Sun, 2004). However, *tmem33* mutants display no phenotype, which may be due to genetic compensation (Rossi et al., 2015) (Figure 3.13). Since my collaborators identified that TMEM33 interacts with the transient receptor potential (TRP) channel family members PKD1 and PKD2, I hypothesised that one such channel may function to compensate for loss of *tmem33* in my mutants.

TRP channels consist of six transmembrane domains, the fourth and fifth of which form part of a tetrameric pore with other TRP channels (Ramsey et al., 2006). It has been suggested that pairs of homodimers form a tetramer in most cases, although cases of three different TRP channels within the same tetramer have

been observed (Heckel et al., 2015; Kobori et al., 2009; Köttgen et al., 2008). It has been shown that PKD2 (TRPP2) and TRPV4 can interact in zebrafish (Heckel et al., 2015), and TRPV4, PKD2 and TRPC1 have been observed to interact in cell culture (Du et al., 2014). Interestingly TRPC1 morphants display a similar phenotype to *tmem33* knockdown (Yu et al 2010). Therefore, the aim of studies presented in this chapter was to investigate whether genetic interaction between *tmem33* and TRP channels could be observed during zebrafish angiogenesis.

I have shown that *tmem33* localises to the ER (Figure 3.4) and current literature has suggested that *pkd2* may be active within the ER, golgi and plasma membranes (Foggensteiner et al., 2000; Obara, 2006; Pazour et al., 2002). Furthermore, recent studies within the zebrafish community have highlighted the importance of understanding genetic compensation between unrelated proteins which localise to similar subcellular domains (Rossi et al., 2015). Since both *tmem33* and *pkd2* localise to the ER membrane, and knockdown produced similar phenotypes, I sought to determine whether any genetic interaction took place, by analysing whether each gene could compensate for the other.

5.2 Knockdown of *tmem33* in *pkd2* mutants does not increase glomerular area.

I hypothesised that since PKD2 and TMEM33 interact in cell culture (Eric Honore, data not shown), they may interact during zebrafish development. Furthermore, both *pkd2* and *tmem33* morphants display expanded glomeruli (Figure 1.5; Sun et al., 2004). However, since neither mutant displays expanded glomeruli, genetic compensation is likely to exist within these mutants. To understand whether

genetic compensation exists between *tmem33* and *pkd2*, I analysed the function of *tmem33* in *pkd2*^{hu2173} mutants (Obara, 2006; Schottenfeld et al., 2007). I sought to determine whether the absence of expanded glomeruli in *pkd2*^{hu2173} mutants was due to compensation via *tmem33* function. Therefore, I knocked down *tmem33* in *pkd2*^{hu2173} mutants and quantified glomerular area to determine whether any difference could be observed in *pkd2*^{hu2173} mutants when compared to siblings.

While *tmem33* knockdown induced glomerular expansion in all embryos observed, no significant difference in glomerular area was observed between sibs or *pkd2*^{hu2173} mutants following *tmem33* knockdown (Figure 5.1). These data suggest that either *tmem33* and *pkd2* function in different pathways during kidney development, or that a different gene serves to compensate for loss of *pkd2* function in *pkd2*^{hu2173} mutants.

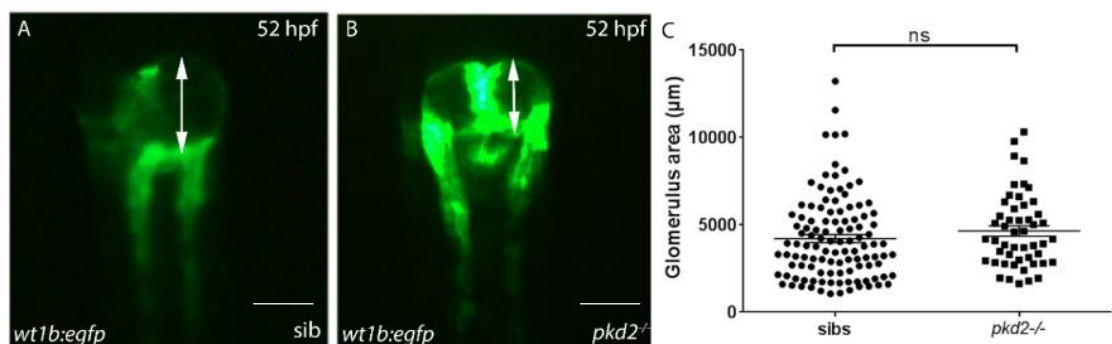


Figure 5.1 Glomerulus area is not affected by *tmem33* knockdown in *pkd2*^{hu2173} mutants. (A-C) Morpholino knockdown of *tmem33* in *pkd2*^{hu2173} mutants induces no statistically significant change in glomerular area (unpaired t-test, ns = not significant). Each data point refers to a single glomerulus.

5.3 Abnormal glomerular development induced by *tmem33* knockdown is not enhanced by knockdown of *pkd2*.

No increase in glomerular area was observed following *tmem33* knockdown in *pkd2^{hu2173}* mutants. I next knocked down both genes independently and simultaneously to determine whether increased glomerular expansion could be observed in double morphants. All three knockdown conditions induced glomerular expansion from 52 hpf in *Tg(-26wt1b:eGFP)li1* embryos (Figure 5.2 A-E), but no significant difference observed between *tmem33* morphants, *pkd2* morphants or double morphants (Figure 5.2 B-D). Analysis of glomerular area confirmed that knockdown of each gene individually and in combination increased glomerular area, but no significant difference was observed between these conditions (Figure 5.2 E). This data is inconclusive and may suggest one of several things: that the genes are unlikely to function in the same pathway at the same developmental time during glomerular development, since no cumulative effect is observed during simultaneous knockdown; that both genes function in the same genetic pathway at the same time but loss of either single gene induces glomerular expansion, regardless of the other; or that both mutants display sufficient compensation by different genes that genetic interaction cannot be assayed in this way.

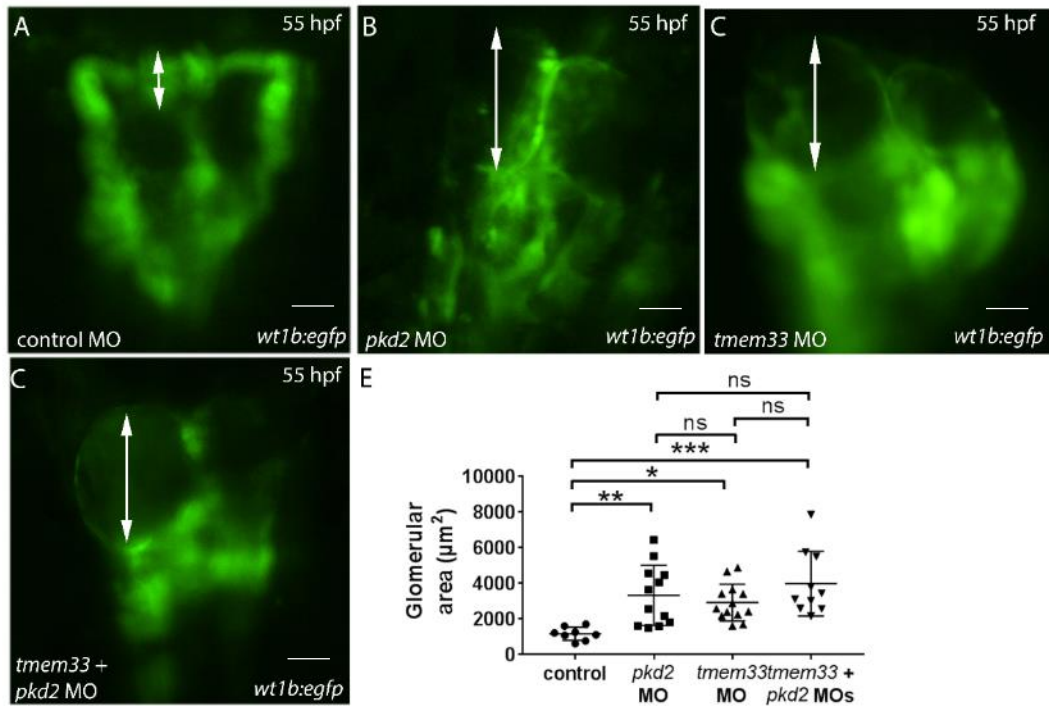


Figure 5.2 Abnormal glomerular development induced by *tmem33* knockdown is not enhanced by knockdown of *pkd2* (A-D) Morpholino knockdown of *pkd2* (B), *tmem33* (C) and both genes in combination increases glomerular area in *Tg(-26wt1b:EGFP)li1* embryos, compared to controls (A) (White arrows). **(E)** By knockdown of *pkd2* and *tmem33* individually and simultaneously induces significant increase in glomerular area, there is no significant difference between each of the knockdown conditions (One-way ANOVA * $p < 0.05$, ** $p < 0.01$, *** $p < 0.0001$). Each data point refers to a single glomerulus. Two experimental repeats were performed.

5.4 *tmem33*^{-/-};*pkd2*^{-/-} double mutants do not display an increase in glomerular area.

Neither *tmem33* knockdown in *pkd2*^{hu2173} mutants (Figure 5.1) nor simultaneous *pkd2* and *tmem33* knockdown (Figure 5.2) induced an enhancement in glomerular expansion, which may suggest an interaction between *pkd2* and *tmem33* exists in zebrafish. To confirm that no interaction can be observed, I

analysed glomerular area in *tmem33^{sh443/sh443};pkd2^{hu2173/hu2173}* double mutants. I incrossed *Tg(-26wt1b:eGFP)li1;tmem33^{sh443/+};pkd2^{hu2173/+}*; zebrafish and selected for *pkd2* mutations using axial curvature. Glomerular areas were measured and embryos retrospectively genotyped to determine *tmem33* allelic status.

No significant increase in glomerular area was observed in *tmem33^{sh443};pkd2^{hu2173}* double mutants when compared to siblings which were either heterozygous or wild type for the *tmem33^{sh443}* allele (Figure 5.3). This suggests it is unlikely that *tmem33* and *pkd2* interact during kidney development in zebrafish. It further indicates that failure to recapitulate kidney abnormalities observed in either *tmem33* or *pkd2* morphants in each respective mutant is not due to compensation from *tmem33* in *pkd2* mutants or vice versa.

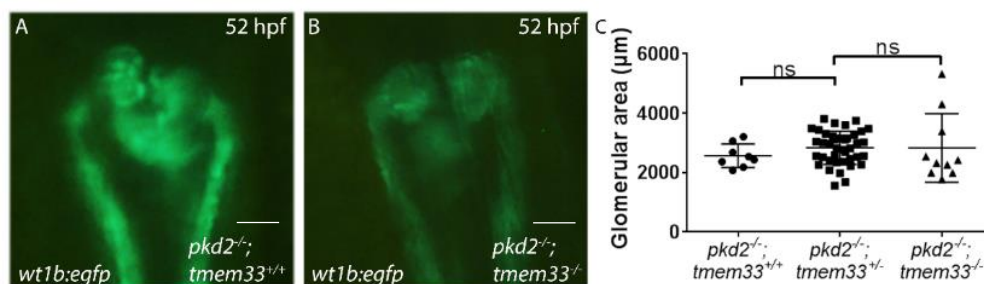


Figure 5.3 No significant change in glomerular area is observed in *tmem33^{sh443};pkd2^{hu2173}* double mutants. (A-C) No significant increase in glomerular area is observed in *tmem33^{sh443};pkd2^{hu2173}* double mutants compared to sibs (One-way ANOVA ns = not significant). Each data point refers to a single glomerulus.

5.4 Axial curvature is not affected in *tmem33*^{-/-};*pkd2*^{-/-} double mutants.

While *pkd2*^{hu2173} mutants do not develop expanded glomeruli, aberrant axial curvature is observed (Obara, 2006; Schottenfeld et al., 2007), which causes the tail of the embryo to bend upwards, which in severe cases points rostrally (Figure 5.4 D). Since combined knockdown of *pkd2* and *tmem33* or *tmem33* knockdown in *pkd2*^{hu2173} mutants indicated no genetic interaction between *tmem33* and *pkd2*, I sought to confirm this in *tmem33*; *pkd2* double mutant embryos.

I incrossed *tmem33*^{sh443/+};*pkd2*^{hu2173/+} zebrafish and sorted for *pkd2*^{hu2173} mutant embryos based on axial curvature. Degree of axial curvature was measured from the centre of the eye, to the end of the yolk cell extension, to the tip of the tail. Axial angle was highly variable, with largely equal numbers of embryos displaying <90°, 90°, or >90° angles (Figure 5.4 A-C). Embryos were genotyped and no significant difference was observed between *tmem33*^{+/+}, *tmem33*^{sh443/+} or *tmem33*^{sh443} mutant embryos. These data suggest one of several possible explanations: either that *tmem33* and *pkd2* interact within the same pathway, or that both mutations induce compensation via different genes, which would mean that loss of a functional Tmem33 in PKD2 mutants may not enhance the axial phenotype of *pkd2*^{hu2173} mutants, since genetic compensation occurs in *tmem33*^{sh443} mutants and they are phenotypically normal. Alternatively, since *tmem33* morphants display no axial defects, *tmem33* is unlikely to function during axial development.

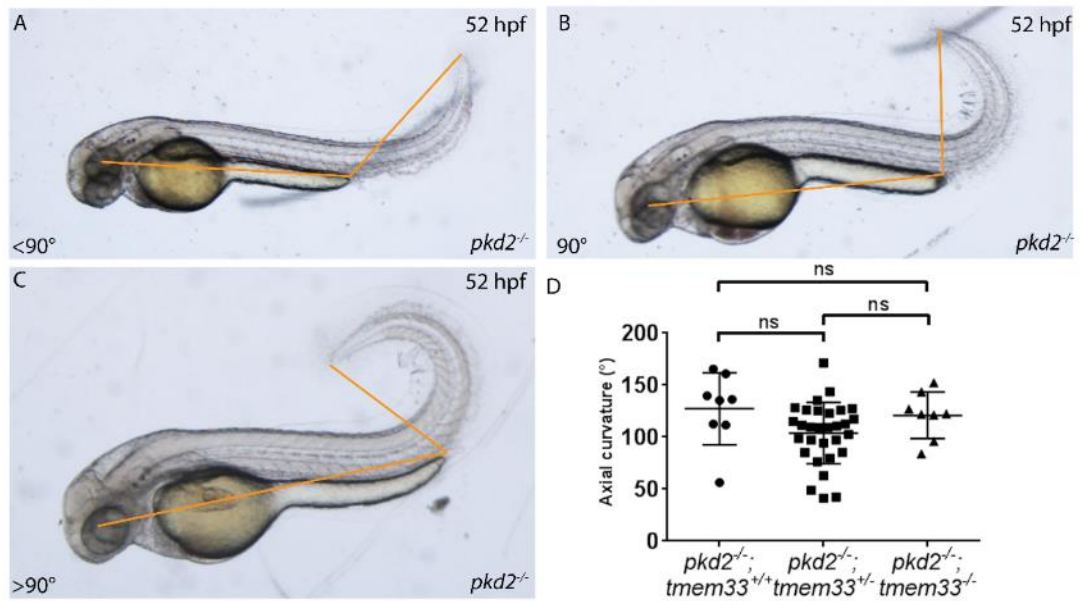


Figure 5.4 *tmem33^{sh443};pkd2^{hu2173}* mutants display no significant difference in axial curvature. (A-D) *pkd2^{hu2173}* mutants develop axial curvature but *tmem33^{sh443};pkd2^{hu2173}* double mutants do not display an increase or decrease in axial curvature compared to sibs (One-way ANOVA ns = not significant).

5.4.1 *tmem33* knockdown in *elipsa* mutants does not increase glomerular area

I have analysed *tmem33* and *pkd2* in kidney development and have been unable to observe interaction between the two genes. I observed no additive effect on glomerular expansion, suggesting *tmem33* and *pkd2* do not interact in the developing zebrafish kidney. However, an alternative explanation is that a physical limit to glomerular expansion exists. Therefore, I performed *tmem33* knockdown in a mutant zebrafish line known to display glomerular expansion, *elipsa* (*traf3ip1*) (J et al., 1996). *Elipsa* functions during ciliogenesis and mutants display developmental defects associated with ciliogenesis defects, including expanded glomeruli and axial defects (J et al., 1996; Omori et al., 2008). I

quantified glomerular area to determine whether *tmem33* knockdown could contribute to increased glomerular expansion in *elipsa* mutants.

While *elipsa* mutants developed extended glomeruli even when injected with control morpholino, control injected siblings did not (Figure 5.5 A, B, E). *tmem33* knockdown in *elipsa* mutants did not significantly increase glomerular expansion observed in *elipsa* mutants (Figure 5.5 B, D, E). However, compared to siblings injected with *tmem33* morpholinos, *elipsa* mutants injected with *tmem33* morpholinos displayed significantly increased glomerular area (Figure 5.5 C, D, E). This suggests that, while *tmem33* and *pkd2* knockdown induce glomerular expansion, the limit of expansion is not reached, since *elipsa* mutants display greater expansion. Furthermore, since no increased expansion was observed when *tmem33* was knocked down in *elipsa* mutants, it is unlikely that *tmem33* and *elipsa* interact. Therefore, I have not established epistasis between *tmem33* and genes required for normal kidney development including *pkd2* and *traf3ip1* (*elipsa*).

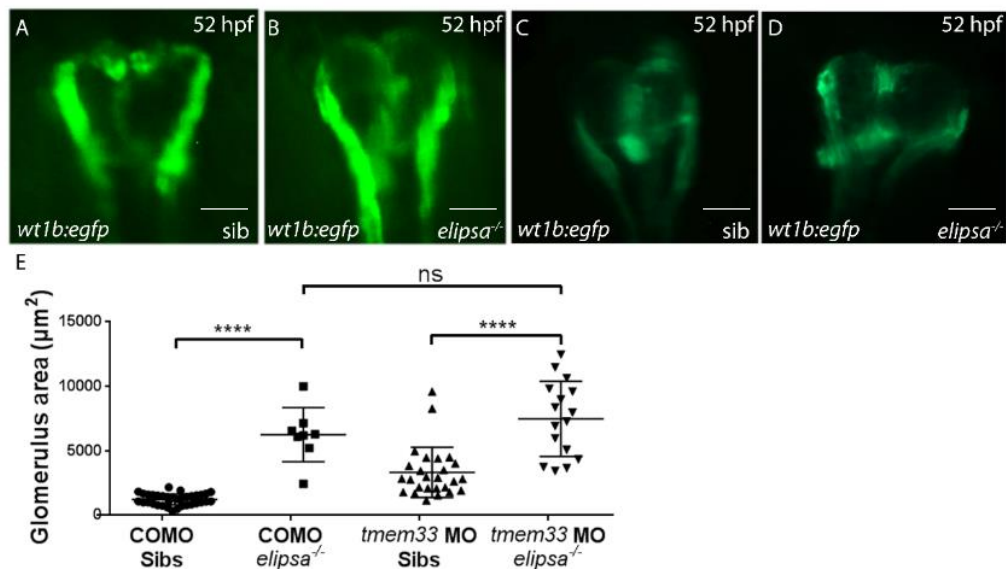


Figure 5.5 *tmem33* knockdown does not increase glomerular expansion in *elipsa* mutants.

(A-D) *elipsa* mutants display increased glomerular area compared to siblings, while *tmem33* knockdown induces glomerular expansion in both siblings and *elipsa* mutants. (E) *elipsa* mutants display significantly increased glomerular area compared to siblings, regardless of whether *tmem33* is knocked down (One-way ANOVA ns = not significant, ****p<0.0001). Each data point refers to a single glomerulus.

5.5 Expression analysis of transient receptor potential (TRP) channels during zebrafish embryogenesis

TRPP2, also known as PKD2/PC2, has been shown by my collaborators to display an increased likelihood of forming a Ca²⁺ channel in the presence of *tmem33* in a lipid bilayer reconstitution assay (Eric Honore, data not shown), suggesting an interaction. I was unable to identify a genetic interaction between *tmem33* and *pkd2* using zebrafish mutants and morphants (Figure 5.2-5.4). Since PKD2 is a member of the TRP channel superfamily of ion channels, I therefore sought alternative TRP channels to test for genetic interaction with *tmem33* and determine their effect on calcium signalling. There are 34 TRP channels in zebrafish. I therefore screened these by *in situ* hybridisation to determine which

were expressed in endothelial or kidney cells. Probes for canonical TRP (TRPC) channels were kindly donated by the Neuhauss lab (Von Niederh??usern et al., 2013). Probes for all other TRP channels were generated by *in vitro* transcription from PCR amplified cDNA (see methods).

I analysed zebrafish at 1 dpf to screen for expression during flow-independent angiogenesis. Expression analysis of all known zebrafish TRPC family members indicate that no TRPC channel displayed endothelial enrichment (Figure 5.6; Figure 5.7, black arrowheads). Expression was only observed in neural tissues (Figure 5.6; Figure 5.7, black arrowheads) and within the head of embryos at 26 hpf (data not shown). TRPA1A and TRPA1B displayed somitic and notochord expression (Figure 5.8 A-D), while TRPM genes were expressed diffusely throughout the trunk (Figure 5.8; Figure 5.9), as were TRPML genes (Figure 5.10 A-F). TRPP1A (PKD1A) displayed enrichment within the neural tube (Figure 5.10 G-H), TRPP1B (PKD1B) displayed enrichment within the pronephric tubules (Figure 5.10, I-J), but no clear enrichment of TRPP2 (PKD2) expression is observed in the trunk (Figure 5.10 K-L). TRPV4 and TRPV6 display posterior notochord enrichment, but TRPV1 does not display any clear enrichment (Figure 5.11 black arrowheads). Interestingly, I was unable to identify *pkd2(trpp2)* expression within the developing vasculature or kidney at 1 dpf, suggesting the gene may not be expressed in the tissue at the time point at which I was analysing function.

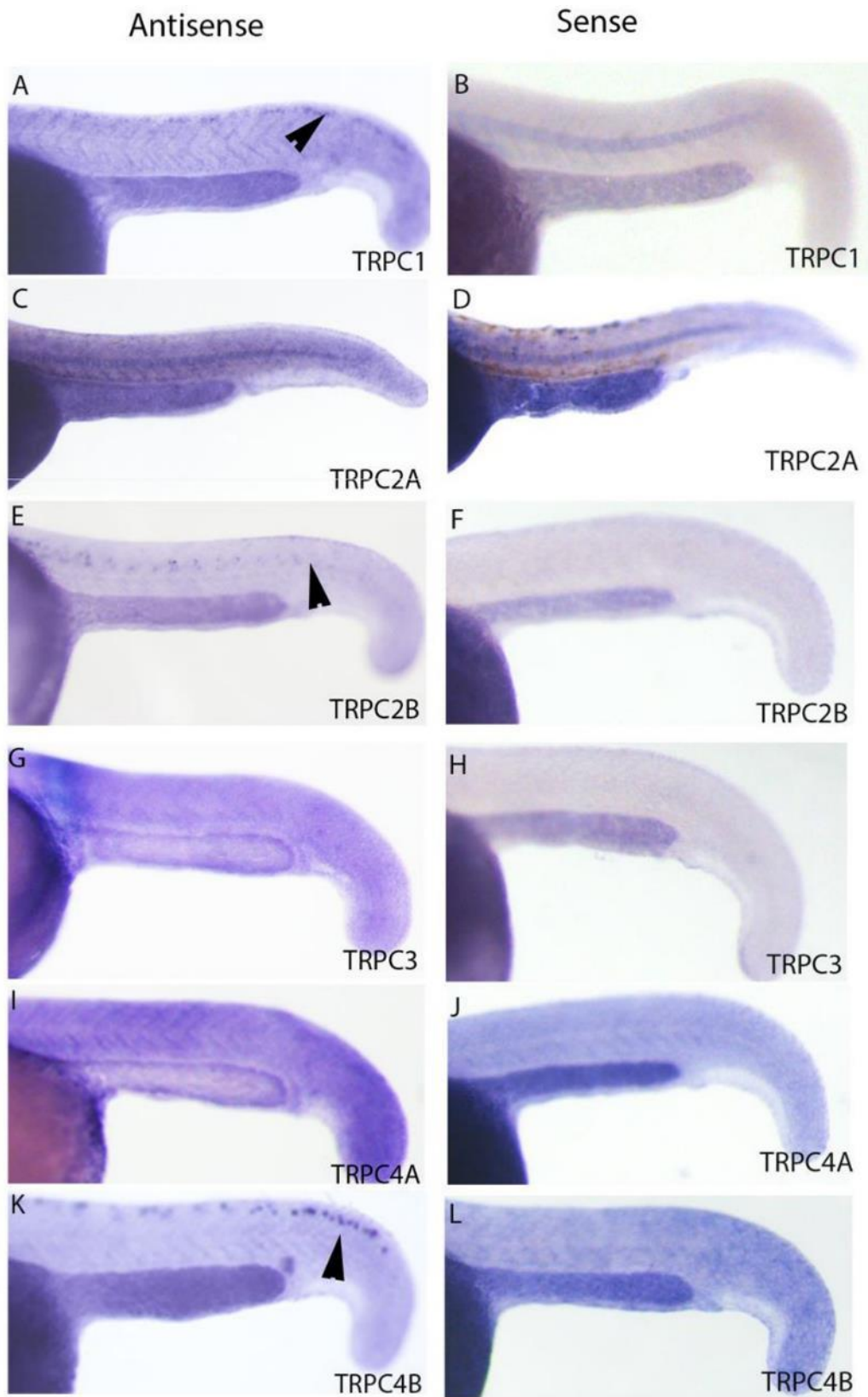


Figure 5.6 No canonical TRP channel displays enrichment in endothelial cells at 24 hpf. (A-L) Canonical TRP channels TRPC1-4B display no enrichment in endothelial cells. TRPC1, TRPC2B and TRPC4B all display enrichment in neural tissues with other genes displaying no enrichment but low-level global expression

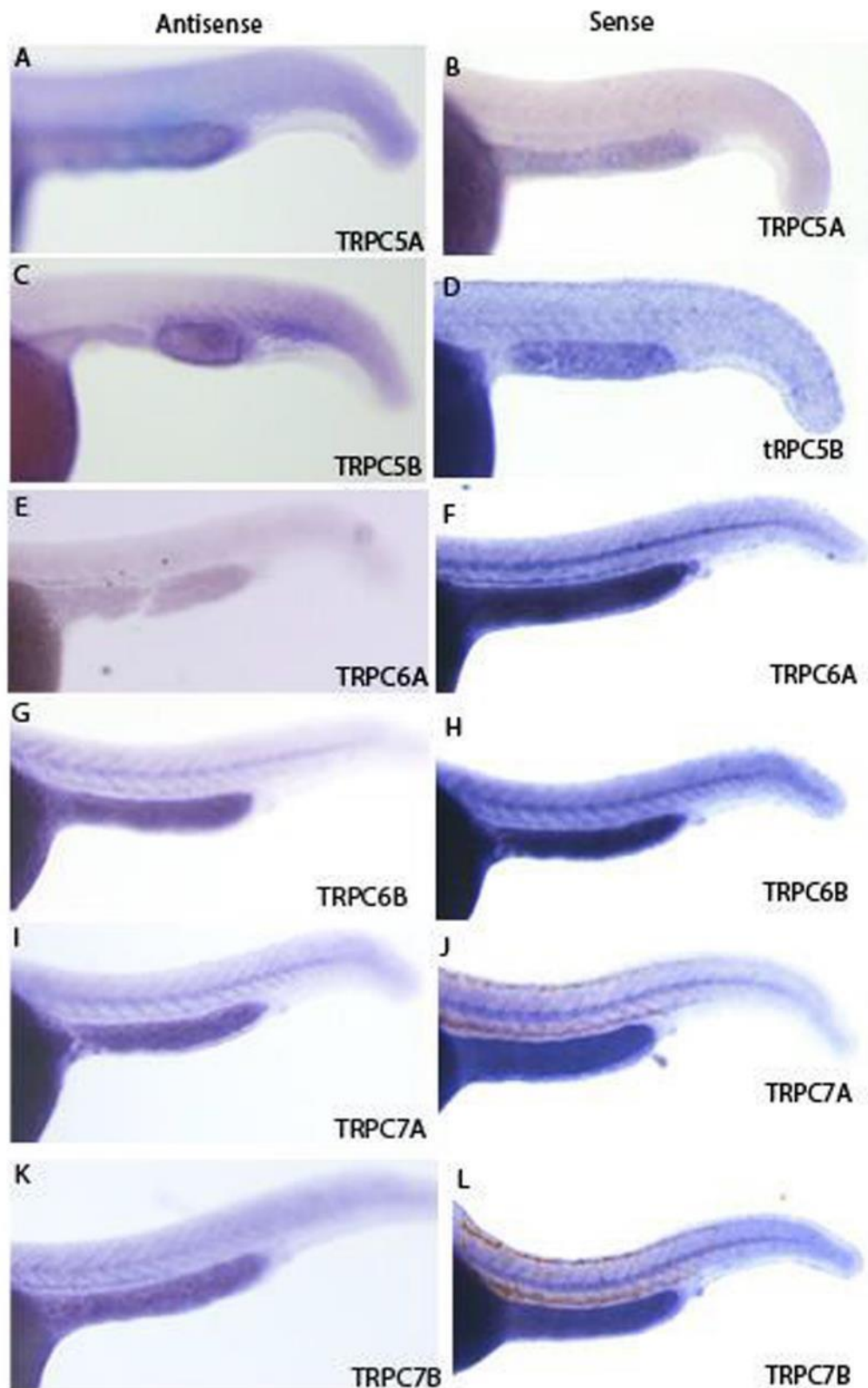


Figure 5.7 No canonical TRP channel displays enrichment in endothelial cells at 24 hpf. (A-L) Canonical TRP channels TRPC5A-7B display no enrichment in endothelial cells, with low-level global expression in all genes.

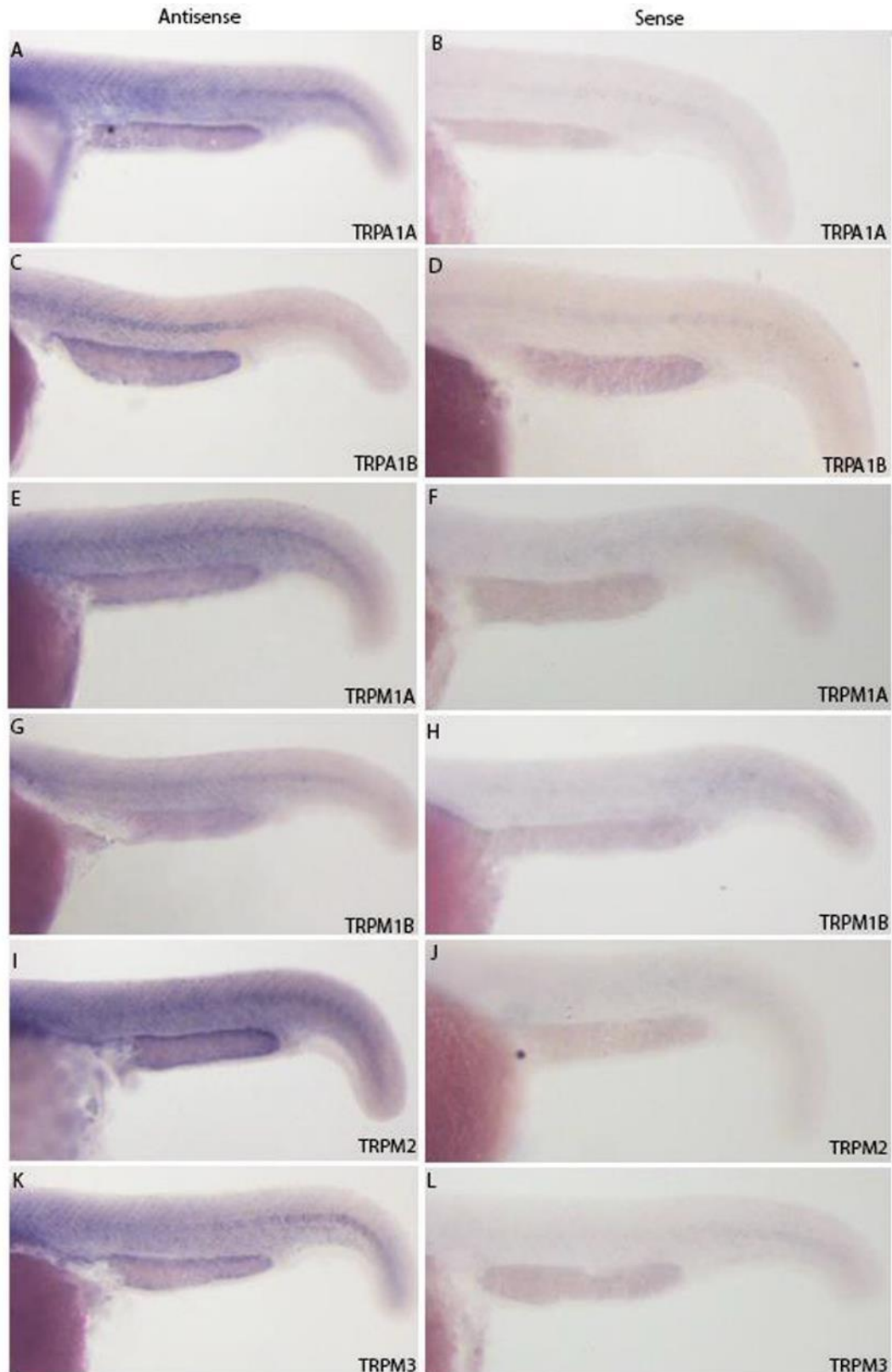


Figure 5.8 No Ankyrin or melanostatin TRP channel displays enrichment in endothelial cells at 24 hpf. (A-L) Ankyrin channels TRPA1A and TRPA1B and melanostatin TRP channels TRPM1A-3 display no enrichment in endothelial cells. TRPA1A, TRPA1B, TRPM1A, and TRPM2 display enriched somitic expression.

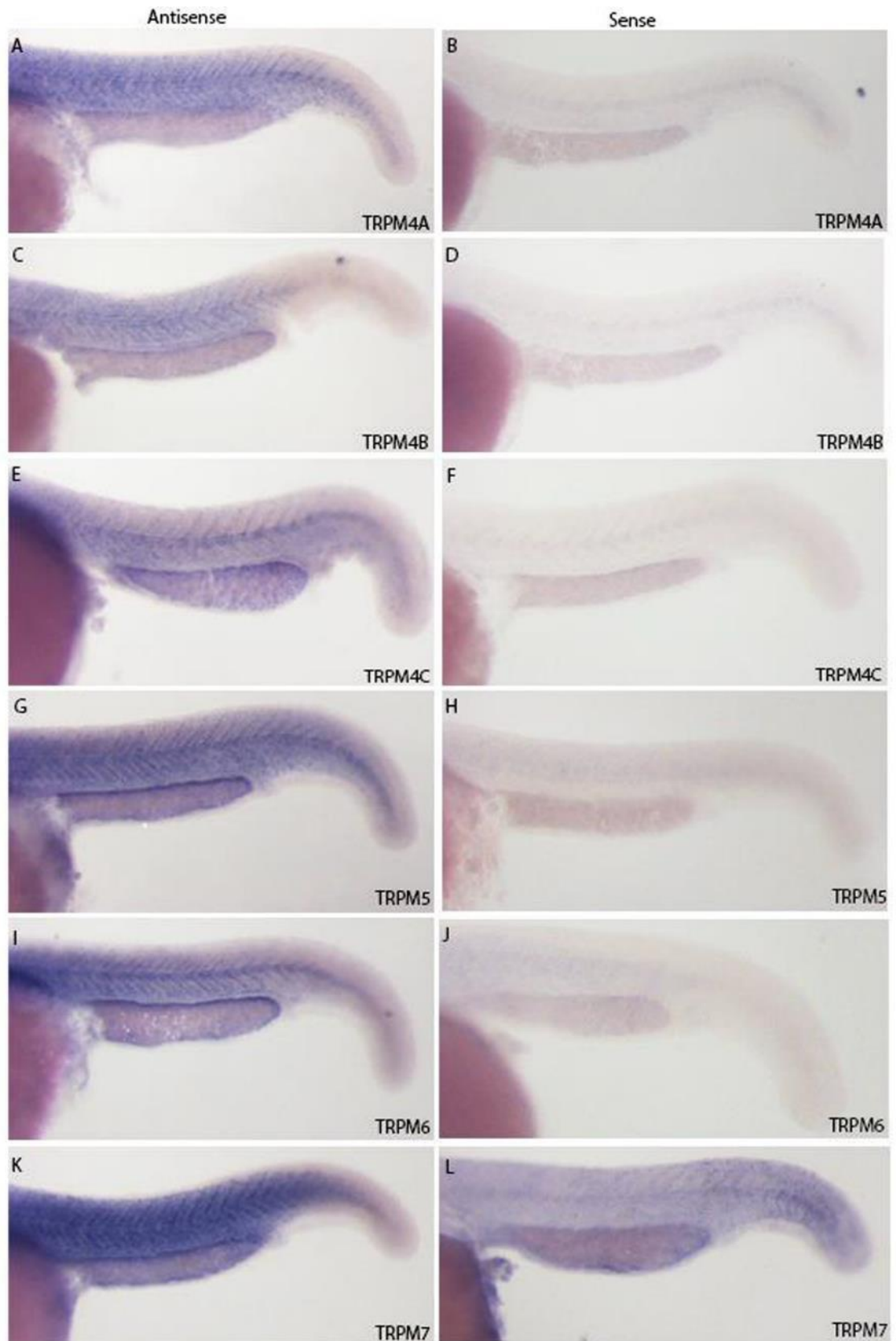


Figure 5.9 No melanostatin TRP channel displays enrichment in endothelial cells at 24 hpf. (A-L) Melanostatin TRP channels TRPM4A-7 display no enrichment in endothelial cells. However, all display enriched somitic expression.

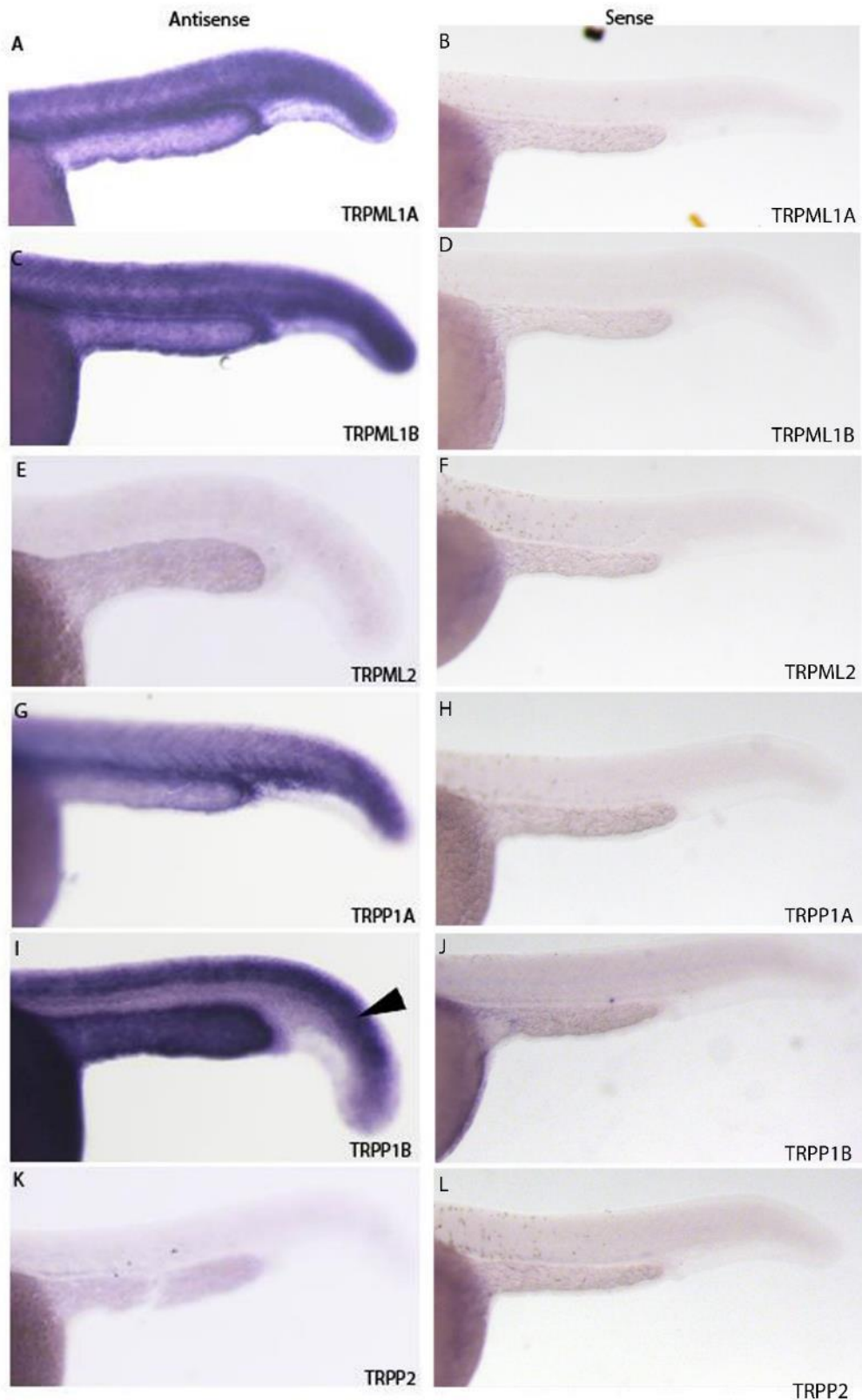


Figure 5.10 No mucolipin or polycystin TRP channel displays enrichment in endothelial cells. (A-L) Mucolipin TRP channels TRPML1A, TRPML1B and TRPML2 and polycystin TRP channels TRPP1A, TRPP1B and TRPP2 display no enrichment in endothelial cells. TRPML1A and TRPML1B display strong global expression, While TRPP1A displays renal expression and TRPP1B displays neural expression.

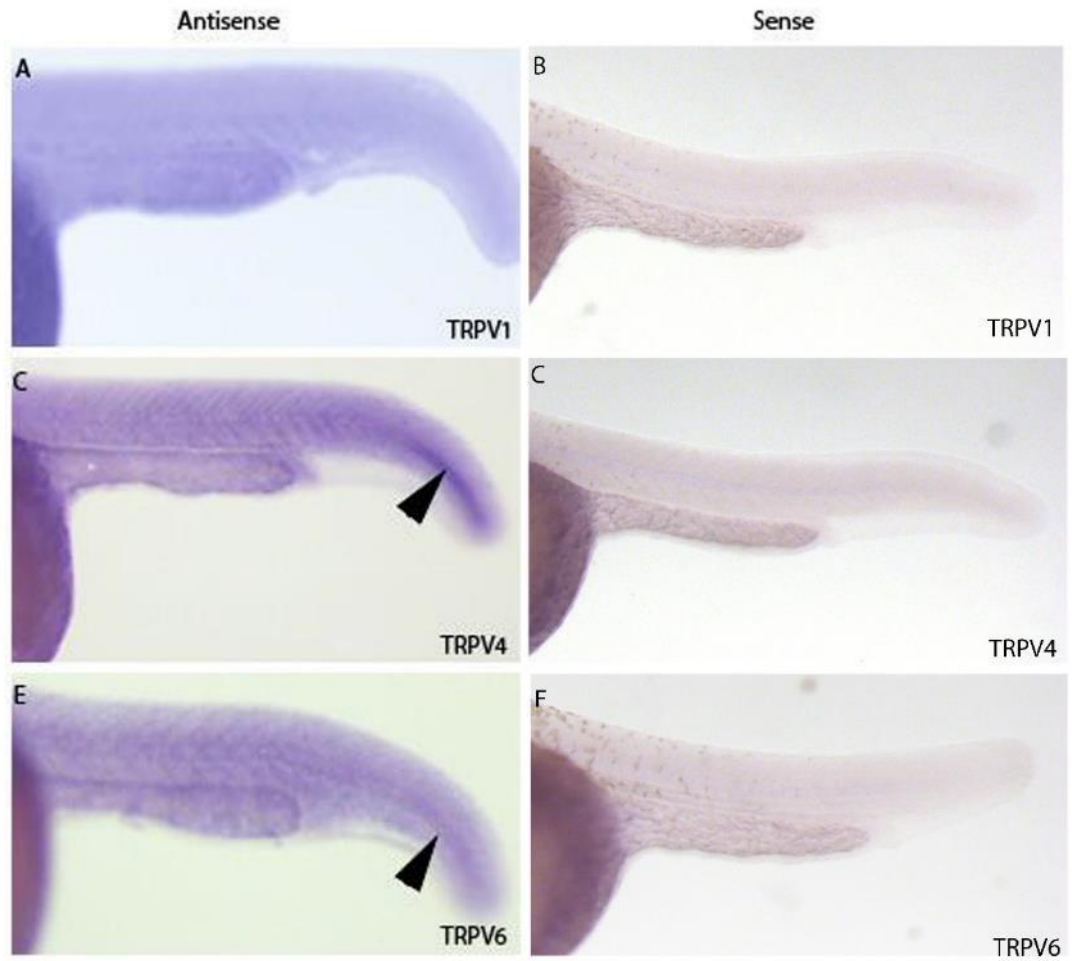


Figure 5.11 No vanilloid TRP channel displays enrichment in endothelial cells. (A-F)

Vanilloid TRP channels TRPV1, TRPV4 and TRPV6 display no enrichment in endothelial cells.

TRPV4 and TRPV6 display enrichment in the posterior notochord.

5.6 TRPV4 is required for calcium signalling during flow-independent angiogenesis

No TRP channel displayed enrichment in endothelial cells (Figure 5.8-5.11) at 1 dpf. However, this does not exclude the possibility that TRP channels function during angiogenesis in ECs. Interestingly, *pkd2* was not expressed at levels detectable by *in situ*, suggesting it along with others, may function ubiquitously at low levels (Figure 5.10); for example, *trpc1* has been suggested to function during angiogenesis in zebrafish (Yu et al., 2010). To study this, loss of function approaches targeting likely candidates are required.

It has been established that TRPV4 interacts with PKD2 in HEK and MDCK cells (Köttgen et al., 2008) and an interaction between *trpv4* and *pkd2* in zebrafish has been suggested in endocardial cells (Heckel et al., 2015). Modulation of TRPV4 is possible using the TRPV4 antagonist, TRPV4 Antagonist III (GSK205), (Kanju et al., 2016; O'Connor et al., 2014; Phan et al., 2009).

5.6.1 *trpv4* antagonist treatment delays angiogenic sprouting in zebrafish embryos.

Calcium signalling is critical for normal angiogenesis, since inhibition of *tmem33* by morpholino or CRISPRi knockdown and inhibition of calcium signalling by SKF96365 reduced calcium signalling and delayed angiogenesis. To determine whether TRPV4 is required during angiogenesis, I treated *Tg(fli1a:eGFP)y1* embryos with a TRPV4 antagonist (Chapter 2.1.6) and measured SeA migration by comparing the length of SeAs in control treated embryos and TRPV4 antagonist treated embryos.

Following three hours incubation, embryos treated with the TRPV4 antagonist displayed a significant decrease in SeA length, suggesting migration of ECs was impaired (Figure 5.12 A-C). Treatment was continued until 5 hours and SeA length was measured. Again, TRPV4 antagonist-treated embryos displayed significantly reduced SeA length (Figure 5.12 D), and SeAs had migrated no further than those measured following 3 hours treatment (Figure 5.12).

These data suggest TRPV4 may be required for EC migration during angiogenesis. Since TRPV4 functions as a calcium channel, reduced migration observed may be due to reduced EC calcium signalling, consistent with observations in *tmem33* knockdown studies.

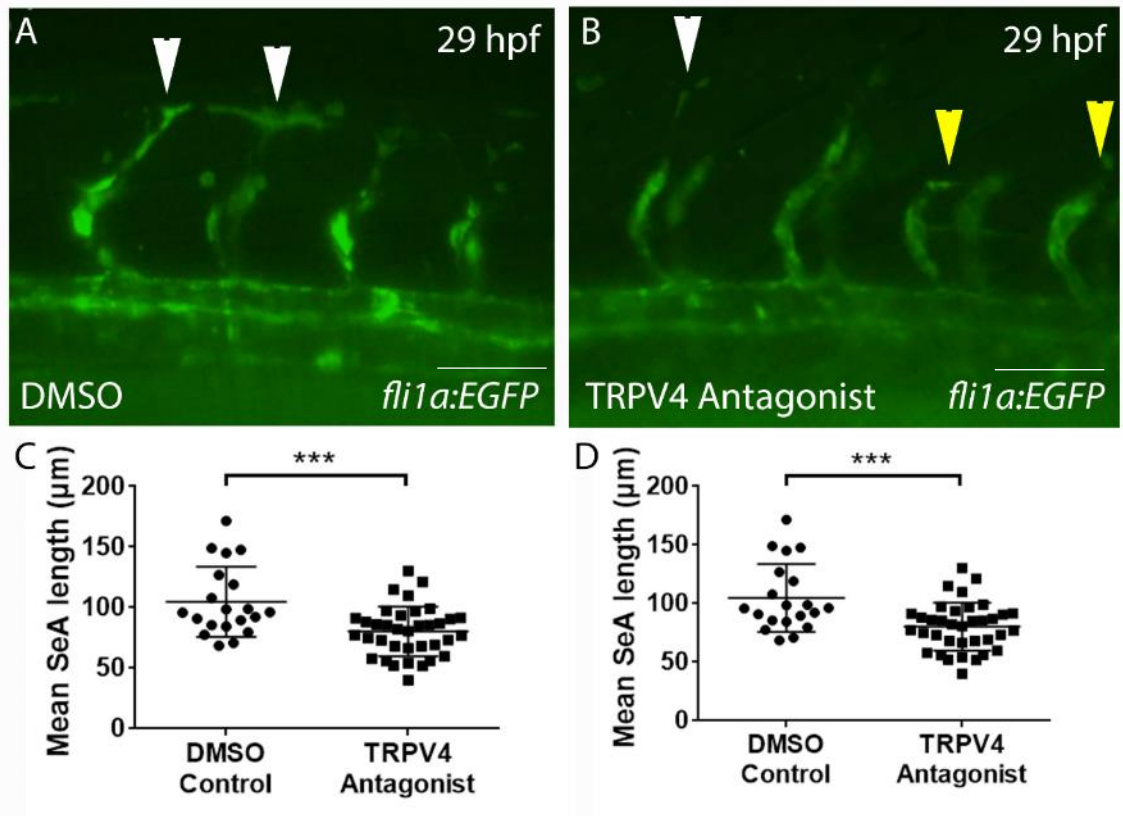


Figure 5.12 TRPV4 Antagonist III treatment causes angiogenesis delays in *Tg(fli1a:EGFP)y1* embryos. (A-B) While DMSO control embryos begin to anastomose by 29 hpf (white arrowheads), TRPV4 antagonist-treated embryos display delayed SeAs (yellow arrowheads). **(C-D)** TRPV4 antagonist treatment delays angiogenesis in treated zebrafish embryos, significantly, by reducing ISV length after both 3 and 5 hours of treatment (unpaired t-test *** $p < 0.001$).

5.6.2 *trpv4* antagonist reduces endothelial calcium oscillations in *Tg(fi1a:gff)ubs3;Tg(uas:GCaMP7a)sh392* embryos.

To determine whether reduced TRPV4 function resulted in reduced calcium transient frequency, *Tg(fi1a:gff)ubs3;Tg(uas:GCaMP7a)sh392* embryos were treated with TRPV4 antagonist for 3 hours. Five minute time-lapse movies were obtained and frequency of calcium oscillations was quantified. Embryos treated with TRPV4 antagonist displayed a significant reduction in endothelial calcium transient frequency (Figure 5.13 A-C), suggesting that TRPV4 function is required

for normal endothelial calcium signalling. Interestingly, these findings suggest that reduced calcium signalling and reduced migration may be linked, supporting data in previous chapters. I have previously shown that calcium signalling is required for normal migration during angiogenesis via *tmem33* function (Figure 3.7; Figure 3.11; Figure 4.16).

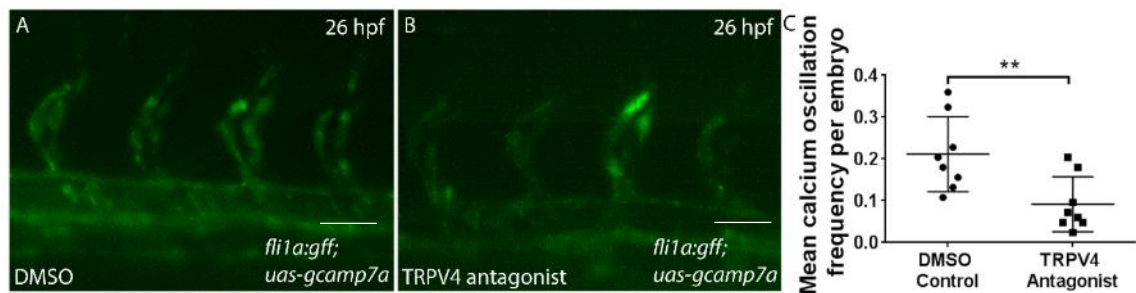


Figure 5.13 TRPV4 Antagonist III treatment reduces calcium oscillation frequency during angiogenesis. (A-C) TRPV4 antagonist-treated zebrafish *Tg(fi1a:gff);Tg(uas:GCaMP7a)sh392* embryos display reduced SeA GCaMP intensity and significantly reduced calcium oscillation frequency (unpaired t-test ** $p < 0.01$).

5.6.3 *trpv4* CRISPRi reduces frequency of calcium oscillations in *Tg(fi1a:gff);Tg(uas:GCaMP7a)sh392* embryos.

TRPV4 inhibition via antagonist treatment reduced both endothelial migration and endothelial calcium signalling. However, it is not known how specific to TRPV4 in zebrafish the TRPV4 antagonist is. Therefore to determine whether the phenotype observed following TRPV4 antagonist treatment is accurate I sought to knock down *trpv4* via CRISPRi. I first performed global knockdown of *trpv4* using CRISPRi in *Tg(fi1a:gff);Tg(uas:GCaMP7a)sh392* embryos. I injected six gRNAs targeting different regions of the gene. Calcium oscillations were still

present following TRPV4 knockdown, with regions of increased GCaMP7a fluorescence observed in endothelial tip cells of both crispants and controls (Figure 5.14 A-B). However, while GCaMP7a fluorescence was not reduced in TRPV4 crispants (Figure 5.14 D), the frequency of calcium transients was significantly reduced (Figure 5.14 C), suggesting TRPV4 is required for normal endothelial calcium signalling during SeA development.

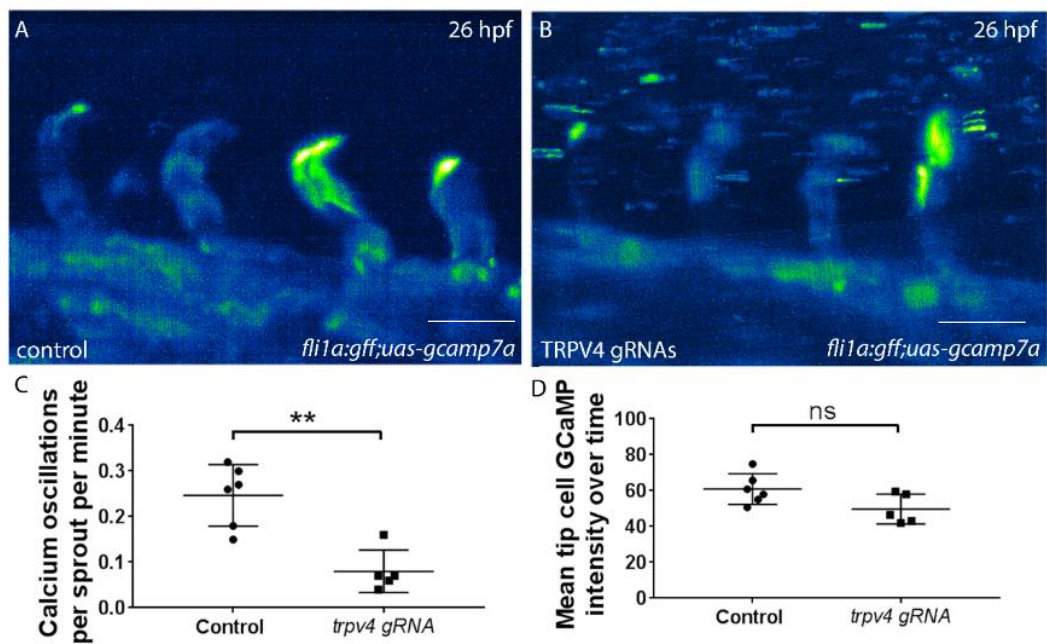


Figure 5.14 TRPV4 CRISPRi reduces endothelial calcium oscillation frequency in migrating SeAs (A-B) *trpv4* CRISPRi knockdown reduced endothelial calcium signalling frequency in *Tg(fli1a:gff)ubs3;Tg(uas:GCaMP7a)sh392* embryos. *Trpv4* crispants display fewer regions of increased intensity compared to controls. **(C-D)** While no significant reduction in GCaMP7a fluorescence is observed in *trpv4* crispants, a significant reduction in calcium oscillation frequency is observed (unpaired t-test **p<0.01).

5.6.4 *trpv4* CRISPRi reduces TRPV4 gene expression.

Having observed reduced calcium oscillation frequency in *Tg(fi1a:gff)ubs3;Tg(uas:GCaMP7a)sh392* embryos following CRISPRi knockdown, I sought to determine the level of knockdown via *in situ* hybridisation. I observed expression of TRPV4 ubiquitously, with enrichment in the posterior notochord in control and TRPV4 crispant embryos at 24 hpf, with no difference in expression observed between groups (Figure 5.15 A-B, black arrowheads). By 30 hpf, control embryos displayed increased staining in the anterior notochord (Figure 5.15 C, red arrowhead), compared to TRPV4 crispants, which only displayed enrichment of expression in the posterior notochord (Figure 5.15 C-D, black arrowheads). I therefore observe a moderate reduction in expression. However, this is sufficient to induce a calcium signalling phenotype.

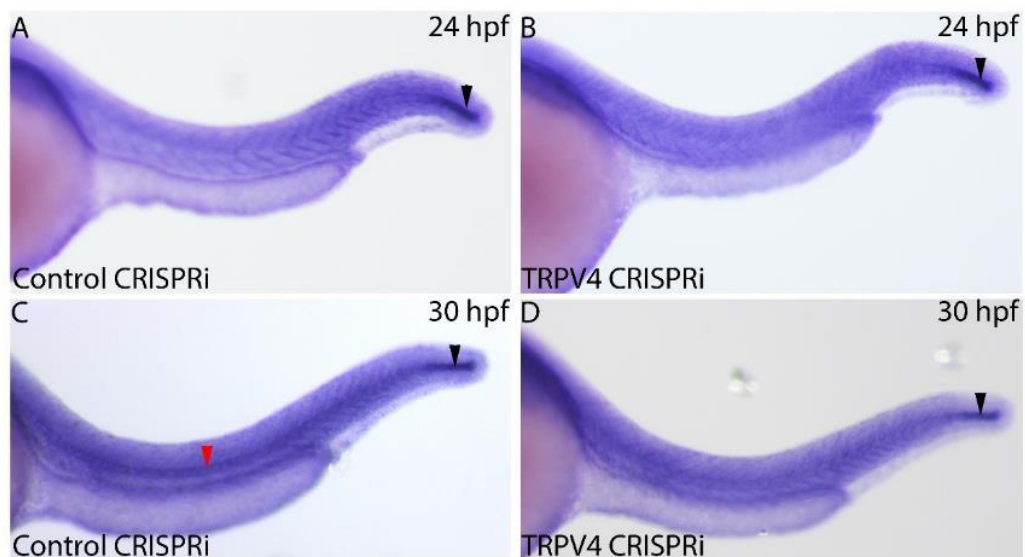


Figure 5.15 TRPV4 CRISPRi reduces TRPV4 expression. (A-B) At 24 hpf, enriched *trpv4* expression in zebrafish embryos is observed caudally, intensity of which is reduced in *trpv4* crispants. **(C-D)** By 30 hpf *trpv4* expression extends rostrally, which is not observed in *trpv4* crispants.

5.6.5 Endothelial-specific knockdown of *trpv4* by CRISPRi reduces calcium oscillation frequency in ECs in *Tg(fi1a:gff)ubs3;Tg(uas:GCaMP7a)sh392* embryos.

I next sought to determine whether TRPV4 was required for calcium signalling in a tissue specific manner during endothelial development. I crossed *Tg(fi1a:gff)ubs3;Tg(uas:GCaMP7a)sh392* and *Tg(fli1a:dCas9)^{sh512}* transgenic zebrafish and injected TRPV4 gRNAs. I found that, similar to global TRPV4 knockdown (Figure 5.14), calcium oscillations were present in TRPV4 crispants (Figure 5.16 A-B), but significantly fewer were observed (Figure 5.16 C). Fluorescence of GCaMP7a in EC tip cells was unaffected by EC-specific *trpv4* CRISPRi (Figure 5.16 D). These data suggest that TRPV4 is required cell autonomously within EC tip cells for calcium signalling during angiogenesis.

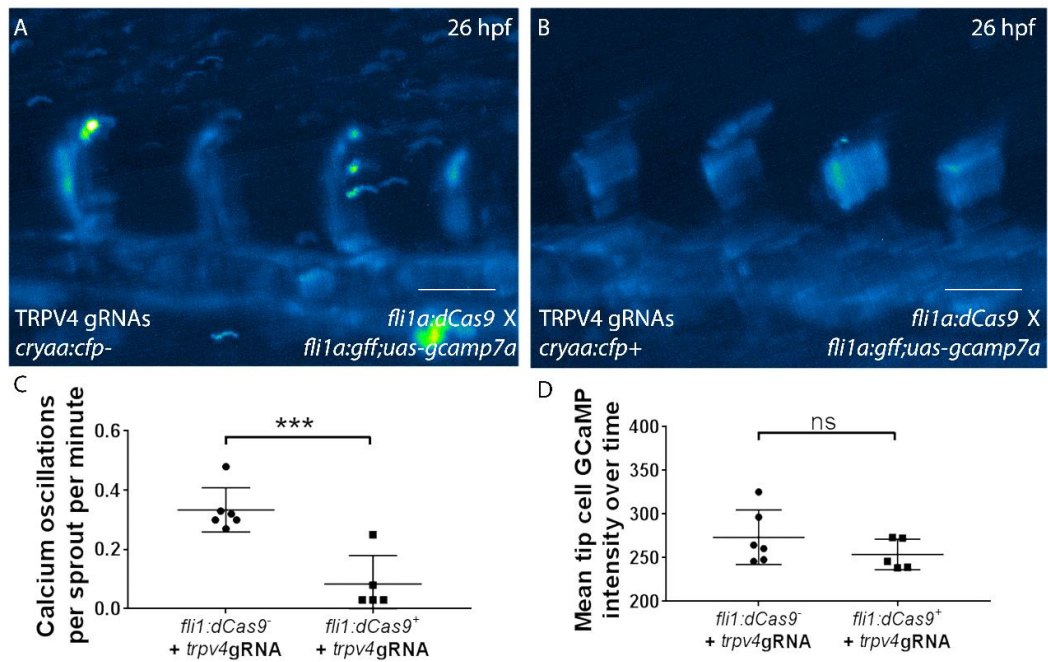


Figure 5.16 Endothelial-specific TRPV4 CRISPRi reduces endothelial calcium oscillation frequency. (A-B) *trpv4* EC-specific CRISPRi knockdown reduced endothelial calcium signalling frequency in *Tg(fli1a:gff)ubs3;Tg(uas:GCaMP7a)sh392* embryos. *Trpv4* EC-specific crispants display fewer regions of increased intensity compared to controls. (C-D) While no significant reduction in GCaMP7a fluorescence is observed in *trpv4* crispants, a significant reduction in calcium oscillation frequency is observed (unpaired t-test *** $p < 0.001$).

5.7 Discussion

5.7.1 My data provides no evidence for genetic compensation between *tmem33* and *pkd2* but does not discount possible interaction during zebrafish development.

Data from my collaborators has shown that TMEM33 increases activity of the PKD2 calcium channel in a lipid bilayer reconstitution assay (Eric Honore, data not shown). This suggests these two proteins interact. *tmem33^{sh443}* mutants used in this thesis display no morphological or developmental abnormalities, while *tmem33* morphants develop expanded glomeruli (Figure 1.4). Furthermore, my analysis has indicated that genetic compensation is likely to exist in *tmem33^{sh443}* mutants (Figure 3.13). In this chapter, I sought to determine whether any interaction takes place, using mutant lines and morpholino knockdown. I also sought to determine whether it is possible that *tmem33* functions to compensate for loss of functional *pkd2* in *pkd2^{hu2173}* mutants and *vice versa*. Interestingly, *pkd2^{hu2173}* mutants do not display expanded glomeruli, unlike *pkd2* morphants (Sun, 2004). My findings in this chapter suggest that in *tmem33^{sh443}* mutants, *pkd2* is not the gene responsible for genetic compensation, while *tmem33* does not compensate in *pkd2^{hu2173}* mutants. However, the data contained within this chapter suggest that there may be a genetic interaction between the two genes.

tmem33 resides within the ER membrane, while *pkd2* has been shown to function both in the ER, golgi and plasma membranes (Foggensteiner et al., 2000; Obara, 2006; Pazour et al., 2002). Recently, genetic compensation has been shown in zebrafish between unrelated proteins which localise to similar subcellular domains (Rossi et al., 2015). Since both *tmem33* and *pkd2* localise to the ER

membrane, and knockdown produced similar phenotypes, I sought to determine whether any genetic interaction took place, by analysing whether each gene could compensate for the other. However, although the mechanisms controlling genetic compensation remain unclear, the data obtained herein suggests that simply because proteins have been shown to interact within a different context, they may not be suitable candidates for compensation. Furthermore, TRP channel family members have been shown to form membrane channels utilising their transmembrane domains, forming a tetrameric pore, with two transmembrane channels contributing to the pore from each protein (Ramsey et al., 2006). Various combinations of TRP channels have been identified, however, pairs of homodimers are most frequent (Kobori et al., 2009; Köttgen et al., 2008; Ramsey et al., 2006). No such data is available for *tmem33* currently and therefore little is known about potential interactors or modes of interaction.

My inability to confirm genetic interaction between *tmem33* and *pkd2* highlights interesting questions regarding the mechanism by which genetic compensation occurs. Therefore, it is possible that although genes may interact during development or adult life, even likely in the same genetic pathway, they may not be sufficiently similar to compensate for the loss of the other. Rather, unrelated genes which display a similar protein structure may serve to function more efficiently during genetic compensation, as previously described (Rossi et al., 2015). Current understanding of how genetic mutations may or may not induce compensatory pathways are limited and little is known regarding what makes a gene more likely to compensate for another (El-Brolosy and Stainier, 2017). Furthermore, nothing is known about how any potential DNA surveillance takes place which may identify suitable candidates for genetic compensation in the

event of a genomic lesion leading to improper protein formation. Interestingly, although mutants which display nonsense-mediated decay (NMD) have been suggested to display genetic compensation via upregulation of other genes, recent evidence has suggested that a lack of phenotype may be due to altered mRNA processing. For example, a loss of NMD machinery may induce an expected phenotype in aphenotypic mutants (Schuermann et al., 2015). I have shown in this thesis that *tmem33* mutants are resistant to the effects of CRISPRi, suggesting that NMD is not the only mechanism by which compensation can occur, since CRISPRi inhibits the formation of mRNA.

Interestingly, my data suggest that that neither a potential similarity in function nor documented interaction may be sufficient to predict a potential compensatory mechanism. However, indicators for likelihood of a given gene to compensate for another remain to be determined. Recent studies have screened for candidate genes (Rossi et al., 2015), however, and an approach combining proteomics and transcriptomics in parallel, with subsequent candidate screening would be required to uncover compensatory genes in mutant lines.

5.7.2 TRPV4 contributes to endothelial calcium oscillations during sprouting angiogenesis

Several TRP channels have been implicated in calcium signalling within endothelial cells, including TRPC1, PKD2 and TRPV4 (Du et al., 2014; Kobori et al., 2009; Köttgen et al., 2008; Zhang et al., 2013). Despite evidence of TRP channel function in endothelial cells (Yu et al., 2010), I was unable to characterise expression of TRP channels within the endothelium of zebrafish during flow-

independent angiogenesis, at which point endothelial calcium signalling is primarily induced by VEGF signalling.

I have shown in this thesis by EC-specific knockdown of *trpv4* that *trpv4* may function during endothelial calcium signalling, however, further experiments are required to confirm this. I disrupted TRPV4 function by both genetic knockdown, utilising CRISPR interference, and chemically, using the TRPV4 antagonist. While knockdown did not result in a clear reduction in mRNA by *in situ* hybridisation, I observed reduced endothelial calcium oscillation frequency, suggesting subtle perturbations in gene expression may cause observable defects. To quantify the extent of genetic knockdown, however, it would be necessary to perform qRT-PCR. Furthermore, endocardial expression and function of *trpv4* has been observed (Heckel et al., 2015; Mangos et al., 2007). Since endothelial and endocardial cells are derived from the same cells, it is possible that *trpv4* may also be expressed in endothelial cells, despite not having yet been described. Interestingly, a reduction in EC calcium oscillation frequency was observed following tissue-specific knockdown, suggesting that *trpv4* may function to regulate endothelial calcium during angiogenesis within ECs. Current literature has shown that TRP channel function within endothelial cells may serve as a mechanism to sense flow and TRP channels may function to induce calcium signalling in response to blood flow in endothelial cells (Du et al., 2014; Heckel et al., 2015; Köttgen et al., 2008). Interestingly, here I report a potential function for TRPV4 in calcium signalling during flow-independent angiogenesis *in vivo* for the first time.

However, while the findings in this thesis indicate a potential role for *trpv4* in endothelial calcium signalling, further testing is required to determine its precise function, particularly in relation to other TRP channels. For example, in this study, I designed six gRNAs (see table 2.2) to target different regions of the TRPV4 gene, including gRNAs flanking the pore-forming transmembrane channels. Therefore, it may be possible to generate not only conditional mutants (Ablain et al., 2015) or perform conditional knockdown (Chapter IV), but also to generate CRISPR mutant lines in which sections of the gene are removed. Therefore the pore-forming domain can be excluded from the protein, removing the functional domain. This would suggest it is possible to obtain a greater understanding of the function of *trpv4* during zebrafish angiogenesis.

5.7.3 Limitations and future work.

In this section, I have analysed TRP channel function, specifically PKD2 and TRPV4. I analysed *pkd2* in relation to *tmem33* function, testing whether either gene is capable of compensating for the other. I analysed *tmem33^{sh443};pkd2^{hu2173}* double mutants and tested *tmem33* knockdown in *pkd2^{hu2173}* mutants but did not have the time to knock *pkd2* down in *tmem33^{sh443}* mutants. Double mutant analysis suggested that neither gene compensated for the other, suggesting that *pkd2* knockdown in *tmem33^{sh443}* mutants would have yielded the same result as *tmem33* knockdown in *pkd2^{hu2173}* mutants. However, although I was unable to clearly identify an interaction utilising the tools available to us, it does not mean the genes do not interact in wild-type zebrafish. Both mutants may undergo genetic compensation via different genes, in which case I would expect no change in phenotype to be observed in *tmem33^{sh443};pkd2^{hu2173}* double mutants.

Likewise, my analysis of *trpv4* function was limited due to time constraints. I showed that *trpv4* functions during calcium signalling in endothelial cells and is required specifically within endothelial cells for normal calcium signalling. However, much more rigorous analysis is required to understand how *trpv4* functions during angiogenesis and how it interacts with known signalling pathways required for angiogenesis. It would also be interesting to determine whether *trpv4* interacts with *tmem33* during angiogenesis.

6 Overall Discussion: A more general role for *tmem33* in calcium signalling?

Current knowledge of intracellular signalling within migratory endothelial cells is incomplete, and many approaches to modulate angiogenesis within a disease context have targeted only VEGF. While VEGF signalling is the major regulator of angiogenesis, most therapies targeting VEGF have been unsuccessful. Therefore investigation of alternative signalling pathways which contribute to angiogenesis may lead to new insights which can be exploited to target disease. In this study I highlight novel functions for the previously uncharacterised *tmem33* gene during multicellular development. I also developed tissue-specific CRISPR interference, a novel technique to conditionally knockdown gene function, and used this to demonstrate an endothelial requirement for *tmem33* during angiogenesis.

tmem33 knockdown delays angiogenesis, and reduces endothelial Ca^{2+} oscillations and filopodia formation, indicating that *tmem33* functions to promote endothelial Ca^{2+} signalling, which in turn governs downstream EC physiology. Furthermore, I demonstrate that *tmem33* functions downstream of VEGF signalling during flow-independent angiogenesis in zebrafish. *TMEM33* is also required for HUVEC migration and angiogenesis *in vitro*, indicating this is an ancestral function of the gene conserved between zebrafish and humans (Data courtesy of collaborators; Figure 6.1). Previous studies have indicated that Ca^{2+} signalling is induced downstream of VEGF signalling (Oike et al., 1994; Vaca and Kunze, 1994; Yokota et al., 2015) and our data is consistent with this. Our study has shown that Ca^{2+} oscillations induced by VEGF contribute to induction of Notch signalling and that *tmem33* mediates this function during angiogenesis.

tmem33 therefore mediates the ability of ECs to respond to VEGF via Ca^{2+} oscillations. *tmem33* knockdown reduces activity of signalling pathways known to function downstream of VEGF signalling, including Notch and MAP kinase signalling. Interestingly, the Notch receptors Jagged-1, DLL-1 and DLL-4 have been shown to bind Notch ligands in a Ca^{2+} -dependent manner via Notch-1 EFG-like repeats, suggesting a link between Ca^{2+} homeostasis and Notch signalling (Andrawes et al., 2013; Chillakuri et al., 2013; Cordle et al., 2008; Rand et al., 1997). Indeed, Ca^{2+} ions have been shown to bind to the Notch-1-DLL-4 complex during ligand-receptor interaction, highlighting that Ca^{2+} signalling is important for Notch signalling (Luca et al., 2015). Therefore, it is likely that Notch and ERK signalling function downstream of Ca^{2+} signalling and are at least partially dependent on Ca^{2+} oscillations for their induction.

While my global knockdown analysis suggests a function for *tmem33* downstream of VEGF during angiogenesis, I did not perform this analysis in a tissue-specific manner. Therefore a non-cell autonomous effect may be present during this analysis. I showed an endothelial cell-specific requirement for *tmem33* during angiogenesis and found that inhibition of calcium signalling via SKF96365 treatment impaired angiogenesis. Furthermore, collaborators showed a requirement for *TMEM33* function during angiogenesis in endothelial cell culture (Figure 6.1).

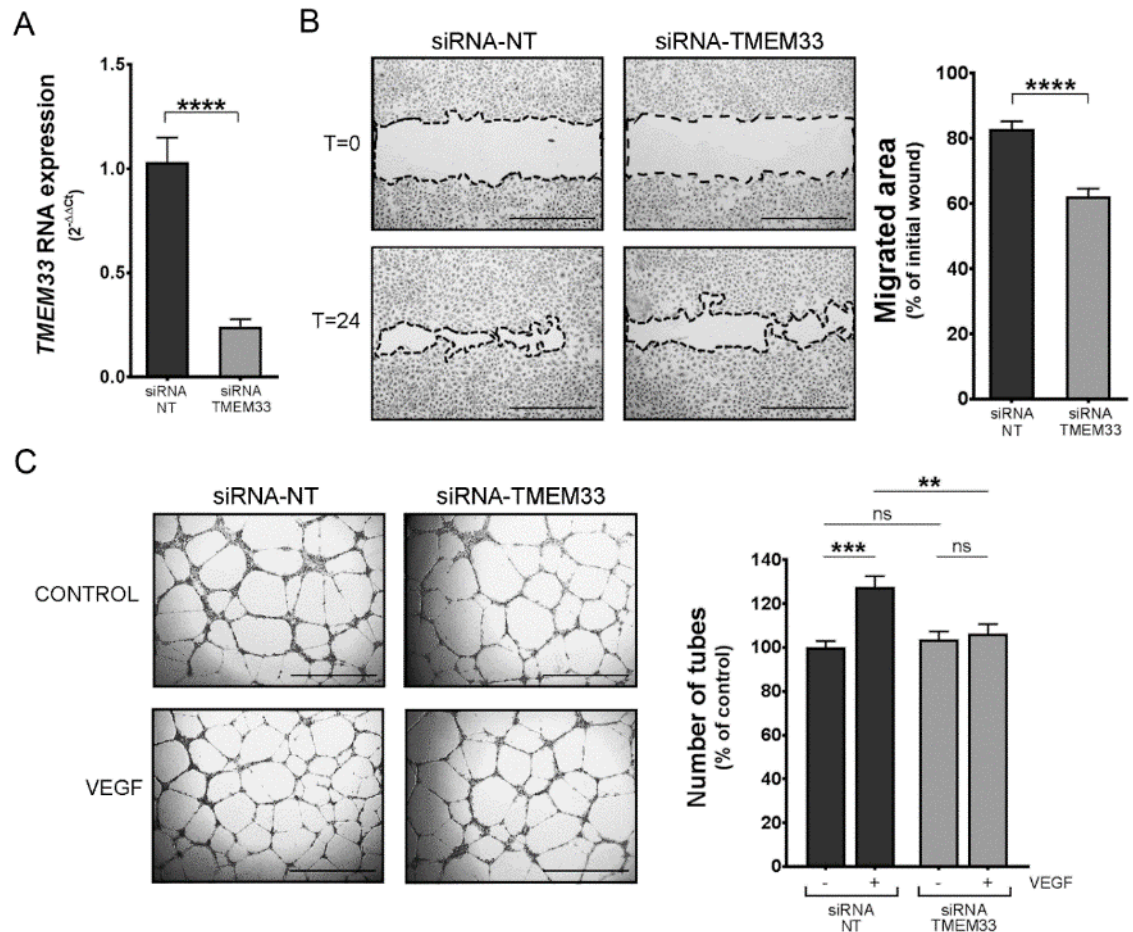


Figure 6.1 *TMEM33* is required for VEGFA-mediated angiogenesis in Human Umbilical Vein Endothelial Cells (HUVECs) (A) *TMEM33* expression is significantly reduced by siRNA knockdown. (B) Representative images of wound-healing migration assays performed with HUVECs transfected with a non-targeting control siRNA (siRNA-NT) or a siRNA specific for human *TMEM33* (siRNA-*TMEM33*). (unpaired *t* test ****, $P \leq 0.001$). Scale bars, 100 μm . (C) HUVECs transfected as described in (A) were plated on Growth-Factor Reduced Matrix (Geltrex) in Medium 200 containing 2% FBS (Control), supplemented with VEGF (25 ng/ml) when indicated (VEGF). Images show representative fields from experiments quantified in the histogram. ns=non-significant; **, $P \leq 0.01$; ***, (one-way ANOVA with *post hoc* Tukey's comparison test $P \leq 0.005$). Scale bars, 1000 μm . Data and analysis courtesy of Dr Sathishkumar Kurusamy and Dr Angel Armesilla.

Interestingly, I observed several phenomena suggestive of a wider function for *tmem33*. Inhibition of SERCA pumps is known to increase cytosolic Ca^{2+} , yet SERCA inhibition following *tmem33* knockdown yielded no increase in cytosolic Ca^{2+} , suggesting *tmem33* may function during regulation of Ca^{2+} efflux from the ER. This indicates a likelihood for a wider role than a downstream effector of VEGF signalling. *tmem33* function is required for both Ca^{2+} oscillations and filopodia formation. Co-dependence between Ca^{2+} homeostasis and the actin cytoskeleton regulates normal cell biology (Hartzell et al., 2016; van Vliet et al., 2017). Furthermore, I observed impaired Ca^{2+} signalling in the developing kidney following *tmem33* knockdown, suggesting that *tmem33* function is not limited to endothelial cells during angiogenesis. Therefore, it is possible that *tmem33* functions in a more general role to promote Ca^{2+} signalling during development.

I also developed tissue-specific CRISPR interference, both transiently and stably, in zebrafish to conditionally modulate *tmem33* expression. Tissue-specific CRISPRi has a broader application, and could be utilised in studies in any multicellular organism. However, the distinct advantage in using the zebrafish lies in external development and transparency enabling live imaging, which I utilised in this study. However, I saw a reduction in knockdown levels between the third and fifth embryonic day. Since zebrafish study is undertaken during the first five days of development, this makes the zebrafish a suitable candidate for CRISPRi study. However, recent studies have shown that guide RNAs can be stably expressed along with Cas9 enzymes, which has the potential to extend guide RNA function (Ablain et al., 2015). Furthermore, modifications to dCas9, such as addition of the KRAB domain (Gilbert et al., 2014) can be utilised to increase transcriptional repression, thereby potentially extending the duration of

knockdown. Both such methods will extend the potential for use in other organisms, such as mice, which develop internally. Of further interest is the potential to not only transcriptionally inactivate genes, but to ectopically activate genetic transcription of genes using CRISPR activation (Gilbert et al., 2014). CRISPR interference and activation provide the means to understand how cell-cell signalling controls morphogenesis during development, which can be a powerful tool to further the development of novel therapies for disease.

I performed analysis on effects of genetic compensation via transcriptional adaptation. Work contained in this thesis shows that genetic knockdown resulting in nonsense-mediated decay can cause transcriptional adaptation. However, I were unable to identify the compensating gene. I first assayed *pkd2*, which interacts genetically with *tmem33* in the kidney of mice and cell culture, wherein *tmem33* increases *pkd2* Ca²⁺ channel function (Eric Honore, data not shown) and performed studies to determine whether *tmem33* and *pkd2* interacted genetically in the developing zebrafish. These results were inconclusive and were unable to identify an interaction at the genetic level. However, since the mechanisms of genetic compensation are as yet unclear, I cannot exclude that the reason I were unable to identify an interaction is due to the limitations of currently approaches (El-Brolosy and Stainier, 2017).

trpv4 is required in endothelial cells for normal Ca²⁺ oscillations during angiogenesis. A role for *trpv4* during calcium signalling in the zebrafish endocardium has previously been described (Heckel et al., 2015), and my data suggest that *trpv4* functions similarly in endothelial cells. Furthermore, TRPV4

and PKD2 have been shown to interact (Köttgen et al., 2008) and may function together, along with TRPC1, during Ca²⁺ signalling in endothelial cells (Du et al., 2014; Goetz et al., 2014; Ma et al., 2013). This is a potentially interesting route to analyse endothelial Ca²⁺ signalling, especially given the development of tissue-specific knockdown within this thesis, which will allow for cell-type specific modulation of gene function *in vivo*. Coupled with the live-imaging capabilities of the zebrafish, this makes for an exciting prospect.

Overall, the findings presented in this thesis indicate VEGF-mediated Ca²⁺ oscillations are mediated by *tmem33* during angiogenesis and are critical for induction of key downstream signalling pathways including Notch and ERK and to promote EC proliferation and filopodia formation (Figure 6.2).

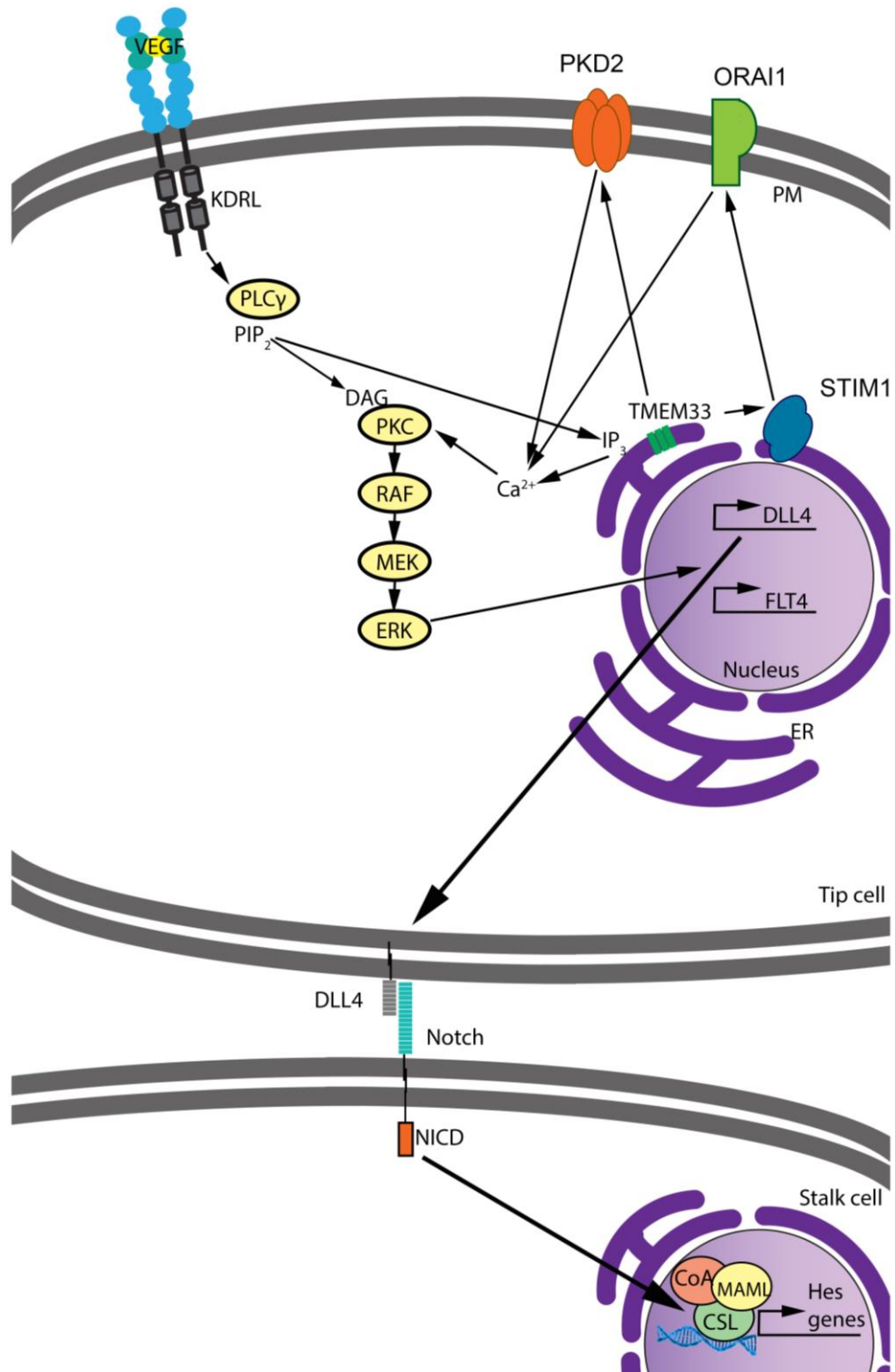


Figure 6.2 *tmem33*-mediated Ca²⁺ signalling functions downstream of VEGF signalling to regulate downstream signalling. During angiogenesis, VEGF signalling via VEGF receptors induces downstream signalling via *plcg1*, inducing Ca²⁺ efflux from the ER. Downstream signalling pathways culminating in Notch signalling are in part Ca²⁺-dependent. *tmem33* functions within the ER to promote endothelial Ca²⁺ oscillations, which contribute to the induction of ERK and Notch signalling, via upregulation of *dll4*.

Future directions:

In this thesis, I have shown that *tmem33* is required during primary sprouting angiogenesis in zebrafish, in the first study of *tmem33* conducted in a multicellular organism. I have shown that *tmem33* is required downstream of VEGF signalling and regulates endothelial cell biology, including regulation of calcium signalling, actin cytoskeleton dynamics and integration of Notch signalling and ERK signalling, downstream of VEGF signalling during angiogenesis. However, much remains unknown regarding Tmem33 function.

To gain greater insight into how Tmem33 regulates calcium signalling, further study on its function within the ER is required. Tmem33 has been implicated in regulation of ER shape, which is important during angiogenesis. Future studies should make use of either a *tmem33*- or ER-reporter transgenic line to analyse ER structure following *tmem33* knockdown. During calcium signalling, the ER must reorganise from a sheet-like to a tubular conformation to maximise contact points between the ER and plasma membrane.

Future interaction studies should be undertaken. It has been suggested that Tmem33 interacts with PERK, which regulates SOCE by interacting with Filamin A, to rearrange the actin cytoskeleton in order to facilitate the translocation of the ER to the plasma membrane. Detailed analysis using cultured endothelial cells should make use of total internal fluorescence (TIRF) microscopy to measure whether *tmem33* knockdown impairs ER translocation to the plasma membrane during SOCE, to determine whether this is the mechanism by which calcium signalling becomes impaired following *tmem33* knockdown.

While the *tmem33* mutant line does not exhibit any phenotype, value still exists in the generation of mutants. For example, recent studies have suggested that aphenotypic mutants may display compensation induced by nonsense-mediated decay (NMD). Furthermore, studies have suggested that genetic abrogation of NMD component function may restore a phenotype previously observed following genetic knockdown. This should be performed in *tmem33* mutants. Furthermore, targeted deletion mutants, in which specific domains of Tmem33 are deleted, may provide a greater understanding of *tmem33* function. For example, deletion of the C-terminal tail may provide information of how Tmem33 interacts with other proteins, such as those previously suggested.

Further conditional experiments using the *Tg(fli1a:dCas9,cryaa:CFP)sh512* transgenic line to validate interaction between *tmem33* and endothelial signalling pathways would strengthen the arguments made in this thesis.

I provided preliminary information on TRPV4 function during angiogenesis. While promising, this requires further investigation. Conditional experiments using the *Tg(fli1a:dCas9,cryaa:CFP)sh512* transgenic line to validate *trpv4* function during angiogenesis would also be beneficial. A similar approach could be applied to *pkd2*, to determine whether it functions during angiogenesis.

7 Bibliography

Ablain, J., Durand, E.M., Yang, S., Zhou, Y., and Zon, L.I. (2015). A CRISPR/Cas9 vector system for tissue-specific gene disruption in zebrafish. *Dev. Cell.*

Andrawes, M.B., Xu, X., Liu, H., Ficarro, S.B., Marto, J.A., Aster, J.C., and Blacklow, S.C. (2013). Intrinsic selectivity of notch 1 for delta-like 4 over delta-like 1. *J. Biol. Chem.* 288, 25477–25489.

Arany, Z., Huang, L.E., Eckner, R., Bhattacharya, S., Jiang, C., Goldberg, M.A., Bunn, H.F., and Livingston, D.M. (1996). An essential role for p300/CBP in the cellular response to hypoxia. *Proc. Natl. Acad. Sci. U. S. A.* 93, 12969–12973.

Aylin Metzner (2016). A study of ADPKD pathogenesis and treatment in zebrafish models. Univeristy of Sheffield.

Bahary, N., Goishi, K., Stuckenholtz, C., Weber, G., Leblanc, J., Schafer, C.A., Berman, S.S., Klagsbrun, M., and Zon, L.I. (2007). Duplicate VegfA genes and orthologues of the KDR receptor tyrosine kinase family mediate vascular development in the zebrafish. *Blood* 110, 3627–3637.

Bansode, R.R., Leung, T., Randolph, P., Williams, L.L., and Ahmedna, M. (2013). Cinnamon extract inhibits angiogenesis in zebrafish and human endothelial cells by suppressing VEGFR1, VEGFR2, and PKC-mediated MAP kinase. *Food Sci. Nutr.* 1, 74–82.

Bates, D.O., and Curry, F.E. (1997). Vascular endothelial growth factor increases microvascular permeability via a Ca(2+)-dependent pathway. *Am. J. Physiol.* 273, H687–H694.

Bayless, K.J., and Johnson, G.A. (2011). Role of the cytoskeleton in formation

and maintenance of angiogenic sprouts. *J. Vasc. Res.* **48**, 369–385.

Bedell, V.M., Person, A.D., Larson, J.D., McLoon, A., Balciunas, D., Clark, K.J., Neff, K.I., Nelson, K.E., Bill, B.R., Schimmenti, L.A., et al. (2012a). The lineage-specific gene *ponzr1* is essential for zebrafish pronephric and pharyngeal arch development. *Development* **139**, 793–804.

Bedell, V.M., Wang, Y., Campbell, J.M., Poshusta, T.L., Starker, C.G., Krug, R.G., Tan, W., Penheiter, S.G., Ma, A.C., Leung, A.Y.H., et al. (2012b). In vivo genome editing using a high-efficiency TALEN system. *Nature* **491**, 114–118.

Benedito, R., Rocha, S.F., Woeste, M., Zamykal, M., Radtke, F., Casanovas, O., Duarte, A., Pytowski, B., and Adams, R.H. (2012). Notch-dependent VEGFR3 upregulation allows angiogenesis without VEGF–VEGFR2 signalling. *Nature* **484**, 110–114.

Bill, B.R., Petzold, A.M., Clark, K.J., Schimmenti, L.A., and Ekker, S.C. (2009). A Primer for Morpholino Use in Zebrafish. *Zebrafish* **6**, 69–77.

Blum, Y., Belting, H.G., Ellertsdottir, E., Herwig, L., Lüders, F., and Affolter, M. (2008). Complex cell rearrangements during intersegmental vessel sprouting and vessel fusion in the zebrafish embryo. *Dev. Biol.* **316**, 312–322.

Bollig, F., Perner, B., Besenbeck, B., Köthe, S., Ebert, C., Taudien, S., and Englert, C. (2009). A highly conserved retinoic acid responsive element controls *wt1a* expression in the zebrafish pronephros. *Development* **136**, 2883–2892.

Bootman, M.D. (2012). Calcium Signaling. *Cold Spring Harb. Lab. Press* **740**, 1039–1071.

Bouché, N., and Bouchez, D. (2001). Arabidopsis gene knockout: Phenotypes wanted. *Curr. Opin. Plant Biol.* **4**, 111–117.

Brenner, S. (1974). The genetics of *Caenorhabditis elegans*. *Genetics* 77, 71–94.

Brock, T.A., Dvorak, H.F., and Senger, D.R. (1991). Tumor-secreted vascular permeability factor increases cytosolic Ca²⁺ and von Willebrand factor release in human endothelial cells. *Am. J. Pathol.* 138, 213–221.

Brown, L.A., Rodaway, A.R.F., Schilling, T.F., Jowett, T., Ingham, P.W., Patient, R.K., and Sharrocks, A.D. (2000). Insights into early vasculogenesis revealed by expression of the ETS-domain transcription factor Fli-1 in wild-type and mutant zebrafish embryos. *Mech. Dev.* 90, 237–252.

Bussmann, J., Bakkers, J., and Schulte-Merker, S. (2007). Early endocardial morphogenesis requires Scf/Tal1. *PLoS Genet.* 3, 1425–1437.

Bussmann, J., Bos, F.L., Urasaki, A., Kawakami, K., Duckers, H.J., and Schulte-Merker, S. (2010). Arteries provide essential guidance cues for lymphatic endothelial cells in the zebrafish trunk. *Development* 137, 2653–2657.

Cao, X., Choi, S., Malhotra, J.J., Park, S., Ahuja, M., and Muallem, S. (2015). The ER/PM microdomain, PI(4,5)P₂ and the regulation of STIM1-Orai1 channel function. *Cell Calcium*.

Cermak, T., Doyle, E.L., Christian, M., Wang, L., Zhang, Y., Schmidt, C., Baller, J.A., Somia, N. V., Bogdanove, A.J., and Voytas, D.F. (2011a). Efficient design and assembly of custom TALEN and other TAL effector-based constructs for DNA targeting (*Nucleic Acids Research* (2011) 39 (e82) DOI: 10.1093/nar/gkr218). *Nucleic Acids Res.* 39, 7879.

Cermak, T., El, D., Wang, C.M., Zhang, L., Schmidt, Y., and Ja, B. (2011b). Efficient design and assembly of custom TALEN and other TAL effector-based constructs for DNA targeting. *Nucleic Acids Res.*

Chakrabarti, S., Streisinger, G., Singer, F., and Walker, C. (1983). Frequency of gamma-ray induced specific locus and recessive lethal mutations in mature germ cells of the zebrafish, *brachydanio rerio*. *Genetics* *103*, 109–123.

Chapman, D.C., Stocki, P., and Williams, D.B. (2015). Cyclophilin C Participates in the US2-Mediated Degradation of Major Histocompatibility Complex Class I Molecules. *PLoS One* *10*, 1–28.

Chavez, A., Scheiman, J., Vora, S., Pruitt, B.W., Tuttle, M., P R Iyer, E., Lin, S., Kiani, S., Guzman, C.D., Wiegand, D.J., et al. (2015). Highly efficient Cas9-mediated transcriptional programming. *Nat. Methods* *12*, 326–328.

Cheng, K.T., Liu, X., Ong, H.L., Swaim, W., and Ambudkar, I.S. (2011). Local Ca^{2+} entry via Orai1 regulates plasma membrane recruitment of TRPC1 and controls cytosolic Ca^{2+} signals required for specific cell functions. *PLoS Biol.* *9*, e1001025.

Cheng, W., Sun, C., and Zheng, J. (2010). Heteromerization of TRP channel subunits: Extending functional diversity. *Protein Cell* *1*, 802–810.

Chhabra, E.S., and Higgs, H.N. (2007). The many faces of actin: Matching assembly factors with cellular structures. *Nat. Cell Biol.* *9*, 1110–1121.

Chi, N.C., Shaw, R.M., Val, S. De, Kang, G., Jan, L.Y., Black, B.L., and Stainier, D.Y.R. (2008). Foxn4 directly regulates *tbx2b* expression and atrioventricular canal formation. *Genes Dev.* 734–739.

Chillakuri, C.R., Sheppard, D., Ilagan, M.X.G., Holt, L.R., Abbott, F., Liang, S., Kopan, R., Handford, P.A., and Lea, S.M. (2013). Structural Analysis Uncovers Lipid-Binding Properties of Notch Ligands. *Cell Rep.* *5*, 861–867.

Chira, S., Gulei, D., Hajitou, A., Zimta, A.A., Cordelier, P., and Berindan-Neagoe,

- I. (2017). CRISPR/Cas9: Transcending the Reality of Genome Editing. *Mol. Ther. - Nucleic Acids* 7, 211–222.
- Choi, K., Kennedy, M., Kazarov, A., Papadimitriou, J.C., and Keller, G. (1998). A common precursor for hematopoietic and endothelial cells. *Development* 125, 725–732.
- Choudhury, S.R., Cui, Y., Lubecka, K., Stefanska, B., and Irudayaraj, J. (2016). CRISPR-dCas9 mediated TET1 targeting for selective DNA demethylation at BRCA1 promoter. *Oncotarget* 7, 46545–46556.
- Ciau-Uitz, A., Pinheiro, P., Gupta, R., Enver, T., and Patient, R. (2010). Tel1/ETV6 Specifies Blood Stem Cells through the Agency of VEGF Signaling. *Dev. Cell* 18, 569–578.
- Ciau-Uitz, A., Pinheiro, P., Kirmizitas, A., Zuo, J., and Patient, R. (2013). VEGFA-dependent and -independent pathways synergise to drive Scl expression and initiate programming of the blood stem cell lineage in *Xenopus*. *Development* 140, 2632–2642.
- Cleaver, O., and Krieg, P.A. (1998). VEGF mediates angioblast migration during development of the dorsal aorta in *Xenopus*. *Development* 125, 3905–3914.
- Clontech (2016). In Vitro Transcription and Screening Kits for sgRNA.
- Cordle, J., Redfield, C., Stacey, M., Van Der Merwe, P.A., Willis, A.C., Champion, B.R., Hambleton, S., and Handford, P.A. (2008). Localization of the delta-like-1-binding site in human Notch-1 and its modulation by calcium affinity. *J. Biol. Chem.* 283, 11785–11793.
- Cosens, D.J., and Manning, A. (1969). Abnormal Electroretinogram from a *Drosophila* Mutant. *Nature* 224, 285–287.

Costa, G., Harrington, K.I., Lovegrove, H.E., Page, D.J., Chakravartula, S., Bentley, K., and Herbert, S.P. (2016). Asymmetric division coordinates collective cell migration in angiogenesis. *Nat. Cell Biol.* 18, 1292–1301.

Coultas, L., Nieuwenhuis, E., Anderson, G.A., Cabezas, J., Nagy, A., Henkelman, R.M., Hui, C.C., and Rossant, J. (2010). Hedgehog regulates distinct vascular patterning events through VEGF-dependent and -independent mechanisms. *Blood* 116, 653–660.

Covassin, L.D., Villefranc, J.A., Kacergis, M.C., Weinstein, B.M., and Lawson, N.D. (2006). Distinct genetic interactions between multiple Vegf receptors are required for development of different blood vessel types in zebrafish. *Proc. Natl. Acad. Sci. U. S. A.* 103.

Covassin, L.D., Siekmann, A.F., Kacergis, M.C., Laver, E., Moore, J.C., Villefranc, J.A., Weinstein, B.M., and Lawson, N.D. (2009). A genetic screen for vascular mutants in zebrafish reveals dynamic roles for Vegf/Plcg1 signaling during artery development. *Dev. Biol.* 329, 212–226.

Coxam, B., Sabine, A., Bower, N.I., Smith, K.A., Pichol-Thievend, C., Skoczylas, R., Astin, J.W., Frampton, E., Jaquet, M., Crosier, P.S., et al. (2014). Pkd1 Regulates Lymphatic Vascular Morphogenesis during Development. *Cell Rep.* 7, 623–633.

Criscuolo, G.R., Lelkes, P.I., Rotrosen, D., and Oldfield, E.H. (1989). Cytosolic calcium changes in endothelial cells induced by a protein product of human gliomas containing vascular permeability factor activity. *J. Neurosurg.* 71, 884–891.

DelNero, P., Lane, M., Verbridge, S.S., Kwee, B., Kermani, P., Hempstead, B., Stroock, A., and Fischbach, C. (2016). 3D culture broadly regulates tumor cell

hypoxia response and angiogenesis via pro-inflammatory pathways. *Pediatr Neurol* 52, 566–584.

Deng, Y., Zhuang, Z.W., Atri, D., Moraes, F., Prahst, C., and Simons, M. (2013a). Endothelial RAF1 / ERK activation regulates arterial morphogenesis. *Blood* 121, 3988–3997.

Deng, Y., Atri, D., Eichmann, A., and Simons, M. (2013b). Endothelial ERK signaling controls lymphatic fate specification. *J. Clin. Invest.* 123, 1202–1215.

Dmitriev, O.Y., Lutsenko, S., and Muyldermans, S. (2016). Nanobodies as Probes for Protein Dynamics in Vitro and in Cells. *J. Biol. Chem.* 291, 3767–3775.

Doyon, Y., McCammon, J.M., Miller, J.C., Faraji, F., Ngo, C., Katibah, G.E., Amora, R., Hocking, T.D., Zhang, L., Rebar, E.J., et al. (2008). Heritable targeted gene disruption in zebrafish using designed zinc-finger nucleases. *Nat. Biotechnol.* 26, 702–708.

Driever, W., Schier, A.F., Neuhauss, S.C.F., Malicki, J., Stemple, D.L., and Stainier, D.Y.R. (1996a). A genetic screen for mutations affecting embryogenesis in zebrafish. *Development* 37–46.

Driever, W., Solnica-Krezel, L., Schier, A.F., Neuhauss, S.C., Malicki, J., Stemple, D.L., Stainier, D.Y., Zwartkuis, F., Abdelilah, S., Rangini, Z., et al. (1996b). A genetic screen for mutations affecting embryogenesis in zebrafish. *Development* 123, 37–46.

Drummond, I.A., and Davidson, A.J. (2016). *Zebrafish kidney development* (Elsevier Ltd).

Du, J., Ma, X., Shen, B., Huang, Y., Birnbaumer, L., and Yao, X. (2014). TRPV4, TRPC1, and TRPP2 assemble to form a flow-sensitive heteromeric channel.

FASEB J.

Duarte, A., Hirashima, M., Benedito, R., Trindade, A., Diniz, P., Bekman, E., Costa, L., Henrique, D., and Rossant, J. (2004). Dosage-sensitive requirement for mouse Dll4 in artery development. *Genes Dev.* *18*, 2474–2478.

Dunworth, W.P., Cardona-Costa, J., Bozkulak, E.C., Kim, J.D., Meadows, S., Fischer, J.C., Wang, Y., Cleaver, O., Qyang, Y., Ober, E.A., et al. (2014). Bone morphogenetic protein 2 signaling negatively modulates lymphatic development in vertebrate embryos. *Circ. Res.* *114*, 56–66.

Durdu, S., Iskar, M., Revenu, C., Schieber, N., Kunze, A., Bork, P., Schwab, Y., and Gilmour, D. (2014). Luminal signalling links cell communication to tissue architecture during organogenesis. *Nature* *515*, 120–124.

Eelen, G., de Zeeuw, P., Treppe, L., Harjes, U., Wong, B.W., and Carmeliet, P. (2018). Endothelial Cell Metabolism. *Physiol. Rev.* *98*, 3–58.

El-Brolosy, M.A., and Stainier, D.Y.R. (2017). Genetic compensation: A phenomenon in search of mechanisms. *PLOS Genet.* *13*, e1006780.

Ema, M., Hirota, K., Mimura, J., Abe, H., Yodoi, J., Sogawa, K., Poellinger, L., and Fujii-Kuriyama, Y. (1999). Molecular mechanisms of transcription activation by HLF and HIF1 α in response to hypoxia: their stabilization and redox signal-induced interaction with CBP/p300. *EMBO J.* *18*, 1905–1914.

Eremina, V., Sood, M., Haigh, J., Nagy, A., Lajoie, G., Ferrara, N., Gerber, H.P., Kikkawa, Y., Miner, J.H., and Quaggin, S.E. (2003). Glomerular-specific alterations of VEGF-A expression lead to distinct congenital and acquired renal diseases. *J. Clin. Invest.* *111*, 707–716.

Fearnley, G.W., Bruns, A.F., Wheatcroft, S.B., and Ponnambalam, S. (2015).

VEGF-A isoform-specific regulation of calcium ion flux, transcriptional activation and endothelial cell migration. *Biol. Open* 4, 731–742.

Feske, S., Gwack, Y., Prakriya, M., Srikanth, S., Puppel, S.-H., Tanasa, B., Hogan, P.G., Lewis, R.S., Daly, M., and Rao, A. (2006). A mutation in Orai1 causes immune deficiency by abrogating CRAC channel function. *Nature* 441, 179–185.

Floch, A.G., Taresté, D., Fuchs, P.F.J., Chadrin, A., Naciri, I., Léger, T., Schlenstedt, G., Palancade, B., and Doye, V. (2015). Nuclear pore targeting of the yeast Pom33 nucleoporin depends on karyopherin and lipid binding. *J. Cell Sci.* 128, 305–316.

Foggensteiner, L., Bevan, A.P., Thomas, R., Coleman, N., Boulter, C., Bradley, J., Ibraghimov-Beskrovnyaya, O., Klinger, K., and Sandford, R. (2000). Cellular and subcellular distribution of polycystin-2, the protein product of the PKD2 gene. *J. Am. Soc. Nephrol.* 11, 814–827.

Fong, T.A.T., Shawver, L.K., Sun, L., Tang, C., App, H., Powell, T.J., Kim, Y.H., Schreck, R., Wang, X., Risau, W., et al. (1999). SU5416 Is a Potent and Selective Inhibitor of the Vascular Endothelial Growth Factor Receptor (Flk-1 / KDR) That Inhibits Tyrosine Kinase Catalysis , Tumor Vascularization , and Growth of Multiple Tumor Types SU5416 Is a Potent and Selective Inhibitor o. *Cancer Res.* 59, 99–106.

Fraccaroli, A., Franco, C.A., Rognoni, E., Neto, F., Rehberg, M., Aszodi, A., Wedlich-Söldner, R., Pohl, U., Gerhardt, H., and Montanez, E. (2012). Visualization of Endothelial Actin Cytoskeleton in the Mouse Retina. *PLoS One* 7, 1–9.

Freedman, S.J., Sun, Z.-Y.J., Poy, F., Kung, A.L., Livingston, D.M., Wagner, G.,

and Eck, M.J. (2002). Structural basis for recruitment of CBP/p300 by hypoxia-inducible factor-1 . *Proc. Natl. Acad. Sci.* 99, 5367–5372.

Gau, P., Poon, J., Ufret-Vincenty, C., Snelson, C.D., Gordon, S.E., Raible, D.W., and Dhaka, A. (2013). The zebrafish ortholog of TRPV1 is required for heat-induced locomotion. *J. Neurosci.* 33, 5249–5260.

Gaudelli, N.M., Komor, A.C., Rees, H.A., Packer, M.S., Badran, A.H., Bryson, D.I., and Liu, D.R. (2017). Programmable base editing of A•T to G•C in genomic DNA without DNA cleavage. *Nature* 551, 464–471.

Ge, R., Tai, Y., Sun, Y., Zhou, K., Yang, S., Cheng, T., Zou, Q., Shen, F., and Wang, Y. (2009). Critical role of TRPC6 channels in VEGF-mediated angiogenesis. *Cancer Lett.* 283, 43–51.

Geisler, R., Rauch, G.J., Baier, H., Van Bebber, F., Broß, L., Dekens, M.P.S., Finger, K., Fricke, C., Gates, M.A., Geiger, H., et al. (1999). A radiation hybrid map of the zebrafish genome. *Nat. Genet.* 23, 86–89.

Gerber, H., McMurtrey, A., Kowalski, J., Yan, M., Keyt, B. a, Dixit, V., and Ferrara, N. (1998). Vascular Endothelial Growth Factor Regulates Endothelial Cell Survival through the Phosphatidylinositol 3⁻Kinase / Akt Signal. *J. Biol. Chem.* 273, 30336–30343.

Gerhardt, H., Golding, M., Fruttiger, M., Ruhrberg, C., Lundkvist, A., Abramsson, A., Jeltsch, M., Mitchell, C., Alitalo, K., Shima, D., et al. (2003). VEGF guides angiogenic sprouting utilizing endothelial tip cell filopodia. *J. Cell Biol.* 161, 1163–1177.

Gering, M., Rodaway, a R., Göttgens, B., Patient, R.K., and Green, a R. (1998). The SCL gene specifies haemangioblast development from early mesoderm. *EMBO J.* 17, 4029–4045.

Gering, M., Yamada, Y., Rabbitts, T.H., and Patient, R.K. (2003). Lmo2 and Scf/Tal1 convert non-axial mesoderm into haemangioblasts which differentiate into endothelial cells in the absence of Gata1. *Development* 130, 6187–6199.

Giacomello, M., Drago, I., Bortolozzi, M., Scorzeto, M., Gianelle, A., Pizzo, P., and Pozzan, T. (2010). Ca²⁺ Hot Spots on the Mitochondrial Surface Are Generated by Ca²⁺ Mobilization from Stores, but Not by Activation of Store-Operated Ca²⁺ Channels. *Mol. Cell* 38, 280–290.

Gilbert, L.A., Larson, M.H., Morsut, L., Liu, Z., Brar, G.A., Torres, S.E., Stern-Ginossar, N., Brandman, O., Whitehead, E.H., Doudna, J.A., et al. (2013). CRISPR-mediated modular RNA-guided regulation of transcription in eukaryotes. *Cell* 154, 442–451.

Gilbert, L.A., Horlbeck, M.A., Adamson, B., Villalta, J.E., Chen, Y., Whitehead, E.H., Guimaraes, C., Panning, B., Ploegh, H.L., Bassik, M.C., et al. (2014). Genome-Scale CRISPR-Mediated Control of Gene Repression and Activation. *Cell* 159, 647–661.

Giroux, S., Tremblay, M., Bernard, D., Cadrin-Girard, J.F., Aubry, S., Larouche, L., Rousseau, S., Huot, J., Landry, J., Jeannotte, L., et al. (1999). Embryonic death of Mek1-deficient mice reveals a role for this kinase in angiogenesis in the labyrinthine region of the placenta. *Curr. Biol.* 9, 369–372.

Glitsch, M.D., Bakowski, D., and Parekh, A.B. (2002). Store-operated Ca²⁺ entry depends on mitochondrial Ca²⁺ uptake. *EMBO J.* 21, 6744–6754.

Goetz, J.G., Steed, E., Ferreira, R.R., Roth, S., Ramspacher, C., Boselli, F., Charvin, G., Liebling, M., Wyart, C., Schwab, Y., et al. (2014). Endothelial cilia mediate low flow sensing during zebrafish vascular development. *Cell Rep.* 6, 799–808.

Graham, D.M., Huang, L., Robinson, K.R., and Messerli, M. a (2013). Epidermal keratinocyte polarity and motility require Ca²⁺ influx through TRPV1. *J. Cell Sci.* 126, 4602–4613.

Graupera, M., Guillermet-Guibert, J., Foukas, L.C., Phng, L.K., Cain, R.J., Salpekar, A., Pearce, W., Meek, S., Millan, J., Cutillas, P.R., et al. (2008). Angiogenesis selectively requires the p110 α isoform of PI3K to control endothelial cell migration. *Nature* 453, 662–666.

Gray, C., Bratt, D., Lees, J., DaCosta, M., Plant, K., Watson, O.J., Solaymani-Kohal, S., Tazzyman, S., Serbanovic-Canic, J., Crossman, D.C., et al. (2013). Loss of function of parathyroid hormone receptor 1 induces notch-dependent aortic defects during zebrafish vascular development. *Arterioscler. Thromb. Vasc. Biol.* 33, 1257–1263.

Grunwald, D.J., Kimmel, C.B., Westerfield, M., Walker, C., and Streisinger, G. (1988). A neural degeneration mutation that spares primary neurons in the zebrafish. *Dev. Biol.* 126, 115–128.

Le Guen, L., Karpanen, T., Schulte, D., Harris, N.C., Koltowska, K., Roukens, G., Bower, N.I., van Impel, A., Stacker, S. a, Achen, M.G., et al. (2014). Ccbe1 regulates Vegfc-mediated induction of Vegfr3 signaling during embryonic lymphangiogenesis. *Development* 141, 1239–1249.

Haffter, P., Granato, M., Brand, M., Mullins, M.C., Hammerschmidt, M., Kane, D. a, Odenthal, J., van Eeden, F.J., Jiang, Y.J., Heisenberg, C.P., et al. (1996). The identification of genes with unique and essential functions in the development of the zebrafish, *Danio rerio*. *Development* 123, 1–36.

Hamdollah Zadeh, J.M. (2008). VEGF-Mediated Elevated Intracellular Calcium and Angiogenesis in Human Microvascular Endothelial Cells In Vitro are Inhibited

by Dominant Negative TRPC6. *Microcirculation*.

Hartzell, C.A., Jankowska, K.I., Burkhardt, J.K., and Lewis, R.S. (2016). Calcium influx through CRAC channels controls actin organization and dynamics at the immune synapse. *Elife* 5, 1–28.

Hasan, S.S., Tsaryk, R., Lange, M., Wisniewski, L., Moore, J.C., Lawson, N.D., Wojciechowska, K., Schnittler, H., and Siekmann, A.F. (2017). Endothelial Notch signalling limits angiogenesis via control of artery formation. *Nat. Cell Biol.* 19.

Heasman, J., Kofron, M., and Wylie, C. (2000). β Catenin Signaling Activity Dissected in the Early *Xenopus* Embryo: A Novel Antisense Approach. *Dev. Biol.* 222, 124–134.

Heckel, E., Boselli, F., Roth, S., Krudewig, A., Belting, H.G., Charvin, G., and Vermot, J. (2015). Oscillatory flow modulates mechanosensitive *klf2a* expression through *trpv4* and *trpp2* during heart valve development. *Curr. Biol.* 25, 1354–1361.

Hellesoy, M., and Lorens, J.B. (2015). Cellular context-mediated Akt dynamics regulates MAP kinase signaling thresholds during angiogenesis. *Mol. Biol. Cell* 26, 2698–2711.

Hellström, M., Phng, L.-K., Hofmann, J.J., Wallgard, E., Coultas, L., Lindblom, P., Alva, J., Nilsson, A.-K., Karlsson, L., Gaiano, N., et al. (2007). Dll4 signalling through Notch1 regulates formation of tip cells during angiogenesis. *Nature* 445, 776–780.

Herbert, S.P., and Stainier, D.Y.R. (2011). Molecular control of endothelial cell behaviour during blood vessel morphogenesis. *Nat. Rev. Mol. Cell Biol.* 12, 551–564.

Herbert, S.P., Cheung, J.Y.M., and Stainier, D.Y.R. (2012). Determination of endothelial stalk versus tip cell potential during angiogenesis by H2.0-like homeobox-1. *Curr. Biol.* 22, 1789–1794.

Hewitson, K.S., McNeill, L.A., Riordan, M. V., Tian, Y.M., Bullock, A.N., Welford, R.W., Elkins, J.M., Oldham, N.J., Bhattacharya, S., Gleadle, J.M., et al. (2002). Hypoxia-inducible factor (HIF) asparagine hydroxylase is identical to factor inhibiting HIF (FIH) and is related to the cupin structural family. *J. Biol. Chem.* 277, 26351–26355.

Hider, J.L., Gittelman, R.M., Shah, T., Edwards, M., Rosenbloom, A., Akey, J.M., and Parra, E.J. (2013). Exploring signatures of positive selection in pigmentation candidate genes in populations of East Asian ancestry. *BMC Evol. Biol.*

Hoenderop, J.G.J., Voets, T., Hoefs, S., Weidema, F., Prenen, J., Nilius, B., and Bindels, R.J.M. (2003). Homo- and heterotetrameric architecture of the epithelial Ca²⁺ channels TRPV5 and TRPV6. *EMBO J.* 22, 776–785.

Hofmann, T., Schaefer, M., Schultz, G., and Gudermann, T. (2002). Subunit composition of mammalian transient receptor potential channels in living cells. *Proc. Natl. Acad. Sci. U. S. A.* 99, 7461–7466.

Hogan, B.M., Herpers, R., Witte, M., Heloterä, H., Alitalo, K., Duckers, H.J., Schulte-Merker, S., Helotera, H., Alitalo, K., Duckers, H.J., et al. (2009a). Vegfc/Flt4 signalling is suppressed by Dll4 in developing zebrafish intersegmental arteries. *Development* 136, 4001–4009.

Hogan, B.M., Bos, F.L., Bussmann, J., Witte, M., Chi, N.C., Duckers, H.J., and Schulte-Merker, S. (2009b). Ccbe1 is required for embryonic lymphangiogenesis and venous sprouting. *Nat. Genet.* 41, 396–398.

Hollenbach, M., Stoll, S.J., Jörgens, K., Seufferlein, T., and Kroll, J. (2013).

Different Regulation of Physiological and Tumor Angiogenesis in Zebrafish by Protein Kinase D1 (PKD1). *PLoS One*.

Hong, C.C., Peterson, Q.P., Hong, J.Y., and Peterson, R.T. (2006). Artery/Vein Specification Is Governed by Opposing Phosphatidylinositol-3 Kinase and MAP Kinase/ERK Signaling. *Curr. Biol.* 16, 1366–1372.

Hong, Y., Qi, J., Gong, D., Han, C., and Deng, H. (2011). Replication and Transcription Activator (RTA) of Murine Gammaherpesvirus 68 Binds to an RTA-Responsive Element and Activates the Expression of ORF18. *J. Virol.* 85, 11338–11350.

Horlbeck, M.A., Gilbert, L.A., Villalta, J.E., Adamson, B., Pak, R.A., Chen, Y., Fields, A.P., Park, C.Y., Corn, J.E., Kampmann, M., et al. (2016). Compact and highly active next-generation libraries for CRISPR-mediated gene repression and activation. *Elife*.

Horner, V.L., and Caspary, T. (2011). Creating a “hopeful monster”: Mouse forward genetic screens. *Methods Mol Biol.* 770, 1–27.

Huang, Z., Li, J., Du, S., Tang, Y., Huang, L., Xiao, L., and Tong, P. (2016). FKBP14 overexpression contributes to osteosarcoma carcinogenesis and indicates poor survival outcome. *Oncotarget* 7.

Hughes, J., Ward, C., Peral, B., Aspinwall, R., Clark, K., San Millán, J., Gamble, V., and Harris, P. (1995). The polycystic kidney disease 1 (PKD1) gene encodes a novel protein with multiple cell recognition domains. *Nat. Genet.* 10, 151–160.

Hwang, W.Y., Fu, Y., Reyon, D., Maeder, M.L., Tsai, S.Q., Sander, J.D., Peterson, R.T., Yeh, J.-R.J., and Joung, J.K. (2013). Efficient genome editing in zebrafish using a CRISPR-Cas system. *Nat. Biotechnol.* 31, 227–229.

Ikebuchi, N.W., and Waismanj, D.M. (1990). Calcium-dependent Regulation of Actin Filament Bundling by Lipocortin-85. *J. Biol. Chem.* 265, 3392–3401.

van Impel, A., Zhao, Z., Hermkens, D.M.A., Roukens, M.G., Fischer, J.C., Peterson-Maduro, J., Duckers, H., Ober, E.A., Ingham, P.W., and Schulte-Merker, S. (2014). Divergence of zebrafish and mouse lymphatic cell fate specification pathways. *Development* 141, 1228–1238.

Isogai, S., Horiguchi, M., and Weinstein, B.M. (2001). The vascular anatomy of the developing zebrafish: an atlas of embryonic and early larval development. *Dev. Biol.* 230, 278–301.

Ivan, M., Kondo, K., Yang, H., Kim, W., Valiando, J., Ohh, M., Salic, A., Asara, J.M., Lane, W.S., and Kaelin, W.G. (2001). HIF α Targeted for VHL-Mediated Destruction by Proline Hydroxylation: Implications for O₂ Sensing. *Science* (80-). 292, 464–468.

J.Kallio, P., Okamoto, K., O'Brien, S., Carrero, P., Makino, Y., Tanaka, H., and Poellinger, L. (1998). Signal transduction in hypoxic cells: inducible nuclear translocation and recruitment of the CBP/p300 coactivator by the hypoxia-inducible factor-1 α . *EMBO J.* 17, 6573–6586.

Jaakkola, P., Mole, D.R., Tian, Y.-M., Wilson, M.I., Gielbert, J., Gaskell, S.J., Kriegsheim, A. v., Hebestreit, H.F., Mukherji, M., Schofield, C.J., et al. (2001). Targeting of HIF- α to the von Hippel-Lindau Ubiquitylation Complex by O₂-Regulated Prolyl Hydroxylation. *Science* (80-). 292, 468–472.

Jayaraman, T., Ondriaì, K., Ondriaìov, E., and Marks, A.R. (1996). Regulation of the inositol 1,4,5-trisphosphate receptor by tyrosine phosphorylation. *Science* (80-). 272, 1492–1494.

Jho, D., Mehta, D., Ahmmed, G., Gao, X.-P., Tiruppathi, C., Broman, M., and

Malik, A.B. (2005). Angiopoietin-1 opposes VEGF-induced increase in endothelial permeability by inhibiting TRPC1-dependent Ca²⁺ influx. *Circ. Res.* *96*, 1282–1290.

Ji, Q.-S., Winnier, G.E., Niswender, K.D., Horstman, D., Wisdom, R., Magnuson, M.A., and Carpenter, G. (1997). Essential role of the tyrosine kinase substrate phospholipase C-g1 in mammalian growth and development. *Cell Biol.* *94*, 2999–3003.

Jiang, B.H., Rue, E., Wang, G.L., Roe, R., and Semenza, G.L. (1996). Dimerization, DNA binding, and transactivation properties of hypoxia-inducible factor 1. *J. Biol. Chem.* *271*, 17771–17778.

Jin, S.-W., Beis, D., Mitchell, T., Chen, J.-N., and Stainier, D.Y.R. (2005a). Cellular and molecular analyses of vascular tube and lumen formation in zebrafish. *Development* *132*, 5199–5209.

Jin, S.-W., Beis, D., Mitchell, T., Chen, J.-N., and Stainier, D.Y.R. (2005b). Cellular and molecular analyses of vascular tube and lumen formation in zebrafish. *Development* *132*, 5199–5209.

Jones, J.T., Myers, J.W., Ferrell, J.E., and Meyer, T. (2005). STIM Is a Ca²⁺ Sensor Essential for Ca²⁺-Store-Depletion-Triggered Ca²⁺ Influx Jen Liou, Man Lyang Kim, Won Do Heo, leads to an initial peak in cytosolic Ca²⁺ levels and then a plateau. The sustained plateau level is indicative of. *Curr. Biol.* *15*, 1235–1241.

Josephs, E.A., Kocak, D.D., Fitzgibbon, C.J., McMenemy, J., Gersbach, C.A., and Marszalek, P.E. (2015). Structure and specificity of the RNA-guided endonuclease Cas9 during DNA interrogation, target binding and cleavage. *Nucleic Acids Res.* *43*, 8924–8941.

Joukov, V., Pajusola, K., Kaipainen, A., Chilov, D., Lahtinen, I., Kukk, E., Saksela, O., Kalkkinen, N., and Alitalo, K. (1996). A novel vascular endothelial growth factor, VEGF-C, is a ligand for the Flt4 (VEGFR-3) and KDR (VEGFR-2) receptor tyrosine kinases. *EMBO J.* 15, 290–298.

Joung, J.K., and Sander, J.D. (2013). TALENs: A widely applicable technology for targeted genome editing. *Nat. Rev. Mol. Cell Biol.* 14, 49–55.

Jozsef, L., Tashiro, K., Kuo, A., Park, E., Skoura, A., Albinsson, S., Rivera-Molina, F., Harrison, K.D., Iwakiri, Y., Toomre, D., et al. (2014). Reticulon 4 is necessary for endoplasmic reticulum tubulation, STIM1-Orai1 coupling, and store-operated calcium entry. *J. Biol. Chem.* 289, 9380–9395.

Kanju, P., Chen, Y., Lee, W., Yeo, M., Lee, S.H., Romac, J., Shahid, R., Fan, P., Gooden, D.M., Simon, S.A., et al. (2016). Small molecule dual-inhibitors of TRPV4 and TRPA1 for attenuation of inflammation and pain. *Sci. Rep.* 6, 1–12.

Kapustina, M., Elston, T.C., and Jacobson, K. (2013). Compression and dilation of the membrane-cortex layer generates rapid changes in cell shape. *J. Cell Biol.* 200, 95–108.

Katz, M., Amit, I., and Yarden, Y. (2012). NIH Public Access Regulation of MAPKs by growth factors and receptor tyrosine kinases. *Biochim Biophys Acta* v, 265–275.

Kearns, N.A., Pham, H., Tabak, B., Genga, R.M., Silverstein, N.J., Garber, M., and Maehr, R. (2015). Functional annotation of native enhancers with a Cas9–histone demethylase fusion. *Nat. Methods* 12, 401–403.

Kim, E.J., Kang, K.H., and Ju, J.H. (2017). CRISPR-Cas9: a promising tool for gene editing on induced pluripotent stem cells. *Korean J. Intern. Med.* 32, 42–61.

Kim, Y.G., Cha, J., and Chandrasegaran, S. (1996). Hybrid restriction enzymes: zinc finger fusions to Fok I cleavage domain. *Proc. Natl. Acad. Sci.* 93, 1156–1160.

Kimmel, C.B., Warga, R.M., and Schilling, T.F. (1990). Origin and organization of the zebrafish fate map. *Development* 108, 581–594.

Kimura, H., Weisz, A., Kurashima, Y., Hashimoto, K., Ogura, T., D'Acquisto, F., Addeo, R., Makuuchi, M., and Esumi, H. (2000). Hypoxia response element of the human vascular endothelial growth factor gene mediates transcriptional regulation by nitric oxide: control of hypoxia-inducible factor-1 activity by nitric oxide. *Blood* 95, 189–197.

Kimura, H., Weisz, A., Ogura, T., Hitomi, Y., Kurashima, Y., Hashimoto, K., D'Acquisto, F., Makuuchi, M., and Esumi, H. (2001). Identification of hypoxia-inducible factor 1 ancillary sequence and its function in vascular endothelial growth factor gene induction by hypoxia and nitric oxide. *J. Biol. Chem.* 276, 2292–2298.

Kishimoto, Y., Lee, K.H., Zon, L., Hammerschmidt, M., and Schulte-Merker, S. (1997). The molecular nature of zebrafish swirl: BMP2 function is essential during early dorsoventral patterning. *Development* 124, 4457–4466.

Knapik, E.W., Goodman, A., Atkinson, O.S., Roberts, C.T., Shiozawa, M., Sim, C.U., Weksler-Zangen, S., Trolliet, M.R., Futrell, C., Innes, B.A., et al. (1996). A reference cross DNA panel for zebrafish (*Danio rerio*) anchored with simple sequence length polymorphisms. *Development* 123, 451–460.

Knapik, E.W., Goodman, A., Ekker, M., Chevrette, M., Delgado, J., Neuhauss, S., Shimoda, N., Driever, W., Fishman, M.C., and Jacob, H.J. (1998). A microsatellite genetic linkage map for zebrafish (*Danio rerio*). *Nat. Genet.* 18, 231–

Kobori, T., Smith, G.D., Sandford, R., and Edwardson, J.M. (2009). The transient receptor potential channels TRPP2 and TRPC1 form a heterotetramer with a 2:2 stoichiometry and an alternating subunit arrangement. *J. Biol. Chem.* *284*, 35507–35513.

Koch, S., and Claesson-Welsh, L. (2011). Signal transduction by vascular endothelial growth factor receptors. *Biochem J* *437*, 169–183.

Kok, F.O., Shin, M., Ni, C.-W., Gupta, A., Grosse, A.S., van Impel, A., Kirchmaier, B.C., Peterson-Maduro, J., Kourkoulis, G., Male, I., et al. (2014). Reverse Genetic Screening Reveals Poor Correlation between Morpholino-Induced and Mutant Phenotypes in Zebrafish. *Dev. Cell* 1–12.

Kok, F.O., Shin, M., Ni, C.W., Gupta, A., Grosse, A.S., vanImpel, A., Kirchmaier, B.C., Peterson-Maduro, J., Kourkoulis, G., Male, I., et al. (2015). Reverse genetic screening reveals poor correlation between morpholino-induced and mutant phenotypes in zebrafish. *Dev. Cell*.

Koltowska, K., Lagendijk, A.K., Pichol-Thievend, C., Fischer, J.C., Francois, M., Ober, E.A., Yap, A.S., and Hogan, B.M. (2015). Vegfc Regulates Bipotential Precursor Division and Prox1 Expression to Promote Lymphatic Identity in Zebrafish. *Cell Rep.* *13*, 1828–1841.

Konermann, S., Brigham, M.D., Trevino, A.E., Joung, J., Abudayyeh, O.O., Barcena, C., Hsu, P.D., Habib, N., Gootenberg, J.S., Nishimasu, H., et al. (2014). Genome-scale transcriptional activation by an engineered CRISPR-Cas9 complex. *Nature* *517*, 583–588.

Köttgen, M., Buchholz, B., Garcia-Gonzalez, M.A., Kotsis, F., Fu, X., Doerken, M., Boehlke, C., Steffl, D., Tauber, R., Wegierski, T., et al. (2008). TRPP2 and

TRPV4 form a polymodal sensory channel complex. *J. Cell Biol.* 182, 437–447.

Krueger, J., Liu, D., Scholz, K., Zimmer, A., Shi, Y., Klein, C., Siekmann, A., Schulte-Merker, S., Cudmore, M., Ahmed, A., et al. (2011). Flt1 acts as a negative regulator of tip cell formation and branching morphogenesis in the zebrafish embryo. *Development*.

Kwan, K.M., Fujimoto, E., Grabher, C., Mangum, B.D., Hardy, M.E., Campbell, D.S., Parant, J.M., Yost, H.J., Kanki, J.P., and Chien, C.-B. (2007). The Tol2kit: a multisite gateway-based construction kit for Tol2 transposon transgenesis constructs. *Dev. Dyn.* 236, 3088–3099.

Lando, D., Peet, D.J., Gorman, J.J., Whelan, D.A., Whitelaw, M.L., and Bruick, R.K. (2002). FIH-1 is an asparaginyl hydroxylase enzyme that regulates the transcriptional activity of hypoxia-inducible factor. *Genes Dev.* 1466–1471.

Larson, M.H., Gilbert, L.A., Wang, X., Lim, W.A., Jonathan, S., Weissman, and S, L.Q. (2014). CRISPR interference (CRISPRi) for sequence-specific control of gene expression. *Nat. Protoc.* 8, 2180–2196.

Lawson, N.D., and Weinstein, B.M. (2002). In Vivo Imaging of Embryonic Vascular Development Using Transgenic Zebrafish. *Dev. Biol.* 248, 307–318.

Lawson, N.D., Scheer, N., Pham, V.N., Kim, C., Chitnis, A.B., Campos-ortega, J.A., and Weinstein, B.M. (2001). Notch signaling is required for arterial-venous differentiation during embryonic vascular development. *Development* 3683, 3675–3683.

Lawson, N.D., Vogel, A.M., and Weinstein, B.M. (2002). Sonic hedgehog and vascular endothelial growth factor act upstream of the Notch pathway during

arterial endothelial differentiation. *Dev. Cell.*

Lawson, N.D., Mugford, J.W., Diamond, B.A., and Weinstein, B.M. (2003). phospholipase C gamma-1 is required downstream of vascular endothelial growth factor during arterial development. *Genes Dev.*

Leslie, J.D., Ariza-McNaughton, L., Bermange, A.L., McAdow, R., Johnson, S.L., and Lewis, J. (2007). Endothelial signalling by the Notch ligand Delta-like 4 restricts angiogenesis. *Development* 134, 839–844.

Li, F., Abuarab, N., and Sivaprasadarao, A. (2016). Reciprocal regulation of actin cytoskeleton remodelling and cell migration by Ca²⁺ and Zn²⁺: role of TRPM2 channels. *J. Cell Sci.* 129, 2016–2029.

Li, J., Cubbon, R.M., Wilson, L.A., Amer, M.S., McKeown, L., Hou, B., Majeed, Y., Tumova, S., Seymour, V.A.L., Taylor, H., et al. (2011). Orai1 and CRAC channel dependence of VEGF-activated Ca²⁺ entry and endothelial tube formation. *Circ. Res.* 108, 1190–1198.

Li, X., Wu, G., Yang, Y., Fu, S., Liu, X., Kang, H., Yang, X., Su, X.C., and Shen, Y. (2017). Calmodulin dissociates the STIM1-Orai1 complex and STIM1 oligomers. *Nat. Commun.* 8.

Li, Z., Lu, J., Xu, P., Xie, X., Chen, L., and Xu, T. (2007). Mapping the interacting domains of STIM1 and Orai1 in Ca²⁺ release-activated Ca²⁺ channel activation. *J. Biol. Chem.* 282, 29448–29456.

Liao, Y., Erxleben, C., Abramowitz, J., Flockerzi, V., Zhu, M.X., Armstrong, D.L., and Birnbaumer, L. (2008). Functional interactions among Orai1, TRPCs, and STIM1 suggest a STIM-regulated heteromeric Orai/TRPC model for SOCE/Icrac channels. *Proc. Natl. Acad. Sci. U. S. A.* 105, 2895–2900.

Lin, S., Ewen-Campen, B., Ni, X., Housden, B.E., and Perrimon, N. (2015). In vivo transcriptional activation using CRISPR/Cas9 in *Drosophila*. *Genetics* 201, 433–442.

Liou, J., Fivaz, M., Inoue, T., and Meyer, T. (2007). Live-cell imaging reveals sequential oligomerization and local plasma membrane targeting of stromal interaction molecule 1 after Ca²⁺ store depletion. *Proc. Natl. Acad. Sci. U. S. A.* 104, 9301–9306.

Lopez-illasaca, M. (1998). Signaling from G-Protein-coupled Receptors to Mitogen-activated Protein (MAP) -Kinase Cascades. *Biochem. Pharmacol.* 56, 269–277.

Luca, V.C., Jude, K.M., Pierce, N.W., Nachury, M. V., Fischer, S., and Garcia, K.C. (2015). Structural basis for Notch1 engagement of Delta-like 4. *Science* (80- .). 347, 847–854.

Ma, G., Wei, M., He, L., Liu, C., Wu, B., Zhang, S.L., Jing, J., Liang, X., Senes, A., Tan, P., et al. (2015). Inside-out Ca²⁺ signalling prompted by STIM1 conformational switch. *Nat. Commun.* 6, 7826.

Ma, X., Chengc, K.-T., Wonga, C.-O., O’Neild, R.G., Birnbaumere, L., Ambudkarc, I.S., and Yao, X. (2013). Heteromeric TRPV4-C1 channels contribute to store-operated Ca²⁺ entry in vascular endothelial cells. *50*, 1–16.

MacLennan, D.H., Brandl, C.J., Korczak, B., and Green, N.M. (1985). Amino-acid sequence of a Ca²⁺ + Mg²⁺-dependent ATPase from rabbit muscle sarcoplasmic reticulum, deduced from its complementary DNA sequence. *Nature* 316, 696–700.

Mali, P., Yang, L., Esvelt, K.M., Aach, J., Guell, M., DiCarlo, J.E., Norville, J.E., and Church, G.M. (2013). RNA-Guided Human Genome Engineering via Cas9.

Science (80-). 339, 823–826.

Malicki, J., Neuhauss, S.C.F., Schier, A.F., Solnica-krezel, L., Stemple, D.L., Stainier, D.Y.R., Abdelilah, S., Zwartkuis, F., Rangini, Z., and Driever, W. (1996). Mutations affecting development of the zebrafish retina. *Development* 263–273.

Malicki, J., Schier, A., Solnica-Krezel, L., Stemple, D., Neuhauss, S., Stainier, D., Abdelilah, S., Rangini, Z., Zwartkuis, F., and Driever, W. (1997). Mutations affecting development of the zebrafish ear. *Development* 123, 275–283.

Mangos, S., Liu, Y., and Drummond, I.A. (2007). Dynamic expression of the osmosensory channel *trpv4* in multiple developing organs in zebrafish. *Gene Expr. Patterns* 7, 480–484.

Mangos, S., Lam, P., Zhao, A., Liu, Y., Mudumana, S., Vasilyev, A., Liu, A., and Drummond, I. a (2010). The ADPKD genes *pkd1a/b* and *pkd2* regulate extracellular matrix formation. *Dis Model Mech* 3, 354–365.

De Marothy, M.T., and Elofsson, A. (2015). Marginally hydrophobic transmembrane α -helices shaping membrane protein folding. *Protein Sci.* 24, 1057–1074.

Martini, F.J., and Valdeolmillos, M. (2010). Actomyosin Contraction at the Cell Rear Drives Nuclear Translocation in Migrating Cortical Interneurons. *J. Neurosci.* 30, 8660–8670.

Masson, N., Willam, C., Maxwell, P.H., Pugh, C.W., and Ratcliffe, P.J. (2001). Independent function of two destruction domains in hypoxia-inducible factor-?? chains activated by prolyl hydroxylation. *EMBO J.* 20, 5197–5206.

Mavria, G., Vercoulen, Y., Yeo, M., Paterson, H., Karasarides, M., Marais, R., Bird, D., and Marshall, C.J. (2006). ERK-MAPK signaling opposes Rho-kinase to

promote endothelial cell survival and sprouting during angiogenesis. *Cancer Cell* 9, 33–44.

Maxwell, P.H., Dachs, G.U., Gleadle, J.M., Nicholls, L.G., Harris, A.L., Stratford, I.J., Hankinson, O., Pugh, C.W., and Ratcliffe, P.J. (1997). Hypoxia-inducible factor-1 modulates gene expression in solid tumors and influences both angiogenesis and tumor growth. *Proc. Natl. Acad. Sci. U. S. A.* 94, 8104–8109.

McMullen, M.E., Bryant, P.W., Glembotski, C.C., Vincent, P.A., and Pumiglia, K.M. (2005). Activation of p38 has opposing effects on the proliferation and migration of endothelial cells. *J. Biol. Chem.* 280, 20995–21003.

McNeill, L.A., Hewitson, K.S., Gleadle, J.M., Horsfall, L.E., Oldham, N.J., Maxwell, P.H., Pugh, C.W., Ratcliffe, P.J., and Schofield, C.J. (2002). The use of dioxygen by HIF prolyl hydroxylase (PHD1). *Bioorganic Med. Chem. Lett.* 12, 1547–1550.

Meadows, K.L., and Hurwitz, H.I. (2012). Anti-VEGF therapies in the clinic. *Cold Spring Harb. Perspect. Med.* 2.

Meadows, K.N., Bryant, P., and Pumiglia, K. (2001). Vascular Endothelial Growth Factor Induction of the Angiogenic Phenotype Requires Ras Activation. *J. Biol. Chem.*

Meng, X., Noyes, M.B., Zhu, L.J., Lawson, N.D., and Wolfe, S.A. (2008). Targeted gene inactivation in zebrafish using engineered zinc-finger nucleases. *Nat. Biotechnol.* 26, 695–701.

Mochizuki, T., Wu, G., Hayashi, T., Xenophontos, S.L., Veldhuisen, B., Saris, J.J., Reynolds, D.M., Cai, Y., Gabow, P.A., Pierides, A., et al. (1996). PKD2, a Gene for Polycystic Kidney Disease That Encodes an Integral Membrane Protein. *Science* (80-.). 272, 1339–1342.

Mohr, S.E., Hu, Y., Ewen-Campen, B., Housden, B.E., Viswanatha, R., and Perrimon, N. (2016). CRISPR guide RNA design for research applications. *FEBS J.* 283, 3232–3238.

Moiseenkova-Bell, V., and Wensel, T.G. (2011). Functional and structural studies of TRP channels heterologously expressed in budding yeast. *Adv. Exp. Med. Biol.* 704, 25–40.

Moiseenkova-Bell, V.Y., and Wensel, T.G. (2009). Hot on the Trail of TRP Channel Structure. *J. Gen. Physiol.* 133, 239–244.

Montell, C., and Rubin, G.M. (1989). Molecular characterization of the drosophila *trp* locus: A putative integral membrane protein required for phototransduction. *Neuron* 2, 1313–1323.

Morales-ruiz, M., Fulton, D., Sowa, G., Languino, L.R., Fujio, Y., Walsh, K., and Sessa, W.C. (2014). Vascular Endothelial Growth Factor – Stimulated Actin Reorganization and Migration of Endothelial Cells Is Regulated via the Serine/Threonine Kinase Akt. *Circ. Res.*

Mouillesseaux, K.P., Wiley, D.S., Saunders, L.M., Wylie, L.A., Kushner, E.J., Chong, D.C., Citrin, K.M., Barber, A.T., Park, Y., Kim, J.D., et al. (2016). Notch regulates BMP responsiveness and lateral branching in vessel networks via SMAD6. *Nat. Commun.* 7, 1–12.

Mudumana, S.P., Hentschel, D., Liu, Y., Vasilyev, A., and Drummond, I.A. (2008). Odd Skipped Related1 Reveals a Novel Role for Endoderm in Regulating Kidney Versus Vascular Cell Fate. *Development* 135, 3355–3367.

Mugford, J.W., Sipilä, P., McMahon, J.A., and McMahon, A.P. (2008). *Osr1* expression demarcates a multi-potent population of intermediate mesoderm that undergoes progressive restriction to an *Osr1*-dependent nephron progenitor

compartment within the mammalian kidney. *Dev. Biol.* 324, 88–98.

Mullins, M.C., Hammerschmidt, M., Haffter, P., and Nusslein-Volhard, C. (1994). Large-scale mutagenesis in the zebrafish: In search of genes controlling development in a vertebrate. *Curr. Biol.* 4, 189–202.

Munro, S., and Pelham, H.R.B. (1987). A C-terminal signal prevents secretion of luminal ER proteins. *Cell* 48, 899–907.

Murakami, M., Nguyen, L.T., Hatanaka, K., Schachterle, W., Chen, P.Y., Zhuang, Z.W., Black, B.L., and Simons, M. (2011). FGF-dependent regulation of VEGF receptor 2 expression in mice. *J Clin Invest* 121, 2668–2678.

Murray, P.D.F. (1932). The Development in vitro of the Blood of the Early Chick Embryo. *Proc. R. Soc. B.*

Myat, M.M., Lightfoot, H., Wang, P., and Andrew, D.J. (2005). A molecular link between FGF and Dpp signaling in branch-specific migration of the *Drosophila* trachea. *Dev. Biol.* 281, 38–52.

Naghdi, S., Waldeck-Weiermair, M., Fertschai, I., Poteser, M., Graier, W.F., and Malli, R. (2010). Mitochondrial Ca²⁺ uptake and not mitochondrial motility is required for STIM1-Orai1-dependent store-operated Ca²⁺ entry. *J. Cell Sci.* 123, 2553–2564.

Nakadai, T., Kishimoto, T., Kokura, K., Ohkawa, N., Making, Y., Muramatsu, M., and Tamura, T.A. (1998). Cloning of a novel rat gene, DB83, that encodes a putative membrane protein. *DNA Res.* 5, 315–317.

Nakai, J., Ohkura, M., and Imoto, K. (2001). A high signal-to-noise Ca(2+) probe composed of a single green fluorescent protein. *Nat. Biotechnol.* 19, 137–141.

Nasevicius, a, and Ekker, S.C. (2000). Effective targeted gene “knockdown” in

zebrafish. *Nat. Genet.* 26, 216–220.

Nasevicius, A., Larson, J., and Ekker, S.C. (2000). Distinct requirements for zebrafish angiogenesis revealed by a VEGF-A morphant. *Yeast* 17, 294–301.

Naylor, R.W., Przepiorski, A., Ren, Q., Yu, J., and Davidson, A.J. (2013). HNF1 β is essential for nephron segmentation during nephrogenesis. *J. Am. Soc. Nephrol.* 24, 77–87.

Naylor, R.W., Dodd, R.C., and Davidson, A.J. (2016). Caudal migration and proliferation of renal progenitors regulates early nephron segment size in zebrafish. *Sci. Rep.* 6, 1–14.

Naylor, R.W., Han, H.I., Hukriede, N.A., and Davidson, A.J. (2017). Wnt8a expands the pool of embryonic kidney progenitors in zebrafish. *Dev. Biol.* 425, 130–141.

Neuhauss, S.C., Solnica-Krezel, L., Schier, A.F., Zwartkuis, F., Stemple, D.L., Malicki, J., Abdelilah, S., Stainier, D.Y., and Driever, W. (1996). Mutations affecting craniofacial development in zebrafish. *Development* 123, 357–367.

Von Niederhausern, V., Kasthuber, E., Stauble, A., Gesemann, M., and Neuhauss, S.C.F. (2013). Phylogeny and expression of canonical transient receptor potential (TRPC) genes in developing zebrafish. *Dev. Dyn.* 242, 1427–1441.

Nilsson, I., Bahram, F., Li, X., Gualandi, L., Koch, S., Jarvius, M., Söderberg, O., Anisimov, A., Kholová, I., Pytowski, B., et al. (2010). VEGF receptor 2/3 heterodimers detected in situ by proximity ligation on angiogenic sprouts. *EMBO J.*

Noh, D.Y., Shin, S.H., and Rhee, S.G. (1995). Phosphoinositide-specific

phospholipase C and mitogenic signaling. *BBA - Rev. Cancer* 1242, 99–113.

Noonan, H.R., Metelo, A.M., Kamei, C.N., Peterson, R.T., Drummond, I.A., and Iliopoulos, O. (2016). Loss of *vhl* in the zebrafish pronephros recapitulates early stages of human clear cell renal cell carcinoma. *Dis. Model. Mech.* 9, 873–884.

Nusslein-Volhard, C., and Wieschaus, E. (1980). Mutations affecting segment number and polarity in *Drosophila*. *Nature* 287, 795–801.

O'Connor, C.J., Leddy, H.A., Benefield, H.C., Liedtke, W.B., and Guilak, F. (2014). TRPV4-mediated mechanotransduction regulates the metabolic response of chondrocytes to dynamic loading. *Proc. Natl. Acad. Sci.* 111, 1316–1321.

Obara, T., Mangos, S., Liu, Y., Zhao, J., Wiessner, S., Kramer-Zucker, A.G., Olale, F., Schier, A.F., and Drummond, I.A. (2006). Polycystin-2 Immunolocalization and Function in Zebrafish. *J. Am. Soc. Nephrol.* 17, 2706–2718.

Oggier, D.M., Lenard, A., Küry, M., Hoeger, B., Affolter, M., and Fent, K. (2011). Effects of the protein kinase inhibitor PKC412 on gene expression and link to physiological effects in zebrafish *Danio rerio* eleuthero-embryos. *Toxicol. Sci.* 119, 104–115.

Oike, M., Gericke, M., Droogmans, G., and Nilius, B. (1994). Calcium entry activated by store depletion in human umbilical vein endothelial cells. *Cell Calcium*.

Omori, Y., Zhao, C., Saras, A., Mukhopadhyay, S., Kim, W., Furukawa, T., Sengupta, P., Veraksa, A., and Malicki, J. (2008). *elipsa* is an early determinant of ciliogenesis that links the IFT particle to membrane-associated small GTPase. *Nat. Cell Biol.* 10.

- Oubaha, M., Lin, M.I., Margaron, Y., Fillion, D., Price, E.N., and Zon, L.I. (2012). Formation of a PKC ζ/β -catenin complex in endothelial cells promotes angiopoietin-1 – induced collective directional migration and angiogenic sprouting. *120*, 3371–3381.
- Panza, P., Maier, J., Schmees, C., Rothbauer, U., and Sollner, C. (2015). Live imaging of endogenous protein dynamics in zebrafish using chromobodies. *Development* *142*, 1879–1884.
- Pazour, G.J., San Agustin, J.T., Follit, J.A., Rosenbaum, J.L., and Witman, G.B. (2002). Polycystin-2 localizes to kidney cilia and the ciliary level is elevated in orpk mice with polycystic kidney disease. *Curr. Biol.* *12*, R378–R380.
- Perens, E.A., Garavito-Aguilar, Z. V., Guio-Vega, G.P., Peña, K.T., Schindler, Y.L., and Yelon, D. (2016). Hand2 inhibits kidney specification while promoting vein formation within the posterior mesoderm. *Elife* *5*, 1–21.
- Perner, B., Englert, C., and Bollig, F. (2007). The Wilms tumor genes *wt1a* and *wt1b* control different steps during formation of the zebrafish pronephros. *Dev. Biol.* *309*, 87–96.
- Pescador, N., Cuevas, Y., Naranjo, S., Alcaide, M., Villar, D., Landázuri, M.O., and del Peso, L. (2005). Identification of a functional hypoxia-responsive element that regulates the expression of the *egl nine* homologue 3 (*egl3/phd3*) gene. *Biochem. J.* *390*, 189–197.
- Pfeffer, P.L., Gerster, T., Lun, K., Brand, M., and Busslinger, M. (1998). Characterization of three novel members of the zebrafish Pax2/5/8 family: dependency of Pax5 and Pax8 expression on the Pax2.1 (*noi*) function. *Development* *125*, 3063–3074.
- Phan, M.N., Leddy, H.A., Votta, B.J., Kumar, S., Levy, D.S., Lipshutz, D.B., Suk,

H.L., Liedtke, W., and Guilak, F. (2009). Functional characterization of TRPV4 as an osmotically sensitive ion channel in porcine articular chondrocytes. *Arthritis Rheum.* *60*, 3028–3037.

Phng, L.K., and Gerhardt, H. (2009). Angiogenesis: A Team Effort Coordinated by Notch. *Dev. Cell* *16*, 196–208.

Phng, L.-K.K., Stanchi, F., and Gerhardt, H. (2013). Filopodia are dispensable for endothelial tip cell guidance. *Development* *140*, 4031–4040.

Pocock, T.M., Foster, R.R., and Bates, D.O. (2004). Evidence of a role for TRPC channels in VEGF-mediated increased vascular permeability in vivo. 1015–1026.

Pollard, T.D., and Cooper, J.A. (2009). Actin, a central player in cell shape and movement. *Science* (80-.). *326*, 1208–1212.

Pozzan, T., Magalhães, P., and Rizzuto, R. (2000). The comeback of mitochondria to calcium signalling. *Cell Calcium* *28*, 279–283.

Prudent, J., Popgeorgiev, N., Bonneau, B., Thibaut, J., Gadet, R., Lopez, J., Gonzalo, P., Rimokh, R., Manon, S., Houart, C., et al. (2013). Bcl-wav and the mitochondrial calcium uniporter drive gastrula morphogenesis in zebrafish. *Nat. Commun.* *4*, 1–15.

Prudent, J., Popgeorgiev, N., Gadet, R., Deygas, M., Rimokh, R., and Gillet, G. (2016). Mitochondrial Ca²⁺ uptake controls actin cytoskeleton dynamics during cell migration. *Sci. Rep.* *6*, 1–13.

Putney, J.W. (2010). Store-operated Calcium Channels. *10*, 209–218.

Qi, L.S., Larson, M.H., Gilbert, L.A., Doudna, J.A., Weissman, J.S., Arkin, A.P., and Lim, W.A. (2013). Repurposing CRISPR as an RNA-guided platform for sequence-specific control of gene expression. *Cell* *152*, 1173–1183.

Quillien, A., Moore, J.C., Shin, M., Siekmann, A.F., Smith, T., Pan, L.Y., Moens, C.B., Parsons, M.J., and Lawson, N.D. (2014). Distinct Notch signaling outputs pattern the developing arterial system. *Development* 141, 1544–1552.

Radzsheuskaya, A., Shlyueva, D., Müller, I., and Helin, K. (2016). Optimizing sgRNA position markedly improves the efficiency of CRISPR/dCas9-mediated transcriptional repression. *Nucleic Acids Res.* 44.

Rajendran, P., Rengarajan, T., Thangavel, J., Nishigaki, Y., Sakthisekaran, D., Sethi, G., and Nishigaki, I. (2013). The vascular endothelium and human diseases. *Int. J. Biol. Sci.* 9, 1057–1069.

Ramsey, I.S., Delling, M., and Clapham, D.E. (2006). An introduction to TRP channels. *Annu. Rev. Physiol.* 68, 619–647.

Ran, F.A., Hsu, P.D., Wright, J., Agarwala, V., Scott, D.A., and Zhang, F. (2013). Genome engineering using the CRISPR-Cas9 system. *Nat. Protoc.*

Rand, M.D., Lindblom, A., Carlson, J., Villoutreix, B.O., and Stenflo, J. (1997). Calcium binding to tandem repeats of EGF-like modules. Expression and characterization of the EGF-like modules of human Notch-1 implicated in receptor-ligand interactions. *Protein Sci.* 6, 2059–2071.

Reischauer, S., Stone, O.A., Villasenor, A., Chi, N., Jin, S.-W., Martin, M., Lee, M.T., Fukuda, N., Marass, M., Witty, A., et al. (2016). Cloche is a bHLH-PAS transcription factor that drives haemato-vascular specification. *Nature* 535, 294–298.

Ribeiro, C., Ebner, A., and Affolter, M. (2002). In vivo Imaging reveals different cellular functions for FGF and Dpp signaling in tracheal branching morphogenesis. *Dev. Cell* 2, 677–683.

Ridley, A.J. (2011). Life at the leading edge. *Cell* 145, 1012–1022.

Riedl, J., Crevenna, A.H., Kessenbrock, K., Yu, J.H., Bista, M., Bradke, F., Jenne, D., Holak, T. a, Werb, Z., Sixt, M., et al. (2008). Lifeact: a versatile marker to visualize F-actin. *Nat. Methods* 5, 1–8.

Riedl, J., Flynn, K.C., Raducanu, A., Gärtner, F., Beck, G., Bösl, M., Bradke, F., Massberg, S., Aszodi, A., Sixt, M., et al. (2010). Lifeact mice for studying F-actin dynamics. *Nat. Methods* 7, 168–169.

Rizzuto, R., Pinton, P., Carrington, W., Fay, F.S., Fogarty, K.E., Lifshitz, L.M., Tuft, R.A., and Pozzan, T. (1998). Close Contacts with the Endoplasmic Reticulum as Determinants of Mitochondrial Ca²⁺ Responses Close Contacts with the Endoplasmic Reticulum as Determinants of Mitochondrial Ca²⁺ Responses. *Science* (80-.). 280, 1763–1766.

Robu, M.E., Larson, J.D., Nasevicius, A., Beiraghi, S., Brenner, C., Farber, S.A., and Ekker, S.C. (2007). p53 activation by knockdown technologies. *PLoS Genet.*

Rofstad, E.K., and Danielsen, T. (1998). Hypoxia-induced angiogenesis and vascular endothelial growth factor secretion in human melanoma. *Br. J. Cancer* 77, 897–902.

Rooijen, E. Van, Voest, E.E., Logister, I., Korving, J., Schwerte, T., Giles, R.H., and Eeden, F.J. Van (2009). Zebrafish mutants in the von Hippel-Lindau (VHL) tumor suppressor display a hypoxic response and recapitulate key aspects of Chuvash polycythemia Hubrecht Institute - KNAW & University Medical Center Utrecht , The Netherlands * R . H . G and F . J . V . *Hematology* 113, 6449–6461.

van Rooijen, E., Voest, E.E., Logister, I., Bussmann, J., Korving, J., van Eeden, F.J., Giles, R.H., and Schulte-Merker, S. (2010). von Hippel-Lindau tumor suppressor mutants faithfully model pathological hypoxia-driven angiogenesis

and vascular retinopathies in zebrafish. *Dis. Model. Mech.* 3, 343–353.

Roos, J., DiGregorio, P.J., Yeromin, A. V., Ohlsen, K., Liudyno, M., Zhang, S., Safrina, O., Kozak, J.A., Wagner, S.L., Cahalan, M.D., et al. (2005). STIM1, an essential and conserved component of store-operated Ca²⁺ channel function. *J. Cell Biol.*

Rossi, A., Kontarakis, Z., Gerri, C., Nolte, H., Hölper, S., Krüger, M., and Stainier, D.Y.R. (2015). Genetic compensation induced by deleterious mutations but not gene knockdowns. *Nature Aug 13*, 230–233.

van Rossum, D.B., Patterson, R.L., Kiselyov, K., Boehning, D., Barrow, R.K., Gill, D.L., and Snyder, S.H. (2004). Agonist-induced Ca²⁺ entry determined by inositol 1,4,5-trisphosphate recognition. *Proc. Natl. Acad. Sci.* 101, 2323–2327.

Sainson, R.C.A., Aoto, J., Nakatsu, M.N., Holderfield, M., Conn, E., Koller, E., and Hughes, C.C.W. (2005). Cell-autonomous notch signaling regulates endothelial cell branching and proliferation during vascular tubulogenesis. *FASEB J.* 1, 1–24.

Sakabe, I., Hu, R., Jin, L., Clarke, R., and Kasid, U.N. (2015). TMEM33: a new stress-inducible endoplasmic reticulum transmembrane protein and modulator of the unfolded protein response signaling. *Breast Cancer Res. Treat.* 153, 285–297.

Sakurai, T., Kurokawa, H., and Nonomura, Y. (1991). The Ca²⁺-dependent actin filament-severing activity of 74-kDa protein (adseverin) resides in its NH₂-terminal half. *J. Biol. Chem.* 266, 4581–4585.

Sanger, F., and Coulson, A.R. (1975). A rapid method for determining sequences in DNA by primed synthesis with DNA polymerase. *J. Mol. Biol.* 94, 441–448.

Santhakumar, K., Judson, E.C., Elks, P.M., McKee, S., Elworthy, S., Van Rooijen, E., Walmsley, S.S., Renshaw, S.A., Cross, S.S., and Van Eeden, F.J.M. (2012). A zebrafish model to study and therapeutically manipulate hypoxia signaling in tumorigenesis. *Cancer Res.* *72*, 4017–4027.

Sathish Srinivasan, R., and Oliver, G. (2011). Prox1 dosage controls the number of lymphatic endothelial cell progenitors and the formation of the lymphovenous valves. *Genes Dev.* *25*, 2187–2197.

Sauteur, L., Krudewig, A., Herwig, L., Ehrenfeuchter, N., Lenard, A., Affolter, M., and Belting, H.G. (2014). Cdh5/VE-cadherin promotes endothelial cell interface elongation via cortical actin polymerization during angiogenic sprouting. *Cell Rep.*

Sawamiphak, S., Seidel, S., Essmann, C.L., Wilkinson, G.A., Pitulescu, M.E., Acker, T., and Acker-Palmer, A. (2010). Ephrin-B2 regulates VEGFR2 function in developmental and tumour angiogenesis. *Nature* *465*, 487–491.

Schaefer, K.A., Wu, W., Colgan, D.F., Tsang, S.H., Bassuk, A.G., and Mahajan, V.B. (2017). Unexpected mutations after CRISPR – Cas9 editing in vivo Digenome-seq web tool for profiling CRISPR specificity. *Nature* *14*, 547–548.

Scheer, N., and Campos-Ortega, J.A. (1999). Use of the Gal4-UAS technique for targeted gene expression in the zebrafish. *Mech. Dev.* *80*, 153–158.

Schier, A.F., Neuhauss, S.C., Harvey, M., Malicki, J., Solnica-Krezel, L., Stainier, D.Y., Zwartkuis, F., Abdelilah, S., Stemple, D.L., Rangini, Z., et al. (1996). Mutations affecting the development of the embryonic zebrafish brain. *Development* *123*, 165–178.

Schottenfeld, J., Sullivan-Brown, J., and Burdine, R.D. (2007). Zebrafish curly up encodes a Pkd2 ortholog that restricts left-side-specific expression of southpaw. *Development* *134*, 1605–1615.

Schuermann, A., Helker, C.S.M., and Herzog, W. (2015). Metallothionein 2 regulates endothelial cell migration through transcriptional regulation of vegfc expression. *Angiogenesis* 18, 463–475.

Schulte-Merker, S., and Stainier, D.Y.R. (2014). Out with the old, in with the new: reassessing morpholino knockdowns in light of genome editing technology. *Development* 141, 3103–3104.

Seiler, C., and Pack, M. (2011). Transgenic labeling of the zebrafish pronephric duct and tubules using a promoter from the enpep gene Christoph. *Gene Expr. Patterns* 175, 777–783.

Selcher, J.C. (2001). Mice Lacking the ERK1 Isoform of MAP Kinase Are Unimpaired in Emotional Learning. *Learn. Mem.* 8, 11–19.

Serban, D., Leng, J., and Cheresh, D. (2008). H-ras regulates angiogenesis and vascular permeability by activation of distinct downstream effectors. *Circ. Res.*

Sharif-Naeini, R., Folgering, J.H.A., Bichet, D., Duprat, F., Lauritzen, I., Arhatte, M., Jodar, M., Dedman, A., Chatelain, F.C., Schulte, U., et al. (2009). Polycystin-1 and -2 Dosage Regulates Pressure Sensing. *Cell* 139, 587–596.

Shibata, M., Nishimasu, H., Kodera, N., Hirano, S., Ando, T., Uchihashi, T., and Nureki, O. (2017). Real-space and real-time dynamics of CRISPR-Cas9 visualized by high-speed atomic force microscopy. *Nat. Commun.* 8, 1430.

Shimoda, N., Knapik, E.W., Ziniti, J., Sim, C., Yamada, E., Kaplan, S., Jackson, D., de Sauvage, F., Jacob, H., and Fishman, M.C. (1999). Zebrafish Genetic Map with 2000 Microsatellite Markers. *Genomics* 58, 219–232.

Shin, M., Beane, T., Quillien, A., Male, I., Zhu, L.J., and Lawson, N.D. (2016a). Vegfa signals through ERK to promote angiogenesis, but not artery

differentiation. *Development* dev.137919.

Shin, M., Male, I., Beane, T.J., Villefranc, J.A., Kok, F.O., Zhu, L.J., and Lawson, N.D. (2016b). Vegfc acts through ERK to induce sprouting and differentiation of trunk lymphatic progenitors. *Development* dev.137901.

Shweiki, D., Itin, A., Soffer, D., and Keshet, E. (1992). Vascular endothelial growth factor induced by hypoxia may mediate hypoxia-initiated angiogenesis. *Nature* 359, 843–845.

Siekman, A.F., and Lawson, N.D. (2007). Notch signalling limits angiogenic cell behaviour in developing zebrafish arteries. *Nature* 445, 781–784.

Singh, A., Hildebrand, M.E., Garcia, E., and Snutch, T.P. (2010). The transient receptor potential channel antagonist SKF96365 is a potent blocker of low-voltage-activated T-type calcium channels. *Br. J. Pharmacol.* 160, 1464–1475.

Sneyd, J., Tsaneva-Atanasova, K., Yule, D.I., Thompson, J.L., and Shuttleworth, T.J. (2004). Control of calcium oscillations by membrane fluxes. *Proc. Natl. Acad. Sci. U. S. A.* 101, 1392–1396.

Soboloff, J., Rothberg, B.S., Madesh, M., and Gill, D.L. (2012). STIM proteins: Dynamic calcium signal transducers. *Nat. Rev. Mol. Cell Biol.* 13, 549–565.

Solnica-Krezel, L., Stemple, D.L., Mountcastle-Shah, E., Rangini, Z., Neuhaus, S.C., Malicki, J., Schier, a F., Stainier, D.Y., Zwartkuis, F., Abdelilah, S., et al. (1996). Mutations affecting cell fates and cellular rearrangements during gastrulation in zebrafish. *Development* 123, 67–80.

Srinivasan, R., Zabuawala, T., Huang, H., Zhang, J., Gulati, P., Fernandez, S., Karlo, J.C., Landreth, G.E., Leone, G., and Ostrowski, M.C. (2009). Erk1 and erk2 regulate endothelial cell proliferation and migration during mouse embryonic

angiogenesis. PLoS One 4.

Stainier, D.Y., Weinstein, B.M., Detrich, H.W., Zon, L.I., and Fishman, M.C. (1995). Cloche, an early acting zebrafish gene, is required by both the endothelial and hematopoietic lineages. *Development* 121, 3141–3150.

Stainier, D.Y., Fouquet, B., Chen, J.N., Warren, K., Weinstein, B.M., Meiler, S., Mohideen, M., Neuhauss, S.C., Solnica-Krezel, L., Schier, A., et al. (1996). Mutations affecting the formation and function of the cardiovascular system in the zebrafish embryo. *Development* 123, 285–292.

Stainier, D.Y.R., Raz, E., Lawson, N.D., Ekker, S.C., Burdine, R.D., Eisen, J.S., Ingham, P.W., Schulte-Merker, S., Yelon, D., Weinstein, B.M., et al. (2017). Guidelines for morpholino use in zebrafish. *PLOS Genet.*

Streisinger, G., Singer, F., Walker, C., Knauber, D., and Dower, N. (1986). Segregation analyses and gene-centromere distances in zebrafish. *Genetics* 112, 311–319.

Suchting, S., Freitas, C., le Noble, F., Benedito, R., Bréant, C., Duarte, A., and Eichmann, A. (2007). The Notch ligand Delta-like 4 negatively regulates endothelial tip cell formation and vessel branching. *Proc. Natl. Acad. Sci. U. S. A.* 104, 3225–3230.

Sullivan-Brown, J., Schottenfeld, J., Okabe, N., Hostetter, C.L., Serluca, F.C., Thiberge, S.Y., and Burdine, R.D. (2008). Zebrafish mutations affecting cilia motility share similar cystic phenotypes and suggest a mechanism of cyst formation that differs from *pkd2* morphants. *Dev. Biol.* 314, 261–275.

Sumanas, S., and Lin, S. (2006). Ets1-related protein is a key regulator of vasculogenesis in zebrafish. *PLoS Biol.* 4, 0060–0069.

Sun, Z., Amsterdam, A., Pazour, G.J., Cole, D.G., Miller, M.S., and Hopkins, N. (2004). A genetic screen in zebrafish identifies cilia genes as a principal cause of cystic kidney. *Development* 131, 4085–4093.

Swanhart, L.M., Takahashi, N., Jackson, R.L., Gibson, G.A., Watkins, C., Dawid, I.B., and Hukriede, N.A. (2010). Characterization of an *lhx1a* transgenic reporter in zebrafish. *54*, 731–736.

Tabas, I., García-Cardena, G., and Owens, G.K. (2015). Recent insights into the cellular biology of atherosclerosis. *J. Cell Biol.* 209, 13–22.

Takahashi, T., and Shibuya, M. (1997). The 230 kDa mature form of KDR/Flk-1 (VEGF receptor-2) activates the PLC-gamma pathway and partially induces mitotic signals in NIH3T3 fibroblasts. *Oncogene* 14, 2079–2089.

Takahashi, T., Yamaguchi, S., Chida, K., and Shibuya, M. (2001). A single autophosphorylation site on KDR / Flk-1 is essential for VEGF-A-dependent activation of PLC-g and DNA synthesis in vascular endothelial cells. *EMBO J.* 20, 2678–2778.

Tao, S., Witte, M., Bryson-Richardson, R.J., Currie, P.D., Hogan, B.M., and Schulte-Merker, S. (2011). Zebrafish *prox1b* mutants develop a lymphatic vasculature, and *prox1b* does not specifically mark lymphatic endothelial cells. *PLoS One* 6.

Terman, B.I.I., Dougher-Vermazen, M., Carrion, M.E.E., Dimitrov, D., Armellino, D.C.C., Gospodarowicz, D., Böhlen, P., and Bohlen, P. (1992). Identification of the KDR tyrosine kinase as a receptor for vascular endothelial cell growth factor. *Biochem. Biophys. Res. Commun.* 187, 1579–1586.

Thakore, P.I., D'Ippolito, A.M., Song, L., Safi, A., Shivakumar, N.K., Kabadi, A.M., Reddy, T.E., Crawford, G.E., and Gersbach, C.A. (2015). Highly specific

epigenome editing by CRISPR-Cas9 repressors for silencing of distal regulatory elements. *Nat. Methods* 12, 1143–1149.

Turner, R.W., Anderson, D., and Zamponi, G.W. (2011). Signaling complexes of voltage-gated calcium channels. *Channels (Austin)*. 5, 440–448.

Urade, T., Yamamoto, Y., Zhang, X., Ku, Y., and Sakisaka, T. (2014). Identification and characterization of TMEM33 as a reticulon-binding protein. *Kobe J. Med. Sci.* 60, E57–E65.

Urnov, F.D., Rebar, E.J., Holmes, M.C., Zhang, H.S., and Gregory, P.D. (2010). Genome editing with engineered zinc finger nucleases. *Nat. Rev. Genet.* 11, 636–646.

Vaca, L., and Kunze, D.L. (1994). Depletion of intracellular Ca²⁺ stores activates a Ca(2+)-selective channel in vascular endothelium. *Am. J. Physiol.* 267, C920–5.

Vacaru, A.M., Narzo, A.F. Di, Howarth, D.L., Tsedensodnom, O., Imrie, D., Cinaroglu, A., Amin, S., Hao, K., and Sadler, K.C. (2014). Molecularly defined unfolded protein response subclasses have distinct correlations with fatty liver disease in zebrafish.

Vasilyev, A., Liu, Y., Mudumana, S., Mangos, S., Lam, P.Y., Majumdar, A., Zhao, J., Poon, K.L., Kondrychyn, I., Korzh, V., et al. (2009). Collective cell migration drives morphogenesis of the kidney nephron. *PLoS Biol.* 7.

Verma, A.K., Filoteo, A.G., Stanford, D.R., Wieben, E.D., Penniston, T., Strehler, E.E., Fischer, R., Heim, R., Vogel, G., Mathews, S., et al. (1988). Complete Primary Structure of a Human Plasma Membrane Ca²⁺ Pump. 263, 14152–14159.

Veron, D., Reidy, K., Marlier, A., Bertuccio, C., Villegas, G., Jimenez, J., Kashgarian, M., and Tufro, A. (2010a). Induction of podocyte VEGF164 overexpression at different stages of development causes congenital nephrosis or steroid-resistant nephrotic syndrome. *Am. J. Pathol.* 177, 2225–2233.

Veron, D., Reidy, K.J., Bertuccio, C., Teichman, J., Villegas, G., Jimenez, J., Shen, W., Kopp, J.B., Thomas, D.B., and Tufro, A. (2010b). Overexpression of VEGF-A in podocytes of adult mice causes glomerular disease. *Kidney Int.* 77, 989–999.

Vig, M., Peinelt, C., Beck, A., Koomoa, D.L., Rabah, D., Koblan-Huberson, M., Kraft, S., Turner, H., Fleig, A., Penner, R., et al. (2006a). CRACM1 is a plasma membrane protein essential for store-operated Ca²⁺ entry. *Science* (80-). 312, 1220–1223.

Vig, M., Peinelt, C., Beck, A., Koomoa, D.L., Rabah, D., Koblan-Huberson, M., Kraft, S., Turner, H., Fleig, A., Penner, R., et al. (2006b). CRACM1 is a plasma membrane protein essential for store-operated Ca²⁺ entry. *Science* (80-). 312, 1220–1223.

Villefranc, J.A., Amigo, J., and Lawson, N.D. (2007). Gateway compatible vectors for analysis of gene function in the zebrafish. *Dev. Dyn.* 236, 3077–3087.

Villefranc, J.A., Nicoli, S., Bentley, K., Jeltsch, M., Zarkada, G., Moore, J.C., Gerhardt, H., Alitalo, K., and Lawson, N.D. (2013). A truncation allele in vascular endothelial growth factor c reveals distinct modes of signaling during lymphatic and vascular development. *Development*.

van Vliet, A.R., Giordano, F., Gerlo, S., Segura, I., Van Eygen, S., Molenberghs, G., Rocha, S., Houcine, A., Derua, R., Verfaillie, T., et al. (2017). The ER Stress

Sensor PERK Coordinates ER-Plasma Membrane Contact Site Formation through Interaction with Filamin-A and F-Actin Remodeling. *Mol. Cell* 65, 885–899.e6.

Wales, P., Schuberth, C.E., Aufschnaiter, R., Fels, J., Garcia-Aguilar, I., Janning, A., Dlugos, C.P., Schafer-Herte, M., Klingner, C., Walte, M., et al. (2016). Calcium-mediated actin reset (CaAR) mediates acute cell adaptations. *Elife* 5, 1–31.

Wang, H., La Russa, M., and Qi, L.S. (2016). CRISPR/Cas9 in Genome Editing and Beyond. *Annu. Rev. Biochem.* 85, 227–264.

Watson, O., Novodvorsky, P., Gray, C., Rothman, A.M.K., Lawrie, A., Crossman, D.C., Haase, A., McMahon, K., Gering, M., Van Eeden, F.J.M., et al. (2013). Blood flow suppresses vascular Notch signalling via *dll4* and is required for angiogenesis in response to hypoxic signalling. *Cardiovasc. Res.* 100, 252–261.

Wei, C., Wang, X., Chen, M., Ouyang, K., Song, L.-S., and Cheng, H. (2009). Calcium flickers steer cell migration. *Nature* 457, 901–905.

White, J.K., Gerdin, A.K., Karp, N.A., Ryder, E., Buljan, M., Bussell, J.N., Salisbury, J., Clare, S., Ingham, N.J., Podrini, C., et al. (2013). Genome-wide generation and systematic phenotyping of knockout mice reveals new roles for many genes. *Cell* 154.

Whiteley, G., Collins, R.F., and Kitmitto, A. (2012). Characterization of the molecular architecture of human caveolin-3 and interaction with the skeletal muscle ryanodine receptor. *J. Biol. Chem.* 287, 40302–40316.

Whitfield, T.T., M., G., van Eeden, F.J.M., Schach, U., Brand, M., Furutani-Seiki, M., Haffter, P., Hammerschmidt, M., Heisenberg, C.-P., Jiang, Y.-J., et al. (1995). Mutations affecting development of the zebrafish inner ear and lateral line. *Dev*

123, 240–254.

Wiley, D.M., Kim, J.-D., Hao, J., Hong, C.C., Bautch, V.L., and Jin, S.-W. (2011). Distinct signalling pathways regulate sprouting angiogenesis from the dorsal aorta and the axial vein. *Nat. Cell Biol.* 13, 686–692.

Wilkinson, R.N., Koudijs, M.J., Patient, R.K., Ingham, P.W., Schulte-Merker, S., and Van Eeden, F.J.M. (2012). Hedgehog signaling via a calcitonin receptor-like receptor can induce arterial differentiation independently of VEGF signaling in zebrafish. *Blood* 120, 477–488.

Wong, C., and Jin, Z.-G. (2005). Protein Kinase C-dependent Protein Kinase D Activation Modulates ERK Signal Pathway and Endothelial Cell Proliferation by Vascular Endothelial Growth Factor. *J. Biol. Chem.*

Wu, L., Gao, X., Brown, R.C., Heller, S., and O’Neil, R.G. (2007). Dual role of the TRPV4 channel as a sensor of flow and osmolality in renal epithelial cells. *Am. J. Physiol. Renal Physiol.* 293, F1699-713.

Yadav, L., Puri, N., Rastogi, V., Satpute, P., and Sharma, V. (2015). Tumour angiogenesis and angiogenic inhibitors: A review. *J. Clin. Diagnostic Res.* 9, XE01-XE05.

Yang, Y., García-Verdugo, J.M., Soriano-Navarro, M., Srinivasan, R.S., Scallan, J.P., Singh, M.K., Epstein, J.A., and Oliver, G. (2012). Lymphatic endothelial progenitors bud from the cardinal vein and intersomitic vessels in mammalian embryos. *Blood* 120, 2340–2348.

Yang, Y.H., Wang, Y., Lam, K.S.L., Yau, M.H., Cheng, K.K.Y., Zhang, J., Zhu, W., Wu, D., and Xu, A. (2008). Suppression of the Raf/MEK/ERK Signaling cascade and inhibition of angiogenesis by the carboxyl terminus of angiopoietin-like protein 4. *Arterioscler. Thromb. Vasc. Biol.* 28, 835–840.

Yaniv, K., Isogai, S., Castranova, D., Dye, L., Hitomi, J., and Weinstein, B.M. (2006). Live imaging of lymphatic development in the zebrafish. *Nat. Med.* *12*, 711–716.

Yokota, Y., Nakajima, H., Wakayama, Y., Muto, A., Kawakami, K., Fukuhara, S., and Mochizuki, N. (2015). Endothelial Ca²⁺ oscillations reflect VEGFR signaling-regulated angiogenic capacity in vivo. *Elife*.

Young, C.L., Feierstein, A., and Southwick, F.S. (1994). Calcium regulation of actin filament capping and monomer binding by macrophage capping protein. *J. Biol. Chem.* *269*, 13997–14002.

Yu, F., White, B., Zhao, Q., and Lee, F. (2001). HIF-1 α binding to VHL is regulated by stimulus-sensitive proline hydroxylation. *Proc. Natl. Acad. Sci.* *98*, 9630–9635.

Yu, P., Gu, S., Bu, J., and Du, J. (2010). TRPC1 is essential for in vivo angiogenesis in zebrafish. *Circ. Res.* *106*, 1221–1232.

Zadeh, M.A.H., Glass, C.A., Magnussen, A., Jules, C., and Bates, D.O. (2009). VEGF-Mediated Elevated Intracellular Calcium and Angiogenesis in Human Microvascular Endothelial Cells In Vitro Are Inhibited by Dominant Negative TRPC6. *Analysis* *15*, 605–614.

Zeng, H., Sanyal, S., and Mukhopadhyay, D. (2001). Tyrosine Residues 951 and 1059 of Vascular Endothelial Growth Factor Receptor-2 (KDR) Are Essential for Vascular Permeability Factor/Vascular Endothelial Growth Factor-induced Endothelium Migration and Proliferation, Respectively. *J. Biol. Chem.*

Zhang, D., and Oliferenko, S. (2014). Tts1, the fission yeast homolog of TMEM33 family, functions in NE remodeling during mitosis. *Mol. Biol. Cell* *25*, 2970–2983.

Zhang, Y., Qin, W., Lu, X., Xu, J., Huang, H., Bai, H., Li, S., and Lin, S. (2017). Programmable base editing of zebrafish genome using a modified CRISPR-Cas9 system. *Nat. Commun.* 8, 6–10.

Zhang, Z.-R., Chu, W.-F., Song, B., Gooz, M., Zhang, J.-N., Yu, C.-J., Jiang, S., Baldys, A., Gooz, P., Steele, S., et al. (2013). TRPP2 and TRPV4 form an EGF-activated calcium permeable channel at the apical membrane of renal collecting duct cells. *PLoS One* 8, e73424.

Zhou, Y., Meraner, P., Kwon, H.T., Machnes, D., Oh-, M., Zimmer, J., Huang, Y., Stura, A., Rao, A., and Patrick, G. (2010). STIM1 gates the store-operated calcium channel ORAI1 in vitro. *Nat. Struct. Mol. Biol.* 17, 112–116.

Zou, P., Wu, S.Y., Koteiche, H.A., Mishra, S., Levic, D.S., Knapik, E., Chen, W., and Mchaourab, H.S. (2015). A conserved role of α A-crystallin in the development of the zebrafish embryonic lens. *Exp. Eye Res.* 138, 104–113.

Zweifach, A., and Lewis, R.S. (1995). Slow calcium-dependent inactivation of depletion-activated calcium current. Store-dependent and -independent mechanisms. *J. Biol. Chem.* 270, 14445–14451.